Evolution and remediation of ground failure risk for temporary roads carrying cyclic heavy haul traffic

by
Christopher Jan Krechowiecki-Shaw

A thesis submitted to
the University of Birmingham
for the degree of
DOCTOR OF PHILOSOPHY

Department of Civil Engineering
School of Engineering
College of Engineering and Physical Sciences
University of Birmingham
September 2017

Abstract

Increasing popularity of offsite modular construction has increased demand for transportation of very large (1000-3000 tonne) indivisible loads. Crossing poor soils presents a serious risk of ground failure, particularly as larger vehicles' greater influence depths produce a very different soil response to conventional vehicles. Temporary haul roads designed conventionally may be excessively conservative and unaffordable as a temporary asset; cost reduction through observational risk management is sought.

This thesis experimentally investigates soft silt and clay soils through cyclic triaxial testing. Particular focus is given to anisotropically normally consolidated silt, carefully manufactured through slurry consolidation to replicate liquefiable fabric. Soil samples are tested under the unusual loading conditions associated with heavy haul roads (slow, large-strain, infrequent).

A new design approach for temporary heavy haul roads is demonstrated: cyclic traffic load can be used to improve soil, either by gradually rearranging fabric (medium-strain treatment) or remoulding and consolidating excess pore water pressure (large-strain treatment). Liquefiable silt benefits from both, plastic clay only from the latter. These findings, combined with a robust monitoring regime and management of heavy traffic, could be used to improve soil strength over time during operations. This could realise significant project savings and increase viability of modular construction.

"There is a theory which states that if ever anyone discovers exactly what the Universe is for and why it is here, it will instantly disappear and be replaced by something even more bizarre and inexplicable.

There is another theory which states that this has already happened."

Douglas Adams, from

"The Restaurant at the End of the Universe"

Acknowledgements

Firstly I would like to thank EPSRC and the University of Birmingham Civil Engineering Department for funding this study, without which this study would not have been possible.

I would like to thank my supervisors, Prof. Ian Jefferson, Dr. Alexander Royal and Dr. Gurmel Ghataora, for their continued help, support, insight and enthusiasm through the ups and downs of the project. Thanks also to Imad Alobaidi of Atkins, Peter Gilbert (formerly of Atkins, now at Jacobs) and the Atkins TCO team for inspiring this study and providing real-world context and practical advice.

I must also thank the lab staff, particularly Jim, Luis and Seb, for helping me find and fix equipment, move heavy bags of soil and generally being friendly, approachable and good company. Similarly, thanks to the other lab occupants, Omar, Giulio, Anna, James and Atiku, for making my time there enjoyable and sympathising with me when soil samples got inadvertently squashed.

Thanks to my parents, Rob and Irene, for taking the time to read and comprehend my thesis, and patiently explaining to me the importance of proper grammar and how not to split infinitives.

Special thanks must be given to my wife, Laura, for looking after me during the hard times, listening to gibberish explanations in response to ‘how was your day?’ and helping me focus on the important things. Appropriate credit must also be given to her cat, Biggles, whose habit of walking on my keyboard has contributed more to this thesis than many would believe.

Contents

List of Figures

List of Tables

List of Symbols

General

A – sample representative cross-sectional area (mm^2)

A_0 – initial sample A prior to consolidation (mm^2)

A_c – sample A following anisotropic consolidation (mm^2)

B – Skempton's pore pressure parameter, defined in Equation 4.1.

c' – effective cohesion (kPa)

c_v – coefficient of consolidation (m^2/s)

c_{vi} – coefficient of consolidation under isotropic consolidation (m^2/s)

D – sample diameter (mm)

D_0 – sample diameter prior to consolidation (mm)

D_1 – sample diameter after initial, isotropic consolidation stage (mm)

D_c – sample diameter after final, anisotropic consolidation stage (mm)

E – Secant Young's Modulus (MPa)

E_0 – Young's Modulus at top of layer (MPa)

E_L – Cyclic Load Modulus (MPa) = $\Delta q_{cyc}/\Delta \varepsilon_{cyc}$

e – void ratio (dimensionless)

e_0 – initial void ratio prior to consolidation (dimensionless)

e_1 – void ratio after initial, isotropic consolidation stage (dimensionless)

e_c – void ratio after final, anisotropic consolidation stage (dimensionless)

Δe_1 – change in void ratio during initial, isotropic consolidation stage (dimensionless)

$\Delta e_1/e_0$ – sample quality metric, similar to that proposed by Lunne et al. (1997)

G – Shear modulus (MPa)

k – coefficient of permeability (m/s)

K – coefficient of lateral earth pressure (dimensionless)

$K_{0,NC}$ – normally consolidated coefficient of lateral earth pressure at rest (dimensionless)

$K_{0,OC}$ – overconsolidated coefficient of lateral earth pressure at rest (dimensionless)

L_d – effective drainage length for consolidation (mm)

L – sample length (mm)

L_0 – sample length prior to consolidation (mm)

L_1 – sample length after initial, isotropic consolidation stage (mm)

L_c – sample length after final, anisotropic consolidation stage (mm)

LL – Liquid Limit as determined by the fall cone method in BS 1377-2 (BSI, 1990a) (%)

OCR – overconsolidation ratio (dimensionless)

P – axial ram load (N)

p' – mean normal effective stress (kPa)

p/p'_e – normalised mean normal effective stress, after Schofield and Wroth (1968) (dimensionless)

PI – Plasticity Index (%) (= $LL - PL$)

PL – Plastic Limit as per BS 1377-2 (BSI, 1990a) (%)

q – deviator stress (kPa)

q/p' – deviator stress ratio (dimensionless)

q/p'_e – normalised deviator stress, after Schofield and Wroth (1968) (dimensionless)

q_{max} – deviator stress at cycle maximum (kPa)

q_{min} – deviator stress at cycle minimum (kPa)

q_{peak} – pre-liquefaction peak (monotonic) deviator stress (kPa)

Δq – increment in deviator stress from start of loading (kPa)

Δq_c – increment in deviator stress to the critical state (kPa)

Δq_{cyc} – peak cyclic deviator stress range (kPa) = q_{max} - q_{min}

Δq_{peak} – increment in deviator stress from start of (monotonic) shear to pre-liquefaction peak (kPa)

$\Delta q_{\varepsilon,max}$ – cyclic deviator increment at peak strain (kPa) (defined in Figure 3.1)

S_u – Undrained shear strength (kPa)

t – time (s)

t_{100} – time to end of primary consolidation, after Head (1986)

t_{90} – time to 90% completion of primary consolidation, after Head (1986)

u –sample pore water pressure (kPa)

u_{base} –pore water pressure measured on base transducer (kPa)

u_{back} – pore water pressure measured on back pressure (Hydraulic APC) (kPa)

u_e – estimated mean excess pore water pressure (kPa)

Δu – change in pore water pressure during a saturation B-test stage (kPa)

u_{max} – maximum value of u attained in a particular cycle (kPa)

u_{pl} – irrecoverable (plastic) value of u attained at the end of a particular cycle (kPa)

Δu_{pl} – increment of irrecoverable (plastic) value of u attained in a particular cycle (kPa)

V – sample volume (mm^3)

V_0 – sample initial volume prior to consolidation (mm^3)

ΔV – change in sample volume from consolidation (mm^3)

ΔV_1 – change in sample volume from initial isotropic consolidation (mm^3)

x – lateral distance from vehicle or wheel centreline (m)

y_m – rolling mean of any variable over n results, defined in Equation 4.3.

y_n – an individuall result of any variable (used in calculation of y_m)

Z_C – mechanical coordination number, defined in Gong (2008)

δ - imposed axial displacement (mm)

λ – gradient of Normal Compression Line in p'-e space (dimensionless)

κ – gradient of swell back lines in p'-e space (dimensionless)

ε – axial strain (dimensionless) = δ/L

ε_{max} – maximum axial strain experienced in a particular cycle (dimensionless) (defined in Figure 3.1)

ε_{pl} – cumulative plastic axial strain in a particular cycle (dimensionless) (defined in Figure 3.1)

$\Delta\varepsilon_{cyc}$ – cyclic strain range for a particular cycle (dimensionless) (defined in Figure 3.1)

$\Delta\varepsilon_{el}$ – recoverable (elastic) axial strain in a particular cycle (dimensionless) (defined in Figure 3.1)

$\Delta\varepsilon_{q,max}$ – increment in axial strain to reach q_{max} in a particular cycle (dimensionless) (defined in Figure 3.1)

$\Delta\varepsilon_{pl}$ – increment in plastic axial strain in a particular cycle (dimensionless) (defined in Figure 3.1)

ε_v – volumetric strain (dimensionless) = $\Delta V/V_0$

ε_{v1} – volumetric strain during initial isotropic consolidation stage (dimensionless) = $\Delta V_1/V_0$

ε_{tv} – axial strain at the volume change threshold, determined after Hsu and Vucetic (2006) (dimensionless)

ε_{tl} – axial strain at initiation of liquefaction (dimensionless)

v – Poisson's ratio (dimensionless)

σ_1 – axial total stress (kPa)

σ_1 – confining total stress (kPa)

σ'_1 – axial effective stress (kPa)

σ'_3 – confining effective stress (kPa)

$\Delta\sigma'_3$ – increment in confining effective stress during saturation B-test stage (kPa)

ϕ' – angle of internal shearing resistance (degrees)

Ψ – cyclic stress normalised to pre-liquefaction peak (dimensionless), = $\Delta q_{cyc}/\Delta q_{peak}$

χ - cyclic stress normalised to critical state (dimensionless), = $\Delta q_{cyc}/\Delta q_c$

Used specifically for modelling (Chapter 2)

b – loaded width (m)

d – pavement depth (m)

m_1 – increase in Young's modulus with depth (MPa/m)

N_{Su} – shear strength ratio (dimensionless),$= S_u/\gamma_p' d$

s_E – settlement for linear elastic model (m)

s_P – settlement for Mohr-Coulomb model (m)

z_{NC} – depth to normal consolidation (m)

γ_p' – effective unit weight of pavement fill (kN/m^3)

γ_p– total unit weight of pavement fill (kN/m^3)

γ_S – unit weight of subgrade (kN/m^3)

Λ – Utilisation of ultimate capacity, ω/ω_{ult} (dimensionless)

ω – uniformly distributed wheel load stress on pavement (kPa)

ω_{ult} – ultimate ω at failure in Mohr-Coulomb model (kPa)

σ_z – vertical total stress (kPa)

σ'_z – vertical effective stress (kPa)

$\Delta\sigma_z$ – increment in total effective stress from wheel load (kPa)

$\Delta\sigma'_z$ – increment in vertical effective stress from wheel load (kPa)

Abbreviations

CPT – (Electronic) Cone Penetration Test

DCP – Dynamic Cone Penetration test

K_0 – consolidated under zero lateral strain conditions.

K_0-NCL - K_0 Normal Compression Line

NC – Normally Consolidated

NCL – Normal Compression Line (also referred to as virgin compression line)

OC – Overconsolidated

PWP – Pore Water Pressure

SHANSEP – Stress History And Normalised Soil Engineering Properties, after Ladd and Foott (1974).

SPT – Standard Penetration Test

CHAPTER 1: INTRODUCTION

1.1. Background

In the construction industry, use of modular, prefabricated units is gaining popularity as they provide a range of benefits over on-site construction:

- In factory conditions, cost is reduced whilst improved quality and whole-life performance is possible (Southern, 2016). Reduced construction waste can also reduce environmental impact.
- Factory conditions reduce exposure of workforce to confined or dangerous working conditions (e.g. adjacent to roads/railways, at height) and adverse weather.
- They can bring digital innovation and increased collaboration on buildability into the industry through use of Building Information Modelling (BIM) technology and Early Contractor Involvement (Cronin, 2015; Southern, 2016), with potential to improve consistency in delivery and reduce potential for expensive on-site changes to design.
- Access constraints (e.g. closure of motorways or railway lines for construction) can require infrastructure to be installed quickly on site; construction off-site is thus a necessity.

Mining, oil and gas and power generation projects which need to develop remote sites, often in inhospitable locations, are particularly suited to modular construction and often perform as much work off-site as possible, resulting in a need to transport very large indivisible loads. For example, platforms composed of multiple Self-Propelled

Modular Transporters (SPMTs, Figure 1.1) can carry 40 metric tonnes per axle (Mammoet 2017a) and cover an area up to 6m wide by 60m long (Mammoet 2017b). The load (up to 3000 tonnes) is transferred to the road surface by around 80 relatively closely spaced axles, stressing a significantly greater volume of soil than conventional traffic. These vehicles typically travel at low speeds, i.e. approximately 5 km/hr, and may recur in the order of once per day.

Temporary haul roads capable of safely conveying these exceptional loads are required. Crossing problematic ground presents a novel engineering challenge; high spend on a robust temporary pavement and earthworks may render the project unaffordable, particularly if the remote location engenders logistical difficulties. Traditional ground improvement techniques may not be feasible for a temporary asset and new, more cost-efficient methods to manage the risk are needed. A temporary haul road is by definition a short-term venture, facilitating the transportation of equipment to site; emphasis is placed on minimal capital cost whilst remaining fit-for-purpose over its short life. Long-term resilience, a key function of permanent roads, is not of concern.

Figure 1.1: Heavy equipment being transported on a platform composed of Self-Propelled Modular Transporters (SPMTs), Courtesy of and ® of Mammoet BV.

1.2. Need for Research

The subgrade response to exceptionally large, heavy vehicles is expected to be fundamentally different to that for conventional traffic: firstly greater volumes and depths of soil are expected to be mobilised by the larger vehicle sizes and interaction between adjacent wheel loads; secondly the temporary nature of these roads means importance may be placed upon different criteria, i.e. more settlement and strength degradation may be permissible than in the conventional case provided ultimate failure does not occur. Running repairs to the road may be acceptable, depending on logistical implications (delays, material supply, etc.).

Larger vehicles, stressing deeper, potentially saturated and weaker deposits, present an increased failure risk compared to the same load transported on a greater number of smaller vehicles, potentially jeopardising these multimillion-dollar payloads. The response of such deep deposits to cyclic traffic loads is not typically considered in pavement engineering and carries unusual risks; plastic yield is more common and in

low-plasticity (silty) soils catastrophic liquefaction failure can occur. Foundation and earthquake engineering research consider similar deep-seated failure problems, however the specifics of heavy haul road loading, i.e. stresses closer to the failure state, entirely transient but low-frequency application and large settlement tolerance, are unusual in these fields. As the soil response is not thoroughly understood, numerical modelling alone will not be sufficient to describe risks or devise solutions; experimental study of these unusual stress conditions in problematic soils is required.

Under cyclic load, soils can 'condition', i.e. gradually become stiffer, as a result of alteration of their internal structure. Positive excess pore water pressures are also typically accumulated, causing consolidation and possible strengthening. Both of these phenomena require plastic strain; enhanced settlement tolerance for temporary roads may thus allow greater improvement via these mechanisms than conventional roads. A method of using operational traffic loads to effect this is sought.

1.3. Aim and Objectives

The aim of this study is to determine, through experimental testing, how management of heavy traffic loads supplemented by *in-situ* monitoring can be used to control residual risk and improve geologically recently deposited deep, problematic subsoil, thus delivering smaller haul road earthwork construction depth whilst remaining fit for purpose, i.e. avoiding failure during the prescribed number of heavy passes.

To achieve this, the following objectives are set:

- Review research on cyclic degradation and liquefaction in soft soils at depth, in particular fine, low-plasticity (silty) soils and ascertain the likely influence of

unusual features of heavy haul road loading, i.e. large stress/strain, transient low-frequency loads and opportunities for consolidation.

- Investigate the nature of stress fields in the subgrade and how the pavement-subgrade response varies in comparison to conventional roads through numerical modelling, in order to determine which subgrade zones cannot be adequately analysed by conventional pavement engineering and require further experimental testing to describe their behaviour.
- Develop and refine experimental soil testing methods to test problematic (i.e. low-plasticity, soft and/or liquefiable) soils under conditions which are representative of deep (i.e. below the water table and normally consolidated) deposits beneath heavy haul roads.
- Experimentally investigate factors which accelerate or arrest degradation, in order to develop methods which improve subgrade strength through select application of traffic loads and manage failure risk throughout the infrastructure life.
- Consider properties which can be measured in-situ to give a real-time indication of failure risk.

1.4. Structure of Research

This study is predominantly laboratory-based experimental work, although it has progressed in collaboration with a live project undertaken by Atkins Ground Engineering in Central Asia where large prefabricated units are transported over soft, relatively young, alluvial and marine low to medium plasticity silty clay deposits. Soil properties and loading characteristics are thus based loosely upon this project; testing

of silt and clay soil samples provides upper and lower bounds on the range of properties expected. Due to the commercial sensitivity and incomplete nature of the project, further details are not supplied.

The experimental work was primarily performed using cyclic triaxial testing. Samples were reconstituted from commercially available geomaterials to obtain the desired properties. Testing incorporated undrained static and cyclic shear on anisotropically consolidated samples. In some cases, rest periods for consolidation were included between load applications.

The pavement and subgrade behavioural differences between heavy haul roads and conventional roads are considered in Chapter 2, supplemented with basic Finite Element Analysis to corroborate assertions. In particular, the effect of vehicle size on localised yielding in the sub-soil, expected to control cyclic degradation, is studied.

The soil mechanics literature pertinent to the novel properties of heavy haul roads, as discussed in Chapter 2, is critically reviewed in Chapter 3.

The development of the laboratory testing methodology is detailed in Chapter 4. This details the engineering descriptions of soils used, efforts in development of sample preparation techniques and evaluation of the reliability and consistency of techniques employed and errors inherent. A limited series of test results pertinent to this evaluation are also presented.

The specifics of the various triaxial tests performed are detailed in Chapter 5.

The test results, with discussion appropriate to development of soil mechanics theory, are presented in Chapter 6. The bulk of testing and analysis is devoted to meta-stable liquefaction of silt soil, although some testing and analysis is also devoted to behaviour of plastic clay under similar loading conditions.

Chapter 7 discusses the practicalities of applying an observational design to a heavy haul road project, with reference to experimental results, to develop recommendations for the identification, investigation, and monitoring of geohazards and the management of large traffic loads to mitigate or remediate these hazards.

Conclusions and recommendations for further work are provided in Chapter 8.

The overall contribution to knowledge this study makes is an improved understanding of deep failure risk beneath large surface loads, particularly in liquefiable soils, and how controlled load application can produce an optimised foundation system through improving the soil.

Findings have been disseminated in several peer-reviewed journal papers:

- Krechowiecki-Shaw, C.J.; Jefferson, I.; Royal, A.; Ghataora, G.S.; Alobaidi, I.M. (2016). *Degradation of soft subgrade soil from slow, large, cyclic heavy-haul road loads: A review*. Canadian Geotechnical Journal, Vol.53(9), pp.1435-1449
- Krechowiecki-Shaw, C.J.; Jefferson, I.; Royal, A.; Ghataora, G.S. (2017) *Temporary routes for exceptional loads: a new soil mechanics perspective.* Proceedings of the ICE – Transport. *In Press, https://doi.org/10.1680/jtran.16.00109.*

A further paper is undergoing amendments following peer review:

- Krechowiecki-Shaw, C.J.; Jefferson, I.; Royal, A. (2017) *Investigating and controlling liquefaction in soft silts.* Canadian Geotechnical Journal

CHAPTER 2: PROBLEM DEFINITION

2.0. Introduction

This chapter defines key novel aspects of temporary heavy haul road behaviour requiring further investigation. Through a systematic review of pavement literature, combined with basic finite element analysis, differences in pavement and subgrade behaviour from more conventional roads, due to the heavy loads and large vehicles, are identified. It is demonstrated that the conventional practice of limiting strains and minimising local yield, when applied to large vehicles, can be prohibitively expensive for temporary assets.

2.1. Subgrade performance concerns for conventional pavements

In his Rankine lecture on this topic, Brown (1996) defines the governing geotechnical conditions for pavement foundation soils; they tend to resist large numbers of load repetitions which are small with respect to the ultimate failure load and experience predominantly recoverable strain. Soil strength arises from (isotropic) negative pore water pressures due to partial saturation. Longevity of pavement foundations therefore can be considered to depend principally upon protecting surface soils from both excessive stress/strain and saturation by water ingress, an opinion widely shared by pavement engineers and researchers (e.g. Hyde, 1974; Little, 1992; Frost, 2000; Thom, 2014).

2.1.1. Performance requirements

For conventional roads with bound surfaces, typically the primary foundation design concern is limitation of cumulative subgrade strain to avoid pavement rutting (Hyde,

1974; Thom, 2014). Pavements with unbound surfaces and railway track formations can be more easily re-profiled: in these cases larger cumulative strains may be tolerated (Little, 1992; Network Rail, 2005, 2011). The rate of strain accumulation, which dictates maintenance frequency, may in fact be more important (Heath et al., 1972; Brown and Selig, 1991). In the extreme case of a temporary road used to infrequently carry very heavy loads, frequent re-profiling may be acceptable provided the route remains trafficable.

Unbound roads often show rapid initial rutting after construction followed by stabilisation (Little, 1992; Frost, 2000), thought to be primarily related to compaction of the granular materials and amenable to correction by re-profiling. Under higher loads, subgrade strain accumulation can produce a dished surface profile, attracting water and accelerating degradation (Frost, 2000; Brown, 2004). If a limiting cyclic traffic load is exceeded, as observed by Little (1992), the large induced subgrade strains can cause softening, leading to a progressive failure and uncontrollable deflections.

A granular sub-base layer, by virtue of its greater stiffness relative to the subgrade, spreads the traffic load and protects the subgrade (Brown and Selig, 1991). A common analytical approach is to specify layer thickness and stiffness to control subgrade strains under transient load: for example, Hyde (1974) summarises a number of case studies which suggest strain limits of 0.06% to 0.09% for bound pavements. Tannant and Regensburg (2001) suggest a limit of 0.15% to 0.20% strain for unbound mine haul roads, in order for the road structure to remain composite. Loss of composite action

reduces stiffness, but also the attending inter-layer slippage accelerates permanent deformation and rutting (Frost, 2000). It is interesting to note these strain limits are below the elastic strain level separating stabilisation and failure under cyclic load determined by Heath et al. (1972) of 0.6% to 0.7%. A design approach focused principally on avoidance of failure with some relaxation of performance criteria may be able to reduce capital cost. The risk of high cumulative strains, deep rutting and frequent roadway maintenance needs to be balanced against the reduced construction costs to achieve optimal asset economy. The increased cumulative settlement expected for temporary roads, combined with wide dish-shaped settlement due to the deeper influence depths of multi-wheeled heavy haul vehicles (Section 2.4.1.), is likely to reduce performance of the granular layers through loss of composite action, inter-layer shearing and water ingress. Design and specification of the granular road layers must consider this risk of reduced performance and aim to maintain trafficability of heavy loads with the granular materials in this degraded state.

2.1.2. Development of failure mechanisms

If the principal aim of heavy haul road design is to avoid ultimate failure, understanding how failure mechanisms develop under surface loads will form an important part of this. An unstable rut formed by subgrade failure tends to exhibit settlement under the wheel path and heave some distance away (Little, 1992; Frost, 2000; Boulbibane et al., 2005), implying a ‘slip circle’ type of failure common with shallow foundation bearing failure (Figure 2.1). For a monotonically increasing surface load, initially the response is fully elastic. At some point, increasing stresses will cause the first local yield; plastic deformation occurs at a single point. Further increase in

load now depends upon yielding, which redistributes stresses until the shear strength is mobilised over the full slip surface at failure (Osman and Boulton, 2005; Madabhushi and Haigh, 2015). There is thus an additional reserve of strength which depends upon plasticity to redistribute stresses.

The presence of a strong granular surface layer increases the subgrade failure load; this can be analysed as a punching shear problem, where the granular layer provides additional passive resistance (Meyerhof, 1974), or as a load-spread problem through the granular layer at a certain angle (Houlsby and Burd, 1999). The apparent simplicity of a load-spread analysis is attractive, however Houlsby and Burd (1999) demonstrate that load-spreading must induce lateral shear at the pavement/subgrade boundary, which reduces subgrade bearing capacity. Capacities calculated assuming load spread but neglecting lateral shear are thus overestimates, conversely estimates of load-spread angles derived empirically (or from numerical models) by simply comparing resistance with and without a granular layer in fact underestimate the lateral extent of load spread. This in turn may underestimate the influence depth of a wheel load – simple Boussinesq analysis demonstrates the depth of a stress bulb depends upon its width.

Load spreading on the subgrade is greater if the ratio of the pavement stiffness to subgrade stiffness (pavement relative stiffness) is higher (Brown, 2004). If a pavement is too stiff, resultant shear and tension can cause localised failure in the pavement (Brown, 2004). An optimal pavement relative stiffness exists where load is spread as widely as possible without overstressing the pavement (Sharp and Booker, 1984).

Similarly, the equivalent load-spread angle for bearing capacity (i.e. a ratio of capacity improvement from the pavement layer, not an actual measure of load spread) was found in numerical analyses by Burd and Frydman (1997) to reduce with increasing shear strength ratio, N_{Su}:

Equation 2.1: $$N_{Su} = S_u/\gamma_p^{'}d$$

Deeper pavements spread loads on the subgrade more widely, but the composite system's ultimate bearing resistance and cyclic shakedown resistance (discussed in Section 2.1.3.) as a function of depth tends asymptotically to a limit, where behaviour is completely controlled by the pavement (Sharp and Booker, 1984; Burd and Frydman, 1997; Houlsby and Burd, 1999; Boulbibane et al., 2005). This effect has also been observed in scale foundation tests (Laman et al., 2012; Ismail Ibrahim, 2016).

Subgrade stress history, in particular the degree of overconsolidation and hence locked-in lateral stress, is influential. Elastic-plastic finite element modelling by D'Appolonia et al. (1971) varied soil shear strengths and lateral stresses in a manner which is typical for varying degrees of overconsolidation; first local yield was found to occur at lower utilisation (ratio of applied to ultimate load, Λ) for normally consolidated soil (12-15%) than for overconsolidated soil (>50%):

Equation 2.2: $$\Lambda = \omega/\omega_{ult}$$

D'Appolonia et al. (1971) corroborated this variation in yielding behaviour through field tests. Local yield at low estimated utilisation was similarly observed by Berardi and Lancellotta (2002) for oil tank settlements on very recent alluvium. N_{Su} is

effectively a measure of overconsolidation and Burd and Frydman (1997) show it also influences the shape of the failure mechanism: normally consolidated subgrades mobilise yield over larger volumes of soil, particularly in the compression zone directly beneath the load. This compressive yield will be partly influenced by the lower ultimate strength, but also by the anisotropic stress state; the vertical axis carries more stress than the horizontal, meaning a lesser vertical increment is needed to reach failure. This is not a common occurrence for conventional roads, which are usually governed by overconsoliated, isotropically stressed near-surface soils (Brown, 1996) but may be more influential for the deeper stress bulbs of heavy haul vehicles.

2.1.3. Progressive failure and shakedown theory

Houlsby and Burd (1999) note that failure of an unbound road under a single wheel passage is extremely rare; failure tends to manifest progressively, with ruts developing from large numbers of wheel loads. They suggest shakedown theorems as a useful tool for understanding progressive failure.

A stable equilibrium ('shakedown'), whereby only recoverable strain occurs under load, is reached if the pavement-subgrade system can effectively become 'prestressed' by a residual stress field to remain within elastic limits both under load and at rest (Sharp and Booker, 1984; Ponter et al., 1985; Zhao et al., 2008). Yielding is assumed to be necessary to mobilise these residual stresses and thus this additional reserve of resistance above the first local yield load (i.e. elastic limit). Shakedown limits are typically only slightly above the first local yield load and significantly below the static collapse load (Pande, 1982; Sharp and Booker, 1984). n.b. the shakedown limit differs from cyclic threshold stress observed experimentally (e.g. Heath et al., 1972); the

former considers the whole pavement-subgrade system theoretically whereas the latter indicates loss of strength of a single soil element once sufficiently large strains occur (e.g. Wang et al., 2014).

If the residual stress field required to counteract loads cannot be achieved without yielding at rest, strain accumulates with each load application and the road fails progressively, typically accompanied by rising subgrade pore water pressures which reduce the strength (e.g. Frost, 2000; Erken and Ulker, 2007; Gräbe and Clayton, 2009).

In addition to subgrade degradation from repeated yield strains, the continuous principal stress rotation associated with a moving wheel load (Brown, 1996) is expected to cause significantly larger cumulative strains and more rapid degradation when compared to a static load or a cyclic load that does not move (Arthur et al., 1980; Gräbe and Clayton, 2009; Xiao et al., 2014; Jefferies et al., 2015). For surface soils this is of considerable importance as self-weight stresses are low (Brown, 1996; Figure 2.1); Deeper soils may be less subject to principal stress rotation as a result of larger and more anisotropic overburden stresses.

Full scale pavement tests (Sharp and Booker, 1984) and scale laboratory experiments on a range of soils (Juspi, 2007) compare well to theoretical shakedown limits. This suggests residual stresses are the dominant factor in achieving equilibrium and common assumptions of constant material strengths and stiffness made in analysis are appropriate. Subgrade soils may only degrade appreciably for loads above the shakedown limit. Overconsolidated surface soils in particular are predominantly elastic when loaded well below their shear strength (Schofield and Wroth, 1968; Brown,

1996) so shakedown behaviour appears predominantly controlled by small strains with little change to strength and stiffness.

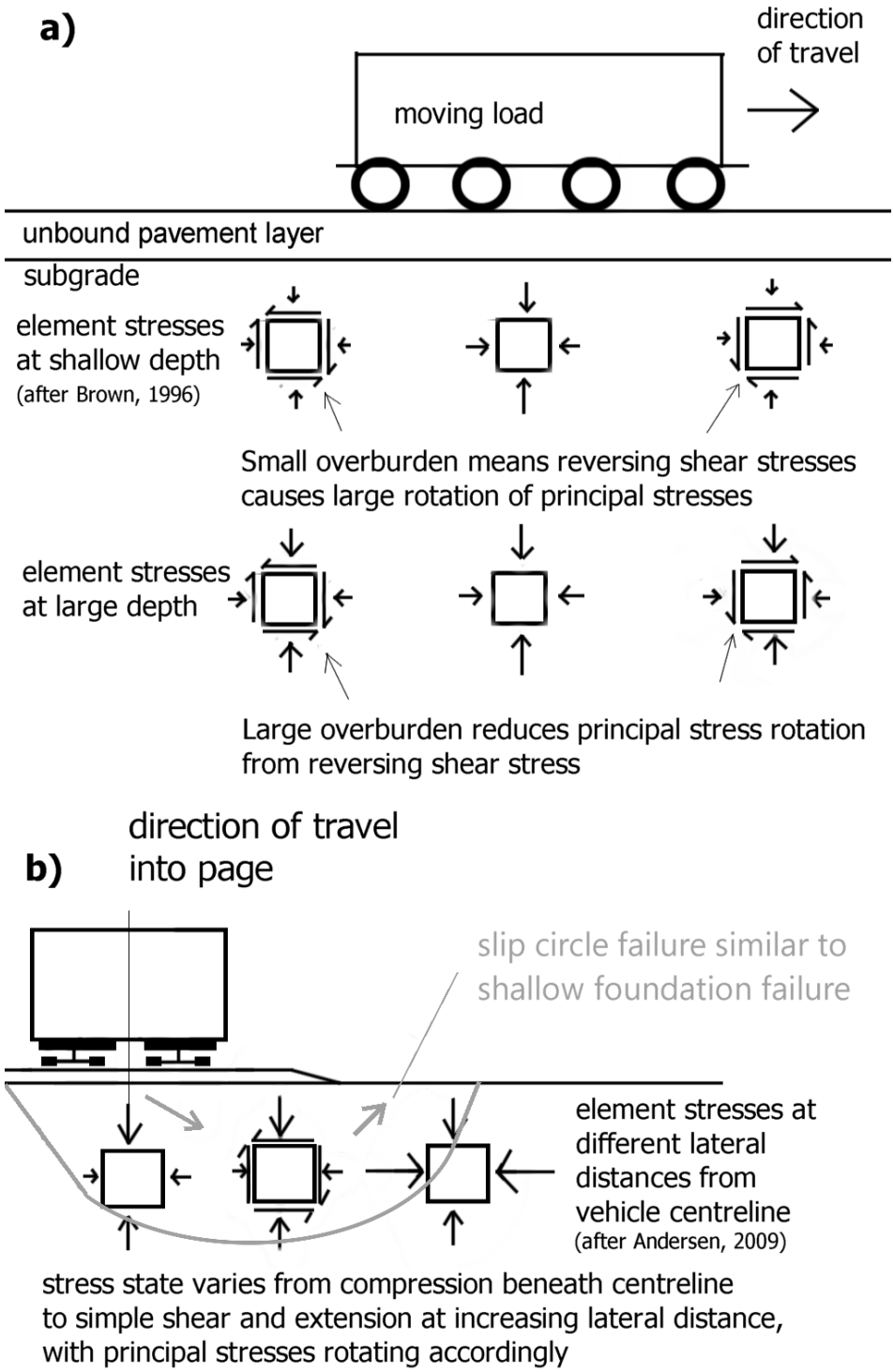

Figure 2.1: Rotation of principal stresses in (a) longitudinal and (b) transverse directions resulting from passage of a heavy-haul vehicle.

Given the importance of local yielding to shakedown solutions, the implications of an approach which aims to limit strains in a similar manner have been explored through a parametric finite element analysis study which investigates local yielding due to passage of large vehicles. Simple analysis methods are purposefully used to allow yielding behaviour to be isolated and examined.

2.2. Examination of pavement modelling assumptions

Linear-elastic and linear-elastic, perfectly-plastic ('Mohr-Coulomb') models are often used in foundation engineering (D'Appolonia et al., 1971) and pavement shakedown analysis (Sharp and Booker, 1985; Boulbibane et al., 2005; Juspi, 2007). Whilst being unrealistic descriptors of element-level behaviour, over a soil mass they can:

1. Offer good agreement with yield development and failure mechanisms of site trials (D'Appolonia et al., 1971; Ismail Ibrahim, 2016).
2. Allow study of local yielding effects in isolation (D'Appolonia et al., 1971).

As this exercise aims to identify broad behavioural trends associated with yielding, these models are considered fit for purpose.

In conventional pavement engineering interaction between wheels normally only occurs at depths where stresses are low (Boulbibane et al. 2005; Thom, 2014); single wheel loads usually govern design. Thom (2014) does recognise the importance of interaction in situations with heavier loads and deep pavements; heavy haul vehicles are likely to fall into this category.

Pavement engineering is typically concerned with very shallow soils whose effective stresses arise predominantly from suction; soil weight is often neglected in analysis (Sharp and Booker, 1984; Boulbibane et al., 2005). Considering the deeper stress bulbs of interest to this study, self-weight stresses are likely to be highly influential to the system's response to load, as they are found to be in foundations research (e.g. D'Appolonia et al, 1971; Burd and Frydman, 1997).

2.3. Finite Element modelling methodology

A key feature of this modelling exercise was to compare single-wheel with multi-wheeled vehicles and identify behavioural changes dependent on the interaction between wheels. The vehicle considered is long relative to its width and wheels are closely spaced in the longitudinal direction (Figure 2.2), thus the three-dimensional layout was simplified to a two-dimensional, plane strain analysis based on the section view. Whilst a single wheel is more accurately represented by an axisymmetric (circular) load, conventional haulage vehicles often have multiple axles with small longitudinal spacing; some longitudinal interaction is likely to occur, making the response more similar to a strip load, hence single wheel loads were also simplified to a plane-strain strip load. Sharp and Booker (1984), Boulbibane et al. (2005) and Juspi (2007) similarly analysed moving single wheel loads as plane-strain strips.

Overconsolidation was represented using a simplified model, presented by Foye et al. (2008), in which the overconsolidated layer is modelled with a constant stiffness and shear strength. The deeper normally consolidated soil increases in stiffness and

strength with depth (Figure 2.2). The properties of the pavement layer were varied to investigate its influence on single and multiple wheel loads.

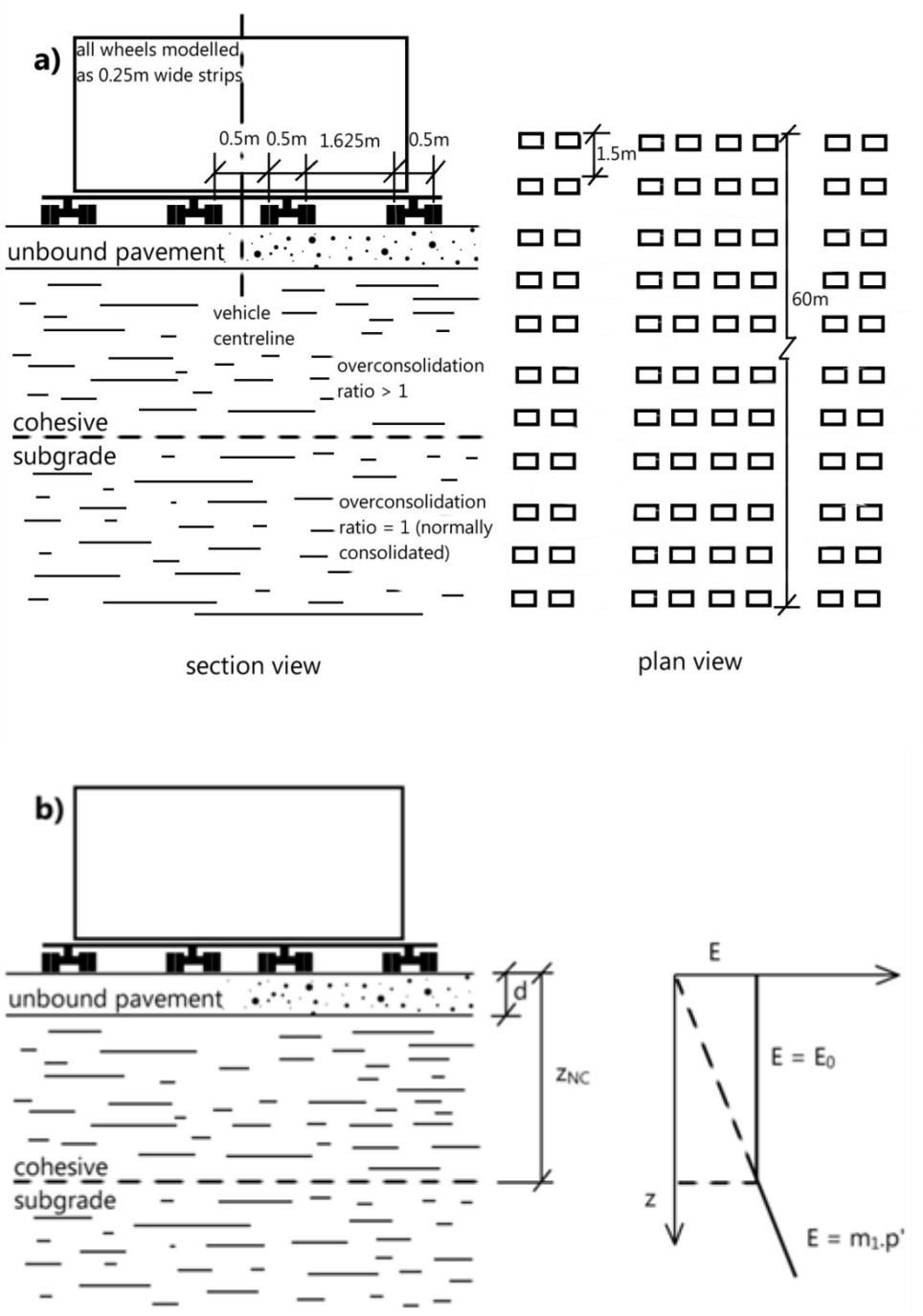

Figure 2.2: Problem definition: a) vehicle geometry and b) ground model for analysis. n.b. as a plane strain analysis is used, the model geometry is based solely on the section view; plan view is for information only.

A range of subgrade models, incorporating soil self-weight, were simulated to represent normally consolidated to lightly overconsolidated, soft to very soft deposits with a high water table, i.e. areas with low bearing capacity likely to present difficulties to temporary roads, such as alluvial deltas. Soil parameters are chosen to reflect a low plasticity (*PI* = 10-15%) silty to very silty clay.

Whilst principal stress rotation is known to influence the soil stress-strain response (Jefferies et al., 2015), such effects were not modelled for the sake of simplicity and due to difficulty in obtaining realistic parameters. General trends in stress rotation are discussed, as this can have a large influence on the subgrade degradation environment. The MIDAS GTS NX finite element software was used for all the finite element analyses.

2.3.1. Soil models

2.3.1.1. Linear-elastic models

Three separate linear-elastic clay subgrade models of soft to very soft alluvial clays with varying surface strength (i.e. representing varying degrees of surface overconsolidation) and a single granular pavement model, with properties as per Table 2.1, were analysed. Below the depth to normal consolidation, z_{NC} (Figure 2.2), the subgrade soil Young's Modulus is described by Equation 2.3:

Equation 2.3: $$E = m_1 \cdot p'$$

The Case 1 subgrade model is such that z_{NC} coincides with the top of subgrade, to provide a theoretical minimum strength and stiffness with no history of

overconsolidation, to provide a reference state for purely normally consolidated behaviour.

The value of m_1 is derived using Modified Cam-Clay equations (Roscoe and Burland, 1968) for the undrained critical state strength of normally consolidated clay as a function of *p'*, i.e. where the yield surface and critical state line intersect. A full derivation is presented in Appendix 2.

Table 2.1: Parameters assumed for linear-elastic and Mohr-Coulomb models: subgrade models are based on normally consolidated or lightly overconsolidated, soft to very soft alluvial clay of low plasticity (i.e. PI = 10-15%). m_1 = 0.457 MPa/m (i.e. 0.001m_1 = 0.457kPa/m).

Material	**Unit weight, *γ* (kN/m^3)**	***S_u* at top of layer, (kPa)**	***E_0* (MPa)**	**Poisson's Ratio, *ν***	***K***
Unbound pavement	21	-	50	0.263	0.36
Cohesive subgrade, Case 1	17	=0.001m_1.p'	=m_1.p'	0.495	0.45
Cohesive subgrade, Case 2	17	5.91	5.91	0.495	0.45
Cohesive subgrade, Case 3	17	15.26	15.26	0.495	0.45

The clay subgrade *K* was assumed to take the normally consolidated value, following Brooker and Ireland (1965; Equation 2.4). The granular pavement follows Jaky (1948; Equation 2.5):

Equation 2.4: $$K_{0,NC} = 0.95 - \sin(\phi')$$

Equation 2.5: $$K_{0,NC} = 1 - \sin(\phi')$$

For the purpose of determining $K_{0,NC}$ in the low plasticity clay subgrade ϕ' = 30° (BSI, 2015a).

Several road thicknesses were considered, overlying each subgrade model. Subgrade effective stresses vary as a result, thereby changing z_{NC} (Table 2.2).

Table 2.2: Model parameters assumed for various pavement designs and corresponding z_{NC} required to satisfy Equation 2.1.

Pavement thickness (m)	Depth to water table (m)	z_{NC} for Case 2 (m)	z_{NC} for Case 3 (m)
0.25	0	2.700	7.192
0.50	0	2.561	7.053
1.00	0	2.283	6.775
1.50	0	2.005	6.497
0.25*	0.25	2.359	6.851
1.50*	1.50	1.500	4.450

2.3.1.2. Mohr-Coulomb models

The granular pavement was modelled as drained material with zero c' and ϕ' = 40° (unless otherwise stated as 32°), corresponding with typical values for a granular sub-base and general earthworks fill respectively (Sharp and Booker, 1984; Burd and Frydman, 1997; BSI, 2015a). Other parameters were unchanged from the linear-elastic models. The clay subgrade was modelled as undrained cohesive material, i.e. with ϕ' = 0 and S_u set such that [E/S_u = 1000], in agreement with typical values for low plasticity, normally consolidated or lightly overconsolidated clay (D'Appolonia et al.,1971; Jamiolkowski et al., 1979).

To calculate the wheel pressure at failure, ω_{ult}, Strength Reduction Method (SRM) analysis was used with a nominal surface load. SRM reduces (or increases) strength

parameters (i.e. S_u and tanϕ') by a SRM factor until equilibrium is met (MIDAS, 2016). By modifying the surface load accordingly, a SRM factor of 1.0 is achieved, which was taken to correspond to the ultimate pressure. Bearing capacities of single material models (drained and undrained) obtained in this manner were compared to classical closed-form equations of Brinch Hansen (1970) and found to differ by less than 4%, confirming reasonable accuracy.

To improve computational efficiency, artificial symmetry was imposed through the centreline of the wheel or vehicle. This approach is commonly used in modelling single loads (Burd and Frydman, 1997; Ismail Ibrahim, 2016), but is not necessarily applicable to a multi-wheeled vehicle as an asymmetric slip may arise between groups of wheels. A Mohr-Coulomb model with artificial symmetry about the centreline was compared to a full-width model: differences in bearing capacity and surface settlement profiles were negligible (<1%). The failure mechanism was found to remain symmetrical up to 95% of bearing capacity. Above this load the solution struggled to converge and asymmetries noted are most likely as a result of convergence algorithms rather than an asymmetrical failure mode.

For multi-wheel models with 1.5m pavement depth, large, localised movement of nodes at the pavement surface adjacent to wheels caused slow convergence even at 10-30% of the failure load, i.e. Λ = 10-30% as defined by Equation 2.2. By including a small c' of 5kPa over the uppermost 0.25m of the 1.5m thick pavement layers, convergence times were improved. Comparison of the bearing capacity and settlements indicated a negligible effect on the global behaviour (Figure 2.3).

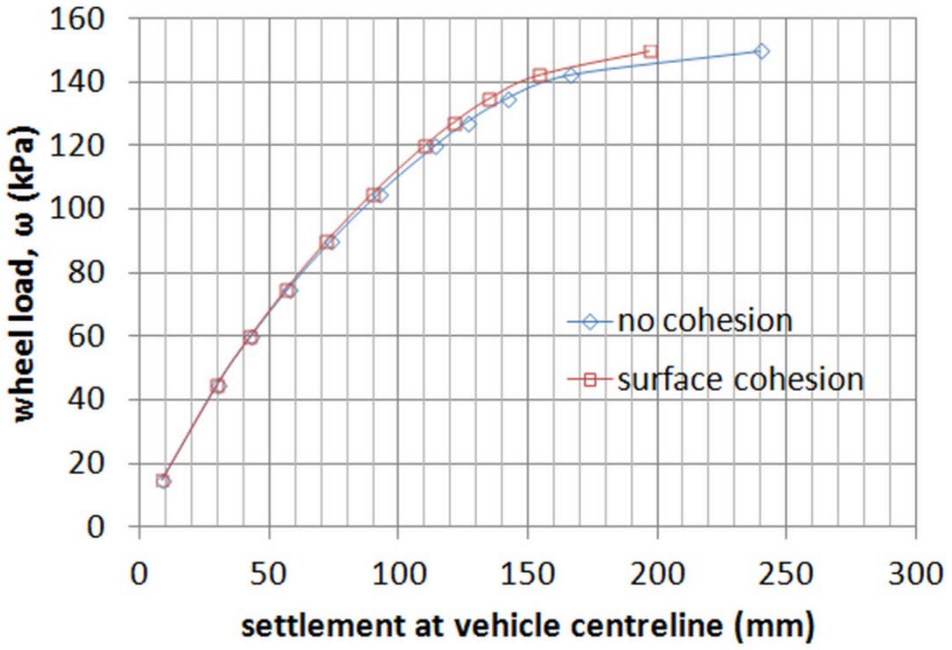

Figure 2.3: Load-settlement response at centreline of multi-wheel Mohr-Coulomb model for 1.5m total pavement depth, showing impact of 5kPa *c'* in the uppermost 0.25m of the pavement layer.

2.3.1.3. Mohr-Coulomb with overconsolidated earth pressures

The previous Mohr-Coulomb models only considered changes to strength and stiffness resulting from overconsolidation. By also including overconsolidated lateral earth pressures, comparison of the relative effects of lateral earth pressures on the composite response is possible. A constant *K* was assumed for the overconsolidated layer, based on $K_{0,OC}$ at the midpoint, which produces reasonable correspondence with the field response (Levenburg and Garg, 2014). $K_{0,OC}$ is calculated following Ladd et al. (1977), Mayne and Kulhawy (1982) and assuming an exponent of 0.8 (as per Burd and Frydman, 1997), (Equations 2.6 and 2.7).

Equation 2.6:
$$\frac{\left(\frac{S_u}{\sigma_{z'}}\right)}{\left(\frac{S_u}{\sigma_{z'}}\right)_{NC}} = \boldsymbol{OCR^{0.8}}$$

Equation 2.7: $$\frac{K_{0,OC}}{K_{0,NC}} = OCR^{sin\phi}$$

2.4. Modelling outcomes

2.4.1. Linear-elastic stress bulbs

Figure 2.4 demonstrates that greater pavement relative stiffness (i.e. softer subgrade, as pavement stiffness does not change) distributes vertical stress more efficiently at a wider load-spread angle, particularly for thin pavements, confirming findings of others discussed in Section 2.1.2. The subgrade stress bulbs are also deeper for thin pavements, particularly with high relative stiffness.

Modelling the large multi-wheeled vehicle confirms that closely-spaced stress bulbs beneath individual wheels join to form a resultant stress bulb on a scale of the whole vehicle (Figure 2.5). This acts similarly to a single load of the same width as the vehicle, meaning even the 1.5m deep pavement behaves as 'thin' in relation to the combined stress bulb, evidenced by the wide load-spread angle in the pavement and deep stress bulb (similar to a single wheel load applied to a thin pavement). Changes to pavement relative stiffness and depth do not significantly affect multi-wheel stress distribution patterns (Figure 2.5), although deeper pavements protect the subgrade from high localised stresses.

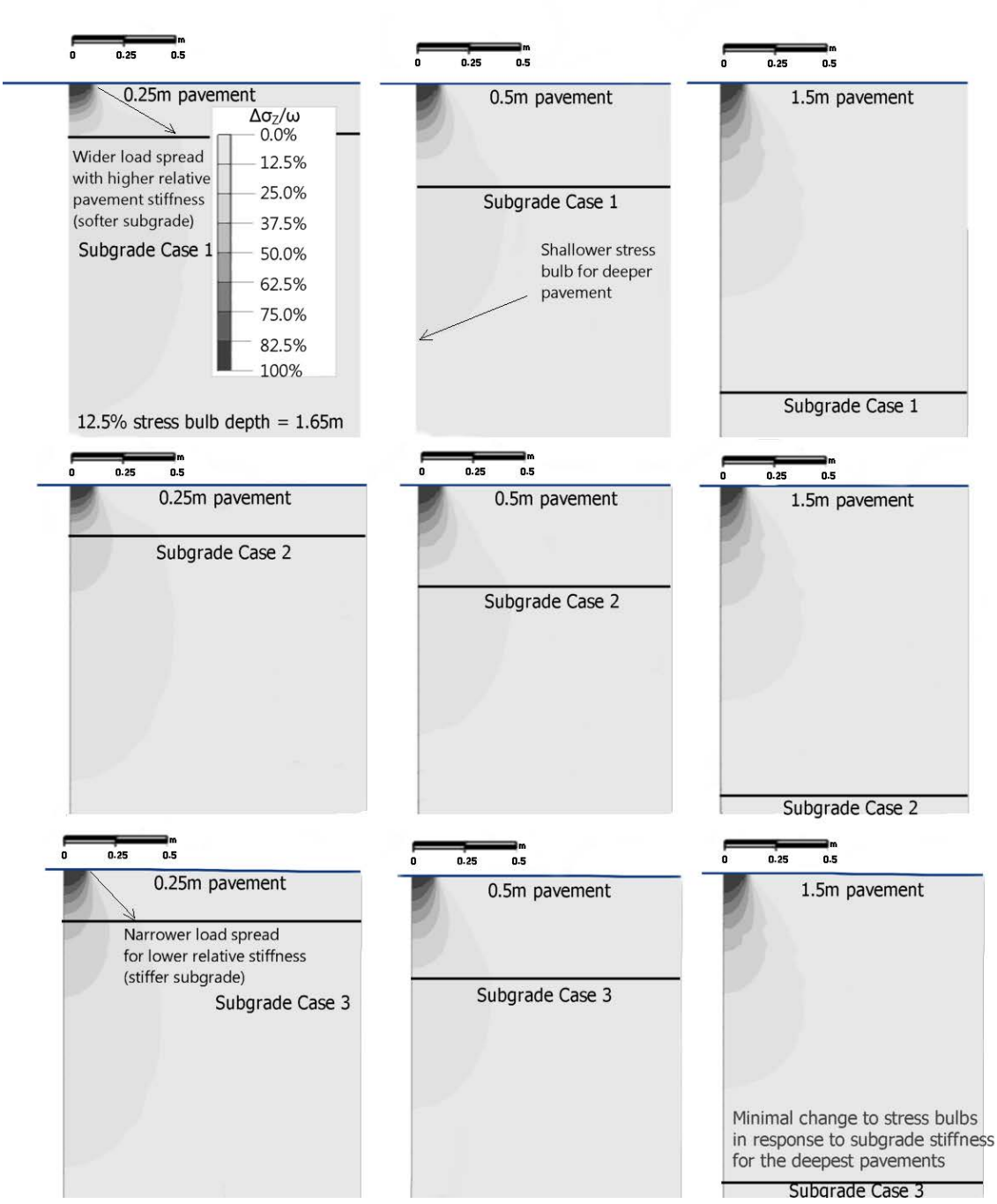

Figure 2.4: Increments in vertical stress, expressed as a percentage of wheel load pressure ω, from a 0.25m wide surface strip load with linear-elastic models of varying subgrade stiffness and pavement depth.

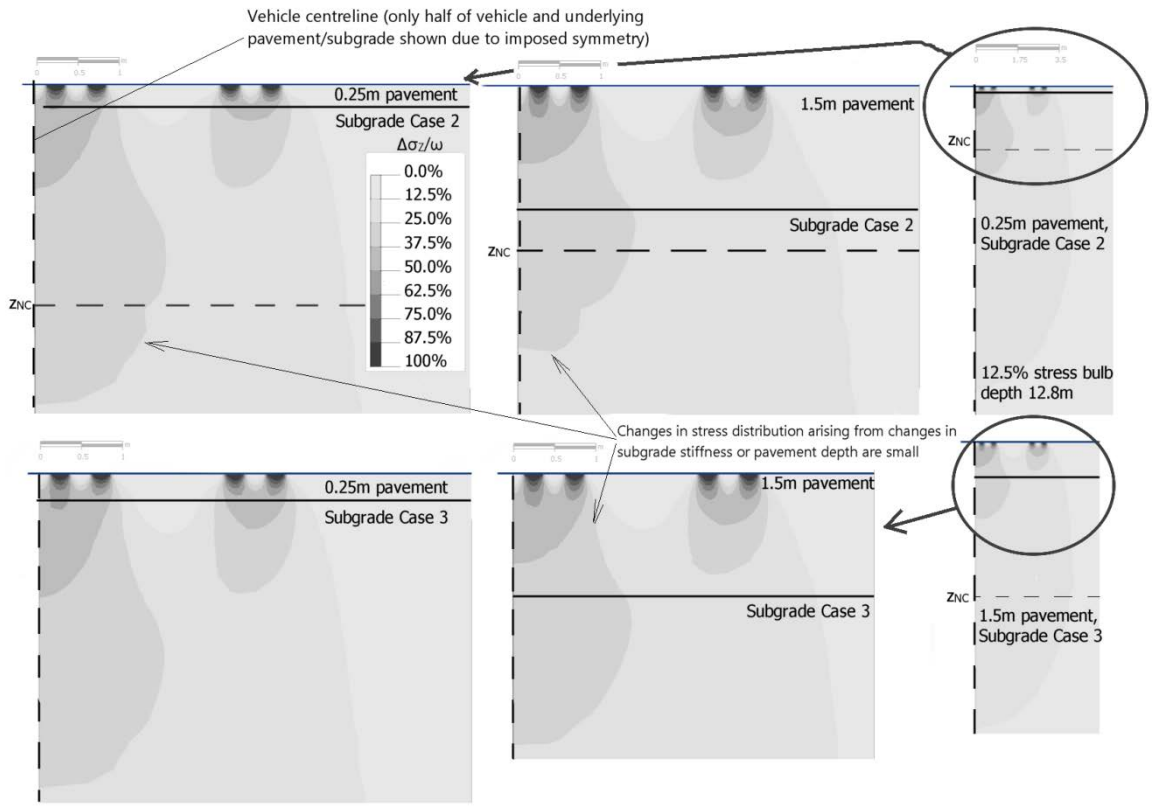

Figure 2.5: Increments in vertical stress from a multi-wheeled vehicle with linear elastic models of varying subgrade stiffness and pavement depth. Left and centre – interaction between individual wheels. Right – Large scale stress bulbs over the whole vehicle width, extending to great depth, similar to the 0.25m pavement depth, Subgrade Case 1 stress bulbs in Figure 2.4.

2.4.2. Local yield of Mohr-Coulomb models

The bearing capacity, ω_{ult}, improves with pavement depth asymptotically to a limit defined by the capacity of the fill itself (Figure 2.6), in agreement with Burd and Frydman (1997) and Ismail Ibrahim (2016). Limited local yielding at the pavement surface is common to all models but is relatively small except at high utilisations (i,e. Λ > 60%, Figure 2.7). Local yield in the subgrade can be identified when behaviour diverges from the 'pavement only' results. Normally consolidated subgrades show local yielding at lower utilisations (Λ = 10-30%), whilst overconsolidated subgrades show little local yield until larger utilisations (Λ = 50-60%), followed by rapid plastic settlement, similar to the findings of D'Appolonia et al. (1971). Differences are more

pronounced for thinner pavements, indicating increased importance of the subgrade in these cases.

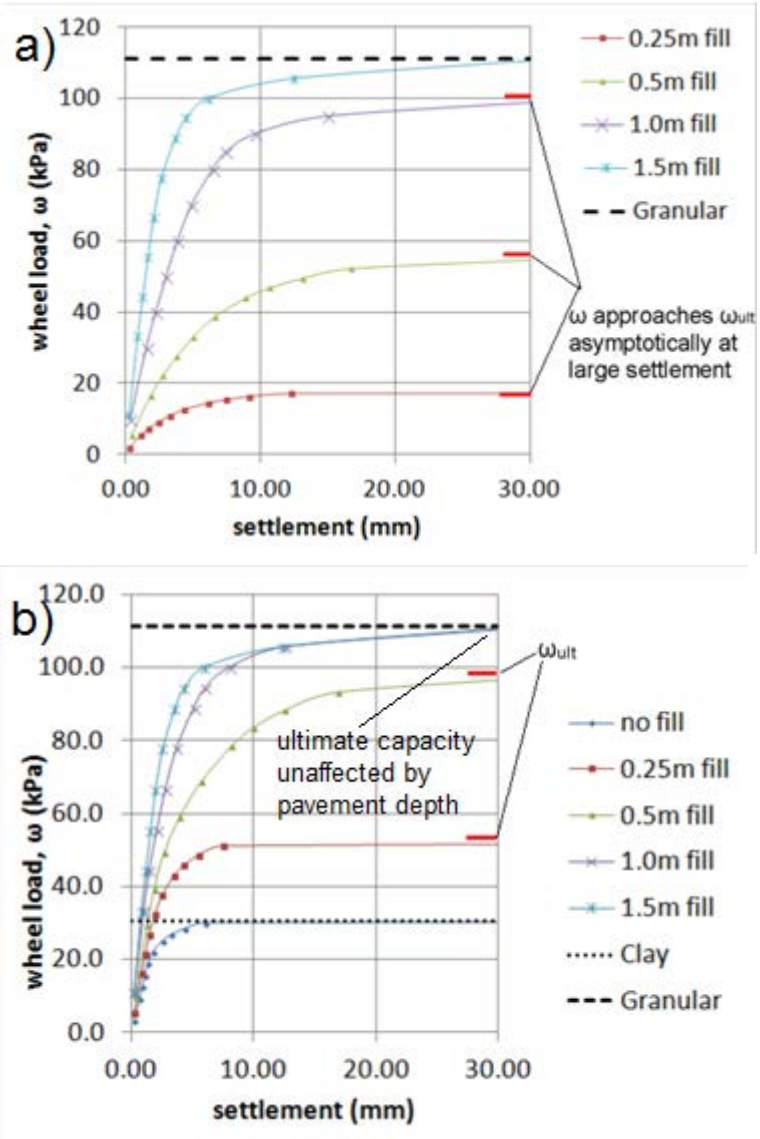

Figure 2.6: Load-settlement response for single-wheel models with varying pavement depths. Dashed lines indicate ω_{ult} calculated after Brinch Hansen, 1970) and Meyerhof (1974). a) - Subgrade Case 1. b) - Subgrade Case 2.

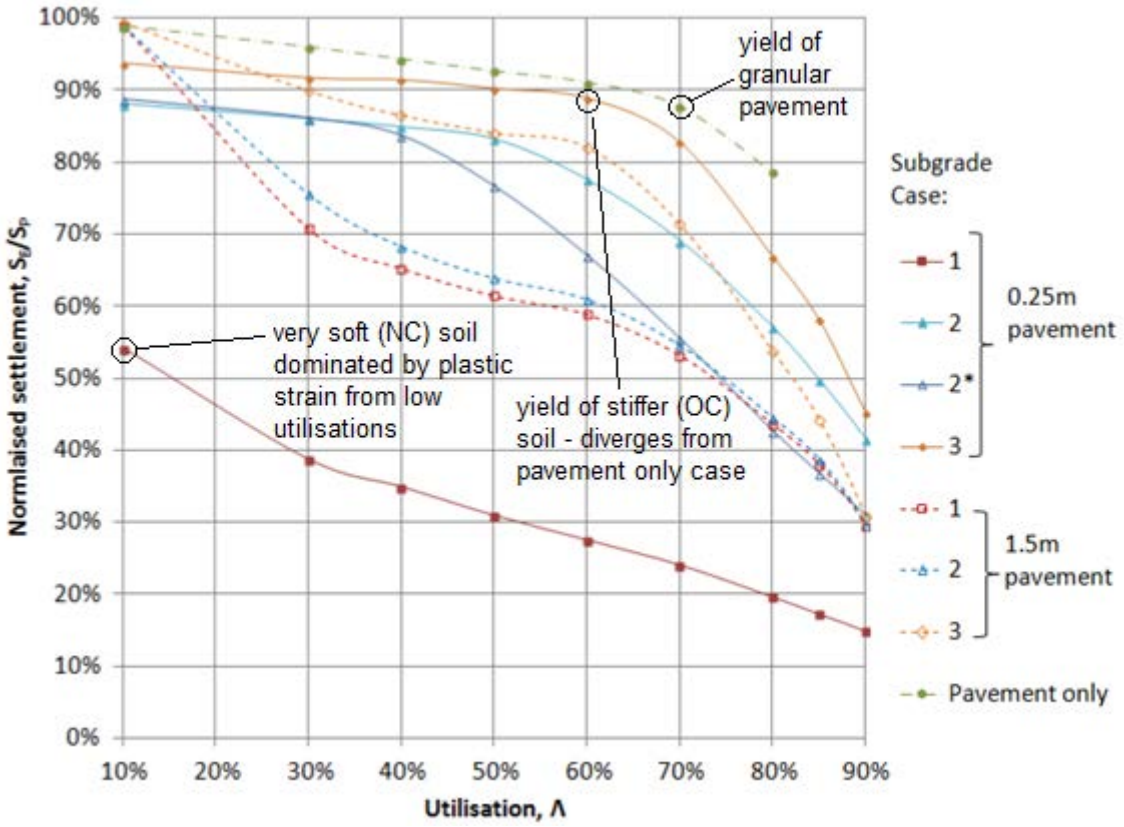

Figure 2.7: Normalised settlement vs utilisation for a range of single wheel Mohr-Coulomb models. S_E/S_P = 100% indicates no yield; decreasing S_E/S_P indicates increasing yield. n.b. * = groundwater level at base of pavement.

Single wheel analyses with differing subgrade strengths, groundwater levels and pavement depths exhibit similar behaviour if their N_{Su} is similar (Figure 2.8); a deeper pavement or lower water table increases subgrade effective stresses, reducing the tendency for overconsolidated-like behaviour. The pavement depth itself also influences local yield; the magnitude of plastic settlement for a constant N_{Su} reduces for a deeper pavement (compare Subgrade Case 1 results in Figure 2.7), but the tendency for local yielding to begin at low utilisation (10-30%) is similar.

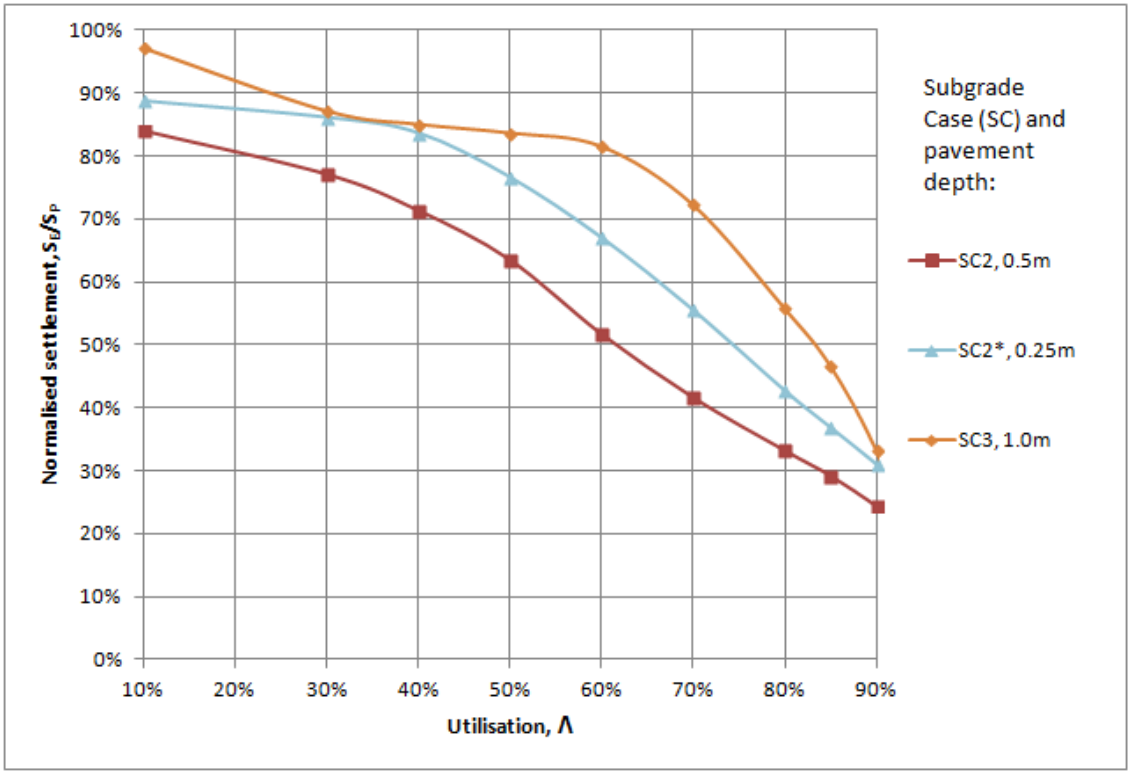

Figure 2.8: Normalised settlement vs utilisation for single-wheel Mohr-Coulomb models with similar N_{Su} (N_{Su} = 1.06, 1.13 and 1.36 respectively, * = groundwater level at base of pavement).

The load-settlement behaviour of multi-wheel analyses cannot be similarly normalised by N_{Su} at the base of the pavement (Figure 2.9). If, following Foye et al. (2008), an influence depth for shear strength equal to one footing width (taken as the vehicle width, 6m) is used to compute N_{Su}, the resultant values are similar to those of normally consolidated single wheel models (Subgrade Case 1), indicating local yield behaviour is also determined by the size of the whole vehicle.

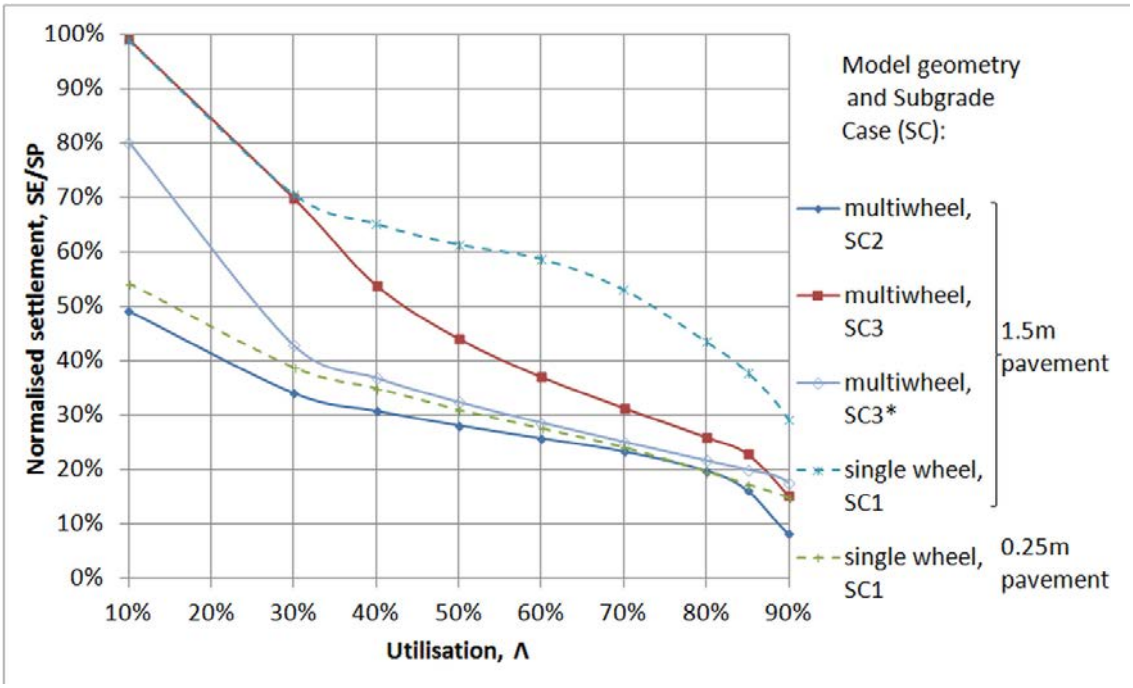

Figure 2.9: Normalised settlement vs utilisation for multiple-wheel Mohr-Coulomb models with varying subgrade models. For comparison, normally consolidated (Case 1) subgrade single-wheel models are also shown. Note that shear strength and stiffness at the influence depth of 6m is the same for Subgrade Cases 3* and 2. n.b. * = groundwater level at base of pavement.

For single-wheel analyses, increasing plastic settlement coincides with shear stresses exceeding the shear strength in the compression zone at the top of the subgrade (Figure 2.10); as the load increases, the yield extent spreads laterally to the passive zone. A similar tendency is apparent for multi-wheel analyses, although yield occurs at low utilisations (10-40%) in the compression zone for all subgrade models, similarly to the normally consolidated single-wheel analyses (Figure 2.10).

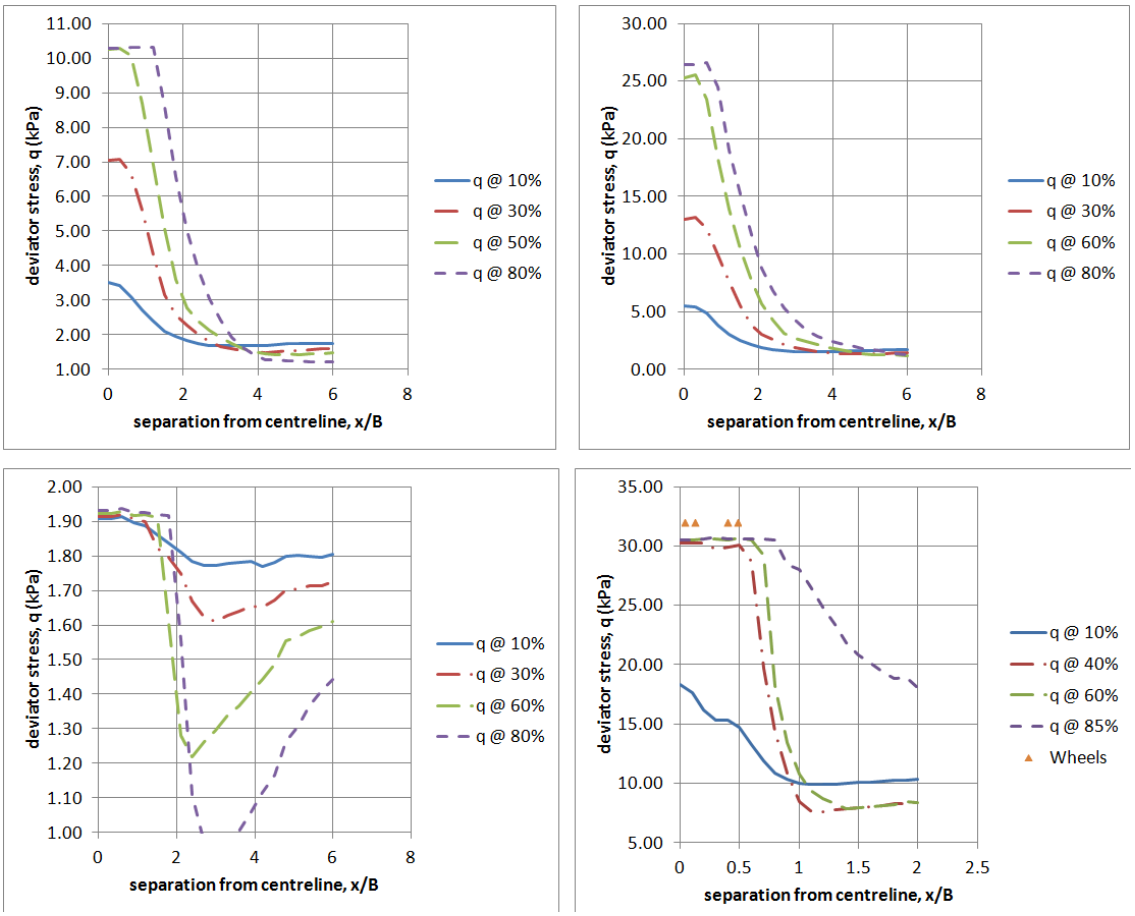

Figure 2.10: Deviator stress, *q*, at base of pavement layer for various degrees of utilisation (*Λ*). a) single wheel, Subgrade Case 2. b) single wheel, Subgrade Case 3. c) single wheel, Subgrade Case 1. d) multi-wheel, Subgrade Case 3. a) – c): *d* = 0.25m, *b* = 0.25m d): *d* = 1.5m, *b* assumed to be 6m (whole vehicle width).

2.4.3. Development of failure mechanisms

The form of the single-wheel failure mechanism is influenced by both the pavement thickness and N_{Su}. Thick pavements and overconsolidated subgrades develop extension strains in a passive wedge confined to the pavement layer, while thin pavements and soft subgrades tend to develop strains in the subgrade compression zone. Figure 2.11 shows progression of failure mechanisms with increasing load by indicating shear strains in excess of 1%, indicating significant post-yield straining. Failure mechanisms extending into overconsolidated subgrades (i.e. through thin

pavements, not localised to the pavement) are smaller, similar to the findings of Burd and Frydman (1997).

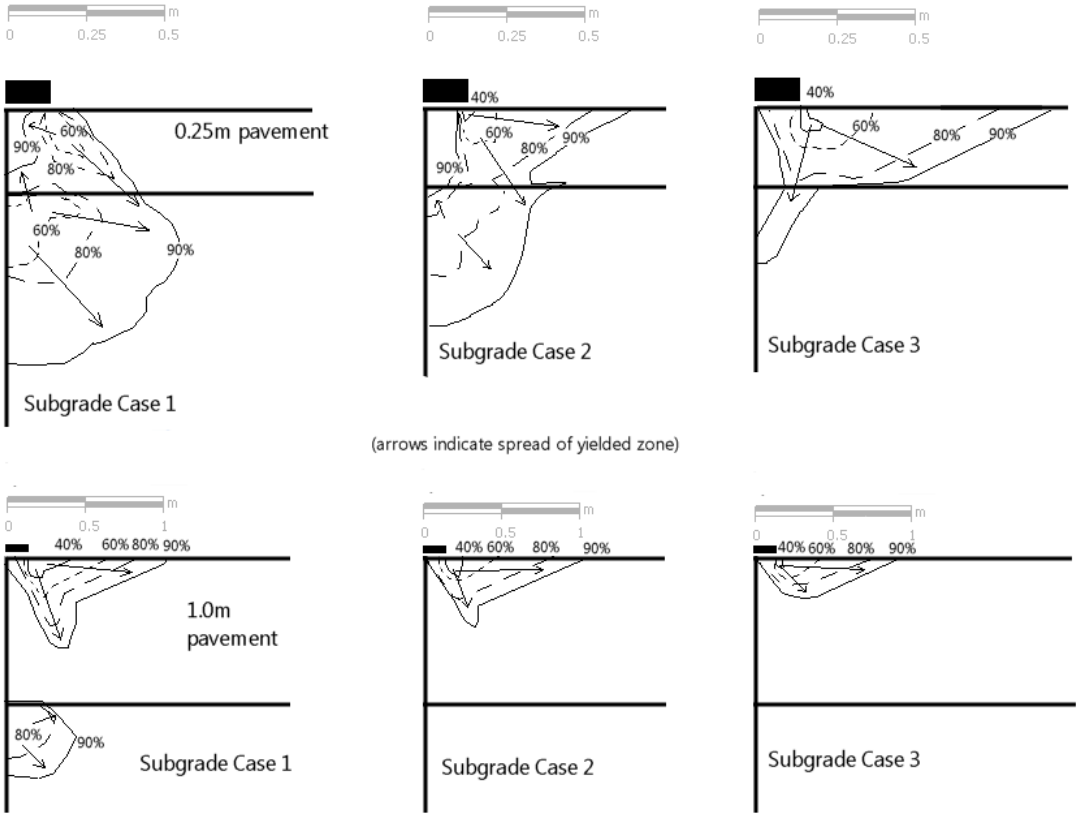

Figure 2.11: Progression of failure mechanisms indicated by 1% shear strain (i.e. large post-yield strain) contour for various degrees of utilisation (percentage values) for single-wheel Mohr-Coulomb models.

The multi-wheel failure mechanism is governed by wheel load interaction: a single wheel load applied to a 1.5m deep pavement causes failure entirely within the pavement layer (Figure 2.11), but the multi-wheel failure is a deep global slip over the vehicle's full width (Figure 2.12). The large yielded volume of soil in the compression zone is also similar to the normally consolidated single-wheel response, validating the assertion that a whole-vehicle scale response is dominated by soil at depth and not the pavement layers (see Table 2.3 and Table 2.4). To limit plasticity at low utilisation, it is

therefore necessary to build a deeper pavement. Assuming minimal changes to multi-wheel stress distribution with pavement depth (as is the case in Figure 2.5), pavement depths of 2.5m to 5.0m may be necessary to limit significant yield at below 40% utilisation (Figure 2.12), i.e. a conventional safety factor of 2.5 (BSI, 1986).

Table 2.3: Ultimate wheel pressures from finite element modelling for single and multi-wheeled models. n.b. the bearing capacity of the pavement-only single-wheel model is 111kPa.

Pavement depth (m)		Ultimate wheel pressure, ω_{ult} (kPa)		
		Subgrade Case 2	Subgrade Case 3	Ratio of ultimate pressures, Case 3:Case 2
0.00	single wheel	32	80	2.54
0.25		54	105	1.94
0.50		98	111	1.13
1.00		111	111	1.00
1.50		111	111	1.00
1.50: multi-wheel		197	320	1.62

Table 2.4: Ultimate wheel pressures for single and multi-wheel models with varying pavement strength parameters. n.b. * = groundwater level at base of pavement.

Subgrade Case (SC) and pavement depth	ω_{ult} with pavement ϕ' = 40° (kPa)	ω_{ult} with pavement ϕ' = 32° (kPa)
Single wheel SC1, 0.25m	18	13
Single wheel SC2, 0.25m	54	29
Single wheel SC2*, 0.25m	63	48
Multi-wheel SC2, 1.5m	197	169
Multi-wheel SC3, 1.5m	320	290
Multi-wheel SC3*, 1.5m	340	320

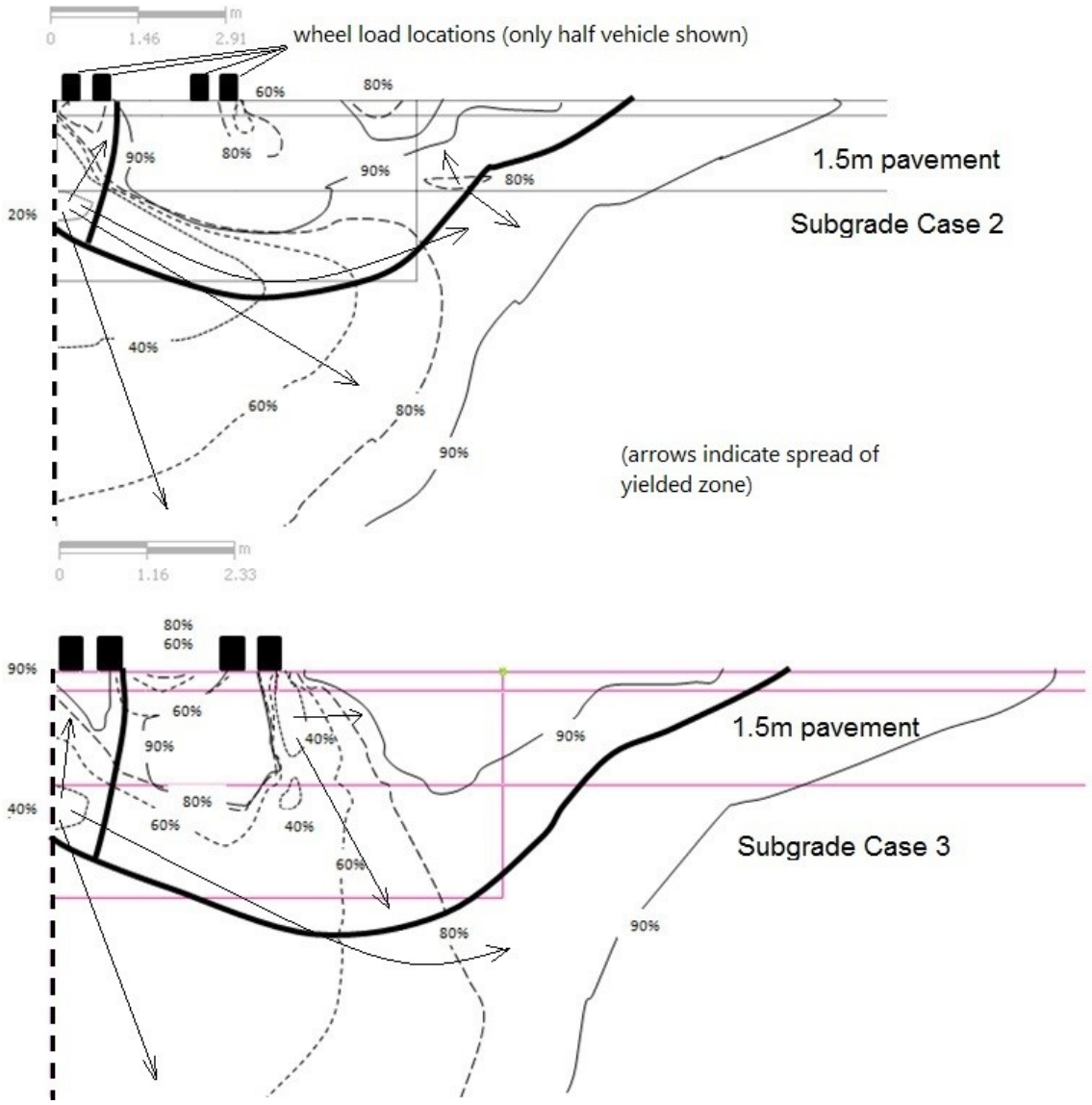

Figure 2.12: Progression of failure mechanisms indicated by 1% shear strain contour for various degrees of utilisation (percentage values) for multi-wheel Mohr-Coulomb models. The thick line follows the maximum shear strains developed at 95% utilisation, i.e. is approximate to the final failure mechanism.

2.4.4. Influence of in-situ stress state

Burd and Frydman (1997) suggest *K* coefficients have little effect on the ultimate bearing capacity; analysis from this study agrees. However, increasing the subgrade *K* is found to reduce local yielding, in agreement with D'Appolonia et al., (1971). This is most pronounced for high overconsolidation and shallow influence depths (Figure 2.13), although the effect on load-settlement response is small when compared to that

arising from changes in shear strength (Figure 2.7). For multi-wheeled models, the behaviour is less influenced by the upper strata and hence the impact of the overconsolidated layer is even less significant.

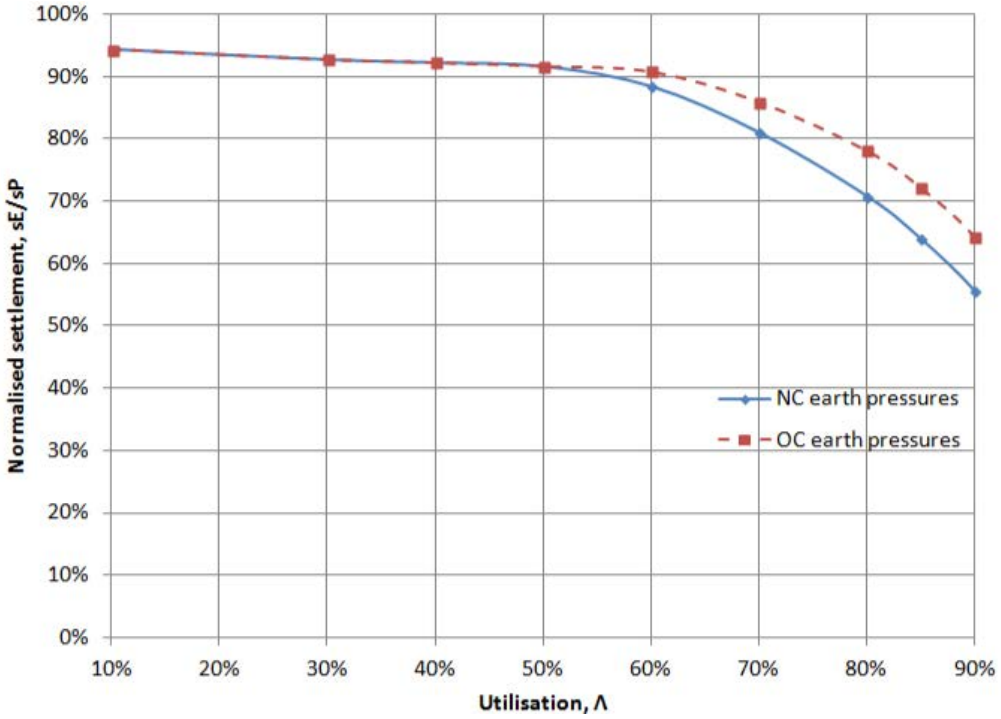

Figure 2.13: Normalised settlement vs utilisation for Mohr-Coulomb single wheel models of Subgrade Case 3* (i.e. groundwater at base of pavement), pavement depth of 0.25m and varying *K* in the overconsolidated subgrade.

2.4.5. Comparison of principal stress rotation

Significant rotation of the principal axes occurs within the pavement layers at relatively low utilisations (i.e. 10-30%, Figure 2.14). Below the pavement, only small principal stress rotation occurs at low utilisation. This is more pronounced for weaker subgrade models, and can be attributed to two factors: firstly lower bearing capacity (and therefore lower wheel pressures for the same Λ) means smaller relative changes to the *in-situ* stress state. Secondly, higher pavement relative stiffness causes greater load spreading (Figure 2.4), reducing principal stress rotation in the subgrade (Figure 2.14).

Inclination of principal stresses reduces with depth, as self-weight stresses become dominant.

For the multi-wheel model at low utilisation (10-30%), the subgrade principal stresses show little inclination, which reduces further with depth and increases with increasing Λ. At Λ = 80%, a zone of principal stress reversal is apparent directly beneath the pavement (Figure 2.15) as the passive part of the failure mechanism is mobilised. This coincides with development of large plastic strains throughout the entire compression zone and yield being initiated in parts of the extension zone (Figure 2.12).

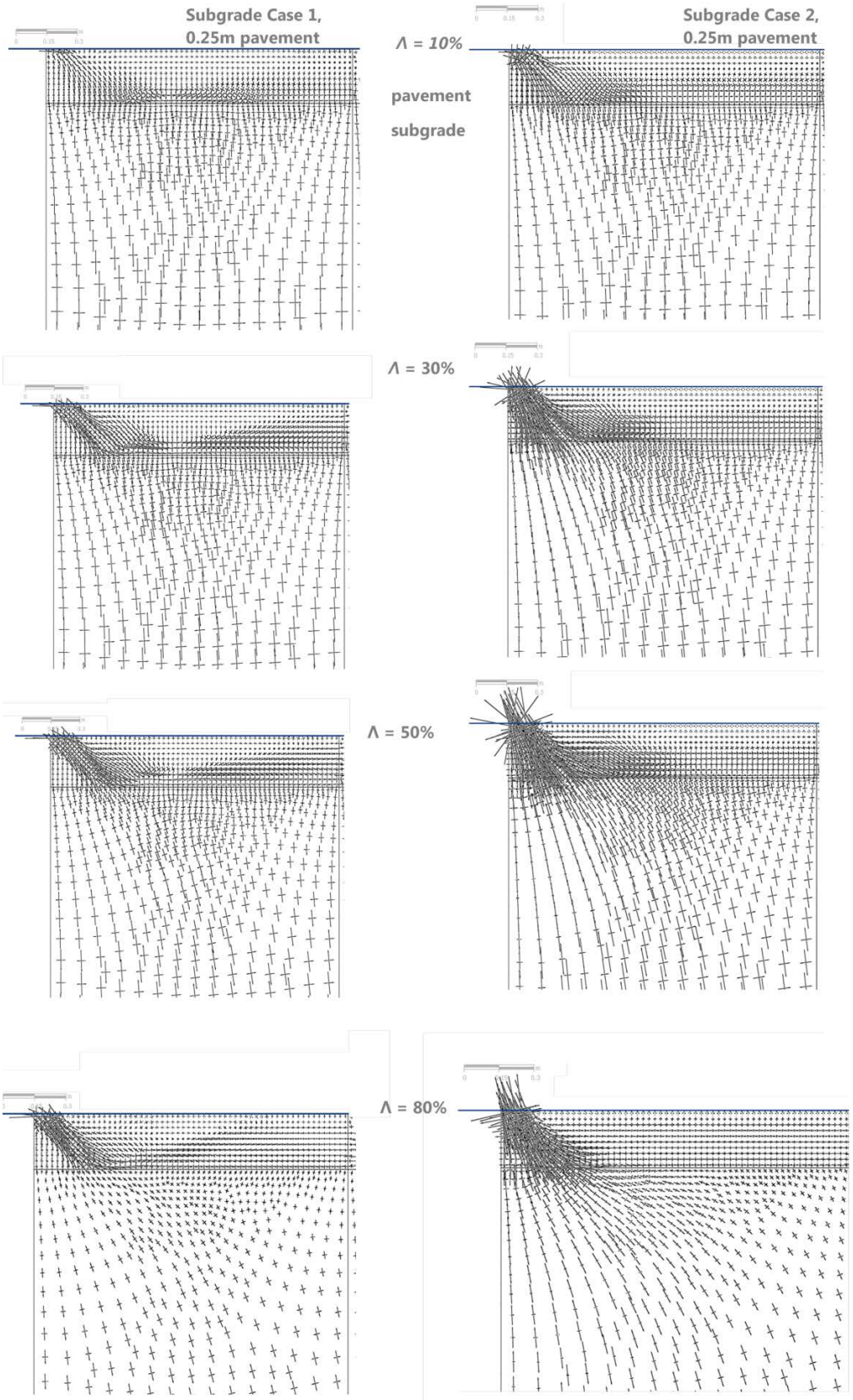

Figure 2.14: Principal stress vectors for single-wheel Mohr-Coulomb models with varying utilisation (Λ).

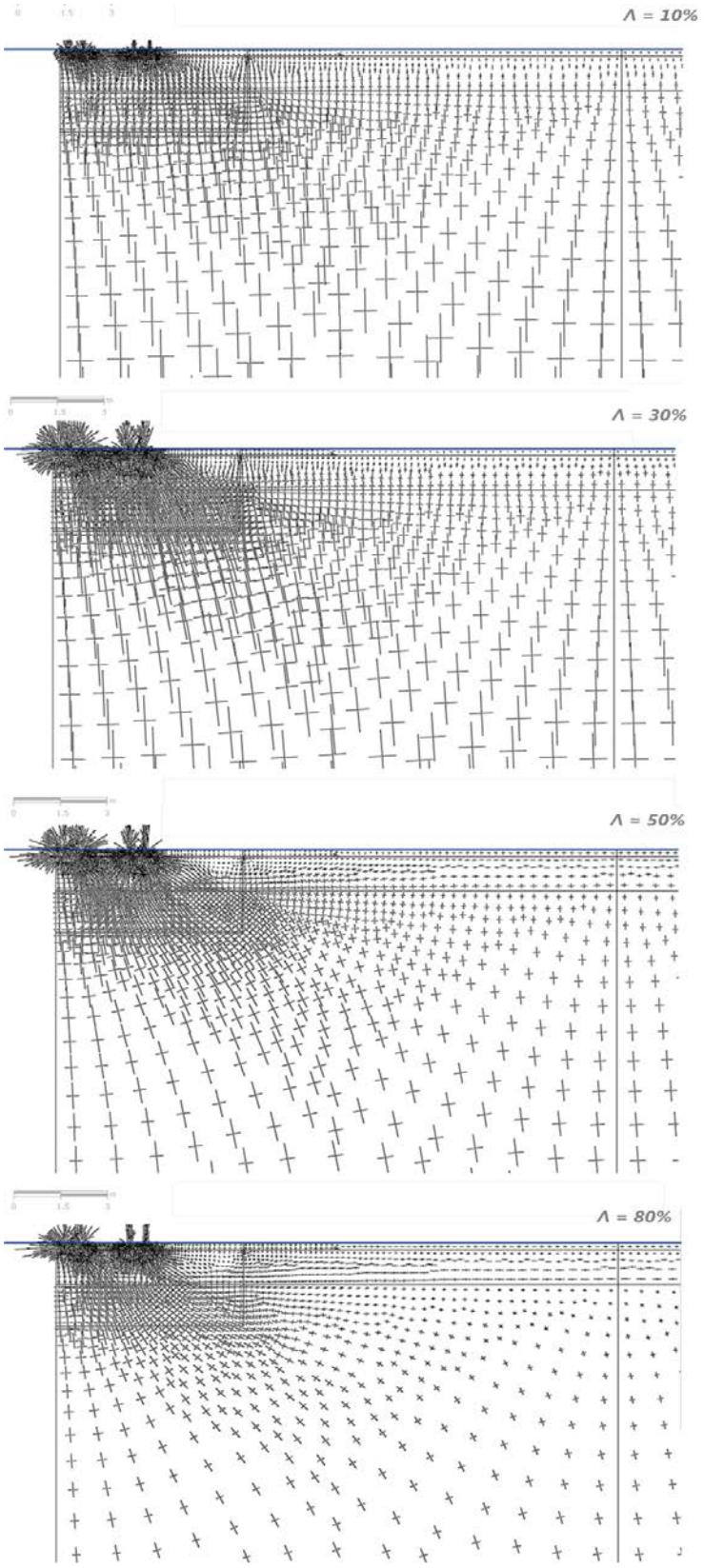

Figure 2.15: Principal stress vectors for multi-wheel Mohr-Coulomb model with Subgrade Case 3 and a 1.5m pavement depth, with varying utilisation (Λ).

2.5. Critical design cases

Figure 2.5 and Figure 2.15 shows the subgrade can be separated into 'upper' and 'lower' zones. The upper, overconsolidated soil resists larger, concentrated wheel stresses and experiences rotation of principal stresses due to low overburden stress. Interaction on a whole-vehicle scale also mobilises a 'lower' zone of normally consolidated soil which has high overburden stress in relation to its strength (in fact N_{Su} reaches a minimum). This normally consolidated state strongly influences the tendency to yield locally (Figure 2.8, Figure 2.9).

The transient stress applied by heavy haul vehicles is largest at subgrade surface (Table 2.5) but comparable to conventional pavement loads: e.g. 50kPa beneath railway sub-ballast (Gräbe and Clayton, 2009) or 60-120kPa beneath road sub-base during construction (Little, 1992; Frost, 2000). Transient stresses in the deep normally consolidated soils (>6.5m below road surface level), whilst of lesser magnitude, are unusual in the context of pavement engineering and are likely to induce a very different response to that in the upper layers.

Table 2.5: Changes in vertical stress for Subgrade Case 3 in response to typical heavy haul vehicle weights (between 10,000 and 30,000 tonnes). n.b. 6.5m is the depth to normal consolidation for Subgrade Case 3.

Loading scenario		Depth below road surface (m)			
		1.5	6.5	10.0	12.0
$\omega = 0$	σ'_z (kPa)	16	53	78	92
3840kN vehicle (ω = 32kPa, Λ = 10%)	$\Delta\sigma_z$ (kPa)	11	5	4	3
	$\Delta\sigma_z / (\sigma'_z @ \omega = 0)$	0.69	0.09	0.05	0.03
11520kN vehicle (ω = 96kPa, Λ = 30%)	$\Delta\sigma_z$ (kPa)	28	13	9	5
	$\Delta\sigma_z / (\sigma'_z @ \omega = 0)$	1.75	0.25	0.12	0.05
19200kN vehicle (ω = 160kPa, Λ = 50%)	$\Delta\sigma_z$ (kPa)	47	24	12	8
	$\Delta\sigma_z / (\sigma'_z @ \omega = 0)$	2.94	0.45	0.15	0.09
26880kN vehicle (ω = 224kPa, Λ = 70%)	$\Delta\sigma_z$ (kPa)	67	40	22	14
	$\Delta\sigma_z / (\sigma'_z @ \omega = 0)$	4.19	0.75	0.28	0.15

Pavement design for the upper subgrade, whilst remaining within the domain of conventional pavement engineering analysis, must consider the implication of larger-than-usual cumulative settlements and reduced performance of the granular layer (see Section 2.1.1.). The granular layer should perform the function of 'cushioning' the upper subgrade to keep stresses within acceptable limits, even after large cumulative settlement. It should be noted that, unlike for smaller-sized single wheel loads, a deeper pavement does not significantly alter how stress is distributed on the subgrade (see Figure 2.5).

During construction, the unprotected subgrade surface is likely to be trafficked by plant and the risk of damage to soft subgrades will be high. Stress bulbs from construction traffic are likely to be shallower and so more amenable to conventional pavement analysis. Larger construction vehicles, applying non-negligible stresses to normally consolidated layers at depth, should be assessed similarly to heavy haul vehicles (Chapter 7.2.2). Further precautionary measures, such as the use of low bearing pressure vehicles with wide tyres or temporary road mats, may be necessary to minimise subgrade surface damage.

The deeper, normally consolidated subgrade soils present a novel and relatively poorly-understood pavement design situation: these soils are likely to be prone to local yield; in some circumstances there may also be a risk of liquefaction under transient load (Chapter 3.3). In addition, the granular pavement layers, due to the thin layer effect (see Figure 2.5: Increments in vertical stress from a multi-wheeled vehicle with linear elastic models of varying subgrade stiffness and pavement depth. Left and

centre – interaction between individual wheels. Right – Large scale stress bulbs over the whole vehicle width, extending to great depth, similar to the 0.25m pavement depth, Subgrade Case 1 stress bulbs in Figure 2.4.) have little influence on the transient stresses at depth. The unusual soil behaviour and the more serious risk of liquefaction in this deep zone, a novel feature of heavy haul traffic, is thus a more sensible focus for this research.

2.6. Conclusions

Local yielding is likely to be much more prominent in subgrade soils beneath heavy haul roads: design which limits plastic strains is likely to be unaffordable over poor ground. Cyclic traffic loads which cause local yield are expected to not reach shakedown but to continually accumulate plastic strains. The shorter design life and possibility of re-profiling for temporary roads may mean shakedown is not a design requirement; they may be able to yield in a manner which is ultimately unstable under large numbers of loads but which does not reach failure within the expected number of passes.

The large difference in scale and magnitude between heavy haul vehicles and conventional vehicles means factors which were previously unimportant can now have a dominant role. Transient subgrade stresses both during construction and beneath a 1.5m deep pavement in service are expected to be comparable to more conventional road/railway pavement design; conventional methods are likely to be applicable for shallow soils, although allowance needs to be made for increased degradation of granular materials due to increased cumulative settlement. As a result of interaction

between adjacent wheel loads, it is expected that a stress bulb on the scale of the whole vehicle is produced; a potentially more critical failure mechanism in normally consolidated soils at depth needs to be considered, which may have more in common with a large shallow foundation. The influence of the pavement layer for soil at depth particularly is likely to be relatively small; analysis of heavy haul roads will need a much more thorough understanding of the deep soils and their response to transient stress.. Further investigation in the following areas is thus necessary:

- **Cyclic response of deep soils:** These are likely to be saturated, anisotropically normally consolidated and subject to significant self-weight overburden stresses, in contrast to highly overconsolidated, unsaturated surface soils usually critical to pavement engineering. Modelling typical vehicle loads and soft soil profiles in this chapter indicates soils at 6m to 12m depth, which are likely to be normally consolidated, may experience transient vertical stresses of 5kPa to 40kPa, i.e. 10% to 75% of the effective overburden stress. Heavy haul vehicles present unusual risks of local yield or liquefaction (see Section 3.3) to soil in this 'deep' zone.
- **Compression zone behaviour:** Yield tends to initiate in the compression zone; strains in the passive zone away from the vehicle only become large once compressive yield is reached and load redistributed. The more damaging effects of cyclic principal stress rotation are dependent upon failure of the compressive zone and it is therefore considered more important to focus on avoiding compressive failure than the final reserve of strength in the extension zone before failure.

- **Yielding and plasticity:** Uneven subgrade strain profiles associated with deep loading is likely to result in more rapid cyclic degradation and more significant changes to soil behaviour. How strength and stiffness change under cyclic loads close to a normally consolidated soil's ultimate capacity and the speed of degradation will be important in understanding how failure risk evolves through a temporary road's life.
- **Contraction and pore pressure generation:** Similarly to the above point, normally consolidated soils are more prone to generation of excess pore pressures. The impact on soil behaviour and potential for pore water flow/consolidation will be more influential than surface soils.

Additionally, as mentioned in Chapter 1.1, these vehicles are likely to travel much more slowly than conventional traffic and the impact of loading rate and duration on degradation requires further investigation.

CHAPTER 3: LITERATURE REVIEW

3.0. Introduction

This chapter comprises a review of soil mechanics literature focusing on the critical domain identified in Chapter 2.5; i.e. deep soil which is soft (normally consolidated), where the stress state is dominated by overburden and transient stresses may result in high cyclic strains. Gaps in the literature are identified and the experimental investigation proposed. Focus is given to the evolving risk of ultimate failure, rather than eventual cessation of irrecoverable strain (as in conventional pavement design).

In response to cyclic load (i.e. transient loading from an intial state q_{min} to a maximum stress q_{max}), cumulative strain (ε_{pl}) and pore pressure (u_{pl}) are of interest generally to determine serviceability and effective stress state changes. Increments of both quantities per cycle (i.e. Δu_{pl} and $\Delta \varepsilon_{pl}$) are also investigated as these can describe stabilising or progressive failure behaviour. For clarity, cyclic stress, strain and pore pressure terms are defined graphically in Figure 3.1 (symbols defined in the nomenclature). The terms *plastic* and *irrecoverable* are used interchangeably, as are *elastic* and *recoverable*.

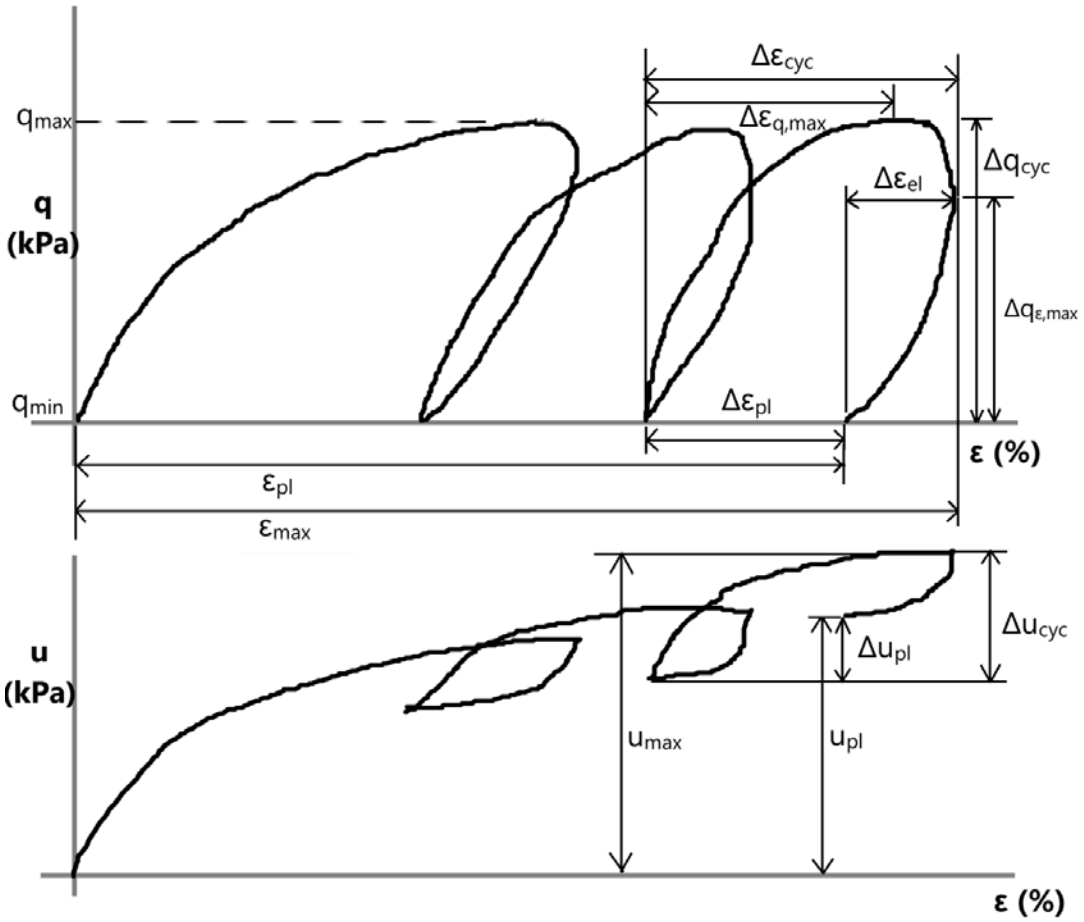

Figure 3.1: Definitions used for description of key cyclic phenomena

3.1. Cyclic failure in deep subsoils

Defining failure of soil under repeated load is not straightforward due to the progressive nature of failure and varying requirements of different engineering applications. As failure approaches, irrecoverable strains accumulate whilst stiffness reduces; much of the literature assumes failure from a certain strain, e.g.: ± 3% cyclic strain (Brown et al., 1977); either 15% average (ε_{pl} + ½.$\Delta\varepsilon_{cyc}$) or 15% cyclic strain (Andersen et al. 1988); 1% plastic strain (Frost et al. 2004). Such disparity may appear an obstacle to clearly defining failure and in some cases (e.g. Frost et al., 2004) relates to serviceability rather than ultimate failure. However as cyclically loaded soil develops most strain in the last few cycles before failure (Overy 1982; Ward 1983; Li et al. 2011), the number of cycles to failure is not significantly affected by the defined failure strain,

within sensible limits (e.g. those stated above). For permanent infrastructure which aims to achieve eventual stability (i.e. $\Delta\varepsilon_{pl}$ tends to zero) under cyclic load, it is likely the precise numbers of cycles to failure are less important and design will tend to err on the side of safety. In the case of a temporary heavy haul road, cyclic stabilisation is not necessarily sought, the requirements may simply be to withstand load during the short service life.

Definitions of cyclic failure related to controllability, i.e. whether external conditions can be maintained in a quasi-static equilibrium (Nicot and Darve 2010; Nova, 2010), may be more applicable. During the rapid failure in the last few cycles of the cyclic tests discussed above, small differences in applied cyclic stress cause an exponential increase in the soil's kinetic energy, i.e. there is a bifurcation of final states from similar initial states (Nova, 2010). Unlike the static failure mechanisms of perfectly plastic material demonstrated in Chapter 2.4.3, which depend on plastic yield to redistribute stresses close to failure, this kinematically unstable cyclic failure could result in progressive failure at a fraction of the static failure load.

At the macro-scale, kinematic instability is apparent in soil through strain-softening. Shear banding, tensile liquefaction and meta-stable liquefaction all follow this behaviour and these mechanisms are therefore discussed in more detail, with consideration of influential factors such as the soil's overconsolidation, the static and cyclic stresses it resists and the soil type.

Heath et al. (1972) found a threshold stress which described the point of divergence in terms of strain accumulation: $\Delta\varepsilon_{pl}$ stabilised for cyclic stress below the threshold and

accelerated for stresses above (Figure 3.2). The threshold stress has commonly been normalised to a soil's static strength. The factors controlling this relationship are not clear and significant variation is observed, suggesting further research into this phenomenon is required. Ward (1983) for example summarises a number of studies on different soils; normalised threshold stresses vary between 37% and 96% with no clear trends apparent. Experiments on natural clays by Frost et al. (2004) show large scatter, with normalised threshold stresses falling within 25% to 100%. The threshold stress for a given soil also varies depending on overconsolidation (Ward, 1983) and the ratio of static to cyclic shear stress (Andersen et al., 1988). Frost et al. (2004) suggest the conservative lower bound on normalised threshold stress of 25% proposed by Heath et al. (1972) is reasonable; however for temporary roads such conservatism is less desirable. Exceeding the threshold stress for a limited number of cycles may be permissible for a temporary road if divergence and ultimate failure only occur after relatively large numbers of cycles (Figure 3.2).

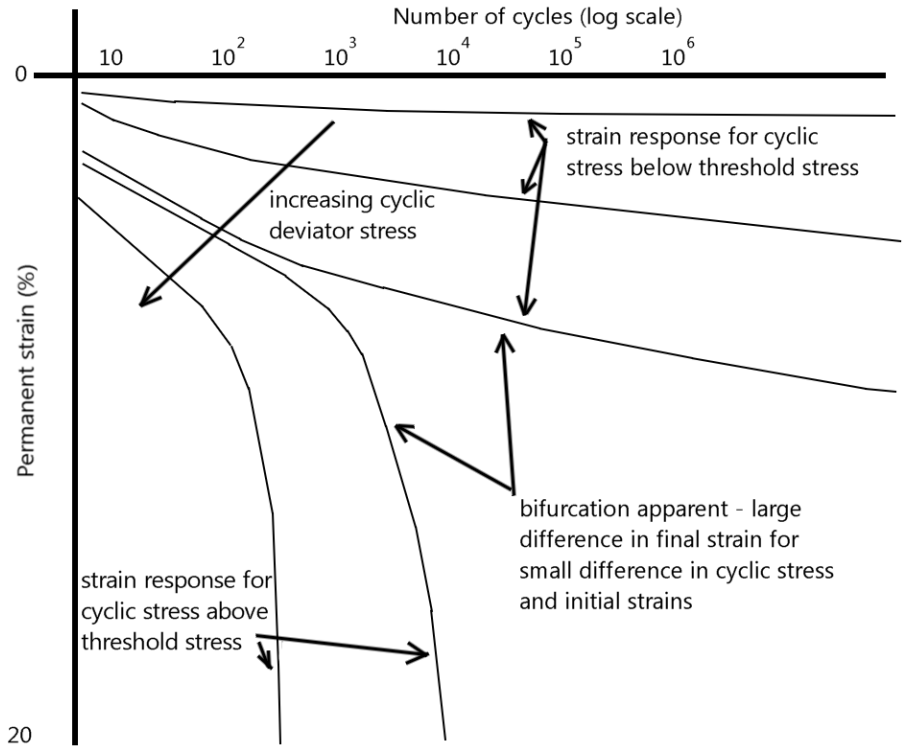

Figure 3.2: Illustration of cyclic failure as a bifurcation dependent upon stress intensity, after Heath et al. (1972)

3.1.1. Influence of stress state

Deep, soft normally consolidated deposits are on the wet side of the critical state (after Schofield and Wroth, 1968) and expected to cyclically accumulate positive pore water pressures (i.e. contractant behaviour). This suggests load shedding from the soil skeleton to pore fluid and loss of effective stress in the confining direction (Andersen, 2009). Cyclic contraction is observed in a range of soils including clays, sands and sand-silt-clay composites (Overy 1982; Marto 1998; Gratchev et al. 2006; Li et al. 2011; Åhnberg and Larsson 2012). Loss of confining pressure moves a soil's stress state towards the dry side of the critical state. Cyclic tests conducted by Ward (1983) on normally consolidated and lightly overconsolidated silty clay reached failure, typically displaying shear banding, when the effective stress paths intercepted the Hvorslev

Surface (Figure 3.3). This failure mode is typical of heavily overconsolidated static tests, implying cyclic load induces overconsolidation through pore pressure accumulation.

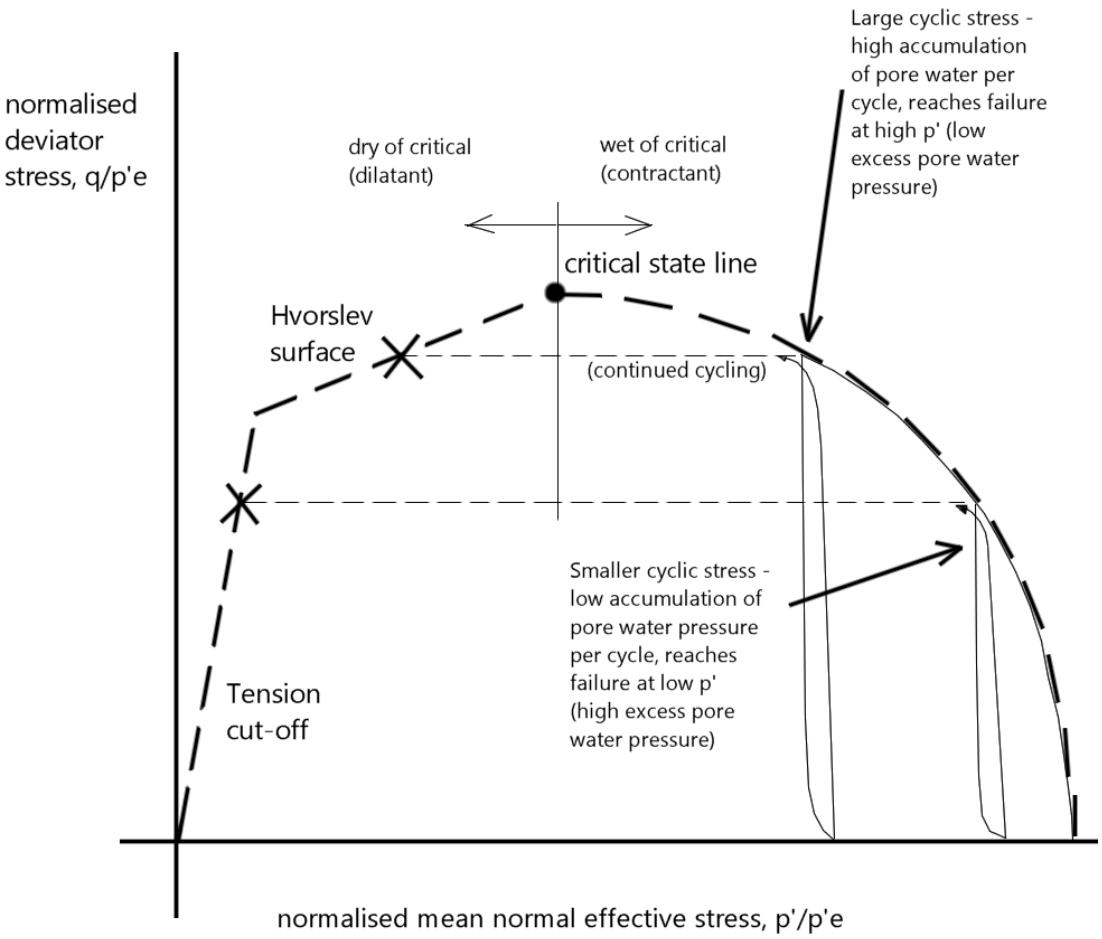

Figure 3.3: Undrained cyclic stress paths to failure for normally consolidated soil in normalised stress invariant space, assuming failure on the Hvorslev Surface or tension cut-off.

The in-situ stresses and the relation to cyclic stress is important in determining failure mode: tests by Selig and Chang (1981) indicate isotropically-stressed undrained sand samples subject to both compression and extension accumulate pore water pressures to fail by tensile liquefaction. Anisotropically-stressed samples purely subjected to compression maintain positive effective confining pressures and exhibit dilatancy (i.e. reducing pore water pressures) at failure. In the former case, large cyclic failure strains

occur with little to no permanent strain accumulation; in the latter case, more pertinent to soils at depth, the reverse is true (Selig and Chang, 1981; Andersen et al., 1988; Qi et al., 2007).

Failure by shear banding as the stress state reaches the Hvorslev Surface, i.e. by increasingly induced overconsolidation, is by no means universal. Whilst static and cyclic tests on Mercia Mudstone (silty clay) samples reconstituted from slurry by Ward (1983) typically failed in this manner, overconsolidated static tests on the same material by Hyde (1974) and Brown et al. (1975) dilated along the Hvorslev Surface to reach the critical state. Tested cyclically (Brown et al., 1975), overconsolidated soil can similarly dilate and tend towards the critical state. Behavioural differences may be due to differences in uniformity introduced by sample preparation and from end restraint (Ward, 1983; Atkinson, 2000); a shear band requires internal stress transfer to a non-homogeneous state to allow separation of the failure planes (Nova, 2010) so formation is likely to be accelerated if the sample or stress field is non-uniform. Early shear band formation is expected to be common in the field; natural soils, particularly soft alluvium which may contain a mixture of sand, silt and clay, are rarely uniform in composition. Slip failures in the field often exhibit a thin failure surface and strain-softening behaviour, suggesting instability due to localisation (Nova, 2010).

3.1.2. Post-cyclic changes to behaviour

The concept of cyclic load inducing overconsolidation in a soil has been proposed by many authors (Ward, 1983; Togrol and Güler, 1984; Li et al., 2011) because post-cyclic monotonic shear follows very closely the response of a sample overconsolidated by removal of the same increment of effective stress. Pore water pressure behaviour can

change from initially contractant to dilatant after cycling if sufficient pore water pressure is induced. Static strength loss following cyclic loading was also apparent (Ward, 1983; Togrol and Güler, 1984; Li et al., 2011), thought to be due to early shear banding as the effective stress path intercepts the Hvorslev Surface. Conversely, Carter et al. (1982) modelled cyclic strength reduction as shrinkage of the wet-of-critical yield surface (Figure 3.4). Whilst able to reproduce experimental results using simple empirical parameters and with good accuracy, conceptually this model implies a wet-of-critical plastic flow failure. Models proposed by Pender (1982) or Li et al. (2011) produce similarly faithful reproductions of experimental phenomena but describe changes to yield surfaces in terms of stress state and overconsolidation.

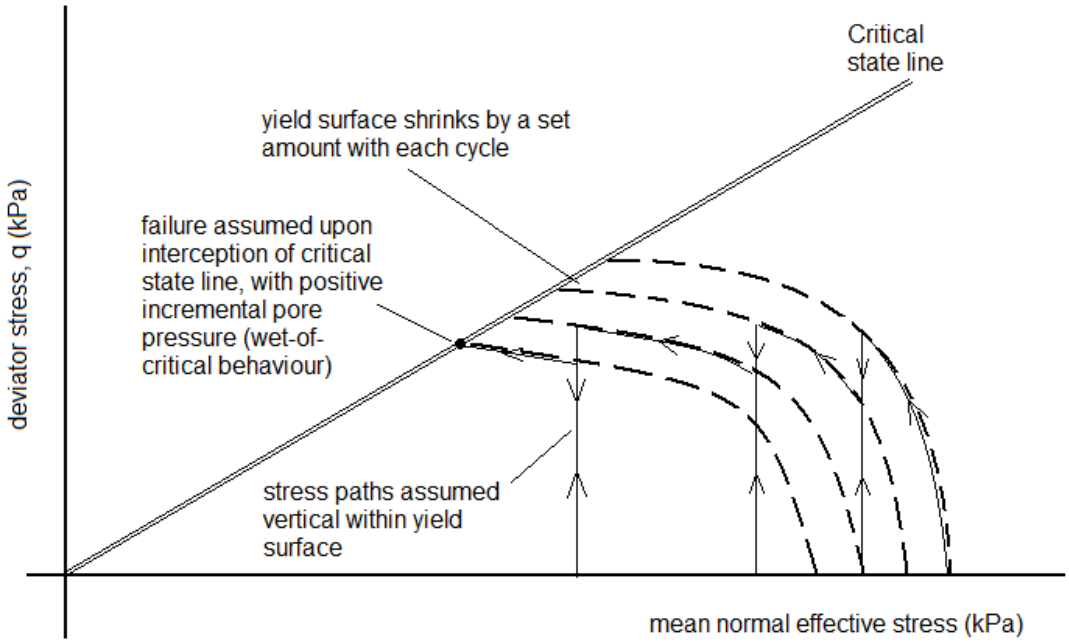

Figure 3.4: Cyclic loading modelled as shrinkage of wet-of-critical yield surface, after Carter et al (1982).

Sensitive clay soils with an open micro-structure , e.g. Åhnberg and Larsson (2012), exhibit gradual strain softening after an initial peak and experience reduction in strength due to cyclic loading as a function of strain. Following cyclic loading, there is often a tendency for sensitive soils to rejoin the intact stress-strain curve unless subject to very high strains (Li et al., 2011; Åhnberg and Larsson, 2012). This apparent invariance of the stress-strain curve may explain strength loss in these cases: increasing strain beyond the peak stress represents an increasing re-structuring of the original, stronger structure. There is evidence that strain is highly influential for all aspects of soil behaviour, including strength loss (discussed further in Chapter 3.2).

Strength is not necessarily reduced after cyclic loading. Brown et al. (1977) found static strength of isotropically normally consolidated silty clay samples experiencing cyclic strains below ±3% immediately improved compared to their pre-cyclic static strength (as opposed to those with cyclic strains above 3%, which lost strength). Beneficial fabric rearrangement is similarly implied by increasing resilient modulus of saturated soil under low cyclic stress (Ward 1983; Ng and Zhou 2014). Cyclically-induced strain may be the best metric for estimating post-cyclic strength changes (Yasuhara et al., 2003).

The failure envelope for improved post-cyclic shear tests in Brown et al. (1977) was translated to match that of overconsolidated samples, i.e. the same internal angle of shearing resistance but greater effective cohesion than normally consolidated samples. For these particular samples, overconsolidation has some beneficial effects. This may be a function of the soil used or the use of 75mm diameter samples, (as opposed to

38mm diameter by Ward, 1983, which were particularly prone to early shear banding). If a soil is able to continue to dilate along the Hvorslev Surface due to its composition and absence of inherent localisations, strength loss may not always follow cyclically-induced overconsolidation.

Reduction in small-strain stiffness following cyclic load is often apparent (Yasuhara et al, 2003; Li and Huang, 2010); the relative reduction is often greater than that of strength, particularly under low-amplitude cyclic load.

3.1.3. Particle-scale interpretation

Soil mass behaviour is the result of numerous inter-particle interactions and Discrete Element Method (DEM) simulations allow inference of 'granular' (i.e. frictional contact laws, predominantly the case for sands and non-plastic silts; Gong, 2008) particle-scale behaviour. Anandarajah (2000) used the technique to model particle-scale interactions in clays (including flexure of slender platelets, electrostatic face and edge forces, and double layer effects). DEM research can identify how different facets of soil macro-behaviour emerge and could offer new insights into how cyclic degradation is effected.

DEM simulations of force distribution in granular assemblies indicate a series of 'strong' networks (i.e. carrying greater than average contact forces) principally supports deviator stress (Gong, 2008) 'Weak' networks, carrying low contact forces, provide orthogonal restraint. As pore pressures rise, force anisotropy increases to maintain the deviator stress; Thornton (2000) found increasing shear strain to cause separation in weak networks. If restraint becomes insufficient, rearrangement and large straining can occur in a buckling-like manner (Nicot and Darve, 2010).

Compression buckling is kinematically unstable and so suggests uncontrollability induced by apparent overconsolidation, as discussed previously.

Under stress-controlled cyclic loading, most strain and thus micro-structural rearrangement develops at the end of each half-cycle at maximum stress anisotropy (Overy, 1982; Åhnberg and Larsson, 2012). Ishihara and Towhata (1982) differentiate between primary plasticity, occurring when the stress path reaches a shrinking yield surface (similar conceptually to Carter et al., 1982) and secondary plasticity, occurring within this yield surface (Figure 3.5). This implies continual small rearrangements under cyclic load, with greater rearrangement when the stress state becomes more anisotropic than previously encountered.

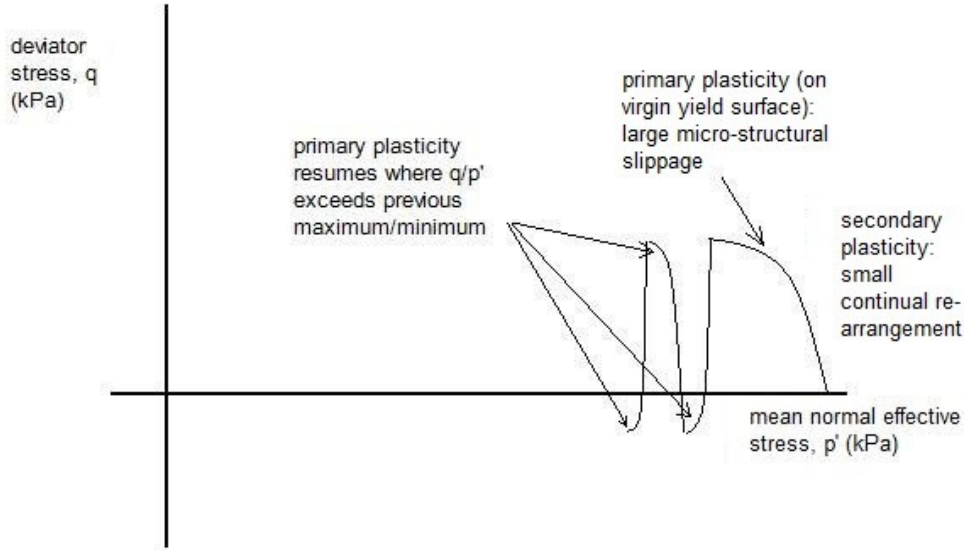

Figure 3.5: Distinction between primary and secondary plasticity, after Ishihara and Towhata (1982), and implied particle-scale behaviour

Soroush and Ferdowsi (2011) found the network of DEM contact forces become more anisotropic with each cycle of strain-controlled loading (Figure 3.6), eventually resulting in disconnected force chains unable to transmit load. A similarly increasing

anisotropy is found during stress-controlled cyclic loading by Xu et al. (2015). These findings support the hypothesis that cyclic degradation is the result of contact breakage, reducing strong network confinement.

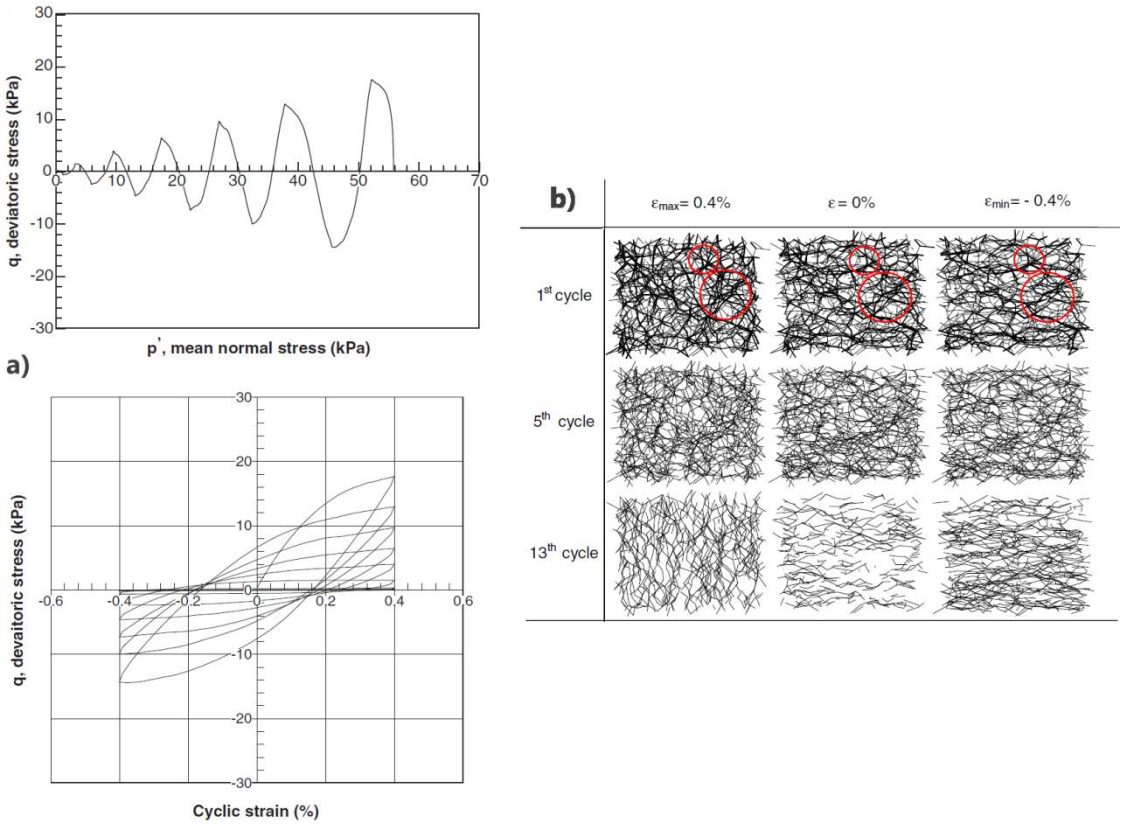

Figure 3.6: Stress-strain response of DEM simulation of undrained cyclic load (a) and vector representations of strong contact force (i.e. greater than average inter-particle force) network (b), taken from Soroush and Ferdowsi (2011). Reducing force magnitude, increasing anisotropy and eventual liquefaction with disconnected regions apparent.

Inter-particle slippage is less likely on strong contacts, which have large tangential resistance due to high normal forces, but more likely on weak contacts (Soroush and Ferdowsi, 2011). Greater plastic strains and rearrangement of strong networks is only possible once restraint is lost. The link between primary plasticity and anisotropy of effective stresses (i.e. *q/p'*) suggests this governs the necessary loss of weak restraint.

In this context, secondary plasticity can be seen as small rearrangements while restraint remains sufficient. This is exemplified in Figure 3.7; strong contact force anisotropy particularly (e) changes rapidly during the stiff part of a cycle, but as the response softens, more strain is required to mobilise the last increments of force anisotropy.

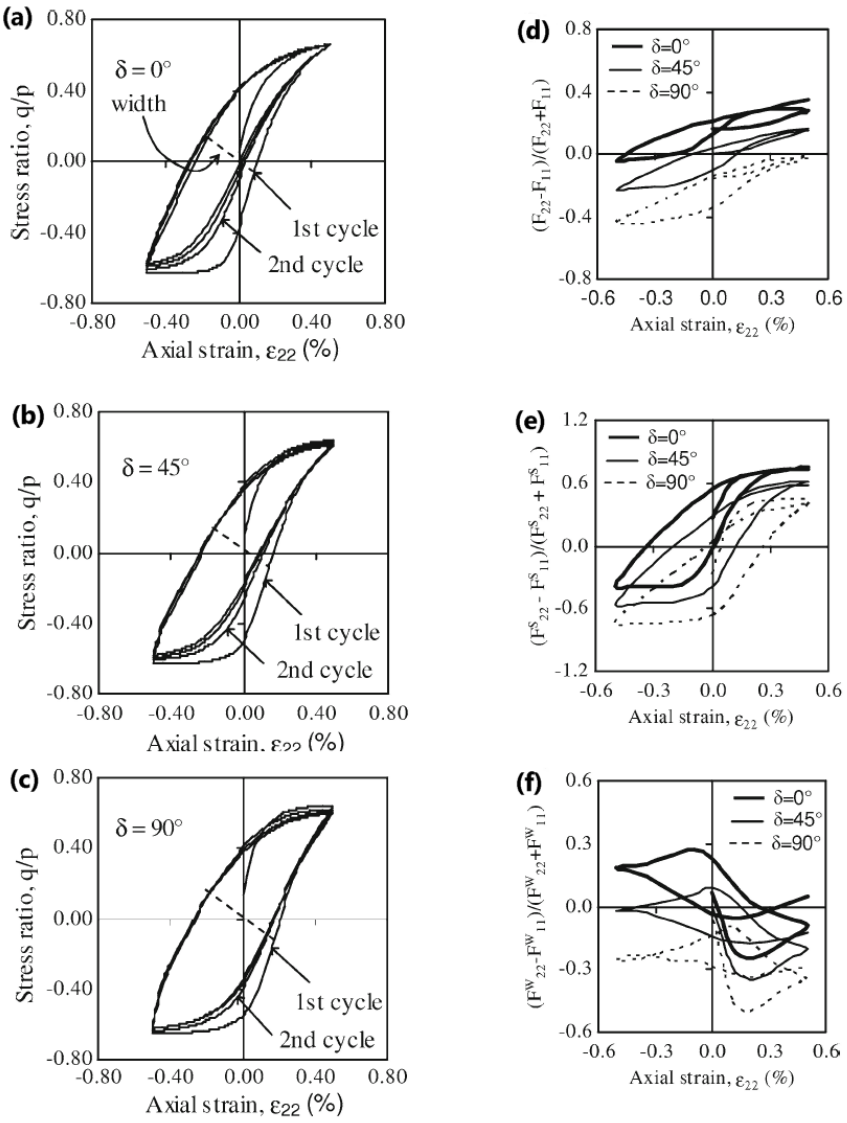

Figure 3.7: Development of hysteretic cyclic stress-strain loops (a, b and c) and normal contact force anisotropy (e, f and g) as a function of strain under cyclic load, taken from Sazzad & Suzuki, 2010. d) is for all contacts, e) is for strong contacts only and f) is for weak contacts only. n.b. δ refers to the mean angle between long axes on oval particles and the horizontal axis.

The previous cyclic degradation behaviour emerges from purely frictional contact laws, but clays modelled by Anandarajah (2000) similarly have small numbers of strong contacts carrying the majority of the force. Platelets typically formed into clusters and force transmission is predominantly transferred at cluster-to-cluster contacts. As clusters behave like malleable particles, the nature of strain-induced fabric rearrangement and contact breakage is more complex than granular materials. Nevertheless, particle orientation similarly becomes more anisotropic during shear towards the direction of the deviator stress, particularly for cluster-to-cluster contacts (Anandarajah, 2000; Figure 3.8). This may explain why the strength of clays is typically governed by effective stresses and 'frictional' behaviour; strength contributions due to true cohesion or electrochemical interaction remain small, particularly in normally consolidated soils (Brown et al., 1977; Atkinson, 2007).

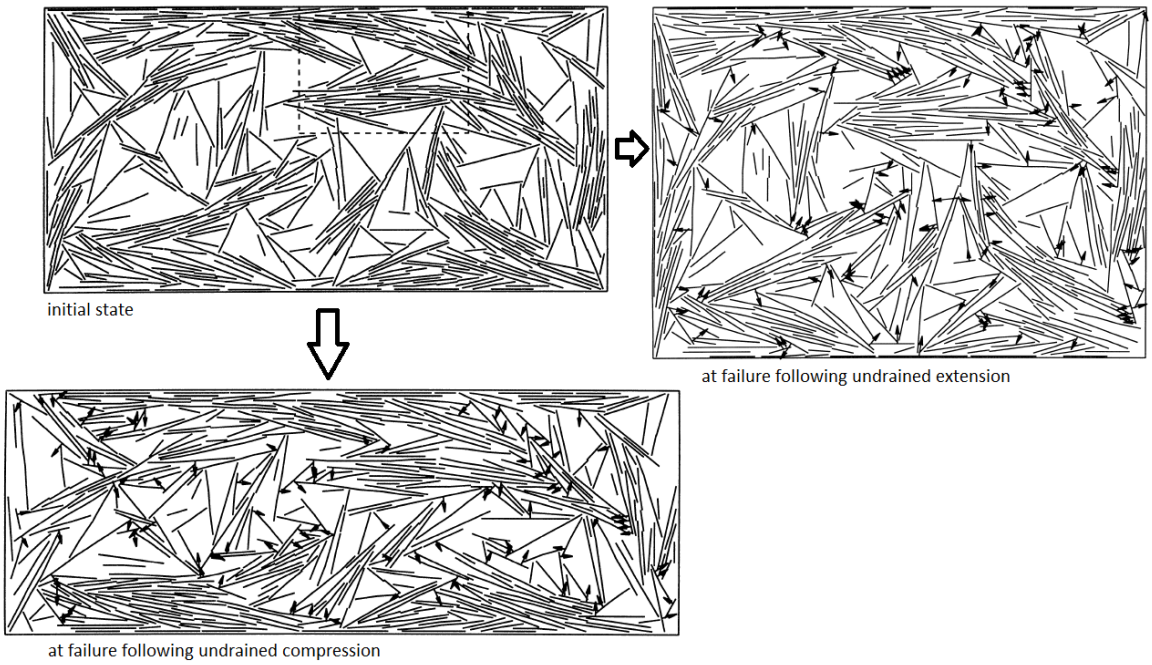

Figure 3.8: Changes in clay microstructure and anisotropy, particularly in terms of cluster-to-cluster contacts and strong interparticle forces (i.e. > average interparticle force, represented by arrows), during undrained shear in compression and extension. Taken from Anandarajah, 2000.

Particle-scale behavioural differences in clays significantly influence cyclic degradation and failure mechanisms. Whilst low plasticity silts reach tensile liquefaction and zero effective stress, clays above a critical Plasticity Index are able to maintain an effective stress (Gratchev et al., 2006; Erken and Ulker, 2007). Some of this apparent cohesion may also be due to low permeability; water trapped in a void may resist extension through generation of negative pressures locally (Erken and Ulker, 2007).

3.2. Strain thresholds

Soil behaviour is dependent upon strain: mechanical response changes from high stiffness with no change to pore pressure (or volume) at very small strain, to low stiffness and irrecoverable strains and pore pressures at medium to large strains (Díaz-Rodriguez and López-Molina, 2008). It is possible to compare this changing macro-scale response to DEM-simulated interactions at a particle-scale to infer controlling factors.

Gu et al. (2014) demonstrate that DEM mobilised shear resistance (i.e. *q/p'*) is the sum of:

1. anisotropy of the inter-particle normal force network;
2. anisotropy of inter-particle tangential forces and;
3. anisotropy of the orientation of the normals of contact points.

Increases in the first two indicate force (but not necessarily particle) realignment to resist the deviator stress, Changes to the third requires particle movements, which tend towards an anisotropic preferential configuration.

Under initial small-strain increments, normal and tangential forces govern resistance (Gu et al., 2014) and stiffness is high. Recoverable strain and pore water pressure behaviour is expected (Díaz-Rodriguez and López-Molina, 2008), implying inter-particle slippage is either non-existent or reversed by unloading. Changing from linear-elastic to hysteretic-elastic between very small-strain and small-strain regimes coincides with the start of stiffness reducing with strain (Díaz-Rodriguez and López-Molina, 2008; Figure 3.9), possibly indicating transition between no slippage and reversible slippage, where noticeable frictional dissipation of energy begins.

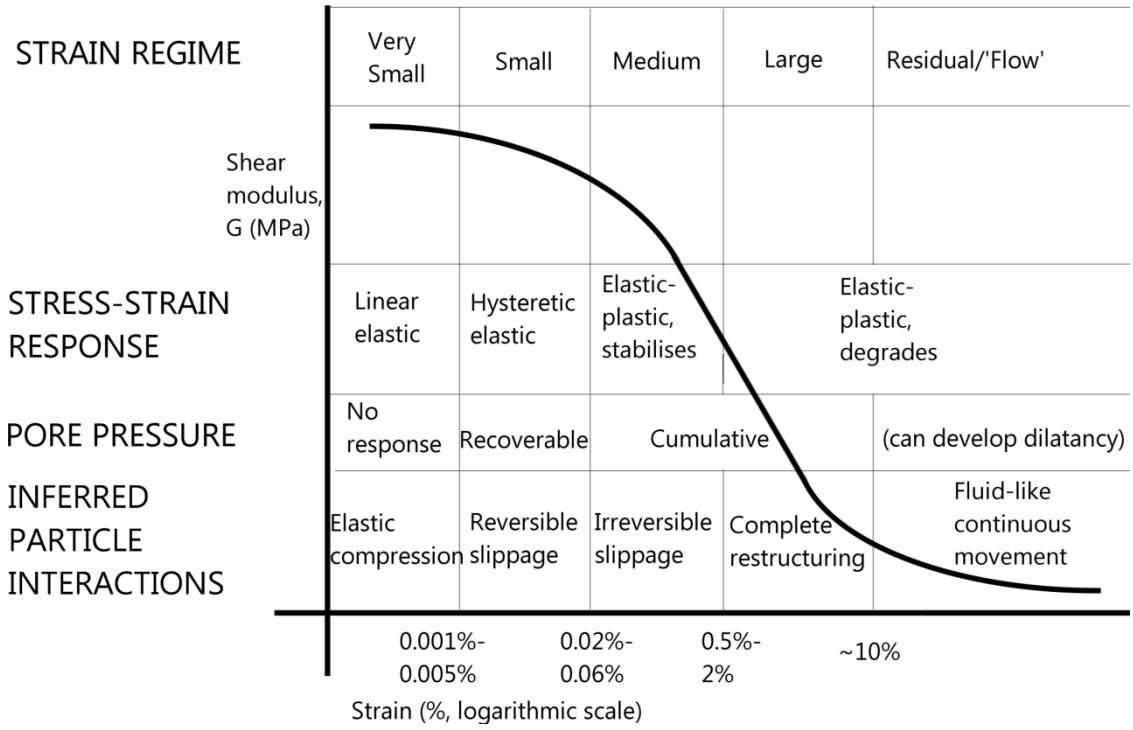

Figure 3.9: Strain regimes and typical strain values after Díaz-Rodríguez and López-Molina (2008) with possible particle interactions inferred from DEM literature

As strains increase, increasingly prevalent inter-particle slippage means tangential forces quickly reach a limit, after which a near-constant proportion of contacts continue to slide (16-20%; Kruyt, 2010 and Gu et al., 2014). Contact realignment and

normal force anisotropy then become dominant (Gu et al., 2014); the structure re-arranges to resist increasing shear through normal contact forces. Accumulation of permanent pore water pressures under cyclic load indicates soil skeleton contraction and medium-strain irreversible fabric rearrangement (Díaz-Rodríguez and López-Molina, 2008), occurring above the volume change threshold strain (after Hsu & Vucetic, 2006). This plasticity-dominated, medium-to-large strain regime is where 'classical' soil mechanics laws, formulated on the basis of effective stresses and plasticity (e.g. the Cam Clay model of Schofield and Wroth, 1968) apply well, particularly for plastic clay soils.

3.2.1. Cyclic degradation: medium and large strain regimes

For the problem of cyclic degradation, the primary focus is small to medium strain (plasticity initiation) and medium to large strain (degradation) transitions.

Non-degrading, cyclically stabilising (medium-strain) and degrading, progressively failing (large-strain) behaviour is typically divided by a threshold stress (Heath et al., 1972; Frost et al., 2004). There is evidence that cyclic degradation is triggered by exceeding a specific plastic (Frost et al., 2004) or cyclic strain (Heath et al., 1972; Erken and Ulker, 2007; Li et al., 2011) which would provide the limit to medium-strain behaviour. Similar to the shakedown analysis discussed in Chapter 2.1.3, a reserve of additional resistance to cyclic load above first yield is apparent, although the mechanisms for this stabilisation differ. DEM modelling implies the additional resistance to yield under medium-strain cyclic load is mobilised by re-arrangement of contact normals into a preferential anisotropic configuration.

Within this stabilising, medium-strain regime, normally consolidated soils accumulate positive pore water pressures at decreasing rate (Hyde, 1974; Ward 1983; Marto 1998; Figure 3.10). Resilient modulus and effective confining stress in clays reduce to a stable value (Brown et al. 1975; Overy 1982; Frost et al. 2004). This implies that a state is attained after sufficient strain where load can be resisted without irreversible contact breakage. This is small-strain behaviour and suggests cyclic loading has raised the volume change (medium-strain) threshold.

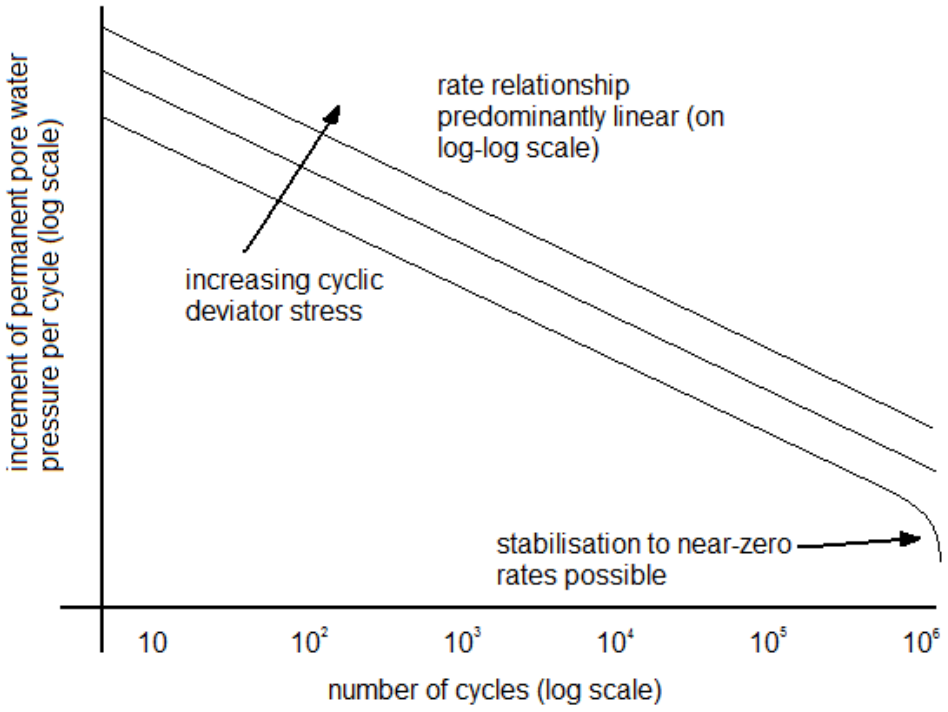

Figure 3.10: Development of pore water pressures under cyclic loading, applicable to one-way cyclic loading (after Hyde, 1974 and Ward, 1983) and two-way cyclic loading (after Marto, 1998); this relationship also applies to accumulation of permanent strains under one-way cyclic loading (after Hyde, 1974 and Ward, 1983).

Hyde (1974) and Ward (1983) integrated rate relationships in Figure 3.10 to predict strains and pore water pressures with some success. Assuming linear rates is initially accurate but after long durations of stable load appears to provide generally

conservative estimates (Walker, 1969). This continuous plasticity implies an increasing component of medium and large-strain behaviour is time-dependent and related to viscous dissipation of energy. Okur and Ansal (2007) similarly noted increasing damping ratio with strain (widely documented by Díaz-Rodriguez and López-Molina, 2008). The implications of time-dependent behaviour are considered in section 3.4.

Static strength degradation correlates with accelerating cyclic strains and pore pressures; post-cyclic static strength only appreciably reduced once the cyclic yield strain was exceeded (Erken and Ulker, 2007). This supports use of the strain limitation design criteria discussed in Chapter 2.1.1. It also suggests that complete fabric restructuring is required for degradation, as suggested by Díaz-Rodriguez and Santamarina (2001) and Díaz-Rodriguez and López-Molina (2008).

It is postulated (Been and Jefferies, 1985; Zhao and Evans, 2011) that at ultimate failure, soil develops a 'flow' structure which enables it to flow at constant velocity under a maintained stress without overall volume change tendency. DEM simulations (Rothenburg and Kruyt, 2004; Zhao and Evans, 2011) indicate the coordination number also reaches a constant value, i.e. no overall gain or loss of particle contacts. This represents the final stage in a soil's strain-dependent transition from a rigid solid to a fluid: resistance arises almost entirely from time-dependent energy dissipation (Díaz-Rodriguez and López-Molina, 2008; Joseph, 2014). Sand and silt can become dilatant at large strains even when normally consolidated and initially contractant. A reserve of additional undrained strength is thus available due to dilation (i.e. as effective stress rises), although as previously discussed this carries the risk of localisation and shear

banding failure. A critical flow condition with zero volume change is often not reached until very large strains (e.g. >25% strain in Wang and Luna, 2012, or >40% strain in Yamamuro and Lade, 1999).

3.2.2. Thermodynamic treatment of soils

Work is done on a soil during load: some is stored as recoverable strain energy whilst some is dissipated frictionally (Figure 3.11). The proportions of recoverable and irrecoverable energy relate to strain magnitude, as seen in DEM simulation by Kruyt and Rothenburg (2006): at small strains, particularly in dilatant soils, sliding contacts are proportionately low and work input is largely retained as strain energy. At larger strains, dissipation from frictional sliding dominates. Consideration of energy becomes particularly important when strain-softening is apparent. As noted by Schofield and Wroth (1968) and Nicot and Darve (2010), strain-softening implies kinematic instability; work is transformed to kinetic energy as static equilibrium is lost.

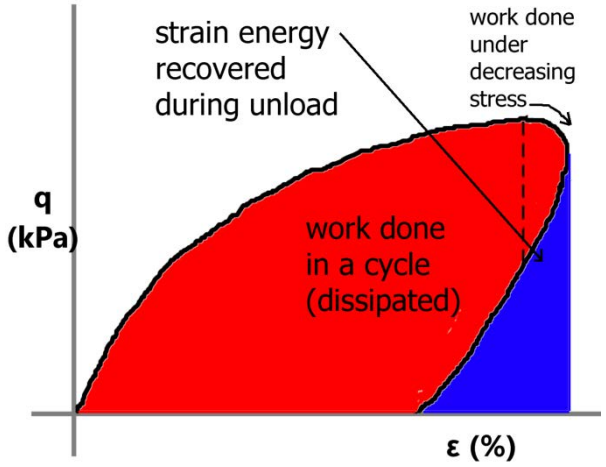

Figure 3.11: Storage, release and dissipation of energy in soil subject to cyclic loading

Edwards et al. (2004) have attempted to modify statistical mechanics for thermodynamic behaviour of gases to provide emergent macro-scale laws for granular

media. Gases are ‘dilute’, i.e. particle movements are effectively random and history-independent. However soils are inherently ‘jammed’, i.e. particles are restrained by frictional contacts, thus unable to explore the energy space. If sufficiently agitated, particles are freed and able to seek lower-energy states. In this context, a quantity termed ‘compactivity’ is proposed which is analogous to temperature in gases; it relates to the potential for re-ordering into a higher-probability, denser packing (Edwards et al., 2004).

Loose soils have high compactivity, reduced by continued agitation. During increasing contractant shear, soil reaches statically determinate states in localised clusters as contacts are lost (Blumenfeld, 2010). A transition point is reached when these clusters connect, allowing large-strain restructuring with dynamic flow between a series of statically determinate states (Kruyt, 2010; Blumenfeld, 2010). The minimum agitation for particle liberation should coincide with the volume change threshold, above which irreversible soil skeleton contraction, i.e. reduction in compactivity, occurs. It is possible that stable cyclic straining corresponds to particle liberation is on a small scale, i.e. when statically determinate clusters are separate, whilst connected zones of particle liberation may correspond to degradation.

As the connectivity of these clusters is proportional to stress (Blumenfeld, 2010) and plastic strain is strongly influenced by this loss of equilibrium, it can be argued that particle agitation is related to mechanical work done on the soil; applying the same stress with higher power input (i.e. more frequently/at faster rates) should also cause more plasticity.

In the case of meta-stable soils, thermodynamic considerations are particularly pertinent: these soils can be kinematically unstable and rapidly convert potential energy to kinetic energy (Lade, 1994).

3.3. Metastability and liquefaction

An unusual feature of loose, 'granular' (i.e. sand and silt) soils in undrained shear is that they can undergo meta-stable liquefaction. There is sudden strain-softening, meaning uncontrollability under stress-controlled conditions, even though the stress state is inside the ultimate failure envelope (Been and Jefferies, 1985; Lade, 1994). This liquefaction is kinematically unstable but not necessarily an ultimate failure mode; recovery can occur (Lade 1994; Wang and Luna, 2012). However strains are so large (Figure 3.12) and rapid that static liquefaction may constitute failure in the sense of stranding or even overturning a vehicle. The combination of small initiation strain and consequent rapid, large strains makes meta-stable liquefaction a nightmare scenario for geotechnical engineers and thus a key focus for this project. The tests shown in Figure 3.12 cover the anticipated effective stress range from Table 2.5, although behavioural changes occur around p' = 150kPa: this effect is dependent on fabric (discussed in Chapter 3.3.3).

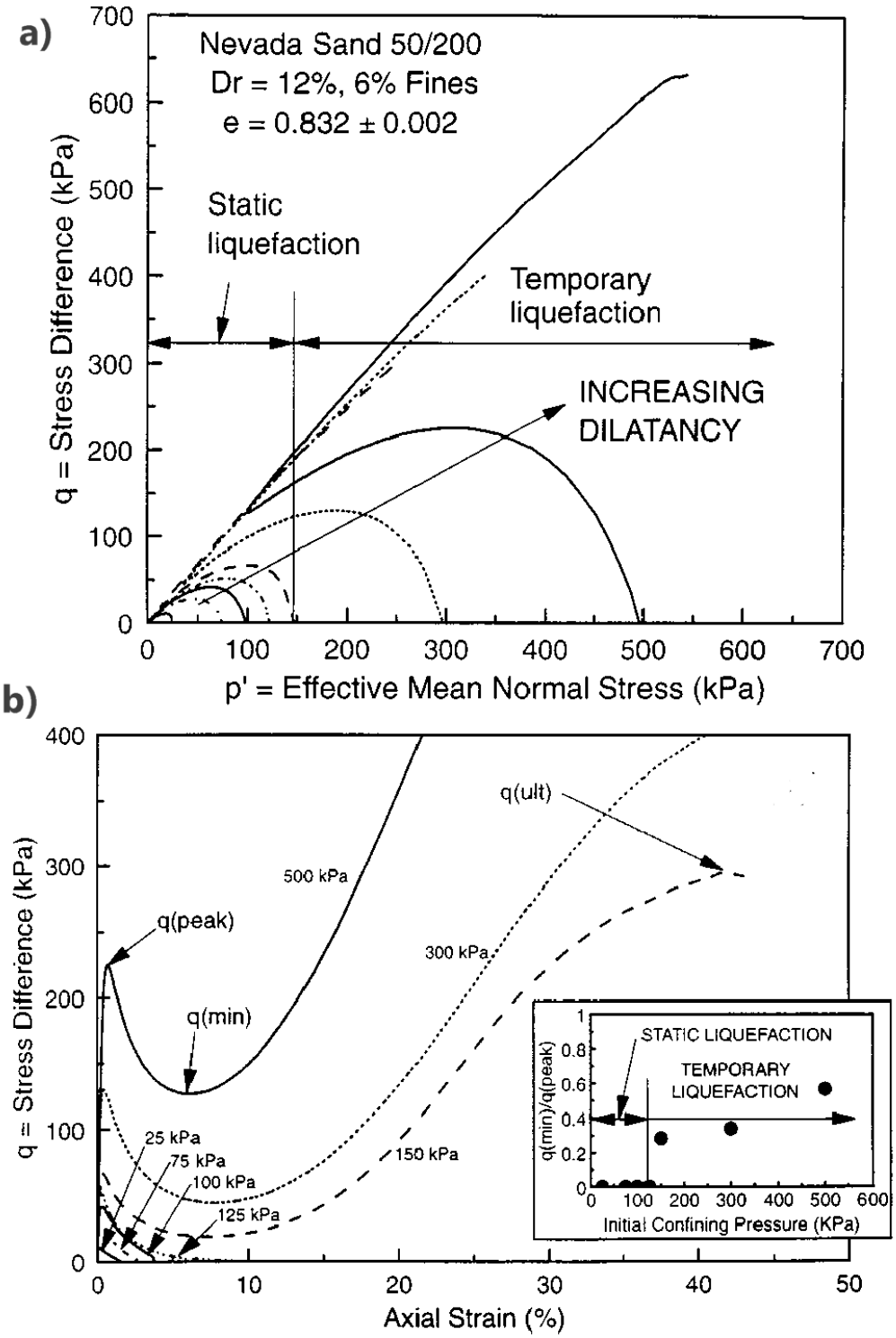

Figure 3.12: Effective stress paths (a) and stress-strain relationships (b) for undrained static triaxial compression tests on loose silty sand, showing static liquefaction, q(peak) to q(min), at small strain and subsequent recovery, q(min) to q(ult) at large strains (taken from Yamamuro & Lade, 1999). Pressures next to lines on the lower stress-strain plot indicate initial confining pressure. n.b. under load-controlled conditions, samples reached q(min) from q(peak) in 0.5 seconds or less.

3.3.1. Conditions for liquefaction

Only contractant soil is able to undergo meta-stable liquefaction (Been and Jefferies, 1985). Dry-of-critical soils can liquefy, but only through pore pressure accumulation and tensile liquefaction (Muhunthan and Worthen, 2011). The degree of contraction is important; Wang and Luna (2012) found overconsolidation in liquefiable silt reduced both pore water pressure generation and strain-softening tendencies. At OCR = 2, no strain softening but a nearly flat stress-strain curve was apparent at strains associated with liquefaction; at higher OCR a more subtle drop in the stress-strain gradient remained (Wang and Luna, 2012). Similar reduction in liquefiability with increasing OCR was observed by Santagata and Germaine (2005). A number of factors may be influential to this phenomenon:

- Reduction in effective stress, resulting in swelling of the soil skeleton but retention of lower void ratio than an equivalent normally consolidated soil (Schofield and Wroth, 1968) with a greater number of inter-particle contacts (Sitharam and Vinod, 2009);
- Less contractant shearing behaviour, reducing collapse risk (Schofield and Wroth, 1968; Sitharam & Vinod, 2009);
- More isotropic stresses due to 'locked-in' lateral stress, thought to provide greater stability through lateral restraint to strong networks (Hu et al., 2010).

Whilst surface soils may therefore be low-risk for liquefaction, deeper soils stressed by heavy haul vehicles (Chapter 2.5) present a much greater risk.

At the pre-liquefaction peak stress, soil reaches a consistent mobilised *q/p'* (Been and Jefferies 1985; Lade, 1994), sometimes termed the 'Instability Line'. A small undrained stress increment to a drained static stress can cause liquefaction, as can closing the drainage valve on a sample already loaded above the Instability Line - ongoing creep contraction initiates the chain reaction collapse (Lade, 1994; Doanh et al., 2012). Static stresses from haul road earthworks (e.g. 30-40kPa) may therefore reduce the undrained increment (Δq_{peak}) required to cross the Instability Line, particularly if not fully consolidated. Δq_{peak} reduces from 12kPa to 3kPa following a vertical effective stress increment of 27kPa in Doanh et al., (2012). Δq_{peak} varies from 2-10% of σ'_1 (Doanh et al., 2012), depending on the consolidation *K* (0.66 to 0.80). Anisotopically normally consolidated soil up to 12m below the road surface (Table 2.5) can thus be at risk of liquefaction. A pavement and earthworks design which limits transient stress below Δq_{peak} may require a depth of 10-12m between the road surface and liquefiable material, i.e. for a z_{NC} depth of 6.5m (as per Table 2.5) this would require 3.5-5.5m high earthworks.

Liquefaction cannot occur if volume contraction (e.g. drainage) is permitted (Lade, 1994; Chu et al., 2015). Bearing in mind the slow speed of heavy haul traffic as compared to earthquake loading (the common motivation for study of meta-stable liquefaction in sands), it is unlikely that loose sands represent a high liquefaction risk. Plastic clays, which are more resistant to liquefaction (section 3.1.3.), are also low-risk (Andrews and Martin, 2000), unless sensitive (e.g. quick clays; Åhnberg and Larsson, 2012). Lower-permeability silts, prone to liquefaction but not pore water drainage under anticipated load durations, are likely to present a worst-case scenario.

3.3.2. Fabric dependence

Low initiation strains suggest meta-stable liquefaction is highly dependent upon a precarious initial fabric arrangement (Lade, 1994). This implies liquefaction initiation is a medium-strain phenomenon. Liquefaction then induces large-strain restructuring which erases the initial fabric (Lade, 1994).

The critical importance of initial fabric is demonstrated by addition of fines to liquefiable soil; increasing non-plastic fines content reduces peak deviator stress (Yamamuro and Lade, 1999), hypothesised to be due to fines acting as spacers between sand grains and forming a more open microstructure. Similarly Gratchev et al. (2006) found adding small quantities (15%) of Kaolinite and Illite clay to fine silica sand reduced cyclic liquefaction resistance. Microscopic imaging confirmed fines forming weak connectors between sand grains. Adding a small quantity of very high plasticity clay can increase liquefaction resistance (e.g. >9% bentonite to fine sand, Gratchev et al., 2006; 2.5% bentonite to silt, Wang et al., 2015b). Mixed soils dominated by the silt/sand fraction are expected to liquefy, whilst those dominated by the clay fraction are not (Andrews and Martin, 2000; Boulanger and Idriss, 2006). Clay dominance and liquefaction resistance is achieved at different clay contents depending on the type of clay added and the material it is added to; use of limiting criteria such as plasticity or clay content need to be considered within the context of a soil's mineralogy and geological history (Andrews and Martin, 2000).

DEM simulations by Gong (2008) found the coordination number (mean number of contacts per particle) reduced during undrained shear. For statical determinacy in three dimensions, a completely frictionless sphere requires six reaction points, which

reduces to four for infinitely frictional particles (Thornton, 2000). Liquefaction coincided with a limiting coordination number in this range, implying a limit to statical determinacy was reached (Gong, 2008; Figure 3.13). The observed phase transformation and liquefaction were considered equivalent to forming a mechanism.

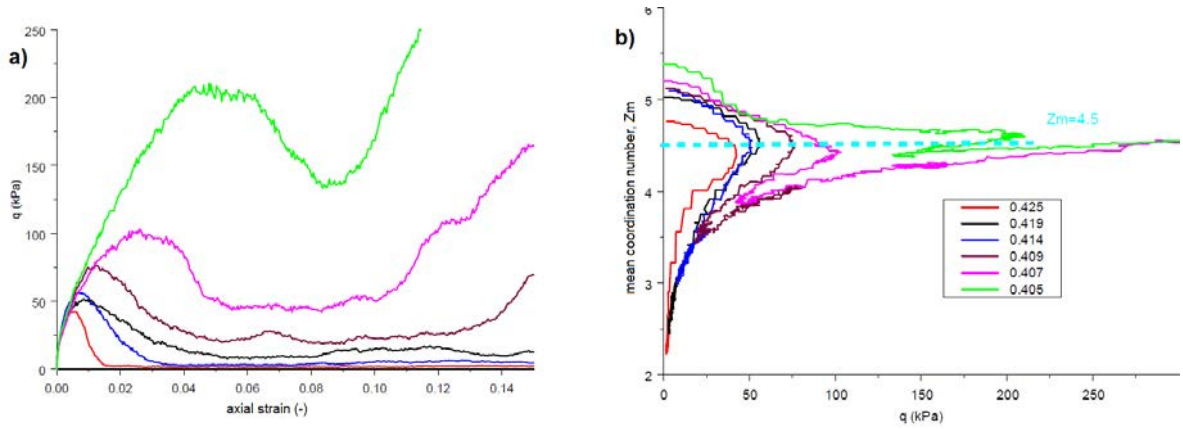

Figure 3.13: Comparison of meta-stable liquefaction in DEM assemblies of varying porosity to evolution of mechanical coordination number (*Zm*) and formation of a mechanism, taken from Gong (2008). a) – deviator stress, b) – mean coordination number as a function of deviator stress; peak deviator stress coincides with the critical coordination number of 4.5.

Liquefaction resistance, and thus the critical coordination number, is influenced by the shape and texture of particles. Resistance was reduced slightly by addition of crushed glass fines to uniform sand but much more significantly when the same proportion of smooth glass spheres were used (Wei and Yang, 2014). Nouguier-Lehon (2010) was able to show that hexagonal particles in DEM simulations developed additional rotation resistance when compared to circular particles, partly due to their ability to make face-to-face contacts. Increasing particle friction coefficients causes greater dilation under shear (Kruyt and Rothenburg 2006), a higher ultimate coordination number at the critical state, and thus a lesser tendency for the soil skeleton to become an unstable mechanism. As frictional, elongated and angular particles remain static

with fewer contacts, more contacts must be broken to liquefy. Well-graded materials also have increased resistance, due to more contacts being initially available.

Fabric rearrangement, which implies inducing micro-structural anisotropy, may cause weakening in another direction: Doanh et al. (2012) showed a cycle of drained compressive deviator stress (in a triaxial cell) applied to contractive sand increases compressive strength, but reduces extension strength (Figure 3.14). Unlike the Mohr-Coulomb failure envelope, which is not significantly altered in these tests by stress history, the Instability Line can be changed by medium or large-strain fabric rearrangement. This suggests fabric rearrangement within the stable domain (in this case, drained loading) can strengthen a liquefiable soil. It also indicates the risk posed by stress rotation, such as observed at high utilisation in Chapter 2.4.5; extension resistance could be significantly lowered by compaction during road construction and traffic loads. It should also be noted that much of the experimental data is from isotropically consolidated samples (e.g. Yamamuro and Lade, 1999; Wang et al., 2014, 2015a and 2015b). Anisotropic stress states, as expected for deep subsoils, may mean a smaller deviator stress increment is required to reach the Instability Line. Conversely, increasing lateral stresses on initially anisotropic stress states reduces the deviator stress, rather than causing the more destabilising effect of full stress reversal.

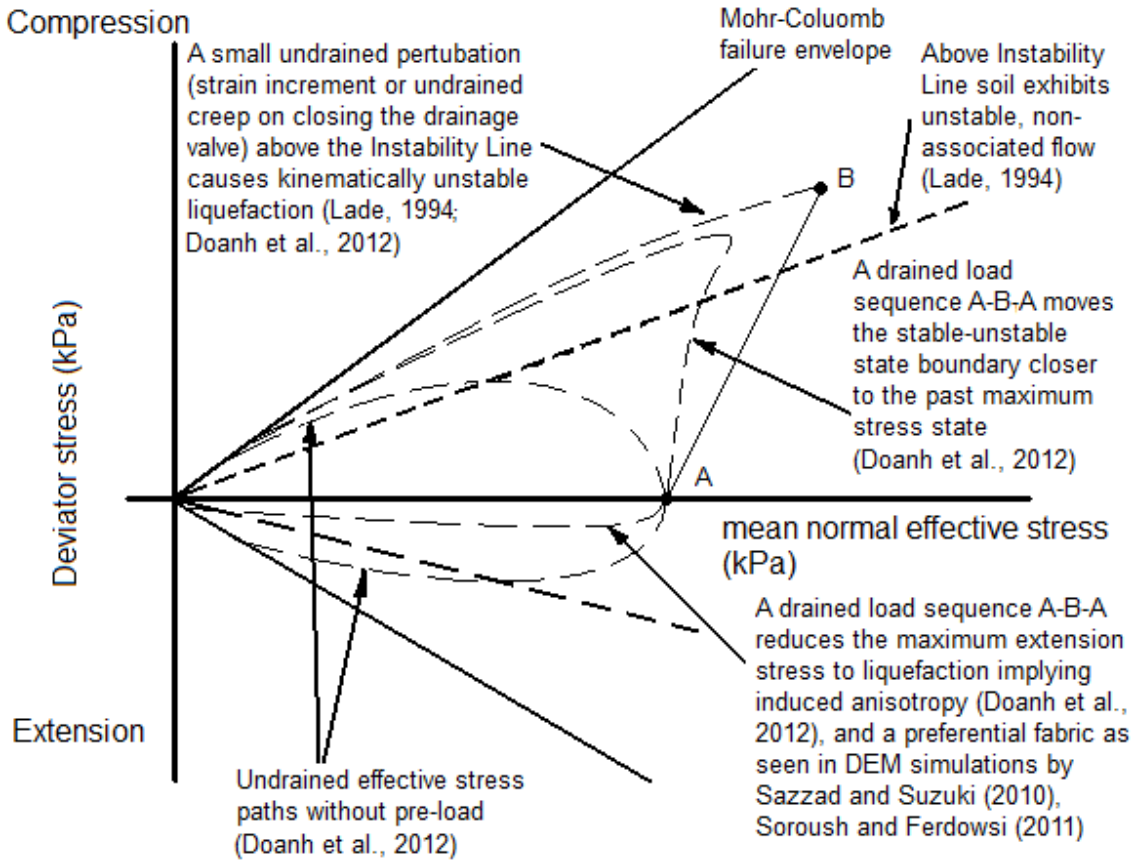

Figure 3.14: Load-induced anisotropy of static liquefaction resistance in undrained triaxial tests on loose sand (after Lade, 1994 and Doanh et al., 2012) as a result of stress history, implying development of preferential fabric.

3.3.3. Post-liquefaction recovery

After large restructuring, the new fabric may be able to restore strength, as is seen in experiments on silty sands by Yamamuro and Lade (1999) and on Mississippi River Valley Silt by Wang and Luna (2012), and DEM simulations by Gong (2008) and Gu et al. (2014). In this condition, the soil becomes dilatant and coordination numbers increase (Figure 3.13; porosities ≤ 0.409). It is noted by Yamamuro and Lade (1999) that increasing effective confining stress ($p' \geq 150$kPa; Figure 3.12) causes greater post-liquefaction recovery, the opposite of that observed in clean sands. This phenomenon is complex and dependent upon interaction between fines and the sand's intergranular pore space (Yamamuro and Lade, 1999; Gratchev et al., 2006; Maleki et al., 2011).

Zhang and Garga (1997) suggest the apparent recovery of strength after liquefaction arises primarily from large-strain triaxial end restraint effects. Numerical simulations by Gong (2008) and Gu et al. (2014), which do not have such physical restraints, suggest recovery may be limited to certain situations; at high porosity, post-liquefaction strength remains low or even tends to zero. Yamamuro and Lade (1999) also demonstrate post-liquefaction strength in sand is reduced by higher non-plastic fines content and slower strain rates. Post-liquefaction recovery may thus not be reliable: the avoidance of liquefaction rather than utilisation of post-liquefied strength should be the preferred strategy.

3.3.4. Thermodynamics of meta-stability

Meta-stable soil is initially in a precarious state and must have a high compactivity: only a small disturbance is necessary for large particle skeleton contraction. As the average coordination number drops below that for statical determinacy, it follows that a large portion must be in a fluidised, dynamic state. Given the loss of controllability at macro-scale and corroborating DEM observations (Figure 3.6), these fluidised regions are likely to become connected, similar to observations by Blumenfeld (2010). Liquefaction skeleton collapse can be considered a chain reaction initiated by sufficient agitation of particles into a low compactivity state.

The conditions for liquefaction can themselves be disrupted: overconsolidation (Wang and Luna, 2012), allowing volume change (Lade, 1994) or a cycle of drained load (Figure 3.14) can increase resistance. Each of these actions decreases the specific volume of a soil relative to normal consolidation at that pressure. Reducing compactivity: such processes applied under stable conditions may stabilise a

liquefiable soil. Medium-strain cyclic loading at sub-liquefaction strains induces pore water pressures and thus a tendency for soil skeleton contraction. If subsequent consolidation is permitted, as discussed in Section 3.5., this will reduce the specific volume and could be effective in remediating liquefiable soils.

3.4. Loading rate-dependent behaviour

Heavy haul vehicles apply longer periods of load due to slower vehicle travel speeds; for example a 60 m long module travelling at 5 km/hr will take around 45 seconds to pass a given point. For the critical design case of normally consolidated soil at depth, vertical stress from the multi-wheeled vehicle can be simplified into a single stress pulse (see Chapter 2.4.1). Transient stress can therefore approximate to a single cycle with an equivalent period of around 0.02 Hz. In contrast, much of the literature uses faster rates: Heath et al. (1972) at 0.5 Hz, the majority of Overy (1982) at 0.1 Hz, Andersen et al. (1988) at 0.1 Hz, Frost et al. (2004) at 2 Hz. It is necessary to consider what impact this slower speed and longer exposure to stress will have on cyclic degradation.

Deformation and pore pressure response of fine-grained soils in particular, has been observed to be a function of the loading rate (Overy 1982; Teachavorasinskun et al. 2002; Li et al, 2011). Patterns of pore water pressure and strain accumulation rates in cyclic loading, as shown in Figure 3.10, also occur during undrained creep (Singh and Mitchell 1968; O'Reilly et al. 1988). This indicates rheology may provide good analogy to cyclic loading at different rates. Hyde (1974) and Li et al. (2011) use creep analogy to predict cyclic deformations of clays below failure. Accuracy is good at low stresses and

strains, but less reliable once strain rates accelerate to failure. Li et al. (2011) find close agreement in accumulation of strain over time under cyclic regimes of the same stress but varying frequency, suggesting that the time spent experiencing a given stress controls cyclic strain accumulation.

Overy (1982) indicates shear strength of silty clay increases at faster strain rates (also found by Andersen, 2009), due to lower pore water pressures generated; the stress path changes but effective strength parameters are unchanged. This could suggest a lower threshold stress for slower loading (as hypothesised by Ward, 1983). The effective stress state and thus accumulation of pore water pressures are expected to control shear-banding initiation, so failure should occur after fewer cycles of slower load. In the large-strain, degradational regime, behaviour is likely to be increasingly viscous and time-dependent. Selection of appropriate cyclic loading rates is important to capture realistic behaviour.

Ultimate failure through shear banding (i.e. as expected in clays and also sands/silts which recover post-liquefaction) requires localised volumetric expansion within the shear band for softening (Schofield and Wroth, 1968; Atkinson, 2000). The reduced time available for localised drainage at faster loading rates implies additional resistance to shear banding (as observed by Atkinson, 2000) and so increased risk of failure for slower cyclic loads.

Vaid (1988) found similarity between failure strain in strain-controlled triaxial tests (at different strain rates) and the strain at which minimum strain rate occurred in stress-controlled creep tests (beyond which strain accelerates to failure) in low plasticity,

sensitive clay. Similar commonalities in strain-dependent failure behaviour in sensitive clays have been observed in cyclic tests by Li et al. (2011) and Åhnberg & Larsson (2012): above the static failure strain in stress-controlled cyclic loading, deformation began to accelerate. Non-failed samples tested by Åhnberg and Larsson (2012) remained below, or marginally exceeded, the static failure strain during cyclic loading. It is possible that liquefiable silts, also dominated by meta-stable structure, behave similarly.

3.5. Influence of excess pore pressure consolidation

Consolidating contractant soil reduces the void ratio, increasing the critical state strength; the swelling of dilatant soil reduces the critical state strength (Schofield and Wroth, 1968). Strengthening from post-cyclic drainage was observed to be dependent on overconsolidation (i.e. degree of contraction or dilation) by Brown et al. (1977), who observed significantly improved static strength in normally consolidated clay, slight improvement of lightly overconsolidated clay and either no effect or slight weakening of heavily overconsolidated clay. Scale model cyclic loading tests on soft, contractant clay subgrade by Ravi et al. (2014) similarly demonstrated that as induced pore pressures consolidated, subgrade stiffness and strength improved. The cyclic pore pressure response also changed from contractant to dilatant, implying induced overconsolidation.

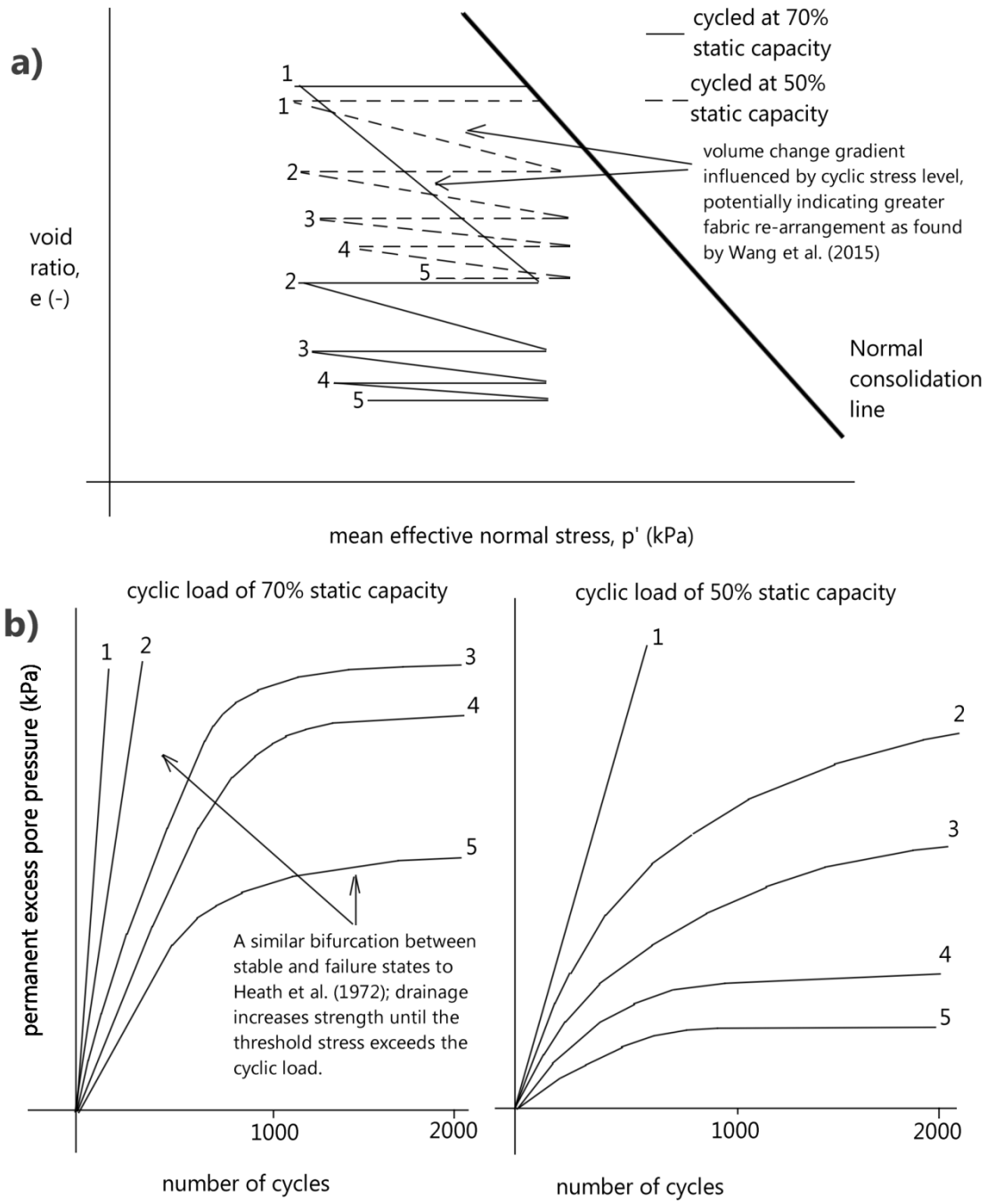

Figure 3.15: Increase in cyclic resistance as a result of drainage intervals between each day of testing (b), after Overy (1982), implying increasing threshold stress. Numbers adjacent to curves refer to the day of testing, with overnight drainage between each. Changes to specific volume during drainage periods (a) after Overy (1982), showing initially steep volume change gradient becoming shallower.

Tests by Overy (1982; Figure 3.15) found samples initially failing under cyclic loading develop increased cyclic resistance if drainage of residual pore water pressures between loading periods was permitted. An increased threshold stress is apparent; it is unclear whether this is simply due to the increased strength or whether a higher cyclic stress normalised to static strength is possible as a result of fabric rearrangement and induced overconsolidation.

Liquefiable silts are similarly strengthened by consolidation, but only if sufficient strain is induced (Wang et al., 2014); samples retained liquefiable behaviour and did not gain strength from consolidation if the cyclic yield strain of 0.5% was not exceeded. This implies that both immediate reduction in post-cyclic strength and consolidation strengthening require large-strain re-structuring. Data in Wang et al. (2014) also demonstrates the difficulty of controlling this behaviour in liquefiable soils; strains increase gradually up to cyclic yield (i.e. requiring 17no. to 26no. cycles of different stresses to achieve 0.8% to 0.9% strain) but rapidly afterwards (after an additional 5no. cycles in each case, strains were 7.1% to 8.5%). The strength increased significantly in post-liquefied reconsolidated samples, by a factor of 2.8 to 2.9 (Wang et al., 2014). After liquefaction the volume change gradient in *e, p'* space is close to that of the Normal Compression Line (NCL), similar to Figure 3.15, implying complete rearrangement and behaviour like a freshly deposited soil (Wang et al., 2014, 2015a, 2015b).

3.5.1. Consolidation-induced stress state changes

Cyclically induced overconsolidation moves the stress state closer to failure (Figure 3.3). Subsequent drainage reduces apparent overconsolidation, provided the gradient of void ratio against effective stress is less than that on the virgin NCL (Figure 3.16). Increasingly contractant behaviour was observed for liquefied samples subject to increasing degrees of reconsolidation (Wang et al., 2015a), although post-cyclic shear behaviour reamined overconsolidated (i.e. reducing pore pressures from >1% strain) even with full reconsolidation. Ultimate strength normalised by confining pressure was similar between reconsolidated samples and those statically unloaded to the same OCR (Wang et al., 2015a).

Consolidation volume change gradient appears to depend upon whether large-strain cyclic degradation is effected: samples failing cyclically are often nearly parallel with the virgin compression line, while stable samples follow a gradient similar to the swell-back line (Brown et al., 1977; Overy, 1982 and Figure 3.15). When liquefaction resistance is increased by addition of bentonite (Wang et al., 2015b), pore pressures generated by reaching 5% double amplitude cyclic strain are lower, the volume change gradient relative to the NCL is shallower and strength gain upon reconsolidation is reduced. In general, plastic clay soils are expected to require more strain to reach strain thresholds than granular ones (Díaz-Rodriguez and López-Molina, 2008) and thus may require higher strains to achieve similar large-strain restructuring.

Strength increase during consolidation should reduce the proportion of strength mobilised, strain experienced and pore water pressures induced under constant cyclic load (Figure 3.16), reducing risk of failure. However a volume change gradient parallel

to the virgin compression line fully retains apparent overconsolidation (Schofield and Wroth, 1968). Liquefaction and reconsolidation can reduce the subsequent strain to failure in post-cyclic static shear and change the failure mode to a brittle, strain-softening one (Wang et al., 2015a). The tendency is reduced in more clay-dominated soils (Wang et al., 2015b), although this may be due to the lesser degree of restructuring and more contractant response. Large strength increases thus carry risk of increasingly brittle behaviour as well as larger road settlements and associated maintenance.

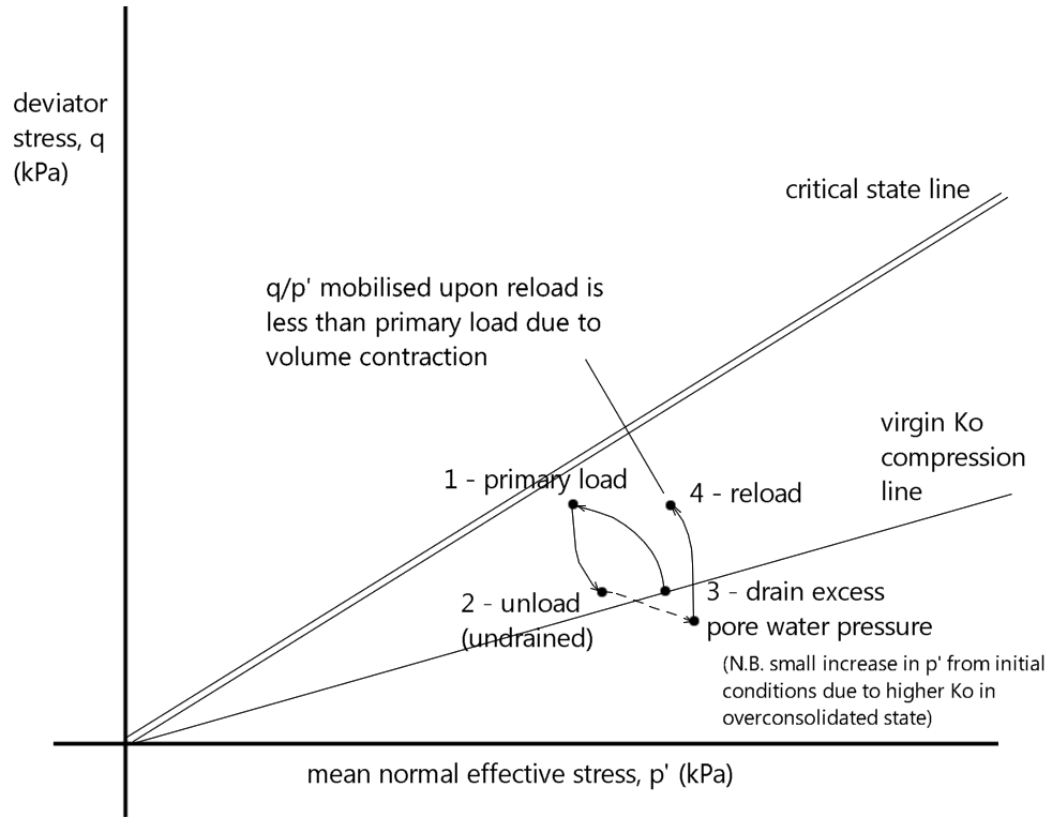

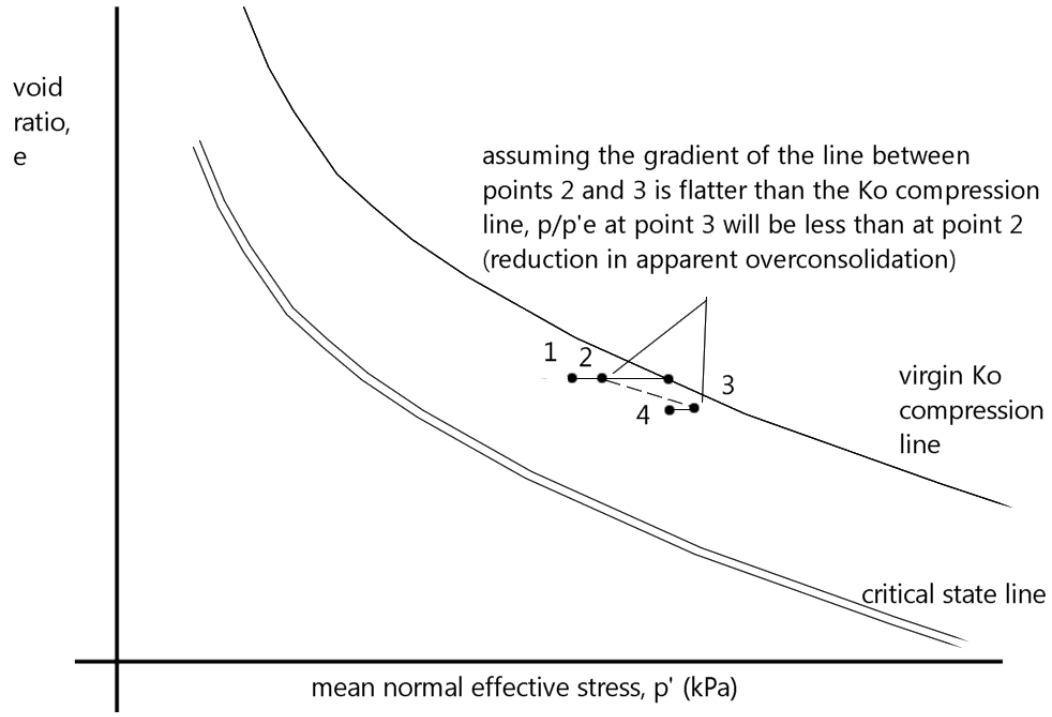

Figure 3.16: Representation of cyclic stress paths with full drainage of excess pore water pressure between loads in e, q, p' space

3.5.2. Induced changes to permeability

In low permeability soils, slow dissipation and retention of excess pore water pressures can result in failure if net accumulation results in effective stresses intercepting the Hvorslev Surface or tension cut-off. Reducing porosity reduces permeability: Dewhurst et al. (1996) found the logarithm of clay permeability (tested range of 10^{-10} m/s to 10^{-12} m/s) decreased linearly with mean normal effective stress during one-dimensional consolidation. A slight reduction of permeability (by a factor of 0.84 to 0.96) was also apparent after liquefaction (Wang et al., 2015b).

A reduced compressibility from densification (O'Riordan, 1991) often counteracts this effect to accelerate consolidation, which depends on the relative changes to both. Cyclically-induced volume collapse of a meta-stable soil could reduce permeability without the expected reduction in compressibility, as is apparent in Overy (1982) and Wang et al. (2015a, 2015b). After liquefaction particularly, excess pore water pressure consolidation may be slower.

Bearing in mind the importance of consolidation to strength and these inherent uncertainties, laboratory values for estimation of consolidation times must be treated as approximate. Consolidation times directly scaled up from laboratory samples are typically overestimated (Davis and Poulos, 1972) due to two or three dimensional drainage paths and permeability anisotropy (particularly silt/sand partings). Where consolidation is critical to performance, in-situ monitoring of pore water pressures can control these uncertainties, avoiding unnecessary delays from overestimated consolidation times and reducing risk of subgrade damage from underestimates.

3.6. Conclusions

A review of soil mechanics literature indicates the following:

- Two failure modes are of primary concern to heavy haul roads; dilatant shear banding and meta-stable liquefaction. The second mode primarily applies to loose silts. Conventional traffic loads are usually too shallow to affect meta-stable soils, however the deeper nature of heavy haul road stresses may mean these soils are now influential. Subgrade soil directly beneath the road is likely to be overconsolidated (Chapter 2.3) and thus not prone to liquefaction (Chapter 3.3.1). Whilst the larger settlement expected from heavy haul loads is likely to reduce the strength and stiffness of the pavement materials and this upper subgrade soil, this part of heavy haul road design is considered to be well-served by more conventional analysis (Chapter 2.5). The greater risk of deep liquefaction from traffic load, currently poorly understood, is instead taken as the focus of the following experimental study.
- Normally consolidated soil, e.g. at 6-12m depth in the analysis in Chapter 2.5, is at risk of liquefaction (as identified in Chapters 2.5 and 3.3) from comparatively small transient vertical stresses (less than 10% of the effective overburden stress of σ'_{z0} = 50-100kPa, i.e. $\Delta\sigma_z$ = 5-10kPa). Such stresses could be applied by vehicles with weights of 390 to 1000 tonnes, i.e. well within the typical working range from Chapter 1.1. Larger vehicles (e.g. 1000 to 3000 tonnes) may apply stresses well in excess of this, i.e. 35-70% of the effective overburden stress.
- Behaviour of soil under load is highly strain-dependent, with inter-particle slippage and fabric rearrangement increasingly important as strains increase.

Large-strain degradational behaviour may be more acceptable for heavy haul roads as stability only needs to be maintained for a small number of loads.

- Meta-stable liquefaction is governed by the initial fabric of a soil, which is prone to catastrophic collapse from small disturbances. This liquefiable state can be disrupted by overconsolidation, stress history and reduction in specific volume. However much of the experimental work is carried out on isotropically consolidated samples and a study of behaviour under anisotropic conditions is necessary as an anisotropic stress state can significantly reduce strength (Chapter 3.3.2).
- Irrecoverable excess pore pressures in a normally consolidated soil have the effect of inducing an apparent overconsolidation, increasing the risk of shear banding failure. As concern is primarily on avoidance of ultimate failure, this condition is of increased importance.
- Cyclic degradation primarily takes place in the large-strain regime associated with complete re-structuring of a soil skeleton; this regime is also associated with strength gain if a cyclically loaded soil is subsequently allowed to consolidate. Increased tolerance of plastic strains may permit utilisation of this additional strength.
- Irrecoverable strain, pore pressure accumulation and initiation of shear banding are sensitive to loading rates and the time spent under a certain stress. Loading rates for heavy haul roads are much slower than typical traffic loads and this may present some unusual hazards.

As such, the following novel elements of the heavy haul road scenario are proposed to be investigated experimentally:

- **Cyclic strain regime:** Cyclic degradation and consolidation strengthening response of soil subject to large strains, concentrated in the compression zone under significantly anisotropic stress conditions. The focus should primarily be upon avoidance of kinematically unstable failure.
- **Liquefiability:** Factors which control initiation of collapse and methods for remediating liquefiable soils through traffic loading. The efficacy of these methods on non-liquefying clay soils, which fail through softening, should also be considered so a strategy that copes with inherent soil variations can be developed. Bearing in mind the potential for sudden, catastrophic collapse, the majority of tests will be on liquefiable silt. Cyclic stresses should be selected close to the threshold stress for liquefaction (expected to be 5-10% of the effective overburden stress) to investigate how liquefaction is initiated and how it can be controlled. There is also a need to investigate the response to small numbers of stress cycles far exceeding the liquefaction threshold stress (i.e. 35-70% of the effective overburden stress, i.e. 4 to 15 times the threshold) to investigate the risks posed by the largest vehicles.
- **Consolidation:** The dissipation of cyclically induced excess pore pressures, the reduction in induced overconsolidation and the effects on soil response are not well understood but are critical to the performance of heavy haul roads, particularly at large strains and in meta-stable soils. The strengthening effects

of full and partial consolidation between loads, replicating variations in in-situ permeability, drainage path and haulage programme, should be investigated.

- **Increased load duration**: The impact of slower loading rates on degradation and failure, particularly on liquefaction and the threshold stress. For a 50-second load passage (Chapter 3.4), a cycle frequency of 0.02Hz may be appropriate, however as slower load is anticipated to be more damaging, testing at lower frequency (i.e. 0.01Hz) and also investigating variation in response to load with frequency variation is proposed to develop an understanding of the risks presented by differences in loading rates.

CHAPTER 4 – LABORATORY TESTING METHODOLOGY DEVELOPMENT

4.0. Introduction

This chapter is split into two parts: the first (Section 4.1) details the development of the test methodology; the second (Section 4.2) evaluates the repeatability of this methodology.

4.1. Development of testing methodology

Meta-stable liquefaction has been identified as the principal geohazard for heavy haul roads (Chapters 3.3 and 3.6); for experimental testing of liquefiable soil, the following necessary conditions have been identified (Chapter 3.3.1 and 3.3.2):

- Low plasticity, principally silty or sandy soil for 'granular' behaviour (Andrews and Martin, 2000; Boulanger and Idriss, 2006)
- Anisotropic normal consolidation
- No volume change permitted (undrained)

A sandy deposit in the field is unlikely to produce an entirely undrained response under load (Chapter 3.3.1); the risk of liquefaction is thus lower. A low plasticity silt soil was therefore chosen to represent the worst-case in-situ liquefaction risk.

Attempts were made to replicate alluvial and delta silt deposits investigated by Atkins in Central Asia (see Chapter 1.4). Proportions of inactive silt and clay were chosen to match the lower bound of Plasticity Index (7-16%), determined by trial and error

(Chapter 4.1.1). Samples with lower plasticity than this were possible to fabricate using a greater silt proportion, but were too easily disturbed to mount in a triaxial cell.

The Central Asia ground investigation identified the silts to be sandy to very sandy (up to 20% sand content). Sand can strongly influence a soil's liquefaction: Maleki et al. (2011) observed a minimum resistance of sand-silt mixtures with between 25% and 65% sand content. The sand fraction's grading is also highly influential (Chapter 4.2.2.2). On this basis, a poorly graded sand fraction of 25% was chosen, providing the additional benefit of higher permeability and faster consolidation. Stress history strongly influences liquefiability (Chapter 3.3.1) so close scrutiny was given to the reconsolidation of samples after production (Chapters 4.1.2 and 4.1.4.2) to ensure a normally consolidated state, representative of recent deposits, is achieved.

Figure 4.1 shows the basic process behind preparation and testing of soil samples.

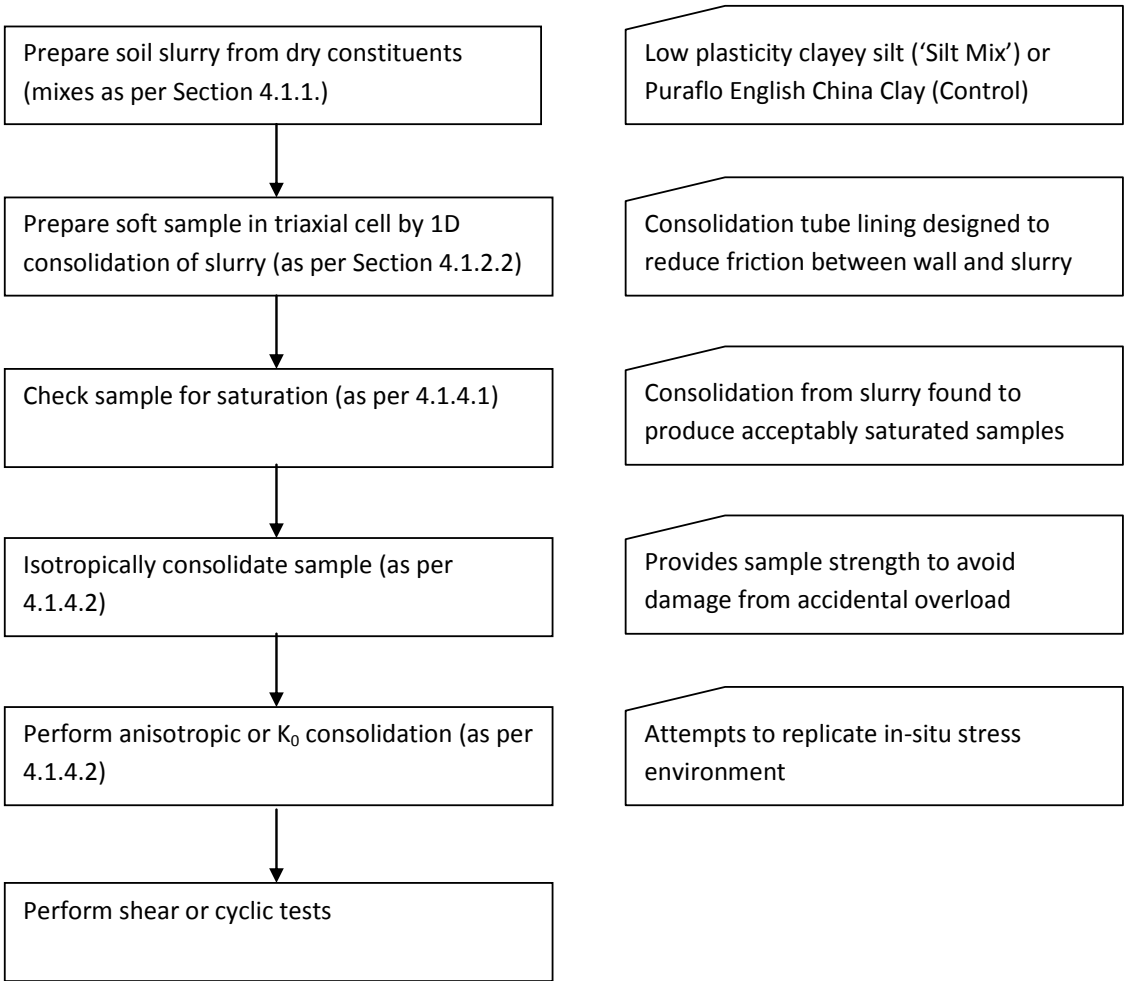

Figure 4.1: Preparation and testing process for soil samples.

4.1.1. Soils used for testing

A source of soil was required which reflects soft, normally consolidated alluvial or marine clay/silt soil deposits. A soil which shows a tendency to liquefy and is measurably affected by strain rate was also desirable as these factors are not commonly problematic for conventional roads but may be influential for heavy haul roads.

Many studies into cyclic response of soils use 'undisturbed' *in-situ* soil samples, e.g. Zapata-Medina et al. (2014) - recovered using Shelby tubes, and Li et al. (2011) and Bradshaw and Baxter (2007) – trimmed from block samples. The aim was to test in the region of 100no. samples of 100mm diameter and 200mm length (i.e. around 300kg of

soil) over the course of the test programme and acquiring this amount of high quality, undisturbed field samples was not considered practical. Instead samples were reproduced from bulk dry soils.

Consistency between samples is important to minimise the impact that variation of soil properties has on the findings of the test programme, therefore it was decided to use commercially available, quality controlled products, rather than site-won fill. Two separate soils were desired:

1. A low plasticity, clayey silt soil which displays more unusual behaviour under load such as liquefaction and non-associated flow.
2. An intermediate to high plasticity clay soil for which behaviour is more conventional, i.e. exhibits perfect plasticity and associated flow, similarly to the Cam-Clay model (Schofield and Wroth, 1968), to act as a control.

Low permeability soils were desired as these will respond in an undrained manner to slow-moving heavy haul vehicles; cyclic degradation is effected through development of excess pore pressures.

The following dry constituents were identified for use:

- **Silverbond M10 Silica Flour** – this is a silt-sized powder derived from attrition of silica sand, which behaves as a fine (slow draining) soil but has very low plasticity. When mixed with water to form a firm solid, it liquefies and flows under repeated hand pressure but reverts to a solid state when not loaded.

- **Puraflo 50 English China Clay** – Kaolinite clay with reasonably well-known properties, as summarised in Valls-Marquez (2009), and not liquefiable under hand pressure (as was observed for the silica flour).
- **Blooma playpit sand (available from B&Q stores)** – a medium to fine, subangular to angular-grained silica sand.

Based on classification tests carried out on these constituents (Section 4.1.1), the following soil mixes were chosen for testing:

- Silt Mix – a liquefiable sandy clayey silt mix: 25% sand, 60% Silica Flour, 15% China Clay. This material displays clear dilatancy and responds to behaves in a manner expected for a clayey silt when subject to hand tests in accordance with BS 5930 (BSI, 2015b).
- Control Mix – 100% Puraflo English China Clay; this material has been extensively studied and as testing on Kaolin clays forms much of the basis of the Cam-Clay model (Schofield and Wroth, 1968), it makes an excellent control.

The dry constituents were mixed with reverse osmosis deionised water (1µS/ml) to maintain consistent soil pore water chemistry.

The particle size distributions for the soil constituents were performed according to BS 1377-2 (BSI, 1990a) using the dry sieve and hydrometer sedimentation methods; results are presented in Figures 4.2 to 4.4.

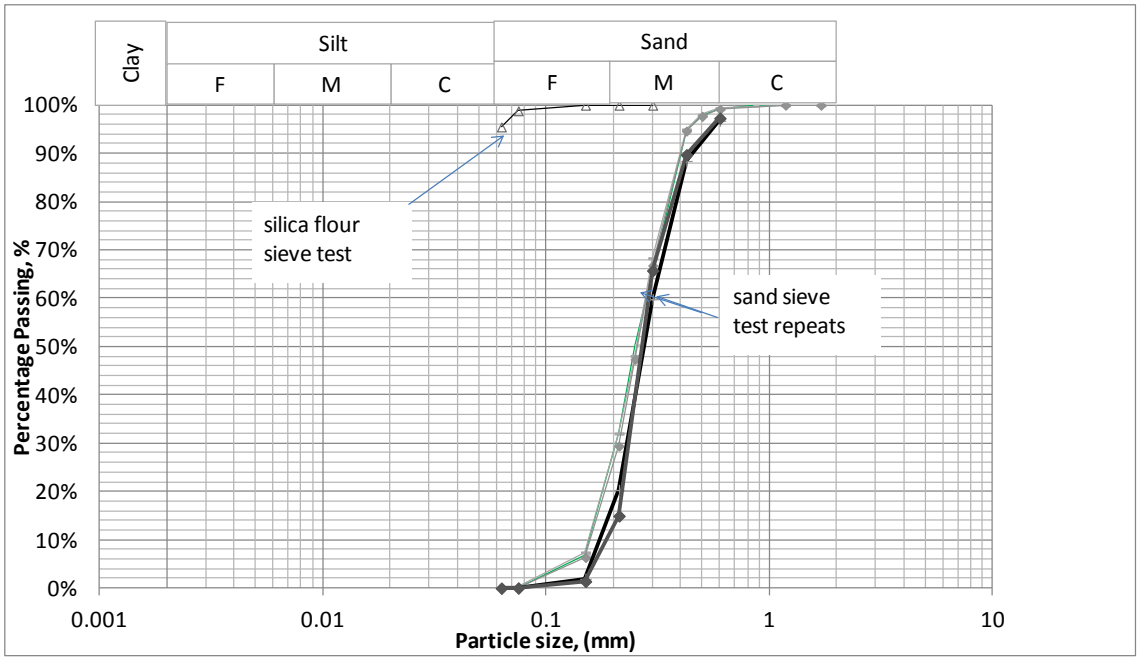

Figure 4.2: Dry sieve Particle Size Distributions

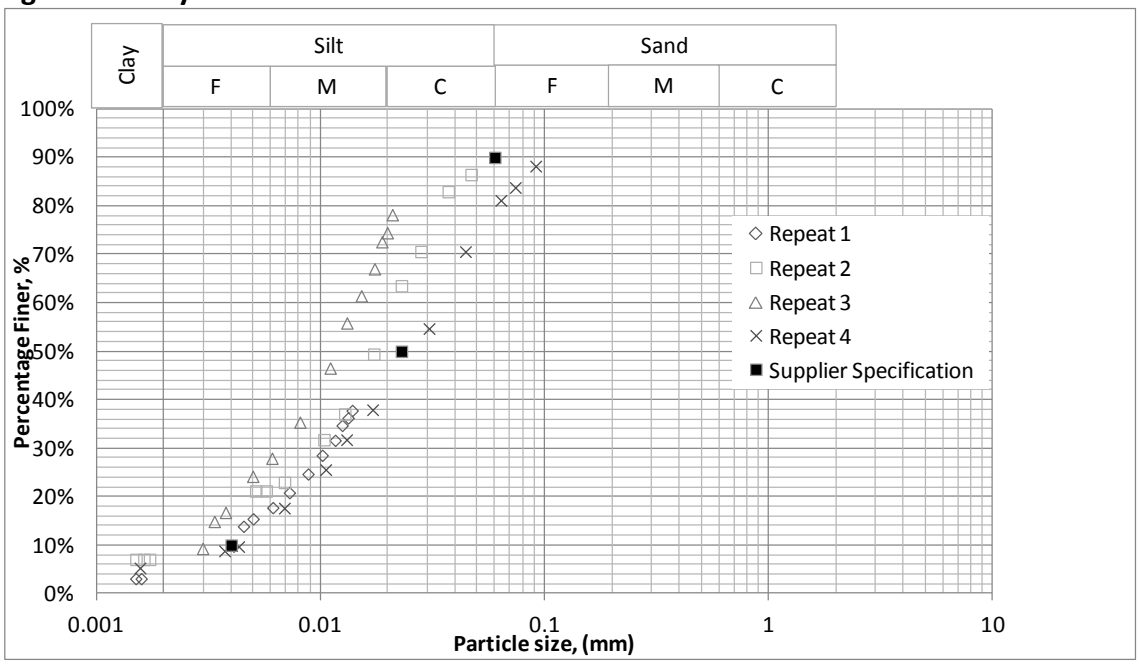

Figure 4.3: Hydrometer Particle Size Distributions for Silica Flour and specification from supplier data sheet (for reference)

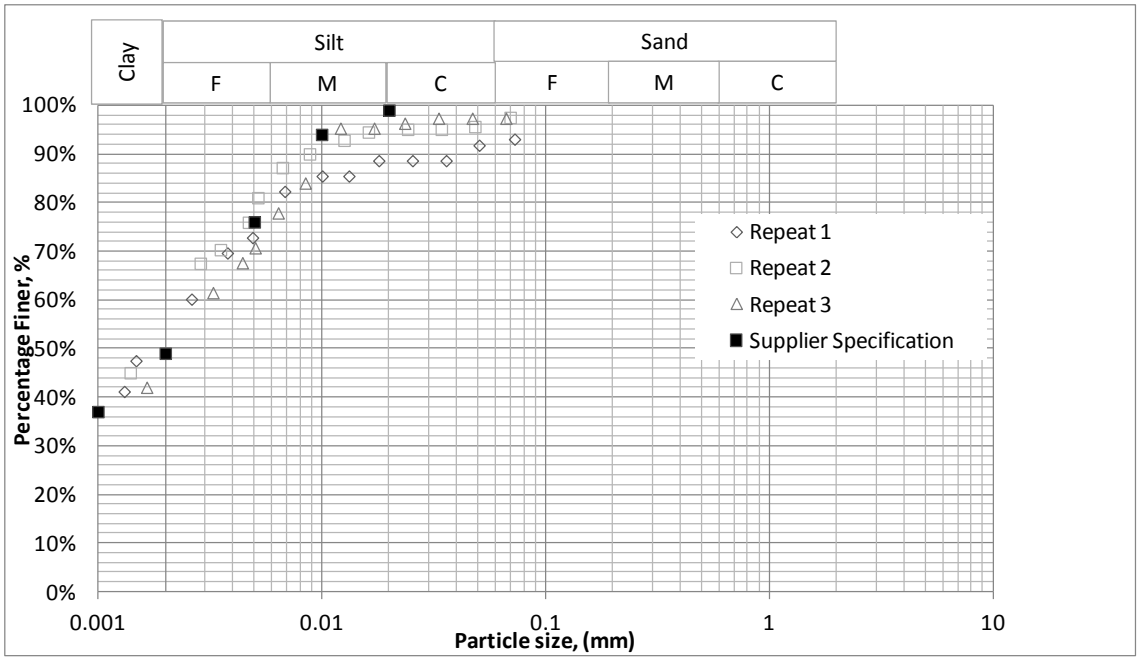

Figure 4.4: Hydrometer Particle Size Distributions for China Clay and specification from supplier data sheet (for reference)

The sand is medium to fine and uniformly graded, with a Coefficient of Uniformity of 2. In order to avoid the need for corrections to plasticity results (BSI, 1990a) only the fraction of the sand passing a 425µm sieve is used in the soil mixes, i.e. the coarser fraction (5% by mass) is disposed of. Particles finer than 63µm are negligible (<0.1%). Part way through the methodology and repeatability testing stages, a new batch of sand (supplied from the same source) was obtained which was found to be slightly coarser: the impact of this change is discussed in detail in Chapter 4.2.2.2.

The Silica Flour has a small proportion (4%) of particles in the fine sand range (63 to 75 µm) when dry sieved and hydrometer tests indicate it is predominantly medium to coarse silt, with a clay-sized particle content of 3-7%.

All of the English China Clay passes the 63µm dry sieve; hydrometer tests indicate it is predominantly clay-sized particles (40-55%) and fine silt (25-45%) with a small (10-20%) proportion of coarse to medium silt.

There is a disagreement between dry sieve and hydrometer particle size distributions. Hydrometer tests tend to overestimate the fraction coarser than 63µm; use of Stokes' Law, which assumes spherical particles (BSI, 1990a) rather than measuring the least dimension, may thus overestimate diameters of elongated platy particles. Microscope imaging (Section 4.1.3) indicates silt and clay particles are elongated and platy which may explain this discrepancy. Furthermore, at the start of a hydrometer test, when the coarse fraction is measured, small errors in timing and measuring have a much greater impact: these errors may cause apparent discrepancies.

Plasticity testing to BS 1377-2 (BSI, 1990a) was carried out on the fine soil constituents. Puraflo English China Clay was found to have a Liquid Limit of 58-61% LL and a Plasticity Index of 36-39%, i.e. is classified as a High Plasticity Clay to BS 5930 (BSI, 2015b). It was difficult to perform repeatable Liquid Limit tests on the Silica Flour; close to its Liquid Limit, it displays rate-dependent strength and liquefaction. Small vibrations and the time between taking readings significantly influenced results. Instead, the Plastic and Liquid Limits were found for mixes of Silica Flour and English China Clay in varying proportions and the results extrapolated, shown in Figure 4.5. The extrapolated Liquid Limit was found to be 20-22% with an extrapolated Plasticity Index of 4-6%, i.e. Silica Flour is classified as Low Plasticity Silt to BS 5930 (BSI, 2015b).

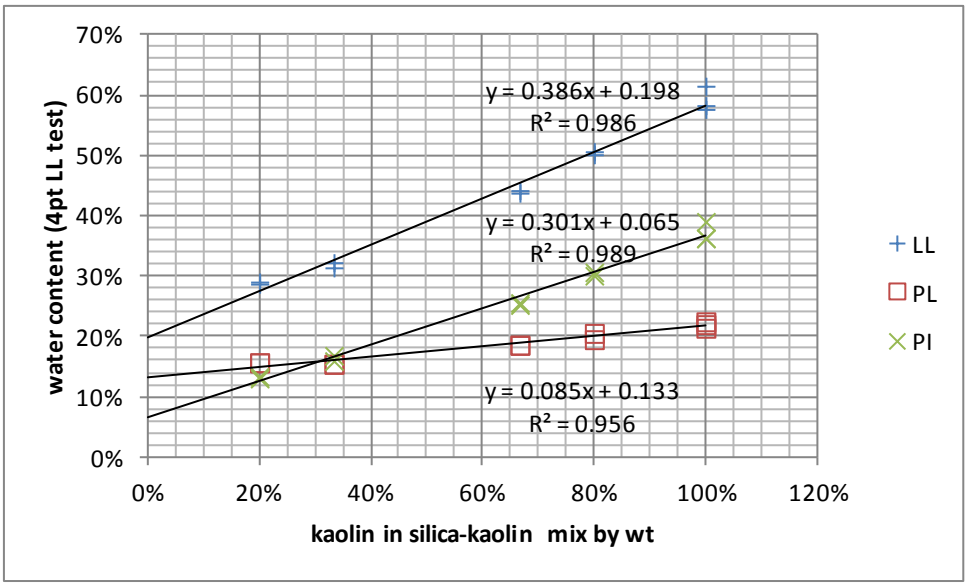

Figure 4.5: Results of Liquid and Plastic Limit tests on Silica Flour:China Clay mixes, with extrapolation of four-point test results following BS 1377-2:1990 (BSI, 1990a) to estimate properties of Silica Flour.

Results from particle density tests using the small pyknometer method to BS 1377-2 (BSI, 1990a) are summarised in Table 4.1:

Table 4.1: Particle densities for various constituents using small pyknometer method in BS 1377-2:1990 (BSI, 1990a)

Material	No. tests	Relative particle density
China Clay	2	2.63 (± 0.01)
Silica Flour	2	2.70 (± 0.01)
Sand	2	2.69 (± 0.02)

Plastic and Liquid Limit testing of the Silt Mix soil from dry constituents indicate:

- Liquid Limit of 21-22% (5no. 4-point tests)
- Plastic Limit of 14-15% (6no. tests)
- Plasticity Index of 7-9%

If each point of the 5no. 4-point Liquid Limit tests is treated as a single 1-point test, the Liquid Limit is in the range 20-23%; this partly indicates the increased error associated

with the 1-point test, but also better illustrates the inherent variability of Liquid Limit results, which are otherwise removed by the use of the best-fit line in the 4-point test. Index tests are comparable to Mississippi River Valley Silt tested by Wang et al. (2011; 2014; 2015a; 2015b), which had PI = 6%, LL = 28% and clay content = 14.5%. These studies, which are concerned with liquefaction, post-liquefaction strength loss and consolidation strengthening, were therefore used as a reference for behavioural changes of a similar material in similar loading conditions.

The Silt Mix soil is classified as a Low Plasticity Clay-Silt to BS 5930 (BSI, 2015b). To examine whether the properties of the soil are altered by sample preparation methods, Plastic and Liquid Limit tests were repeated on slurry-consolidated samples after testing, which indicates:

- Liquid Limit of 20-22% (14no. 4-point tests)
- Liquid Limit of 19-22% (treating the above as 70no. separate 1-point tests)
- Plastic Limit of 13-15% (14no. tests)
- Plasticity Index of 6-8%

It does appear that plasticity is slightly reduced in sample preparation and/or testing; clay may not be transferred from the mixer in full, or particles in suspension within the slurry mix may be removed during consolidation. Bearing in mind experimental variations apparent and the large overlap of the two data sets, these differences are relatively small.

4.1.2. Preparation of triaxial test samples

The response of reconstituted samples can be significantly influenced by the preparation method. The principal aim of the sample preparation method is to replicate the response typical of a young, normally consolidated deposit. Furthermore, when handling these soft soils there is increased potential to induce damage, which must be minimised.

In order to test samples in a normally consolidated state, they must be consolidated in the triaxial cell to effective stresses 1.5 to 4 times their preconsolidation pressure (Overy, 1982; Santagata and Germaine, 2005). Changes in stress-strain behaviour with effective consolidation stress cannot necessarily be described by normalising with respect to the maximum consolidation stress: partial liquefaction observed in normally consolidated reconstituted Blue Boston Clay at low consolidation stress was not apparent at higher stresses (Zapata-Medina et al., 2014) and a greater post-liquefaction undrained shear strength of sand is apparent with increasing effective stress (Yamamuro and Lade, 1999). A compromise needs to reached between soft samples (i.e. consolidated to low effective stresses) and ones which behave like normally consolidated soil (i.e. higher consolidation stresses to erase memory of overconsolidation). A further complication is introduced in the handling of samples prior to triaxial testing; they must be sufficiently strong to resist their own weight and withstand gentle manipulation without slumping.

A commonly used preparation method for clays and plastic silts is to mix with water to form a slurry and then consolidate to the desired water content by application of axial load in a rigid cylinder (i.e. K_0 consolidation); this has been used in a wide range of

studies into cyclic loading (Overy, 1982; Ward, 1983; Wang et al., 2011, 2014). The speed of this procedure is dependent upon the soil permeability and cylinder dimensions; for many authors (Overy, 1982; Ward, 1983), consolidation took several days to complete.

For sands and non-plastic silts, dry or wet deposition methods are often used (Gratchev et al., 2006; Yamamuro and Lade, 1999) whereby soil is poured into a mould with careful control of drop height and then agitated to achieve the required density. This method is less successful for soils of non-uniform grading, as segregation of coarse and fine proportions occurs (Ladd, 1978; Amini and Qi, 2000).

Ladd (1978) instead developed a method for sands where moist soil was compacted to achieve the appropriate density, later adapted by Bradshaw and Baxter (2007) to silt. To avoid the lower layers achieving higher densities as a result of compaction on layers above, the compaction effort is increased for each subsequent layer ('under-compaction'). The required effort is determined by trial and error (Ladd, 1978; Amini and Qi, 2000; Bradshaw and Baxter, 2007). If certain layers have significantly lower densities, failure will localise in these layers (Ladd, 1978; Bradshaw and Baxter, 2007). The layering and intra-layer density gradients in compacted soils are found to not significantly affect the failure mode (Amini and Qi, 2000).

Slurry consolidation and under-compaction methods were investigated further.

4.1.2.1. Development of under-compaction method

Constituents were mixed in a Hobart mixer on its slowest setting for a minimum of 30 minutes until an even consistency was achieved. Significantly longer mixing times were

avoided as the soil tends to dry out. Finished samples showed a maximum water content variation of 0.25% between 6no. equal slices.

Compaction was performed using two separate pieces of equipment, referred to herein as 'heavy' and 'light' equipment. Light compaction used standard Proctor test equipment as per BS 1377-4 (BSI, 1990b), with blows distributed evenly over the soil surface. Heavy compaction used heavy Proctor test equipment with a 100mm diameter rigid steel plate (the same size as the mould). Compaction using only one of these approaches developed inclined compaction planes: concave for light compaction and convex for heavy compaction (see Figure 4.6). Unlike horizontal discontinuities, found to have minimal impact on test results by Amini and Qi (2000), inclined compaction surfaces may intersect a slip plane and thereby have greater influence. Through trial and error, a mixed under-compaction method was used to produce approximately uniform and horizontal compaction planes (Figure 4.7). Compaction effort only varied for the first two layers (Table 4.2), expected to be due to stiffer base support and the soft, plastic nature of the material compacted (as opposed to the non-plastic soils tested by Ladd, 1978 and Bradshaw and Baxter, 2007) through which very little compaction energy appears to be transferred.

Figure 4.6: inclined compaction surfaces highlighted by adding red ink between layers. The sample is constructed from bottom to top. Left – heavy compaction, convex surfaces. Right – light compaction, concave surfaces.

Table 4.2: Under-compaction sequence using mixed 'heavy' and 'light' methods to achieve horizontal compaction planes

Layer	Compaction effort
1	2x heavy
2	4x heavy, 5x light
3 to 10	6x heavy, 5x light

Figure 4.7: A sample following 'mixed' compaction: layers are approximately horizontal and evenly spaced.

Compaction of these soft soil samples was performed in a 100mm diameter, 200mm high split mould with a 50mm extension piece. The surface was trimmed flush using a cheesewire.

4.1.2.2. Development of slurry consolidation method

A serious drawback of the slurry consolidation method is non-uniform water content across the sample, as it is then difficult to determine whether behaviour under load is representative of the whole sample or a localised area. Many authors have noted an uneven distribution of water content within slurry consolidated samples (Overy, 1982; Valls-Marquez et al., 2008; Wang et al., 2011). Additionally, as segregation of coarse and fine particles has been noted when pouring multi-graded sands and silts (Ladd, 1978; Amini and Qi, 2000), this is also a concern in thin slurries.

Water content of slurry for consolidation in the literature varies from around 1.5 times the soil's Liquid Limit (Wang et al., 2011) to up to 3 *LL* (Lin and Penumadu, 2005); 2 *LL* appears to be commonly used (e.g. Brown et al., 1975; O'Reilly et al., 1988; Head, 1986). Silt Mix slurry mixed at 2 *LL* was visually observed to undergo segregation of the coarse and fine fractions, as in Figure 4.8. At 1.5 *LL,* silt slurry was found by Wang et al. (2011) to show negligible segregation, also seen with Silt Mix slurry (Figure 4.8). In fact, Table 4.3 indicates a significantly higher coarse proportion at the top of a sample, implying segregation instead occurs during mixing, resulting in a concentration of coarse particles at the bottom of the vessel (i.e. the slurry poured into the cylinder last).

Figure 4.8: Silt mix slurry mixed and left to stand for 1 hour. Left – slurry mixed at 1.5 *LL*, relatively uniform. Right – slurry mixed at 2 *LL*, varying from thin suspension near the top to predominantly fine soil beneath, becoming coarser at depth.

Originally slurry was mixed by adding dry sand, then Silica Flour and then China Clay before adding water. The procedure was changed with dry constituents added in the reverse order; settlement of the sand observed during mixing would result in a more uniform spatial distribution rather than a concentration at the bottom. As is apparent in Table 4.3, this mixing procedure improves the uniformity of the samples. Figure 4.9 shows the particle size distribution of the fine fraction; bearing in mind the inherent experimental error in this test shown in Figure 4.3 and Figure 4.4, differences are small using the reversed mixing procedure.

Thick slurry has the additional advantage during preparation that it is less prone to squeezing out of the mould under initial consolidation load increments. Further reduction of the water content of the slurry to 1.1 *LL* was attempted but the thicker slurry developed air bubbles during pouring which were not all removed by consolidation.

Table 4.3: Wet sieve results for slurry consolidated samples indicating relative segregation of coarse and fine particles with various slurry mixing methods.

Wet sieve test (to BS 1377-2)		Soil coarser than 63µm	Soil finer than 63µm
Original mixing procedure	Top of sample	31.1%	68.9%
	Base of sample	26.8%	73.2%
Reversed mixing procedure (2no. tests)	Top of sample	28.9 - 29.0%	71.0 – 71.1%
	Base of sample	27.9 - 29.8%	70.2 – 72.1%

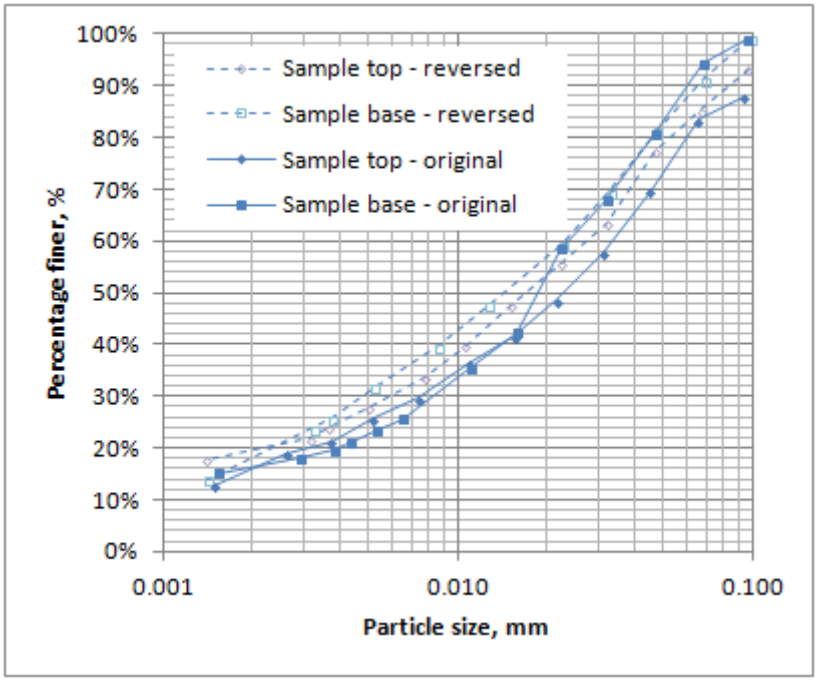

Figure 4.9: Hydrometer Particle Size distribution for the fine fraction of slurry consolidated samples using various mixing techniques.

Before pouring the slurry, it was taken from the Hobart mixer and then stirred by hand in a random pattern to disrupt any anisotropy of the slurry developed by the regular

pattern of the mixer. In order to avoid trapping air during pouring of the slurry, the bottom porous disc was covered with a thin layer of deaired water before pouring, as per Ward (1983). Once the slurry was poured into the mould, it was again gently stirred to remove any preferential arrangement from pouring and then gently shaken to remove air bubbles, as per Valls-Marquez (2009).

Consolidation in a rigid tube is known to be an imperfect replication of *in-situ* stress conditions, as tube boundaries exert some vertical frictional resistance, causing an uneven effective stress distribution throughout the sample, concave lenses and a 'wet' sample mid-section (Valls-Marquez et al., 2008). Differences can be significant; in the case of soil consolidated directly in a Perspex tube, Overy (1982) found 3-6% difference for a silty clay (*PI* = 13%) and Valls-Marquez et al. (2008) found up to 8.7% difference using China Clay (*PI* = 32%). A more advanced consolidation methodology by Wang et al. (2011), in which slurry was consolidated under vacuum in a latex membrane within a split mould to minimise friction, achieved water content differences of less than 1.2% in a silt (*PI* = 6%).

Silt Mix slurry consolidated directly in a Perspex tube was found to have a water content difference of 3-5% between the top and centre. The finished samples were impossible to handle: the mid-section was extremely soft (close to the *LL*) and unable to support its own weight. Pouring the slurry into a sleeve which was free to move relative to the confining tube and lubricating the interface between the two was found to be effective in reducing friction.

A critical part of the consolidation apparatus design was to ensure the sleeve extends over the top cap which applies the load; otherwise as the top cap settles, it can trap a small quantity of slurry between itself and the confining tube, which can cause the cap to stick. This can the result in incomplete consolidation, residual excess pore pressures in the sample centre and a similar wet mid-section, as is apparent in Figure 4.10. Consolidating with extended sleeving reduced water content differences to a maximum of 1.2% (Figure 4.11).

Figure 4.10: Central wet zone in a consolidated sample (a sleeve is used but does not extend to include the top cap). Localised lower strength is apparent from the central bulging.

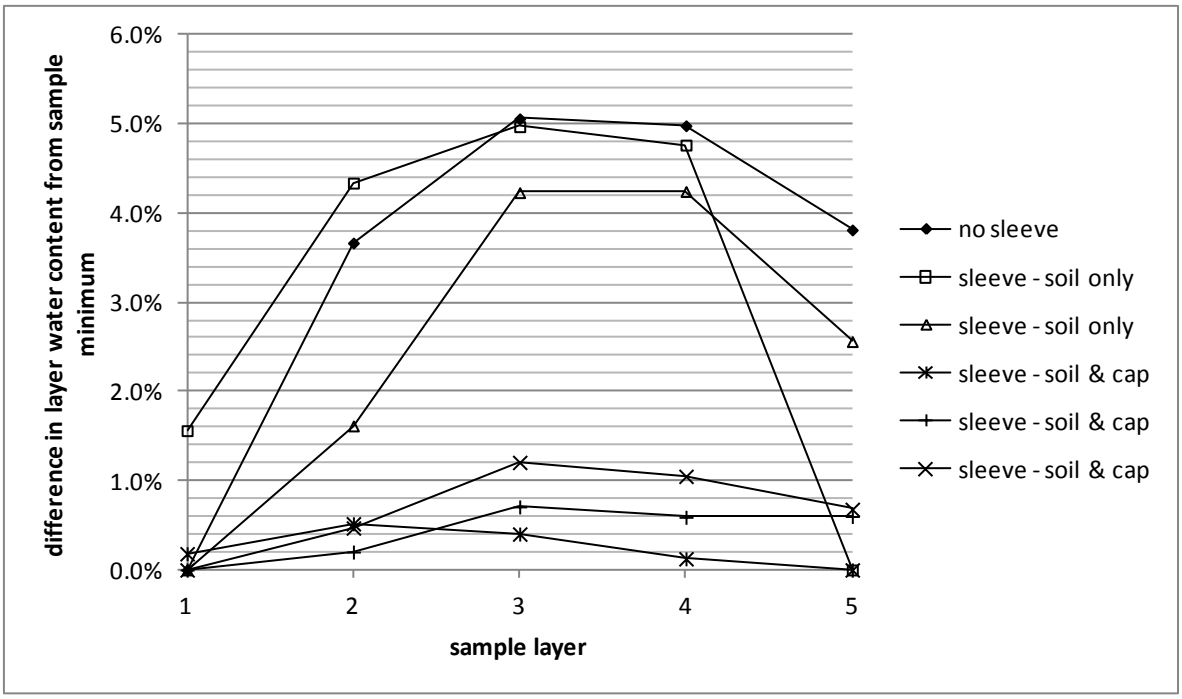

Figure 4.11: Water content differences arising from side friction using various consolidation sleeving approaches

Initially a polythene sheet was used to sleeve the consolidation tube; this reduced friction, particularly when lubricated with WD40 spray. However polythene is a relatively stiff material and generated deep 'creases' within the soil sample as the lining compressed (Figure 4.12). A latex membrane is less stiff and does not form the same creases; it can be initially stretched before consolidation, this tensile strain then relaxes as consolidation progresses. Latex was found to be more frictional than the polythene; a second, outer sleeve of polythene was included in the consolidation apparatus but fixed in place to avoid 'creases' in the sample. This has the additional advantage that the sample does not need a membrane fitted before testing, avoiding a potential source of disturbance to soft samples, similar to the procedures of Wang et al. (2011). Membrane toughness is an important factor when they are used in this way

as they can rip when being stretched – 0.4mm thick membranes were found to perform much better than thinner ones (i.e. 0.2mm).

Figure 4.12: Creases in a soil sample consolidated using a polythene sheet as a compressible sleeve

Handling soft samples was found to be difficult without inducing unacceptable levels of disturbance and damage. Using the triaxial rig to apply the consolidation load to the slurry, similarly to Wang et al. (2011), avoids handling and transporting the sample and allows softer samples to be tested. Extraction from a solid tube (by pulling the tube free whilst holding the sample in place) often caused the sample to slump under its own weight –the restraining load and sliding the tube past the soil may break suction in the sample, which is instrumental in holding it together. A split mould formed from a

plastic pipe held together by worm-drive clips (Figure 4.13) minimised extraction disturbance, again similar to Wang et al. (2011). Okur and Ansal (2007) and Zapata-Medina et al. (2014) similarly split apart liner tubes when recovering high quality *in-situ* samples. The top cap and O-rings securing the membrane at the top can also be fitted with the split mould still in place, a procedure which often damaged soft samples otherwise. As a result, very soft, low strength samples (5kPa shear strength in a quick undrained test) could be produced.

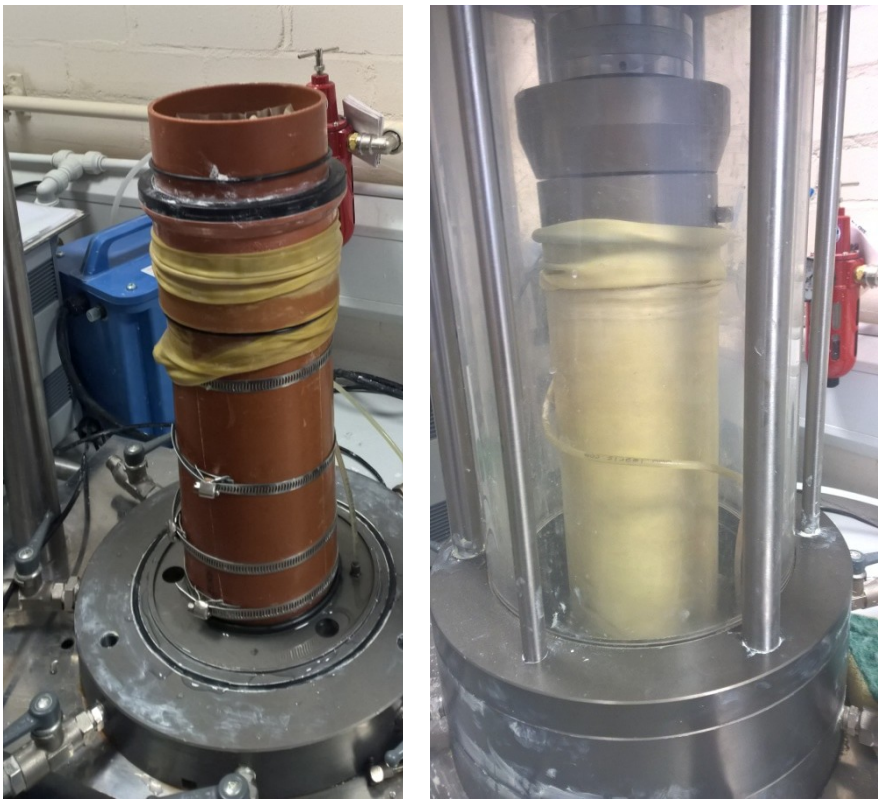

Figure 4.13: Assembled split mould on cyclic triaxial platen filled with slurry prior to loading (left) and finished sample in the triaxial cell (right)

In order to avoid the slurry squeezing out of the liner during consolidation, the load was usually applied incrementally (e.g. Overy, 1982; Ward, 1983; Wang et al., 2011). After the slurry was poured, it was first loaded with the top cap and a sequence of

small weights (1kg, 2kg and 5kg in 30 minute increments), in order to thicken it further and reduce the risk of squeezing out under load. For higher loads, the computer-controlled triaxial rig (see Sections 4.1.3 and 4.1.5) was able to achieve and maintain a given load via instrument feedback to its Digital Servo-Control device. When initially applying small loads, instrument noise was dominant: often the feedback mechanism can cause large, sudden displacements which squeeze the slurry out of the mould. Instead of programming the rig to maintain load increments, a sufficiently slow strain rate (5mm/hr) was applied until the ram load reached the target consolidation load. At this load level, the relative influence of instrument noise was reduced and controlling the load level via feedback was much more effective. Initially, very soft samples were prepared using a 1000N axial load. However the process of removing the split mould often resulted in disturbance, rendering the sample unusable. For improved productivity, a higher axial load of 1500N was used for the Silt Mix samples. Consolidation of samples from slurry under this load displayed a preconsolidation stress (using Casagrande's method, discussed in Chapter 6.1.1) in the order of p' = 70kPa, meaning triaxial consolidation stresses in excess of this were required to develop normally consolidated behaviour. Following anisotropic consolidation to p' = 210kPa, (i.e. 3x the preconsolidation stress; q = 190kPa, $K_{0,NC}$ = 0.45, determined as per Chapter 4.1.4.2) liquefiable behaviour was observed (Chapter 4.2.2.2 and 6.2); this implied sufficiently normally consolidated behaviour and so was used as the consolidation state for the majority of tests.

Upon removal of the split mould it was common for samples to slump slightly, reducing their height whilst increasing their diameter, due to their self-weight. Even

with careful handling, it was possible for 100mm diameter samples to slump to 103-105mm in diameter. This reduced the final length-to-diameter (L_c/D_c) ratio of the sample to below the typical minimum of 2.0 (discussed in more detail in Section 4.2.2.1). To remedy this, before removing the split mould, the top cap was fitted and sealed and a small suction applied via the back pressure line. Combined with careful handling, this method minimised slumping, with sample diameters post-extraction typically less than 101.5mm.

For English China Clay tests, consolidation strains under the desired loads were too large for the triaxial ram (travel limited to 70mm). However the stable and more cohesive nature of the clay means that transporting samples from an external rig did not induce disturbance; slurry consolidated clay samples were therefore consolidated externally in stages (up to 100kg; Figure 4.14) in a split mould, mounted on the triaxial rig and then the mould disassembled as per the Silt Mix.

Figure 4.14: External split-mould slurry consolidation rig for English China Clay

Clay samples manufactured in this way were found to show similar intra-sample water content variation profiles to Silt Mix samples (Figure 4.11); differences of 1.0% to 2.8% between minimum and maximum layer water contents were observed. Estimated average water contents following slurry consolidation under 100kg load varied from

48.2% to 50.4% (0.80 to 0.84 *LL*); this was considered acceptably consistent as a further stage of triaxial consolidation was then applied.

4.1.2.3. Influence of sample preparation on soil fabric

In addition to achieving normal consolidation with an appropriately low strength and stiffness, it is also important that the arrangement of particles on a micro-scale, i.e. the fabric, is representative of the desired depositional environment. Bradshaw and Baxter (2007) prepared samples of non-plastic silt, using both under-compaction and slurry consolidation, to compare to the two-way cyclic loading response of an *in-situ* block sample of overconsolidated and varved soil. For the initial cycles the response was found to be very similar for all three. Differences arose in the large-strain region: the slurry consolidated sample accumulated compression strains rapidly and showed little dilatancy, whilst under-compacted and *in-situ* samples accumulated extension strains and showed greater dilation. It was suggested (Bradshaw and Baxter, 2007) that slurry consolidation produces a fabric more representative of a very 'young' deposit, with no features associated with overconsolidation or ageing, and that the under-compacted and slurry consolidated samples provide reasonable bounds to the behaviour of an undisturbed sample of *in-situ* soil.

When Silt Mix samples were split and examined visually, there appeared to be a difference in the soil texture, compacted samples appearing rougher and more random than slurry consolidated (see Figure 4.15). To better understand the influence of sample preparation technique on fabric, small sub-samples of soil were taken from two separate samples and microscope images compared.

Figure 4.15: Internal fabric of 100mm diameter triaxial samples split in half vertically. Left - prepared using the under-compaction method. Right - prepared by slurry consolidation.

Soil was sub-sampled from the mid-section of each sample by pushing 15mm diameter tubes (approx. 30mm long) into the soil; one vertically along the central sample axis and one horizontally, in order to study differences in fabric in different perpendicular planes. After careful extraction, a small piece of the sub-sample (3mm x 3mm x 10mm long) was cut from the middle of the sub-sample using a razor blade and flash-frozen using liquid nitrogen to retain the soil structure, and then warmed to -90°C under a vacuum to allow the frozen water to sublime.

From the micrographs produced, it is apparent that the soil is predominantly a silt matrix with fine to medium sand particles interspersed throughout. The sand grains were subangular to rounded and approximately spherical/cubical, whilst the silt particles are angular flat plates. Clay-sized particles tended to align with the faces of

larger silt particles and are in sufficiently low concentrations that the inter-particle pore space between silt particles is relatively open (i.e. similar to a granular matrix as described by Collins and McGown, 1974).

Similar to Figure 4.15, the micro-texture of the compacted soil appears more random than that of the slurry consolidated soil; in the latter case, the silt particles particularly appear to be preferentially aligned such that the long sides of the particles are horizontal, i.e. more edges of silt particles visible with a vertical cut plane and more faces visible with a horizontal cut plane (Figure 4.16 to Figure 4.19). This implies the more ordered fabric is a function of the preparation methodology, as was found by Kirkpatrick and Rennie (1972) and Krizek et al. (1977).

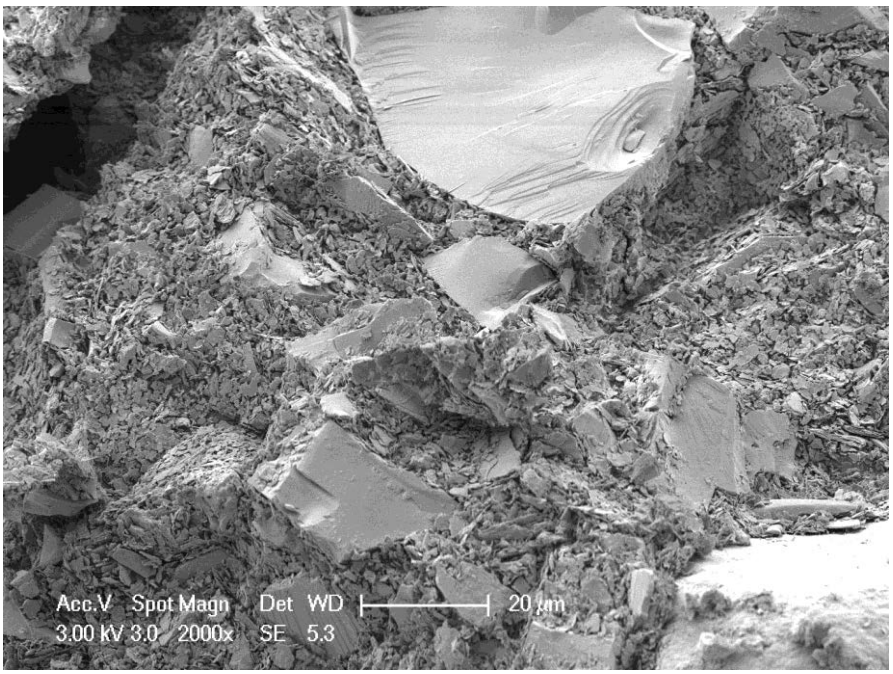

Figure 4.16: Micrograph on vertical cut plane of slurry consolidated Silt Mix soil, illustrating some preferential (edges visible) alignment of silt particles

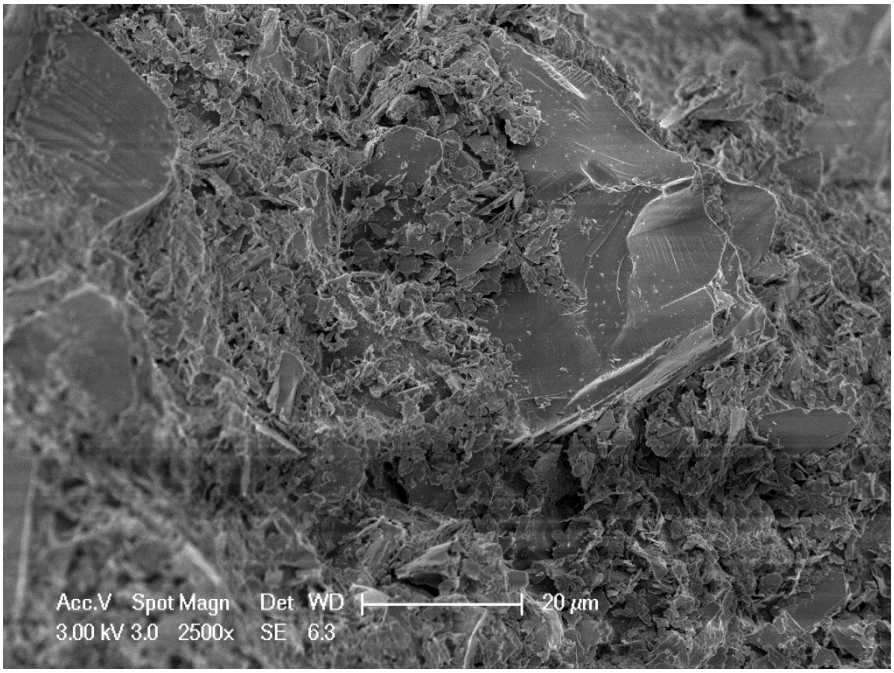

Figure 4.17: Micrograph on horizontal cut plane of slurry consolidated Silt Mix soil, illustrating preferential alignment (faces visible) of silt particles and presence of vertically-aligned circular pores potentially formed by fluid flow.

Figure 4.18: Micrograph on vertical cut plane of under-compacted Silt Mix soil illustrating more random and better interlocking alignment of particles.

Figure 4.19: Micrograph on horizontal cut plane of under-compacted Silt Mix soil illustrating random alignment similar to Figure 4.18.

The slurry consolidated soil, when viewed on a horizontal cut plane, also indicated a different type of pore network to that seen in vertical cut planes or the compacted soil. Roughly circular pores, surrounded by fine silt/clay-sized particles with a strong preference for being oriented with the faces visible, are present (Figure 4.17). These pores bear a resemblance to soil which has been fluidised by a hydraulic gradient (i.e. 'boiling') where effective stresses reach zero and particles are displaced by fluid flow. During slurry consolidation, external stresses will cause vertical fluid flow. Initially, the effective stresses in the slurry will also be low, meaning soil particles can be easily displaced by flowing water. It is reasonable to assume that pore fluid flow under low effective stress, experienced during slurry consolidation but not compaction, will influence the soil fabric.

The differences in preferential particle alignment and pore networks observed between the two sample preparation approaches are likely to affect sample behaviour; variations in pore networks may influence permeability and differences in interlock may change the volumetric strain response under shear (i.e. dilation/contraction), particularly in the large-strain region as observed by Bradshaw and Baxter (2007).

4.1.2.4. Evaluation of sample preparation options

Initially the option of using both under-compacted and slurry consolidated samples and comparing the effects of the different fabrics was considered. However the sole use of slurry consolidation to produce samples was taken forward because:

- Slurry consolidation better represents the geological deposition conditions of normally consolidated marine/alluvial deposits and produces a 'young' fabric.
- The stress history of the soil in this situation is better defined, as the past maximum load will be no greater than the load applied during slurry consolidation (in practice, some stress will be lost to side friction), whereas the past maximum pressures applied by dynamic compaction are unknown.
- Most importantly, due to the mould dimensions, it was difficult to produce under-compacted triaxial samples of soft clayey silt which were able to maintain an L_c/D_c ratio > 2.0 after being extracted (and undergoing some slumping) and then being subject to anisotropic consolidation in the triaxial cell. As is discussed in Section 4.2.2.1, shear tests on Silt Mix samples with an L_c/D_c ratio of < 2.0 were found to suffer from large errors introduced by end restraint.

4.1.3. Triaxial testing equipment

Static and cyclic testing was performed using the VJTech Dynamic Triaxial Testing System (DTTS). The various components of the system are controlled by the Digital Servo Control (DSC) unit which coordinates data logs and governs feedback control of the electric motor controlling the ram. The Automatic Pressure Control (APC) units have their own built-in feedback control systems. Testing parameters for the various instruments are set using VJTech's proprietary software, Clisp Studio, on the desktop PC before testing begins. During testing, data logs from the DSC are transferred to the PC. The DSC itself only monitors the raw data from the instruments, i.e. the electrical signals corresponding to loads, pressures and displacements. Engineering quantities required for test control (e.g. stress, strain) are then calculated by the PC through Clisp Studio.

Measurement of the raw test data is undertaken by numerous instruments, described below:

- **Cell Pressure:** Triaxial cell pressure is controlled by the Pneumatic APC, which uses compressed air and an air-water interface to pressurise water. The Pneumatic APC can pressurise the large cell volume rapidly, making it better suited to maintaining cell pressure during cyclic testing (changes in cell water volume imposed by the movement of the ram can cause corresponding pressure fluctuations). Readings are provided to the nearest 1kPa (i.e. ± 0.5kPa) and the APC controls the pressure to within 1kPa of the target (i.e. ± 1kPa).
- **Back Pressure:** Back pressure, applied via the sample top cap, is controlled by the Hydraulic APC, which uses a cylinder of known volume and a hydraulic ram

to pressurise water. It is slower to react than the Pneumatic APC but is able to measure changes in volume during consolidation. Readings are provided to the nearest 1kPa (i.e. ± 0.5kPa) and the APC controls the pressure to within 1kPa of the target (i.e. ± 1kPa). Volume change is measured to the nearest 0.001ml (i.e. ± 0.0005ml), however inherent creep in the plastic tubing connecting the APC to the test sample (quantified in Section 4.2.1.2) means such precision is not meaningful.

- **Ram Load:** A submersible load cell measures ram load on the sample, avoiding errors introduced by friction on the bushings etc. Readings are provided to the nearest 1N (i.e. ± 0.5N)**.**
- **Pore Water Pressure:** A pore pressure transducer takes readings at the base. Pore pressure readings are provided to the nearest 0.1kPa (i.e. ± 0.05kPa), however the inherent instrument noise (see Section 4.2.1.1.) means such precision is not meaningful.
- **Displacement:** The DTTS has two independent measurements of global displacement; the Encoder for the electric motor controlling the load ram and an external Linear Variable Differential Transducer (LVDT). Both measure displacement to the nearest 0.001mm (i.e. ± 0.0005mm). The LVDT was used initially to cross-check Encoder displacements, however its mounting on the ram reduced available travel and it was subsequently removed.

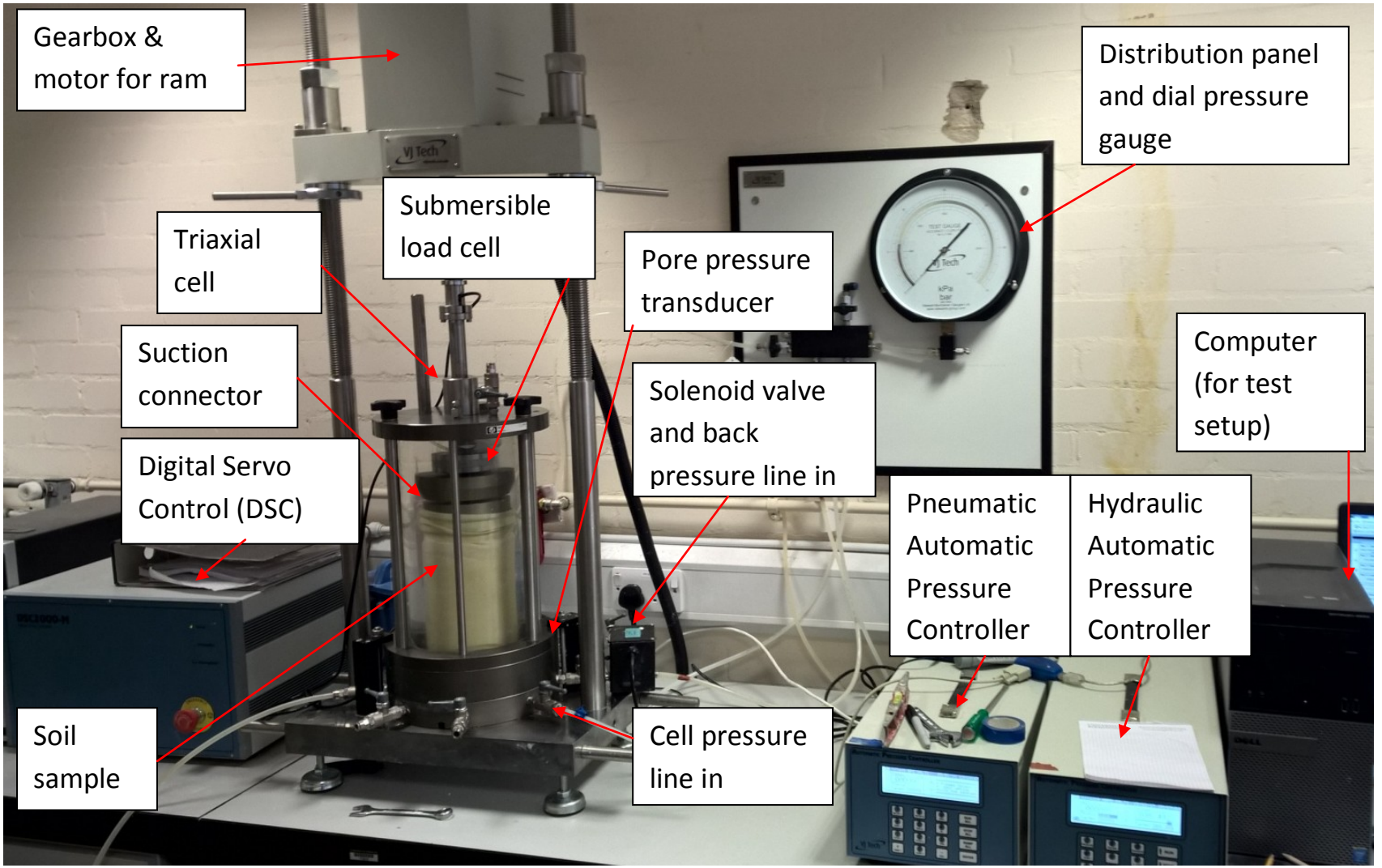

Figure 4.20: Photograph of DDTS with key components labelled

4.1.4. Triaxial pre-test procedures

Before shear and cyclic loading regimes, samples are first tested for saturation and then consolidated to reach the desired normally consolidated state. A well-controlled consolidation stage is intended to reduce the potential impact of variations in the slurry consolidation process and also erase the memory of overconsolidation associated with the removal of the slurry-consolidating load.

The sample dimensions were measured once the mould is removed. The diameter was measured at a minimum of 3no. locations using a pair of vernier callipers which can measure to a precision of ±0.005mm. In practice, measured diameter varies considerably more than this, typically in the order of ±0.25mm; this may be as a result of localised friction between the sample and mould wall, localised slumping, or simply difficulties in defining the edge of a very soft sample. For analysis, the median reading is used as a representative value of the (assumed uniform) sample diameter.

4.1.4.1. Saturation

Sufficient pore air content can invalidate the assumptions of effective stress routinely used in soil mechanics analysis (Head, 1986). To test the validity of assuming saturation, a 'B-test' is carried out; cell pressure is increased and the corresponding increase in pore pressure is measured, quantified through Skempton's pore pressure parameter *B*, i.e.:

Equation 4.1: $$B = \frac{\Delta u}{\Delta \sigma_3}$$

$B \geq 0.95$ is considered sufficient to assume saturated behaviour without significant error (Head, 1986; Bradshaw and Baxter, 2007). Slurry consolidated samples, subject

to an initial cell pressure increment of 100kPa, achieve B = 0.95 to 0.97; additional saturation through back pressure was not necessary. The back pressure during consolidation is maintained at 100kPa to avoid cavitation arising from possible subsequent undrained dilation and also maintains acceptably saturated conditions for testing.

4.1.4.2. Triaxial Consolidation

As samples are heavily overconsolidated following extraction, a normally consolidated state is attained by reloading the sample such that its stress history is erased (e.g. Santagata and Germaine, 2005). The simplest method is to consolidate under isotropic pressure; as was performed for initial shear tests. However this stress state is not representative of normally consolidated soil at depth. Furthermore, errors associated with finding the point of first ram contact (see Section 4.2.1.3 and 4.2.1.4) and bedding errors introduce an initial additional compliance to the sample. Meaningful changes in stress cannot be identified at small strains for isotropically consolidated samples but are apparent for anisotropically consolidated samples (Figure 4.21).

All tests include an initial isotropic consolidation stage to increase the sample strength so any fluctuation in the anisotropic consolidation load does not cause accidental overload and damage.

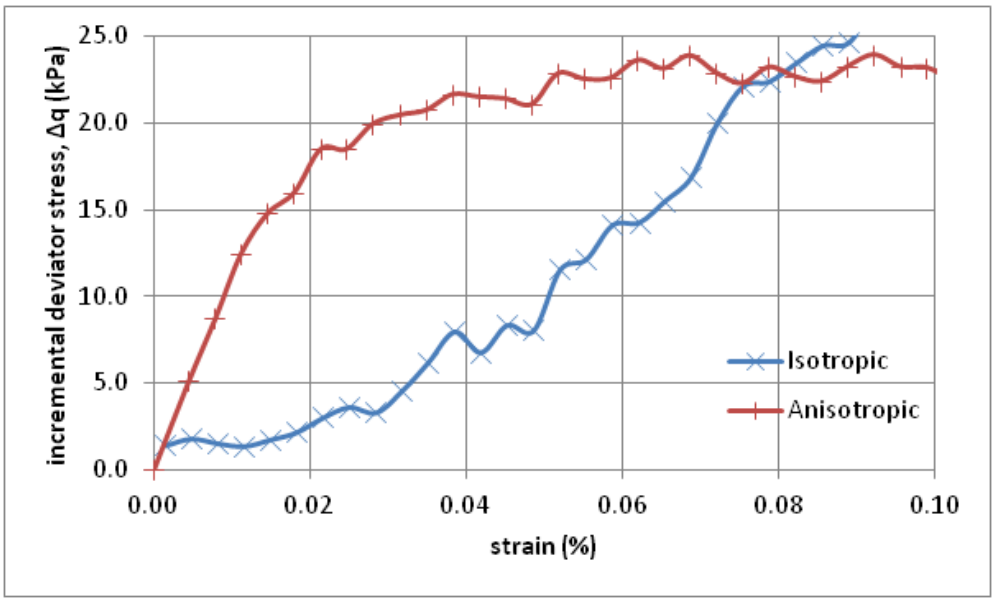

Figure 4.21: Small strain undrained shear response of isotropically and anisotropically consolidated samples, showing initial bedding compliance for the isotropically consolidated sample.

Before anisotropic consolidation, the axial loading ram is brought into contact with the sample. This was initially identified by lowering the ram until the load cell reading increases by 10N, then withdrawing until the original load is attained. Inherent electrical noise (see Chapter 4.2.1.3) introduces a small chance of this occurring without any contact. Therefore a larger change in load (25N) was subsequently used.

Using feedback control it is possible to consolidate soil samples in a condition of zero lateral strain (K_0 consolidation); after an initial isotropic consolidation stage to provide a small effective stress in the sample, the axial strain is then controlled such that the ratio of axial strain to volume change produces no change in the sample's cross-sectional area, i.e. Equation 4.2:

Equation 4.2: $$\delta = \frac{\Delta V}{A}$$

This consolidation method must be carried out at slow speeds, i.e. similar to that of a drained shear test (i.e. 8.5 x t_{100}; Head, 1986), otherwise excess pore pressures and therefore the degree of consolidation can develop non-uniformly and locally invalidate the assumption of zero lateral strain. For an expedient testing programme, a simpler and faster method of anisotropic consolidation was developed. Based on initial K_0-consolidated tests performed as above, the desired stress state (i.e. axial and lateral stresses) is selected. The sample is isotropically consolidated under the desired lateral stress; upon reaching 95% dissipation of base pore pressure, axial stress is slowly increased (at a rate determined by trial and error such that base pore water pressure remains approximately constant) until the desired stress state is achieved.

During consolidation, the default arrangement for drainage of excess pore pressures (i.e. above the target back-pressure of 100kPa) is via the top cap. The pore water pressure which is measured at the sample base is in this case the maximum pore pressure and can be used to accurately determine when primary consolidation is substantially complete. Consolidation can also be accelerated by various different test arrangements:

- **Side filter drains:** Filter paper strips on the vertical edges reduces the drainage path by a factor of around 4 (for a sample with $L = 2D$) and hence consolidation time by 16 times, provided the soil has a permeability less than around 10^{-8} m/s (Head, 1986). Permeability estimates for the Silt Mix soil derived from isotropic consolidation tests of 5 to 9 x 10^{-9} m/s indicate this method is unlikely to

significantly accelerate consolidation. Furthermore, fitting side drains to very soft samples is likely to induce damage.

- **Top and base drainage:** Drainage from both the top and base reduces the drainage path by a factor of 2 and hence consolidation time by 4 times. The pore water pressure transducer is also located in the base pedestal, so pore pressure cannot be measured during consolidation. This approach was used to speed up testing, particularly for repeat tests.

4.1.5. Feedback control

More complex testing conditions, e.g. load-controlled cyclic tests and anisotropic consolidation, require properly specified feedback control to ensure consistent application of load or strain and avoid accidental overload.

During dynamic testing, the computation speed of the PC is insufficient to recalculate parameters to update feedback systems; control is performed entirely by the DSC. As such, cyclic tests are limited to controlling the basic variables only, i.e. ram load or displacement.

The DSC feedback system uses PID (Proportional, Integral and Derivative) feedback to minimise the error between the axial ram's actual load/displacement and the desired waveform. The system accelerates or decelerates the axial ram according to a combination of PID control algorithms.

Proportional (P) control is the simplest; the ram is accelerated or decelerated in proportion to the control error. This works well for directly controlled target variables (i.e. displacement control) but for load-controlled cyclic tests on soil samples, where

load and displacement are not linearly associated and instrument noise introduces additional variability, P control alone can lead to over-correction and oscillation (Figure 4.22). Maximum and minimum cyclic loads are often not well controlled. This is of particular concern with soft samples where the load response requires a greater strain.

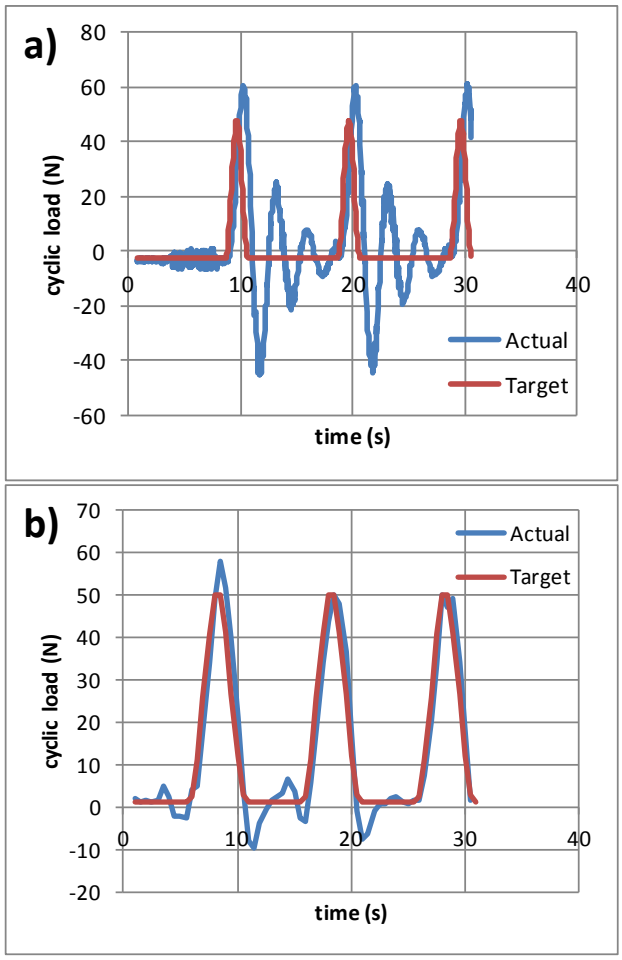

Figure 4.22: Load-controlled tests on foam rubber sample; controlled by P algorithm only (a) and by PID algorithms (b), showing overcorrection and oscillation around the target waveform for P only algorithms.

Derivative (D) control tries to match the time-gradient of the actual and desired waveform. In practice this algorithm is good for smoothing out over-corrections from P control algorithms, particularly at sharp corners on triangular or square waveforms.

Integral (I) control reduces the cumulative error (area under the curve) between the actual and desired waveforms. This algorithm is used to reduce cumulative phase shifts which can be introduced by the other algorithms and maintain desired cyclic frequency.

During undrained cyclic tests, accumulation of permanent axial strain results in an increased cross-sectional area. The deviator stress therefore reduces with increasing axial strain for a given load, meaning purely load-controlled tests undergo a relaxation of the maximum and minimum deviator stresses throughout the test (correction factors used for changes to area from axial and volumetric strains are presented in Section 4.2.1.5). These effects were not discovered until later in the testing programme but were subsequently corrected for by manually changing cyclic load parameters, discussed further in Chapters 5.1 and 6.2.

During a displacement controlled test on an anisotropically consolidated sample, accumulation of plastic strain from a cycle will similarly cause relaxation. This limits displacement controlled testing of anisotropically consolidated samples to the small-strain, elastic region; large plastic strains result in the sample unloading very quickly and reverting to an isotropic stress state (Figure 4.23), an unrealistic stress state for deep soil.

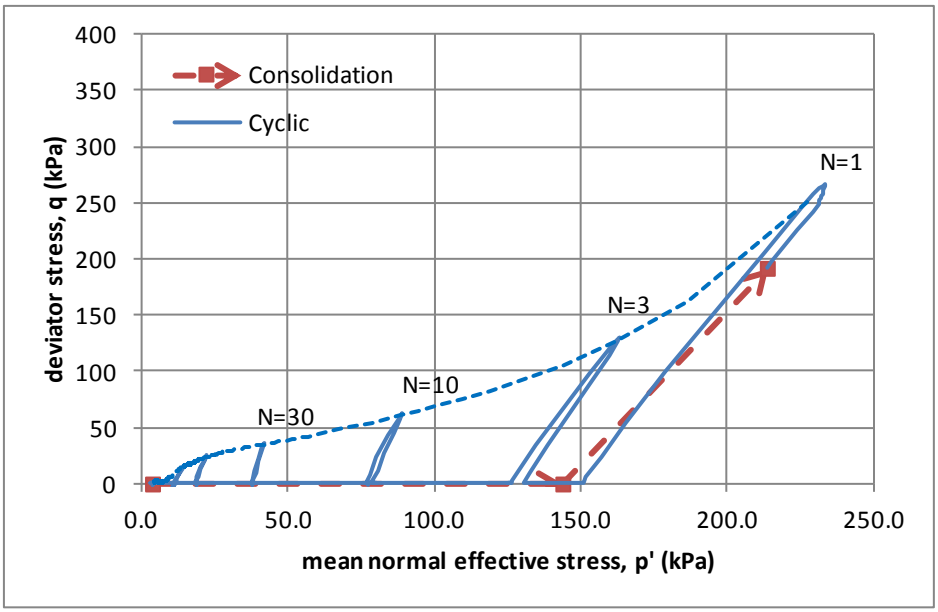

Figure 4.23: Changes in stress state in test B-3; anisotropically consolidated, subject to strain-controlled cycling from 0 to 2%. N = number of strain-controlled cycles. Dashed line connects points of maximum *q*.

4.1.6. Measurement of water content

Following testing, the sample was split in half lengthwise. One half was weighed and dried to determine the whole-sample water content, the second was split into five parts to qualitatively assess the water content uniformity within the sample.

A comparative check of the full sample's wet and dry weights with the sum of all the sub-samples, check can be made and erroneous water content measurements avoided. The sum of the sub-sample weights is lower than the intact sample typically by 1-5g and comparison of half-sample and whole-sample water content indicates an error of less than 0.15% on the absolute value of sample water content.

4.2. Evaluation of experimental variability

This section considers variation arising from;

1. The control and measuring apparatus associated with the DTTS itself
2. Inherent soil variability and preparation procedures

4.2.1. Control and measurement apparatus

The use of digital instruments connected via the DSC allows high-frequency, synchronised readings of multiple variables to be taken simultaneously. The data logging capacity of the DTTS is:

- 1000no. feedback control points per cycle (during cyclic testing using the DSC), up to a cycle frequency of 5Hz.
- 200no. data points recorded per cycle (cyclic testing), up to a cycle frequency of 5Hz.
- 1no. reading per second in non-cyclic tests (saturation, consolidation, static shear).

Electrical noise limits precision. A number of 'dummy tests' were undertaken, which recorded the variation of the instrument readings under apparently constant conditions.

4.2.1.1. Water pressure transducers

Three instruments measure fluid pressure (cell pressure, back pressure and pore pressure) and the extent to which they agree determines the accuracy of readings during tests.

The triaxial cell was filled and pressurised to 200kPa, 400kPa and 600kPa by the Pneumatic APC. Ordering the pore pressure data by magnitude of deviation from the APC target pressure (determined over 1430no. readings for each pressure level) produces a frequency distribution of errors (Figure 4.24). 90% of all pore pressure transducer readings were within +0.5kPa and – 1.0kPa of the target. A median

difference (50th percentile) of 0 to -0.5kPa indicates pore pressure readings are more likely to be below the target than above. It is possible the cell pressure is maintained, on average, slightly below the target pressure: APC feedback control only adjusts if measured pressure is 1kPa or more below the target. As plastic tubing and the triaxial cell will tend to creep slightly under pressure (Head, 1986) there is a tendency for volume expansion of the water within and hence a slow reduction in pressure if not corrected.

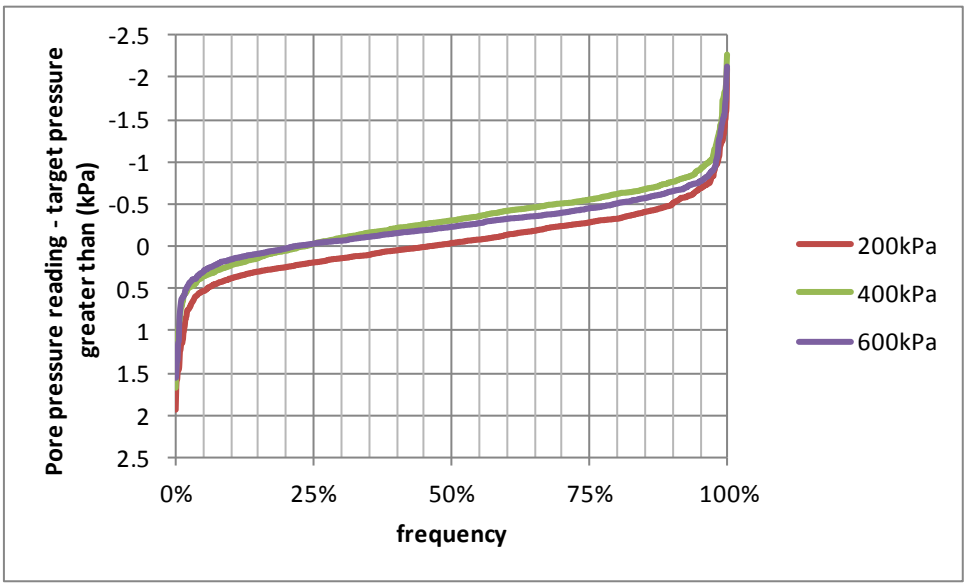

Figure 4.24: Frequency distribution of difference between pore pressure transducer reading and target pressure for 200kPa, 400kPa and 600kPa target pressures

Similarly, when the cell pressure was maintained and back pressure (Hydraulic APC) readings were taken, 90% of readings were within ±1kPa of each other (Figure 4.25).

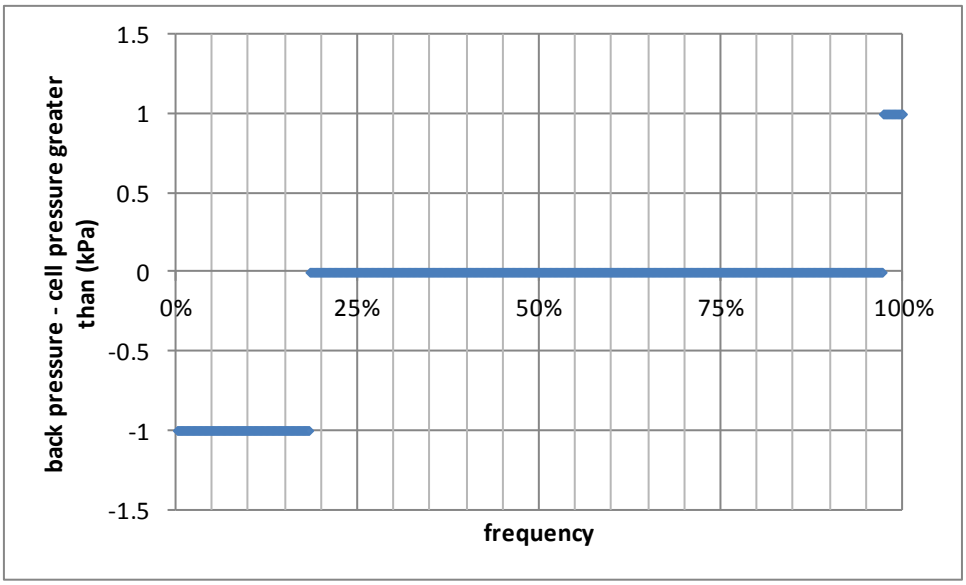

Figure 4.25: Frequency distribution of difference between cell pressure (Pneumatic APC) and back pressure (Hydraulic APC) readings for 100kPa target pressure

To minimise errors in absolute water pressure and so sample effective stresses, before each test the three pressure transducers were cross-checked against one another and also the dial gauge (see Figure 4.20). Instruments are considered to be in agreement if readings between the three transducers and the dial gauge are within ±1kPa. The pore pressure and back pressure (Hydraulic APC) transducers have not been observed to disagree. During consolidation, the volume of water in the air/water interface cylinder reduces and after several tests the water must be replenished by letting out air. This can cause the Pneumatic APC to disagree with other instruments; re-calibration was occasionally performed.

4.2.1.2. Volume change measurement

The Hydraulic APC is connected to the soil sample by lengths of plastic tubing, prone to creep expansion (Head, 1986). To quantify these errors, the Hydraulic APC maintained constant pressure in the tubing only (at 350kPa, i.e. above that used in testing) and

volume change measured. As expected for creep, the relationship was approximately logarithmic (Figure 4.26). Within the expected duration of a single consolidation stage (6 to 12 hours) the error from creep was approximately 0.4ml.

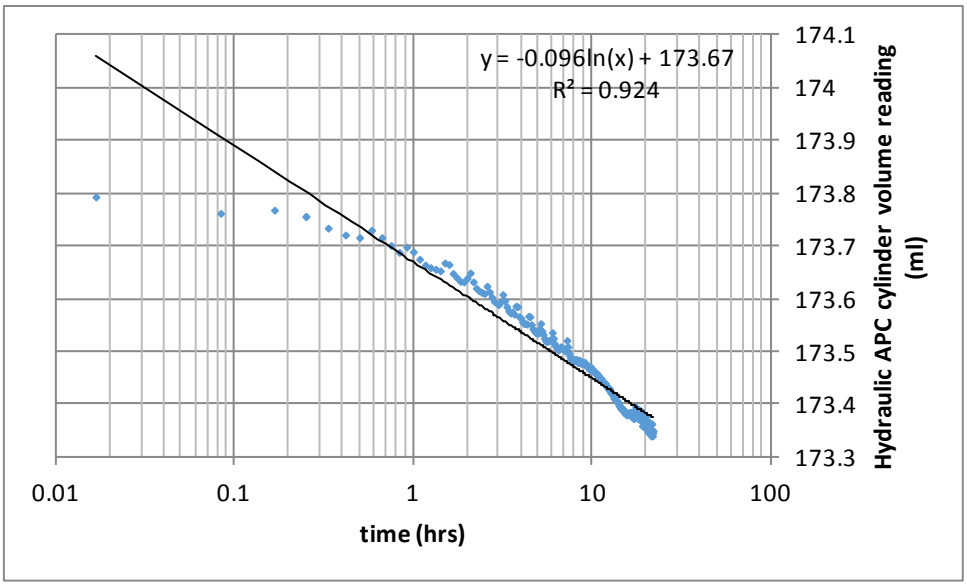

Figure 4.26: Changes to Hydraulic APC cylinder volume (i.e. a decrease indicates an increase in tubing volume) under maintained pressure of 350kPa within plastic tubing connecting Hydraulic APC and soil samples during tests.

4.2.1.3. Submersible load cell

Tests were performed with zero ram load over 24 hours. This indicated 90% of the readings were within ±4N of the mean. Similar results were found in tests with the load maintained constant using feedback control (Figure 4.27).

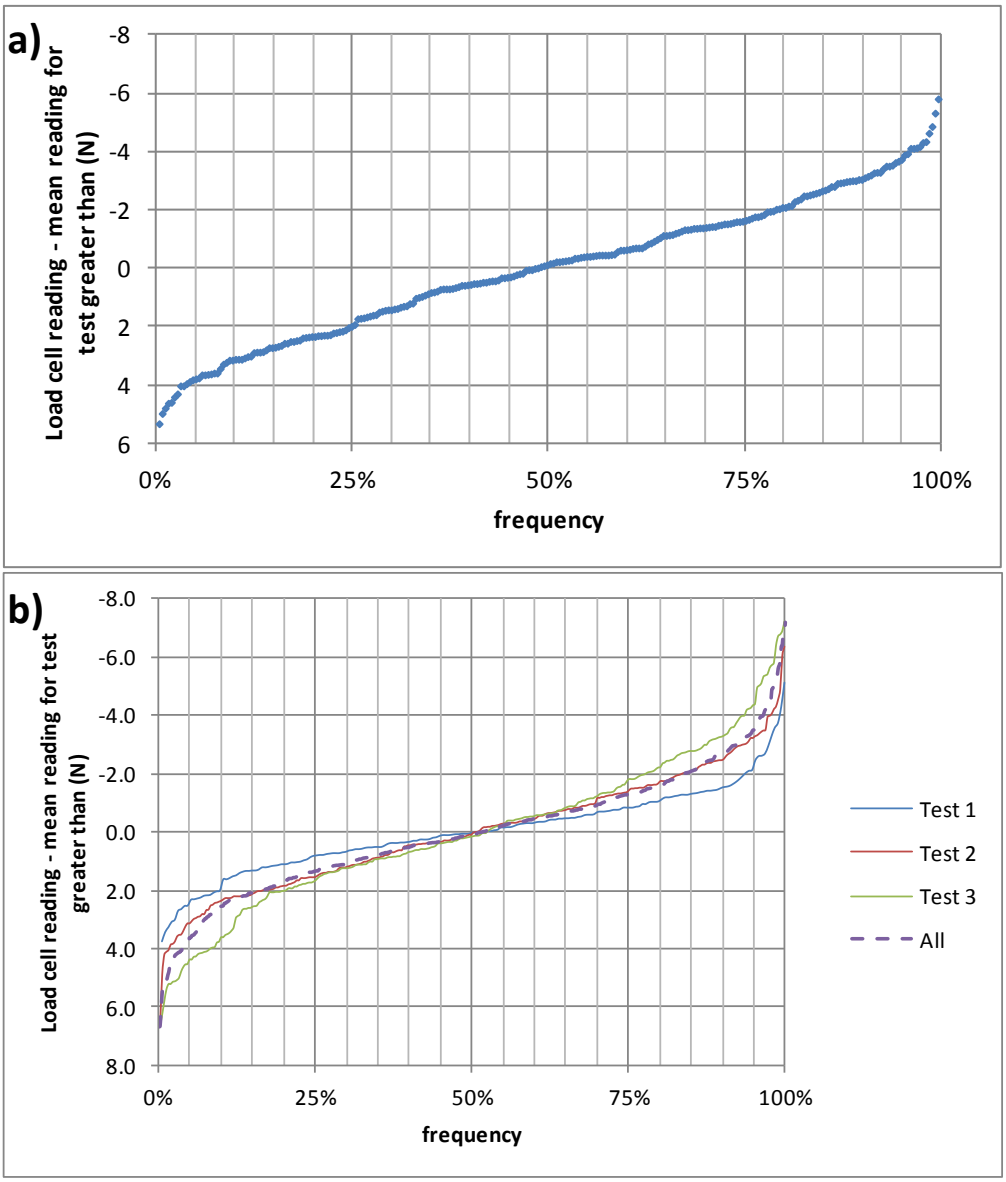

Figure 4.27: Frequency distribution of difference between load cell reading and average reading over 4no. 24 hour tests with zero applied load (a) and with constant non-zero load (1500N) using data obtained during slurry consolidation (b).

In addition to random scatter, the load reading can drift slowly over time (Figure 4.28), at a load drift rate between 0.05N and 1.15N per 10 hours. The drift rate is not constant or predictable so no attempts to correct readings have been made; the variation from the mean reading in Figure 4.27 includes drift.

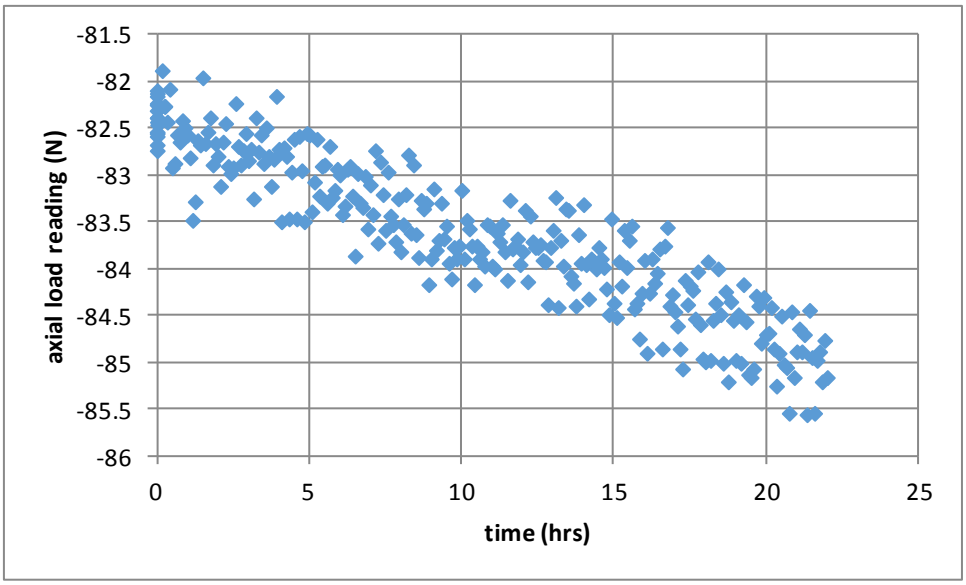

Figure 4.28: Load cell readings during zero external load test, indicating slow drift of the load reading

A foam rubber test sample was subjected to several strain-controlled loading tests (at 1mm/min) in the triaxial cell to assess the similarity of load cell readings. The results in Figure 4.29 show the variation in load readings for a given displacement of up to ±10N. As 90% of results in a zero-load test are within ±4N of the mean (Figure 4.27) this larger variation incorporates additional sources of error. There is a clear systematic component to variation between tests, possibly arising due to differences in positioning of the foam rubber sample or determination of the point at which the ram contacts the sample (performed as per Section 4.1.4.2). With typical instrument noise of ±4N, displacement at the actual zero-load point in Figure 4.29 can be within the range ±0.5mm: this could explain why tests 1 and 5 appear to be translated laterally from tests 2-4. Small differences in setting up the test, e.g. sample alignment, fit of the membrane and top cap, may also be responsible for the systematic error; small imperfections can introduce a variable initial portion of compliance.

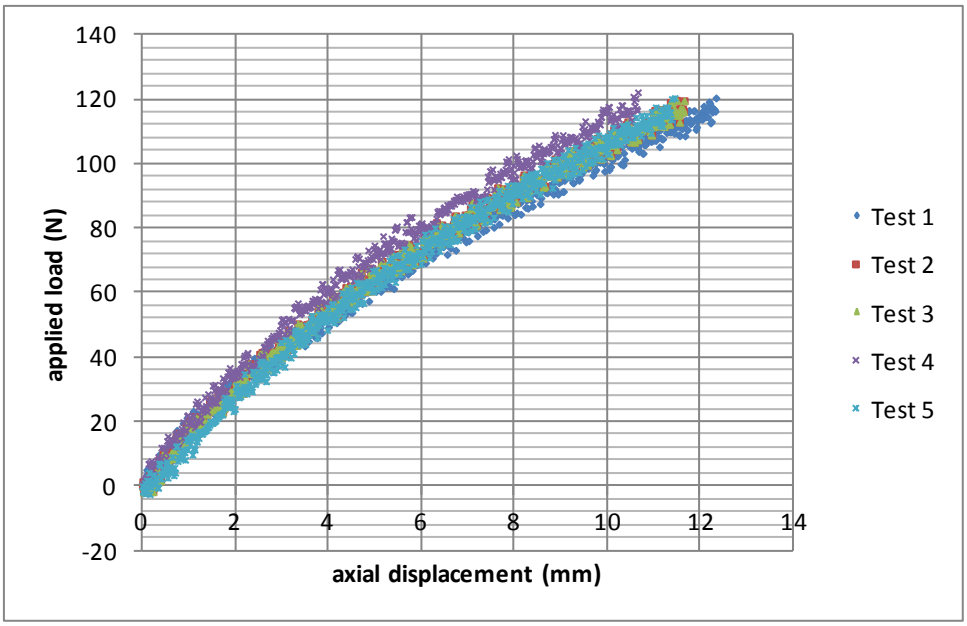

Figure 4.29: Load vs displacement results for 5no. strain-controlled static tests at 1mm/min on a foam rubber sample

Cyclic waveforms change continuously and rapidly; cyclic load errors are likely to be greater, particularly at sharp corners; square waves exhibit the greatest control errors (Figure 4.30), but both waveforms are more poorly-controlled than monotonic loading. 90% of readings are within ±7N (haversine) to ±12N (square wave) of the target load. The square waveforms also have a very low frequency of very large control errors.

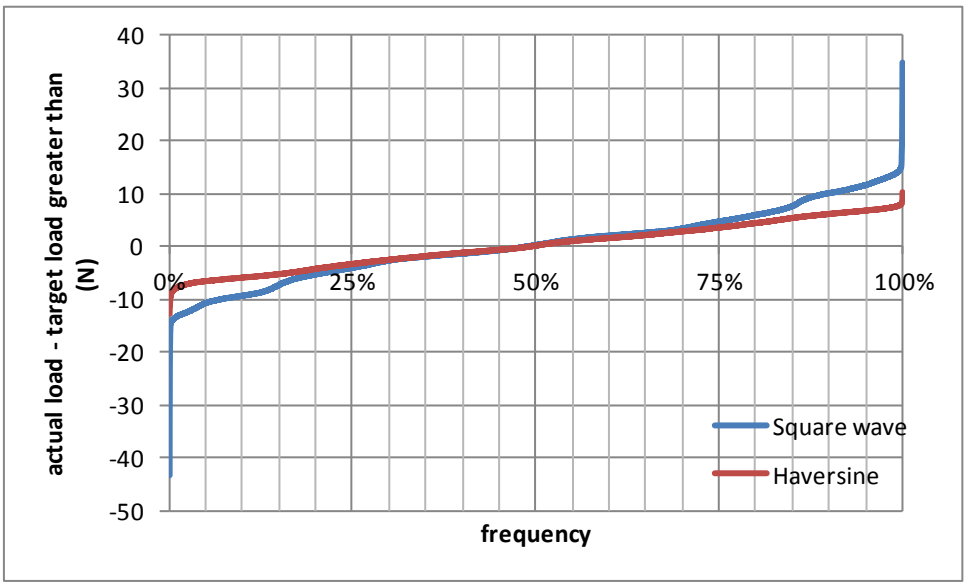

Figure 4.30: Frequency distribution of control errors for cyclic load-controlled tests (data from 100no. cycles of 300N amplitude) for square and haversine waveforms.

The effect of inherent load cell noise on cyclic control is increasingly important at low stresses. For samples consolidated to σ'_1 = 50kPa (i.e. 6.5m depth in Table 2.5), with an estimated threshold stress of 2.5kPa to 5.0kPa (i.e. 5-10%), an overload of 7N (0.9kPa for a 100mm diameter sample) could easily change a sample from stable to liquefying. Such variability and uncertainty in applied cyclic stresses will make it difficult to compute the liquefaction threshold stress. At the higher consolidation stresses (p' = 210kPa), chosen to remove the memory of overconsolidation (Chapter 4.1.2.2), this variation is a much smaller proportion of the threshold stress (26kPa; Chapter 6.2).

4.2.1.4. Instrument noise – data processing

In order to reduce the impact of random noise, a rolling mean over 10 points (y_m, Equation 4.3) to 'smooth' the data was used. As is apparent in Figure 4.31, variation between adjacent data points is significantly reduced.

Equation 4.3: $$y_m = \sum_{n+5}^{n-5} y_n$$

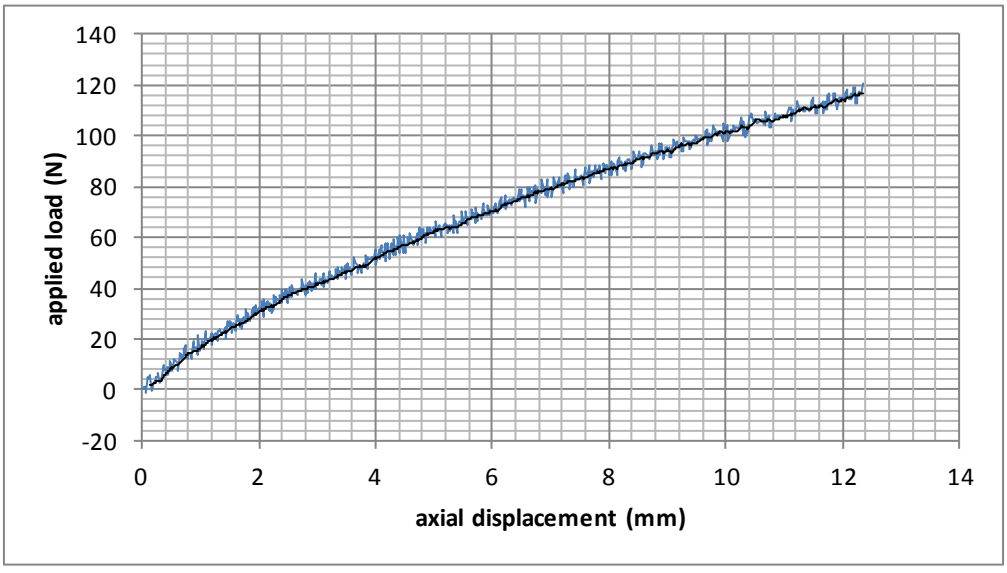

Figure 4.31: Effect of data smoothing through use of a rolling mean (period of 10no. data points) illustrated for a single foam rubber sample test.

Applying a rolling mean to the maintained pressure test data presented in Figure 4.27 reduces the frequency of extreme variation, with 90% of results within +0.6kPa and -0.2kPa of the target (Figure 4.32).

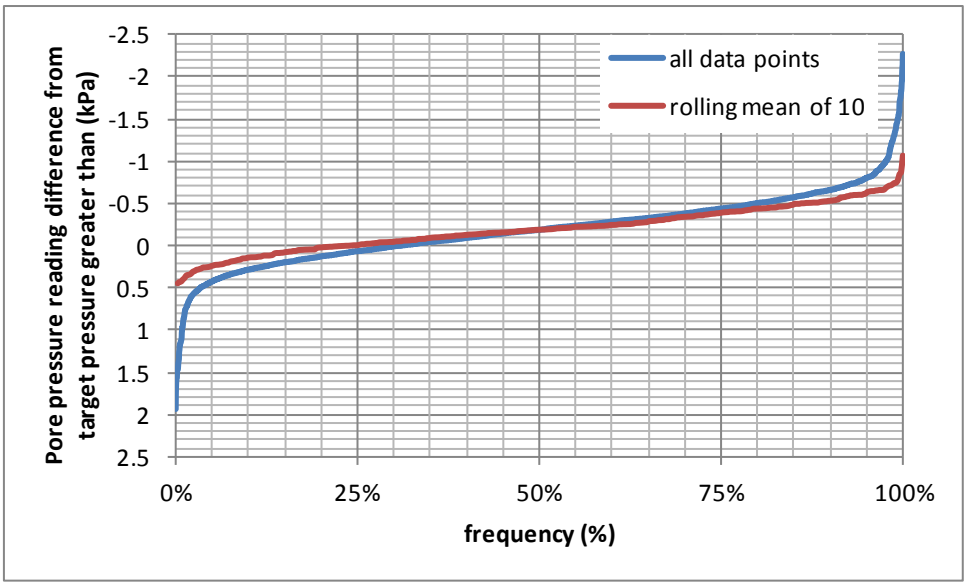

Figure 4.32: Frequency distribution of difference between rolling mean of pore pressure transducer reading and target pressure: variability is reduced (period of 10no. results).

With dynamic data, test variables change more quickly than slow monotonic tests. Applying a rolling mean to cyclically-varying sine wave data adds a phase-shift (Figure 4.33). Furthermore, the points of interest are often cycle maxima and minima; a rolling mean will tend to underestimate the maximum and overestimate the minimum. Moving averages are thus routinely applied to monotonic test data to reduce random error, but not to cyclic test data. The greater potential for random variation in these tests must be considered during analysis.

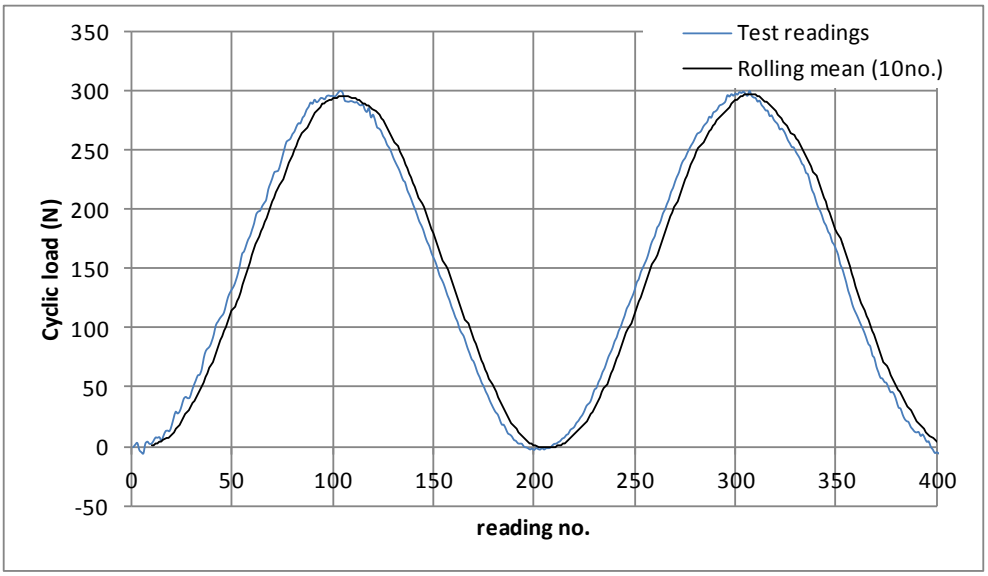

Figure 4.33: Phase-lag effect and underestimation of cycle peak introduced by a rolling mean on cyclic sine wave data.

4.2.1.5. Corrections applied to data

In an undrained (i.e. zero volume change) condition, axial strain will increase sample area (barrelling), which is accounted for as follows (Head, 1986, La Rochelle et al., 1988):

Equation 4.4: $$q = \frac{P}{A_c} \cdot (1 - \varepsilon)$$

During anisotropic consolidation (i.e. shear under drained conditions), the reduction in area as a result of volume change must also be considered, i.e.:

Equation 4.5: $$q = \frac{P}{A_c} \cdot \frac{(1-\varepsilon)}{(1-\frac{\Delta V}{V_0})}$$

In addition to correcting the area for barrelling, the restraining effects of the rubber membrane are also included, after Head (1986). It was apparent, when calculating for larger sample diameters relative to the membrane thickness, that such effects will be

minor, in the order of 1-2kPa deviator stress at 10% strain; this is also confirmed by more recent work by Knodel et al. (1990) and Greeuw et al. (2000).

Following planar slip initiation, the effective area for shear stress calculation should be taken locally over the slip zone (Head, 1986; La Rochelle et al., 1988), although classical concepts of uniform stress and strain are not applicable, due to the highly localised phenomenon (Atkinson, 2000). Further corrections for membrane restraint post-slip are necessary and are more influential; Head (1986) indicates these can be in the order of 20kPa whilst La Rochelle et al. (1988) find post-slip corrections of around 10kPa. For accurate results, analysis requires accurate estimation of when slippage initiated and the out-of-plane movement. Instead of attempting these calculations based on limited and approximate data (bearing in mind the soft nature of the samples and difficulty of local measurements after testing), failure is taken to occur at the point of first slip, i.e. upon propagation of a shear band. Stress-strain data shown subsequent to this is calculated as per samples without a slip plane and shown for illustrative purposes only.

During consolidation, an estimate of the excess pore water pressure distribution is required to determine a sample mean excess pore pressure from base readings. Head (1986) suggests for low excess pore water pressures the distribution can be assumed as linear with little error, i.e. $u_e = (u_{base} - u_{back})/2$, whilst at larger pressures a parabola is more accurate, i.e. $u_e = {}^2/_3 (u_{base} - u_{back})$. Based on the solution to the differential equations of consolidation, Barnes (2000) indicates the theoretical distribution to be half of a sine wave, i.e. that $u_e = 0.636(u_{base} - u_{back})$, close to the parabolic distribution. The latter expression is chosen for analysis of consolidation herein. During undrained

shear, it is recognised that end restraint will produce a non-uniform pore water pressure profile within the sample (as demonstrated by Sheng et al., 1997). However this profile is unknown; for simplicity it is assumed that $u_e = u_{base}$. Lubricated samples with lower restraint offer indications of a more representative uniform pore pressure.

4.2.2. Soil constituents and preparation

4.2.2.1. Repeatability static tests

Multiple monotonic tests on samples under apparently identical conditions were performed with the intention of:

1. Quantifying the likely inherent variations in sample behaviour arising from random variations in soil constituents and preparation procedure
2. Determining whether such variation is acceptable
3. Where possible, informing experimental design to refine the sample preparation procedure and reduce this observed variation in sample behaviour

A number of slurry consolidated Silt Mix samples (15no.), subject to isotropic consolidation to σ'_3 = 150kPa (with u_{back} = 100kPa) followed by anisotropic consolidation to K = 0.45 (and σ'_3 remaining constant, i.e. q = 190kPa, p' = 210kPa) were conducted. The deviator stress increased linearly over 12 hours; further time was allowed for excess pore pressures to dissipate. 90% of isotropic consolidation (following Taylor's method) typically occurred after 100 to 160 minutes, so an additional 4 hours (i.e. a total stage time of 16 hours) was permitted. After this, if the rate of axial strain over the final hour was in excess of 1/30 the intended undrained shear strain rate, the sample was allowed to consolidate further: creep strains above

this are expected to influence the undrained stress-strain response (Zapata-Medina et al., 2014). For the majority of tests, creep strain rates were below the limit and base excess pore pressures were 1-5kPa after 16 hours: testing progressed without delay. Undrained static shear tests were conducted at a constant rate of 2.856mm/hr; sufficiently slow for internal pore pressure equalisation to bring the base pore pressure measurement to a reasonable approximation of the mean pore pressure after a testing duration of 50-80mins, i.e. at strains of 1-2% (Head, 1986).

The undrained shear response of Silt Mix samples can be generalised as follows:

1. At small strains, behaviour is very stiff. The Secant Modulus degrades rapidly from 100-120MPa at 0.01% strain to 20-25MPa by 0.1% strain (i.e. Δq = 20-25kPa; Figure 4.34, Figure 4.40, Figure 6.21). No pore pressure changes are observed; pressures are unlikely to have equalised, base readings are not representative of the sample as a whole.
2. Above 0.1% strain, pore pressure readings rise, whilst the Secant Modulus reduces further. A peak pore pressure is reached, but this does not coincide with peak strength, as would be expected for a normally consolidated Cam-Clay material (Schofield and Wroth, 1968).
3. Pore pressures then drop (Figure 4.35), whilst deviator stress rises, suggesting the soil is now mobilising dilatant strength. Whilst dilation of normally consolidated clays does not occur, this is a phenomenon often observed in undrained shearing of silts and sands (Lee, 1978; Yamamuro and Lade, 1999; Wang et al., 2011).

4. The sample continues to mobilise dilatant strength, maintaining an approximately constant *q/p'* ratio (Figure 4.36; similarly observed by Wang and Luna, 2012) whilst pore pressures drop and deviator stress rises, until failure is reached as a result of a shear band forming within the sample. Shear band initiation is observed to coincide with a sudden drop in deviator stress; in these first 15no. tests at strains of 6-11%. No critical state is apparent; tests by others (Yamamuro and Lade, 1999; Wang and Luna, 2012) indicate this requires attainment of much larger strains (>20%).

The first 15no. samples prepared in this manner exhibited one of two distinctly different responses to undrained shear (Figure 4.34):

1. A 'strong' response with large ultimate strength (Δq = 170-280kPa at failure), reaching peak pore water pressure at 2% strain before dilating strongly, sometimes achieving a negative final excess pore water pressure (i.e. below 100kPa).
2. A 'weak' response with lower ultimate strengths (Δq = 80-130kPa at failure) and peak pore pressure at larger strains (3-4%), showing weaker dilation and retaining positive excess pore water pressure at failure (Figure 4.35).

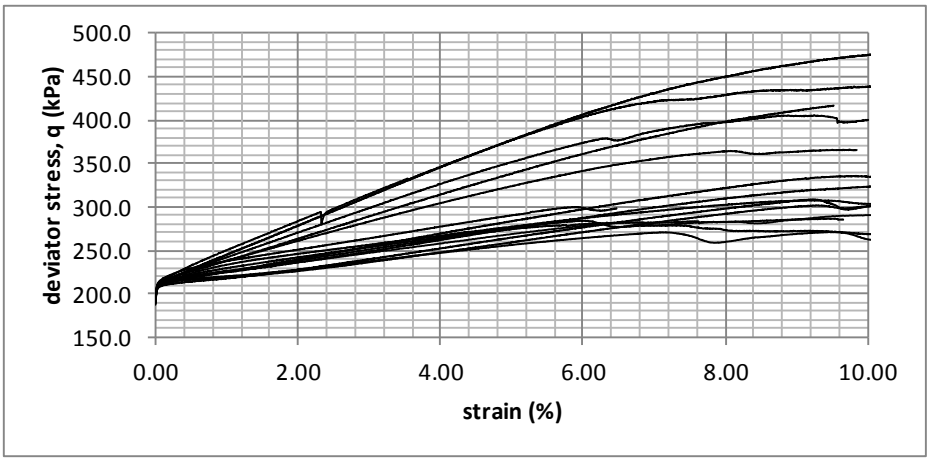

Figure 4.34: Divergent undrained shear response for initial repeatability tests with samples prepared under apparently identical conditions.

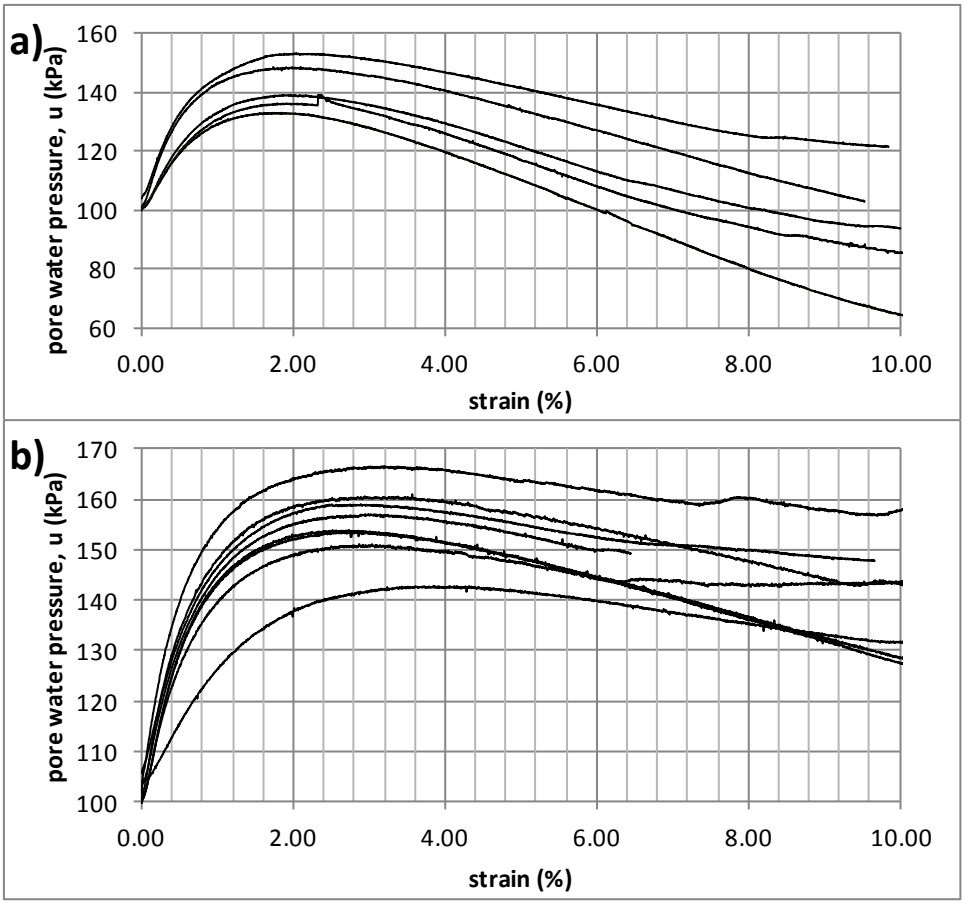

Figure 4.35: Divergent pore water pressure response under undrained shear repeatability tests for apparently identically prepared samples. a) - 'strong' samples (Δq > 170kPa at failure), b) - 'weak' samples.

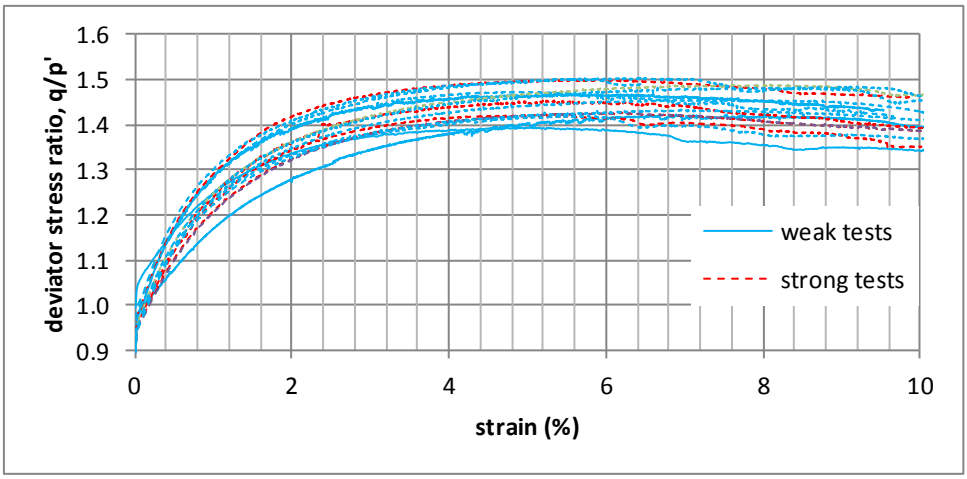

Figure 4.36: Commonality in development of deviator stress ratio with strain between 'weak' and 'strong' samples

This difference in strength and stiffness by a factor of two, under apparently identical conditions, was clearly unacceptable. The cause of this difference was sought so it could be controlled during sample preparation and variability reduced.

It was thought variations in the constituents of the Silt Mix may be influencing behaviour. Atterberg Limit tests were performed on sub-samples after testing to assess any potential soil variation between samples. The procedure for mixing constituents for samples was also changed, so that constituents were taken from bags arising from the same batch (rather than the general laboratory supply). Variations in Atterberg Limits were found to be similar to previous (Chapter 4.1.1) and did not correlate strongly to strength (Figure 4.37). The deviator stress increment at 5% strain, rather than ultimate strength, was used for comparison as shear banding occurs at different strains (6-11%), making comparison of ultimate strengths difficult. Samples prepared using the more rigorous batch control were also found to exhibit the same large strength variability.

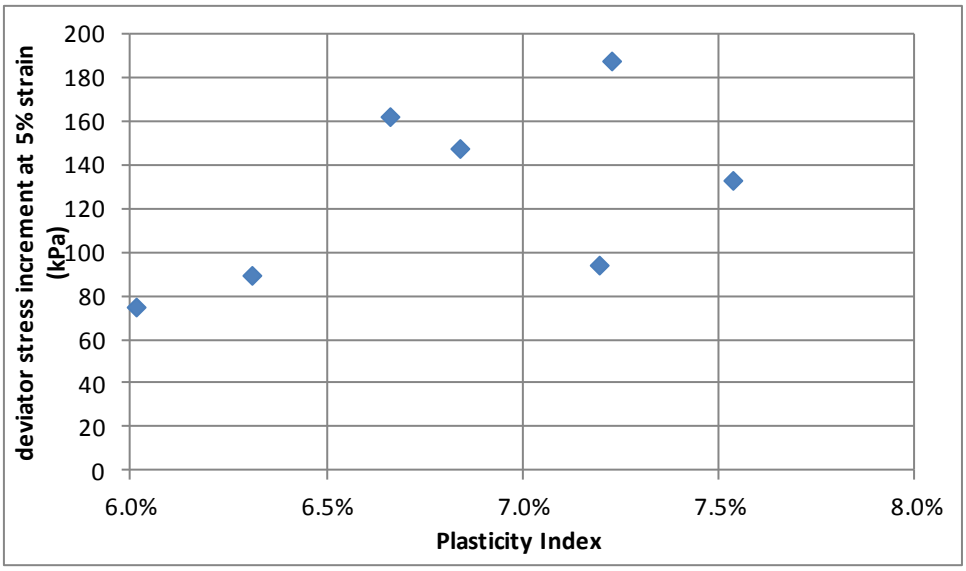

Figure 4.37: Poor correlation of sample stress increment at 5% strain (i.e. a measure of stiffness) to Plasticity Index.

Following extraction from the slurry mould, some samples were found to be misaligned with the vertical, meaning the loading ram was slightly eccentric (up to 5mm). It was thought that this may have caused the large discrepancies. The moulds were re-fabricated more accurately and the mould disassembly procedure refined to reduce the risk of slumping. Both 'weak' and 'strong' responses were still observed with these improved samples.

The slurry mould was originally designed to provide samples 205-210mm long, such that the L_0/D_0 ratio prior to consolidation was in excess of 2.0, as recommended by Bishop and Green (1965), Kirkpatrick and Belshaw (1968) and Head (1986) to avoid interference from end restraint. However following anisotropic consolidation, it was found the pre-shear L_c/D_c ratio (calculated as per equations in Section 4.2.1.5.) in some instances was below 2.0. When mobilised deviator stress is compared to the L_c/D_c

ratio, increased strength and variability for samples with L_c/D_c < 2.0 is apparent (Figure 4.38).

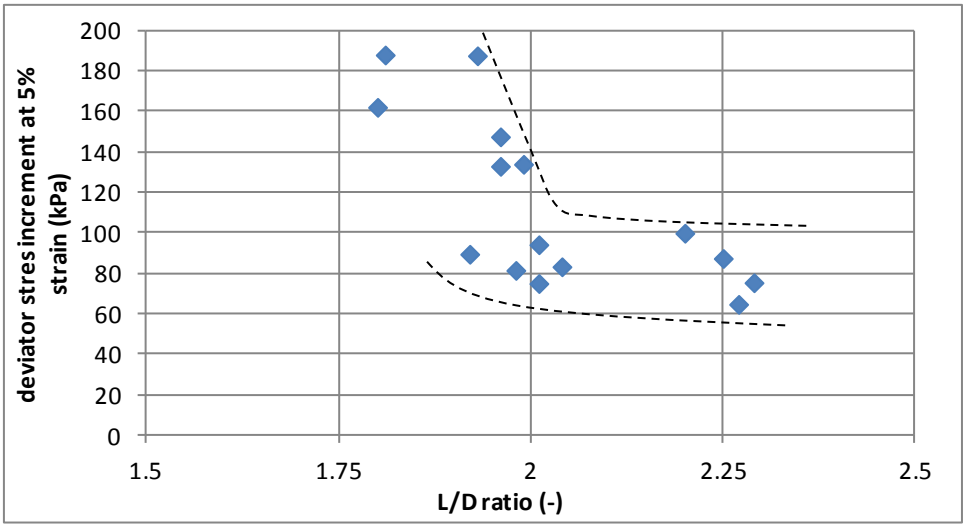

Figure 4.38: Increased variations in stiffness and strength for short L_c/D_c < 2.0) samples

Triaxial samples are known to contain a 'dead zone', extending from each end for 20-30% of the sample height. The rough contact between the sample and porous discs radially restrains the sample (Kirkpatrick and Belshaw, 1968; Sheng et al., 1997). In undrained tests on sands, this increased localised dilatant strength (Zhang and Garga, 1997). The observed increase in dilatancy and strength of Silt Mix samples with L_c/D_c < 2.0 may be due to increased radial restraint from frictional ends. A longer slurry mould was therefore produced which allowed samples of 230-235mm length to be produced; after anisotropic consolidation these samples retained an L_c/D_c ratio > 2.2.

4.2.2.2. Impact of inherent constituent variation

Samples which used material without considering batch control show higher variation in both post-test mean water content and the isotropic stage consolidation coefficient, c_{vi} (Figure 4.39).

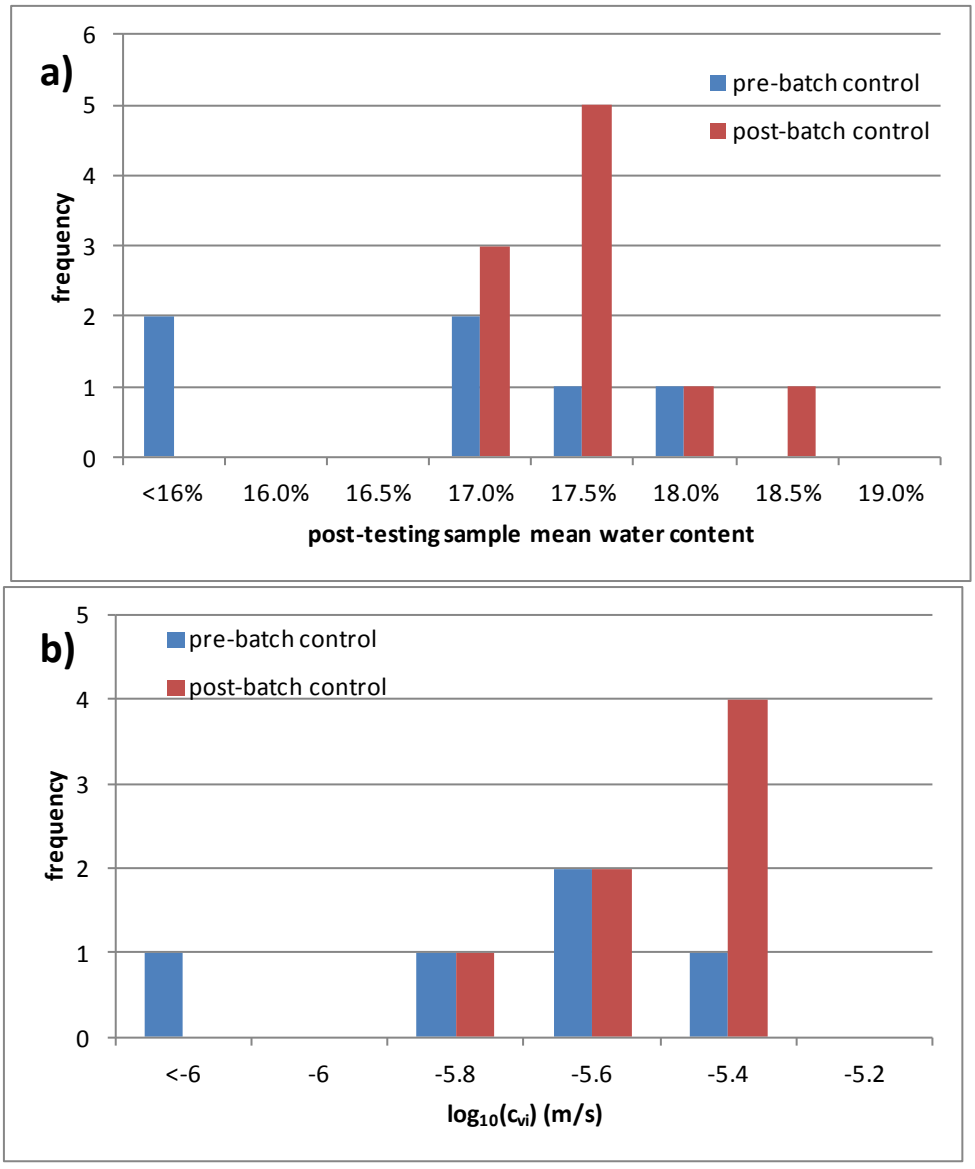

Figure 4.39: Inherent variation of sample mean water content post-test (a) and c_{vi} consolidation coefficient (b) for repeatability samples before and after implementing batch control on constituents

The sand used in the Silt Mix was supplied in 25kg bags; after the first 15no. tests, the supply changed from an older source to one purchased more recently. Dry sieve tests to BS 1377-2 (BSI, 1990a) indicated the sand to be slightly coarser. After passing this sand through a 425µm sieve as before, the grading of the coarser sand became much more uniform than the finer sand.

Despite only being a minor constituent in the Silt Mix, this relatively minor change to the sand fraction significantly changed the undrained shear response. After the initially stiff small-strain response, deviator stress reaches a peak at 0.2-0.3% strain and then dropped to a minimum at 1.5-2.0% strain, implying a partial static liquefaction. Samples then regained strength, at a lesser rate than with the older sand (Figure 4.40): ultimate strength was significantly reduced. The peak pore water pressure also tended to be higher. Increased familiarity with the equipment and refinement of the sample preparation procedure appears to have further reduced variation in response between identically prepared samples (±5kPa deviator stress and ±2kPa pore water pressure up to 8% strain, after which different shear band initiation strains make comparison difficult).

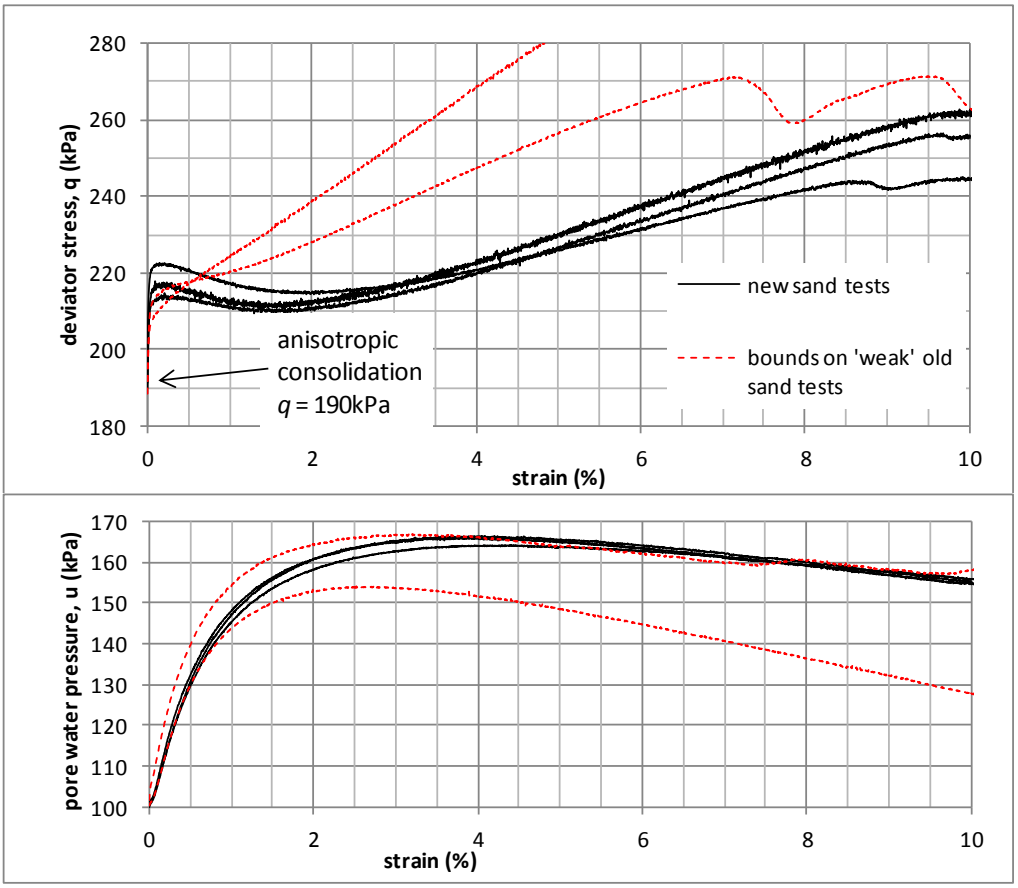

Figure 4.40: Differences in undrained shear response due to changes in sand grading.

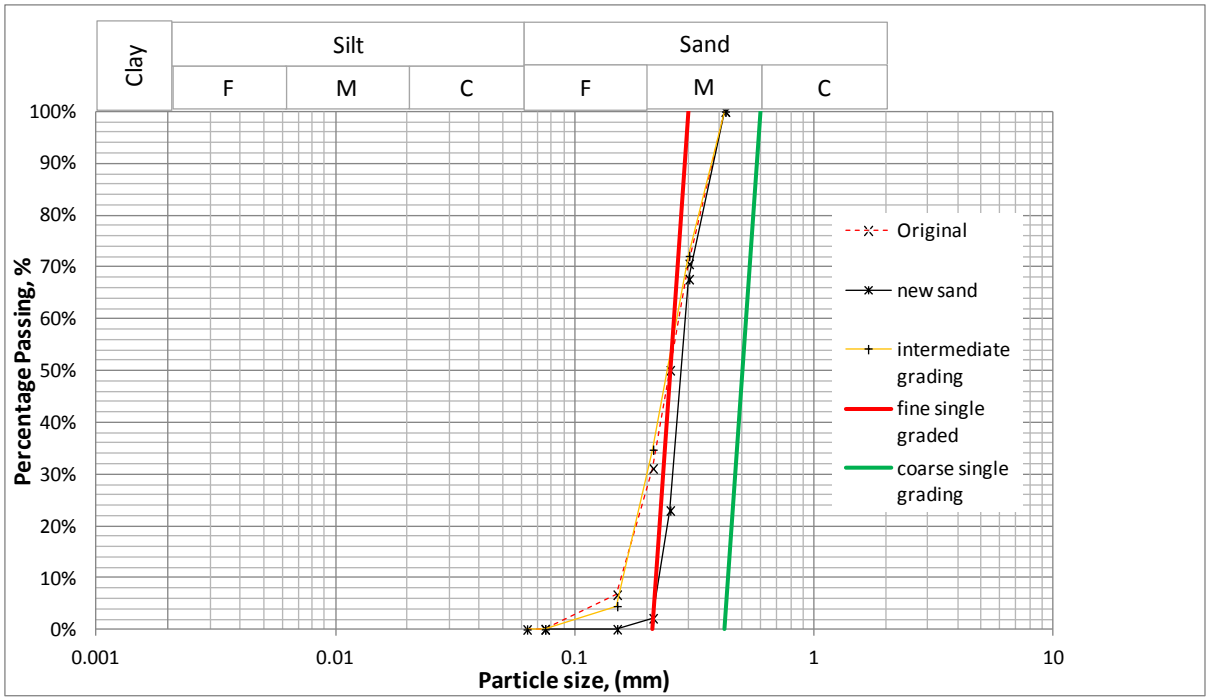

Figure 4.41: Different sand gradings tested (in Silt Mix samples) to determine influence of the sand fraction

The impact of the sand fraction on the overall behaviour was investigated further by deliberately altering the grading of the new sand. Tests were carried out using a fine, single-graded sand (passing a 300µm sieve and retained on a 212µm sieve), a coarse, single-graded sand (425-600µm) and using a blended grading which produced a sand with was better graded than the new sand but more poorly graded than the original sand (Figure 4.41 and Figure 4.42).

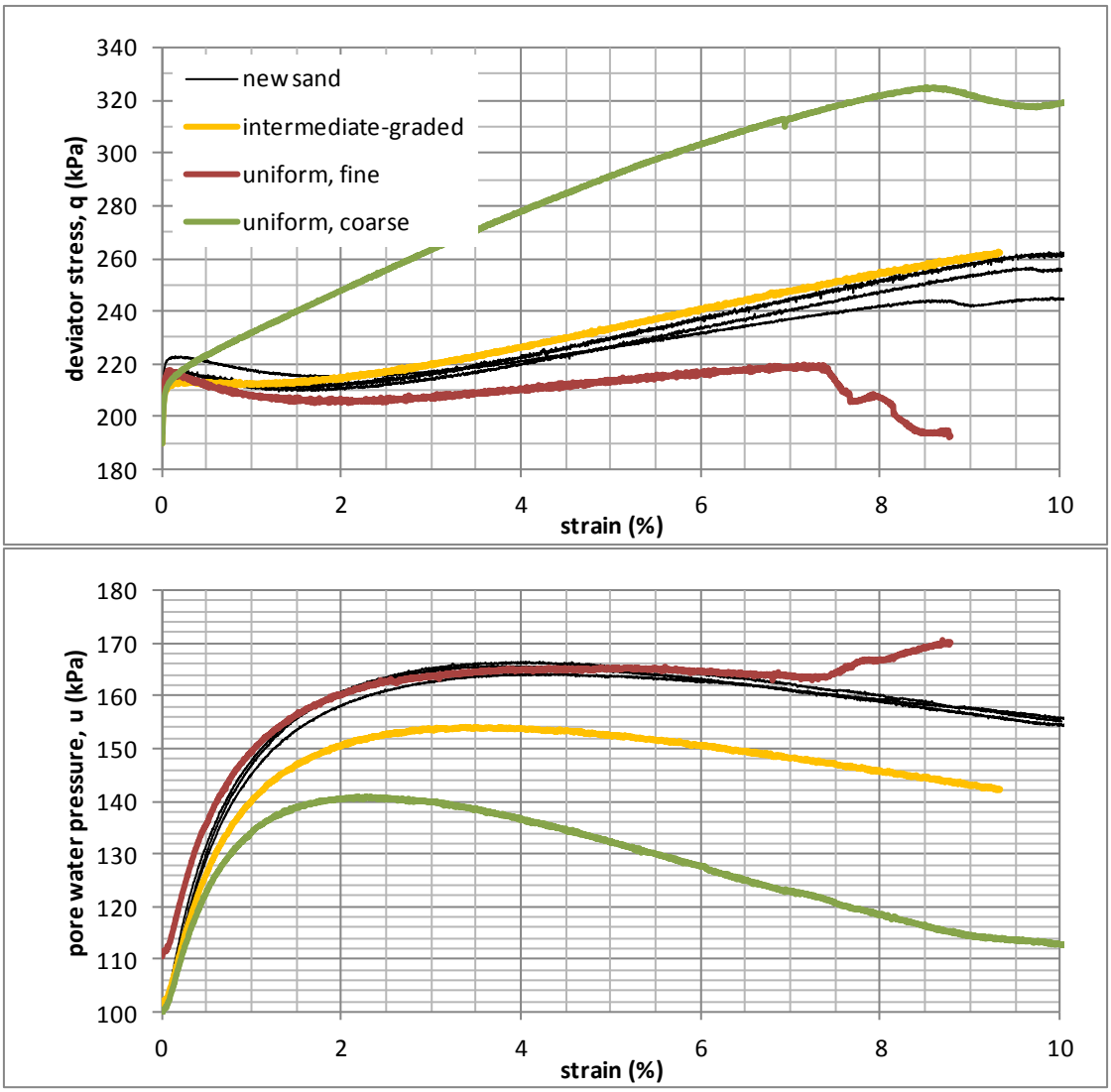

Figure 4.42: Influence of varying sand gradings on undrained shear response

By using single-graded fine sand, strength was clearly reduced, although little difference in the pore pressure response was apparent before shear banding was initiated. The sample with improved grading sand did not experience partial liquefaction (instead deviator stress remains approximately constant between 0.1 and 1.5% strain) and peak pore water pressure was substantially lower. Interestingly, single-sized coarse sand was observed to significantly increase strength and produced a more dilatant response. It is possible that the larger sand particles are able to interlock more strongly.

4.2.2.3. Influence of lubricated end platens

As end restraint significantly altered the behaviour of short samples (see Section 4.2.2.1), the influence of sample-to-platen friction was further investigated. This has been investigated by others by introducing a low-friction interface (silicone grease trapped beneath a layer of latex membrane; Figure 4.43). This generally results in a reduced barrelling tendency and more uniform radial strain distribution (Kirkpatrick and Belshaw, 1968; Zhang and Garga, 1997).

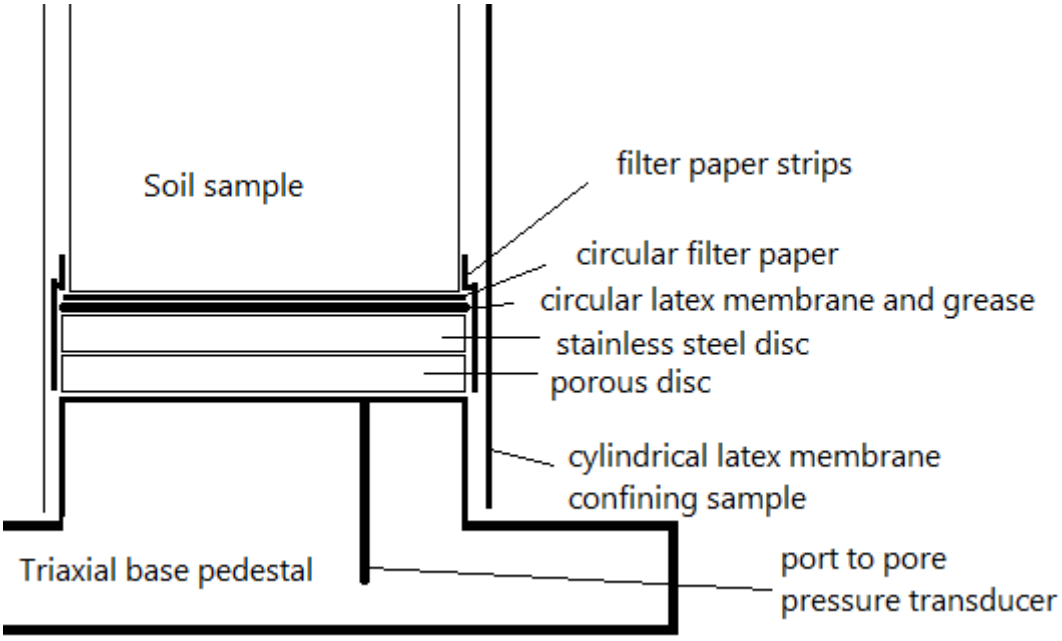

Figure 4.43: Section view through a commonly used setup for lubricated sample ends, after Head (1986). n.b. the lubricated top is arranged in the same manner.

As the slurry samples were consolidated on the triaxial cell's base pedestal, lifting to place the lubricated end assembly at the base was expected to cause unacceptable handling disturbance. It was possible to fit the lubricated end assembly to the sample top (using a low-friction polymer resin disc rather than stainless steel, purely due to availability). A similar technique was used by Kirkpatrick and Belshaw (1968) to simulate a half-sample of double the actual length: top-lubricated samples could be

considered to behave, in terms of the influence of end restraint, like samples with L_c/D_c > 4.0. Three static shear tests were undertaken with such a lubricated top interface. The first was sheared directly after anisotropic consolidation. The other two were sheared after the same consolidation stages but also after accumulating varying amounts of strain from undrained cyclic loading (the impact on cyclic response is discussed in Chapter 6.3.3).

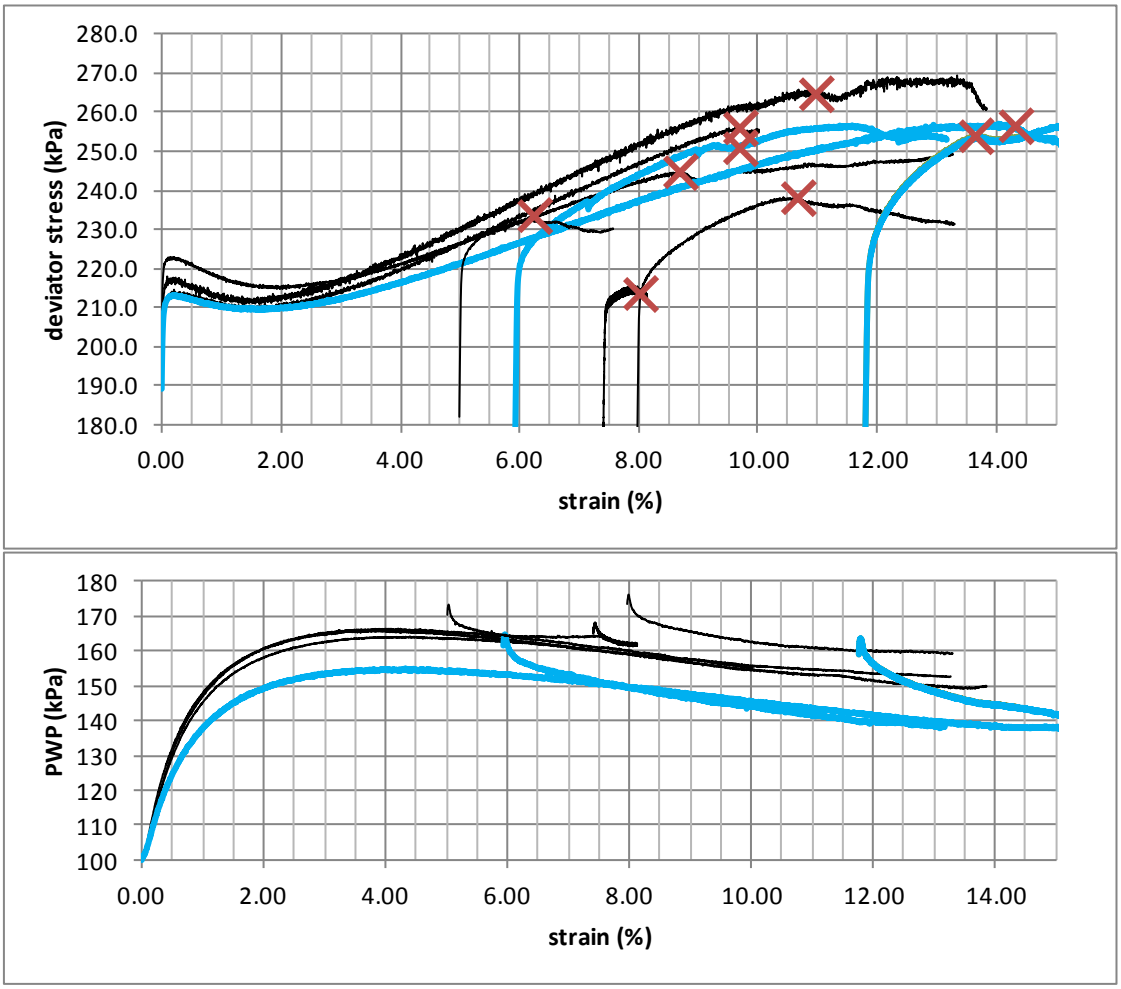

Figure 4.44: A comparison of undrained shear behaviour between standard ends (black) and lubricated ends (blue) for intact and post-cyclic tests. Red 'X' marks indicate the onset of shear banding failure. n.b. curves starting from a non-zero strain are post-cyclic tests; the starting strain represents the cumulative cyclic strain after testing.

The static behaviour without pre-cycling appears largely unaffected at small strains by the end lubrication – liquefaction initiates at 0.2% followed by recovery at 1.7% strain. The results only diverge at large strains, as expected for end restraint phenomena (Lee, 1978; Zhang and Garga, 1997); larger axial strains are required for non-uniform radial strains to manifest (Sheng et al., 1997). The deviator stress response tends to 'lag' non-lubricated samples, producing a lower stress for the same strain but ultimately failing at higher final strain with similar ultimate strength, as is generally expected (Bishop and Green, 1965; Head, 1986). The pore water pressure for the lubricated-top sample diverges from around 0.5% strain to reach a lower peak, in agreement with Lee (1978) and Head (1986) and thought to represent more closely the 'true' response of a homogeneous *in-situ* deposit. Whilst the rate of dilation with respect to strain is similar, lubricated samples can withstand more dilatant strain before shear banding.

The increased capacity for dilation of lubricated samples may relate to observed changes in the failure mode; instead of failing either in a single diagonal shear band, or a double 'X' shaped mechanism, the three top-lubricated samples showed multiple slips in both directions, indicating the samples fail in a more general shearing mechanism of multiple blocks (Figure 4.45), similarly observed by Lunne et al. (2006). It is credible to assume strain localisation is caused by end restraint: finite element modelling of a triaxial sample with rough boundaries (Sheng et al., 1997) indicates locally increased shear stresses along diagonal planes in this 'X' pattern. Silt Mix soil displays dilation after around 4% strain; shear banding dependent upon end restraint is thus reasonable to expect.

Figure 4.45: Differences in triaxial sample failure mode as a result of top lubrication: left - standard ends and single slip, right - lubricated top and multiple slip planes.

A dilatant shear band will draw in water from the surrounding soil, causing the failure zone to soften (Schofield and Wroth, 1968, Atkinson, 2000) such that failure is sudden and kinematically unstable; in fact shear bands are only kinematically possible in dilating soil (Nova, 2010). Whilst the ram load after shear band initiation often remained steady or exhibited a slight increase (Figure 4.44), when the membrane resistance to a planar slip is deducted, i.e. an additional deviator stress of 10-20kPa, it is clear that initiation of the shear band marks a peak strength followed by kinematically unstable, strain-softening failure.

Lubricating the sample top reduces the impact of end restraint on global sample behaviour. However this approach was not taken forward for the main series of tests for the following reasons:

- Setting up the lubricated top increases handling and potential for disturbance; sample quality was considered more important.
- The filter paper arrangement slows down consolidation, reducing the number of tests possible.
- Increased dilation of lubricated samples arises due to greater strain uniformity. For a homogeneous *in-situ* deposit this is certainly more representative but real, non-uniform soil deposits may in fact trigger shear banding failures sooner than a lubricated sample may suggest and the dilatant strength component may be less. Non-lubricated samples, which are more prone to failing by shear banding, may be better to investigate such a risk.

4.2.2.4. Influence of anisotropic consolidation process

Zero lateral strain (K_0) consolidation tests (as per Section 4.1.4.2) was applied to a sample containing the new sand. In addition to determining whether the faster anisotropic process was reasonably representative of K_0 consolidated soil, the lateral earth pressure coefficient *K* for the samples with the new sand were calculated.

The original K_0 consolidation tests (i.e. on samples containing the original, non-liquefying sand) returned *K* = 0.38-0.55. The test on the new sand indicated *K* = 0.48-0.50, i.e. within the expected range, although as *K* = 0.45 was used for repeatability tests, further testing on the influence of variations in *K* were performed (Chapter

6.2.2). The undrained shear response similarly showed partial liquefaction followed by recovery (Figure 4.46). The recovery of deviator stress after liquefaction for the K_0 consolidated sample is less than the anisotropic samples; this may be as a result of the slightly lower final consolidation stress (the confining pressure is the same but the axial stress is lower due to the higher *K*) or may be related to the onset of shear banding at the lower bound of that expected, i.e. 6%.

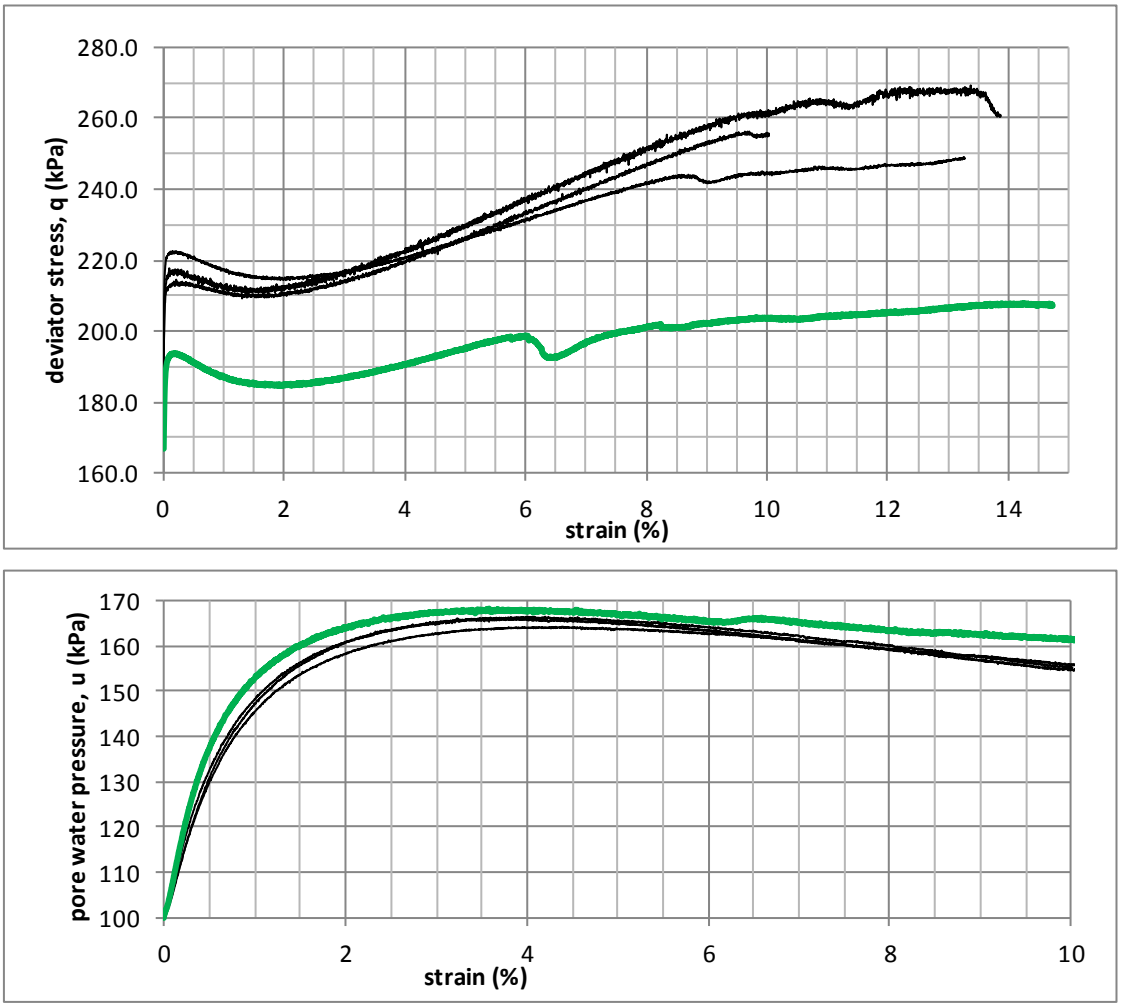

Figure 4.46: Undrained shear response of K_0 consolidated sample (green) in comparison to samples subject to faster anisotropic consolidation. The K_0 consolidated sample achieved a higher K coefficient (σ'_3 = 150kPa, as per the others) and thus the starting q is lower.

4.3. Summary

The methodology developed in this chapter produced soft, normally consolidated samples for static and cyclic triaxial testing via slurry consolidation with minimal handling disturbance. This method was chosen over other methods as it could produce very soft, saturated samples expected to better replicate the fabric of recent alluvial or marine deposits. Consistent liquefiable fabric was demonstrated through repeatability tests but could be easily disturbed; careful, handling-minimised preparation procedures were thus paramount. A liquefiable sandy clayey silt soil (Silt Mix) and English China Clay are to be tested and compared to investigate the influence of liquefiability and dilatancy on the cyclic response and consolidation recovery. Liquefaction of the Silt Mix soil is highly fabric-dependent and can be significantly altered by small changes to the sand fraction.

Control of the sample dimensions is particularly important for the dilatant Silt Mix soil as increased restraint (i.e. for $L_c/D_c < 2.0$) can cause large variations in behaviour. Reduced end restraint (lubricated sample top) affects large-strain behaviour, delays shear band initiation and changes the failure mode to a more general shearing. Medium-strain behaviour, including initiation of liquefaction, is unaffected by end restraint. Due to the greatly increased complexity of setting up end-lubricated tests, only a select number were performed.

Anisotropic triaxial consolidation was used to finely control the stress state of the soil and achieve a response representative of a deep, normally consolidated soil. Liquefiability was not found to be significantly influenced by the intermediate

consolidation stages; K_0 consolidation was replaced by a faster anisotropic consolidation process. The preconsolidation stress developed during sample preparation (p' = 70kPa) is exceeded by appropriately three times (p' = 210kPa) to recapture the behaviour of samples with no unload-reload history. Furthermore, the inherent load cell noise and possible overload during cyclic stages is proportionally less at higher stresses.

The variability of test results was investigated and separated into errors arising from the equipment and measurement apparatus, and errors arising from the soil and sample preparation. The errors inherent from the equipment can be quantified as:

- Water pressure (cell, back and pore) readings: ±1kPa relative to other readings from the same test and ±2kPa on the absolute value of pressure (i.e. between different tests). The use of a rolling mean (for monotonic test data) reduces random variation to ±0.5kPa, with an error of ±1.5kPa on the absolute value.
- Volume change readings: a creep of 0.5ml over 24 hours is recorded; test duration needs to be considered when accounting for this error.
- Axial load readings: ±4N relative to other readings from the same test and ±10N on the absolute value of axial load (0.5kPa and 1.3kPa stress respectively for a 100mm diameter sample), taking into account potential bedding and zero-point errors.
- Axial load control: the feedback mechanism for slow monotonic tests does not display any increase in variability from the target above the inherent instrument noise (±4N or 0.5kPa). For rapidly varying cyclic tests, control is less

accurate; variation from the target is ±7N (0.9kPa) for a smooth haversine waveform and ±12N (1.5kPa) for a square wave. Square waveforms also have a low probability of a large control error of up to 40N (5kPa).

Variation between the results from the 3no. static tests using the new sand, which also included the inherent equipment errors above, is ±5kPa deviator stress and ±2kPa pore water pressure up to a strain of 8%. Larger errors arose at greater strains, to some extent due to the variation in the shear band initiation strain. Errors from these final static tests were reduced significantly from earlier tests as a result of refinements to the sample preparation process.

CHAPTER 5: TESTING PROGRAMME

5.0. Introduction

Laboratory experiments principally investigated the following:

- Monotonic undrained shear of intact and post-cyclic samples, particularly in terms of liquefaction
- Cyclic threshold stress, liquefaction and accumulation of strain and pore water pressure
- Cyclic strain rate and cycle duration-dependent behaviour
- Intermediate consolidation between cyclic load application, pore pressure dissipation and strengthening

The majority of tests were performed on liquefiable Silt Mix soil, but a series of tests on English China Clay, investigating the same phenomena, were performed as non-liquefying controls.

Consolidation stresses were chosen to be sufficiently high that memory of overconsolidation from sample preparation is erased, i.e. p' = 210kPa, three times the preconsolidation stress (p' = 70kPa, see Chapter 4.2.2). As liquefaction is strongly influenced by stress history (Chapter 3.3.1), this aspect of behaviour was considered more critical to reproduce than using the typical stresses computed in Chapter 2.5. The discrepancy in applying strength values derived using higher consolidation stresses was accounted for by normalising with respect to overburden stress, similarly to Ladd and Foott (1977). The effect of different consolidation stresses on the qualitative response

was also investigated in a limited number of tests (Series A and K; see Table 5.1, Table 5.3 and Table 5.4).

The slow loading rates of heavy vehicles has been identified as an important factor in the resistance of subgrade soils, with slower loads more prone to development of plastic strain and pore water pressure (Chapter 3.4). As slower than anticipated vehicle progress may therefore induce greater damage, tests were based on a slower frequency of 0.01Hz (c.f. 0.02Hz in Chapter 3.4). Understanding changes in behaviour dependent on loading rates was also considered important. As changes in strength with loading rate often follow logarithmic relationships (e.g. Overy, 1982; Andersen, 2009) and in order to observe clear and measureable frequency-dependent changes in behaviour, tests to investigate frequency effects were also undertaken at 0.1Hz.

Monotonic tests were used to determine Δq_{peak} and thus inform selection of cyclic stresses for threshold stress testing. The upper bound of cyclic stresses (series G tests) was based on model results of transient stresses normalised against the effective overburden stress (Table 2.5): undrained cyclic tests were able to reach 15% of the effective overburden stress (i.e. 50kPa) before becoming uncontrollable and series G tests incorporating consolidation were able to reach 59% of the effective overburden stress, i.e. equivalent to the transient stress from a 2000 tonne at 6.5m depth in Chapter 2.5.

Tests are divided into a number of 'Test Series' which investigated these different aspects:

Table 5.1: Overview of Test Series undertaken

Series	Principal aim of Test Series
R	Repeatability/method refinement tests (see Chapter 4.2.2.1)
K	Consolidation-only tests for determination of K_0 for use in faster two-stage consolidation and to derive consolidation characteristics. Feedback control matched change in length to measured volume change (i.e. constant area).
A	Monotonic shear tests investigating static liquefaction in samples using new sand. Stress state varied and trial of lubricated top assembly.
B	Strain-controlled cyclic tests to investigate small to medium strain transition (i.e. initiation of plasticity) and determine volume change threshold (after Hsu and Vucetic, 2006; strain magnitudes based on Díaz-Rodriguez and López-Molina, 2008). Attempted to use larger strains to investigate degradation threshold, relaxation of anisotropic stress state found to be a serious obstacle - this aspect of the study was abandoned.
C	Load-controlled tests to determine cyclic accumulation of strain and pore pressure stiffness moduli, and threshold stress. It was found part-way through that for load-controlled tests, the anisotropic stress state gradually unloads. All Series C tests were therefore gradually decreasing in maximum cyclic stress and also changing from one-way to two-way as strain increased.
D	As per series C, these tests aimed to investigate cyclic load response. Manual correction to cyclic load limits was applied to maintain the maximum stress

Series	Principal aim of Test Series
	throughout a test as strain increases. The impact of creep rates under anisotropic stress conditions on strain accumulation at very small cyclic amplitudes was also investigated.
E	These tests further investigated the phenomenon of strengthening in post-cyclic monotonic tests observed in Series D tests and various combinations of cyclic load and monotonic shearing were applied to determine the necessary conditions for post-cyclic strengthening.
F	Cyclic tests with varying frequency and waveform to investigate the impact of strain rates and cycle duration. Some of these tests were performed without area corrections so were only comparable to Series C tests (and not Series D/E).
G	Cyclic tests with various combinations of cyclic load and drainage intervals between loads to investigate excess pore pressure dissipation and strengthening.
CL	Monotonic, undrained cyclic and cyclic with consolidation interval tests, conducted using the same procedures as Series A-G, applied to non-liquefying English China Clay.

5.1. Correction for relaxation

As demonstrated in Section 4.2.1.5., undrained strain increases the cross-sectional area. For anisotropically consolidated samples, cycling between constant maximum

and minimum ram loads causes relaxation of the consolidation axial stress, which can be significant even under relatively small cyclic stress increments (Figure 5.1).

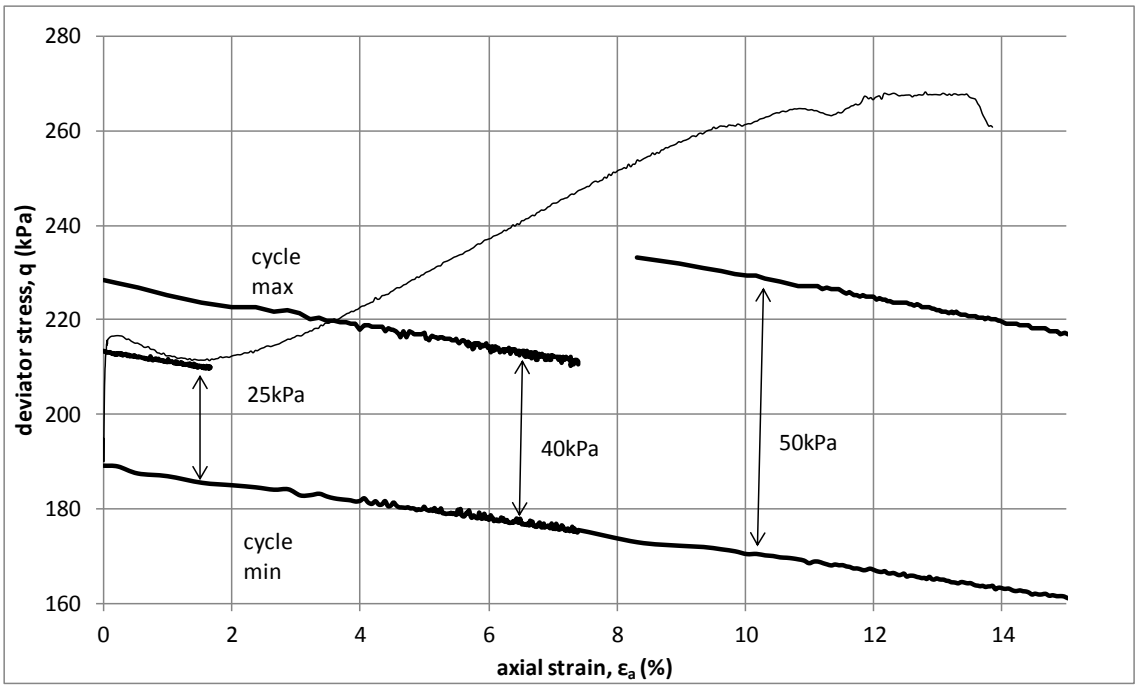

Figure 5.1: Relaxation of the maximum cyclic stress (thick lines) due to feedback control on load readings and accumulated strain in Series C tests. A typical monotonic stress-strain response is shown (thin line) to indicate the relative significance of relaxation.

In subsequent tests (Series D, E, G, CL and some of F), relaxation was corrected by manually changing the maximum and minimum target cyclic loads to maintain constant maximum and minimum stresses over the corrected area. Bearing in mind the anticipated errors in load measurement (Chapter 4.2.1.3), this was performed approximately every 0.5% strain, i.e. equivalent to approximately 1kPa of relaxation.

5.2. Intermediate consolidation stages

Drainage between cyclic loads in Series G and CL tests was intended to model the behaviour of a heavy haul road subgrade allowed to rest without traffic for long enough for pore pressures to dissipate. Due to the complex stress field, the likely

stress conditions experienced are difficult to determine: it cannot be assumed that the lateral effective stresses remain constant as overconsolidation may induce a higher *K*. As the passage of a heavy haul vehicle induces a complex stress/strain field, the assumption of K_0 conditions during consolidation is not necessarily correct. For simplicity, Series G and CL tests simply applied the final consolidation stresses, i.e. with no change to cell pressure, back pressure or *K*. It is likely that some increase in *K* during intermediate consolidation stages will occur in the field, which would be expected to improve resistance in the compression zone particularly (the *in-situ* deviator stress is reduced by higher lateral stress). Investigations using scale models or field trials would be likely to yield much more useful information than changing the assumed *K* in triaxial testing.

5.3. Clay anisotropic consolidation

As the clay tests are intended as a minor part of this research and their low permeability makes K_0 consolidation very slow, it was decided to estimate a $K_{0,NC}$ value based on the Plasticity Index and reported $K_{0,NC}$ values in Valls-Marquez (2009) to save time. Accordingly $K_{0,NC}$ = 0.63 was chosen.

5.4. Test summaries

The testing conditions and any notable observations for each test are presented in Tables 5.2 to 5.11.

Table 5.2: Series R tests

Test	Consolidation	Notes
R-1 to R-15	Anisotropic: p' = 210kPa	Repeatability (Length to diameter ratio variation)
R-16	Anisotropic: p' = 210kPa	Coarse Single-sized sand Mix B
R-17	Anisotropic: p' = 210kPa	Fine Single-sized sand Mix B – liquefying
R-18	Anisotropic: p' = 210kPa	Multi-graded new sand - non-liquefying, but dropping tangent modulus

Table 5.3: Series K tests

Test	Consolidation	Notes
K-1	σ'_3 = 100kPa, K_0	Using original sand. $K_{0,NC}$ = 0.50
K-2	σ'_3 = 100kPa, K_0	Using original sand. $K_{0,NC}$ = 0.38
K-3	σ'_3 = 50kPa, K_0	Using original sand. $K_{0,NC}$ = 0.42
K-4	σ'_3 = 50kPa, K_0	Using original sand. $K_{0,NC}$ = 0.55
K-5	σ'_3 = 150kPa, K_0	Using new sand. $K_{0,NC}$ = 0.48
K-6	σ'_3 = 200kPa, K_0	Using new sand. $K_{0,NC}$ = 0.48

Table 5.4: Series A tests

Test	Consolidation	Notes
A-1	Anisotropic: σ'_1 = 337kPa, σ'_3 = 150kPa	Partially liquefying
A-2	Anisotropic: σ'_1 = 337kPa, σ'_3 = 150kPa	Disturbed by interrupted consolidation, elevated vol. change. Non liquefying.
A-3	Anisotropic: σ'_1 = 348kPa, σ'_3 = 150kPa	Partially liquefying
A-4	Anisotropic: σ'_1 = 316kPa, σ'_3 = 150kPa	Partially liquefying
A-5	Anisotropic: σ'_1 = 336kPa, σ'_3 = 150kPa	Lubricated top - partially liquefying
A-6	Isotropic: $\sigma'3$ = 190kPa	Pressure ramped slowly for more faithful compression line. Non liquefying.
A-7	K_0, $\sigma'3$ = 150kPa	$K_{0,NC}$ = 0.50. Partially liquefying.
A-8	OC: σ'_1 = 267kPa, σ'_3 = 100kPa	Non liquefying
A-9	OC: σ'_1 = 310kPa, σ'_3 = 119kPa	Non liquefying
A-10	Anisotropic: Lower σ'_3 (75kPa), K=0.45	Partially liquefying
A-11	Anisotropic: Lower σ'_3 (50kPa), K=0.45	Partially liquefying

Test	Consolidation	Notes
A-12	Anisotropic: σ'_3 = 150kPa, stepped up to σ'_3 = 200kPa (K= 0.45)	Partially liquefying (test not taken to ultimate failure)
A-13	Anisotropic: σ'_1 = 337kPa, σ'_3 = 150kPa	Clearly disturbed; slumped and tilted. Non liquefying, shear banding failure at ~2%.
A-14	Anisotropic: σ'_1 = 273kPa, σ'_3 = 150kPa	Partially liquefying, lower stress drop in liquefaction.

Table 5.5: Series B tests (all anisotropically consolidated to p' = 210kPa, K = 0.45)

Test	Cyclic strain	Cycle count	Waveform & period	Notes
B-1	0.01% to 0.1%	10no. each stage	Haversine, 10s	Incremental strain to determine volume change threshold. Only max/min stress and pore pressure recorded
B-2	0.005% to 0.1%	10no. each stage	Haversine, 10s	Incremental strain to determine volume change threshold. Full data resolution (200 points per cycle). Period of undrained creep relaxation for 1hr before cyclic stage to determine baseline change in *q* and *u*.
B-3	2%	200	Haversine, 10s	Reverted to isotropic stress state after 1st cycle, i.e. Lift-off due to plastic strain.

Table 5.6: Series C tests (all anisotropically consolidated to p' = 210kPa, K = 0.45)

Test	Cyclic load & count	Waveform & period	Post-shear	Notes
C-1	200no. 0-40 kPa	Haversine, 100s	Y	Cyclic liquefaction and recovery. Final cyclic strain of 5.0%. Post-shear stress-strain curve converges to that of the intact tests, fails at 7.5% strain.
C-2	200no. 0-40 kPa	Haversine, 100s	Y	Cyclic liquefaction and recovery. Final cyclic strain of 8.0%. Post-shear stress-strain curve below that of the intact tests, fails at 10.4% strain.
C-3	200no. 0-40 kPa	Haversine, 100s	N	Cyclic liquefaction and recovery.
C-4	200no. 0-40 kPa	Haversine, 100s	Y	Cyclic liquefaction and recovery. Final cyclic strain of 7.4%. Post-shear stress-strain curve converges to that of the intact tests, fails at 10.4% strain.
C-5	200no. 0-40 kPa	Haversine, 100s	Y	Lubricated top - liquefaction and recovery. Final cyclic strain of 5.9%. Post-shear stress-strain curve converges to intact test, fails at 14.0% strain.

Test	Cyclic load & count	Waveform & period	Post-shear	Notes
C-6	200no. 0-50 kPa	Haversine, 100s	N	Cyclic liquefaction and recovery, reaches limit of ram travel (hence no post-shear)
C-7	200no. 0-50 kPa	Haversine, 100s	N	Disturbed during mould removal, large consolidation volume change, no liquefaction
C-8	200no. 0-50 kPa	Haversine, 100s	Y	Disturbed during mould removal, large consolidation volume change, no liquefaction
C-9	200no. 0-50 kPa	Haversine, 100s	N	Lubricated top - liquefaction and recovery, reaches limit of travel
C-10	200no. 0-50 kPa	Haversine, 100s	N	Over-long sample, disturbed by trimming. Large consolidation volume change, no liquefaction
C-11	200no. 0-50 kPa	Haversine, 100s	N	Cyclic liquefaction and recovery
C-12	200no. 0-25 kPa	Haversine, 100s	Y	Stable strain accumulation. Final cyclic strain of 1.7%. Increased strength and stiffness in post-shear, fails at 7.6% strain.

Test	Cyclic load & count	Waveform & period	Post-shear	Notes
C-13	200no. 0-40 kPa	Haversine, 100s	N	Control error in anisotropic consolidation stage: unload and reload applied. No liquefaction

Table 5.7: Series D tests (all anisotropically consolidated to p' = 210kPa, K = 0.45)

Test	Cyclic load & count	Waveform & period	Post-shear	Notes
D-1	200no. 0-45 kPa	Haversine, 100s	N	Cyclic liquefaction and recovery
D-2	200no. 0-25 kPa	Haversine, 100s	Y	Cyclic liquefaction and recovery. Final cyclic strain of 8.7%. Post-shear not taken to failure, used to derive static small-strain stiffness only.
D-3	200no. 0-20 kPa	Haversine, 100s	Y	Stable strain accumulation. Final cyclic strain of 0.7%. Increased strength and stiffness in post-shear, fails at 9.9% strain.
D-4	200no. 0-8 kPa	Haversine, 100s	Y	Very slow, stable strain accumulation. Final cyclic strain of 0.06%. Partial static liquefaction in post-shear as per intact tests, failure at 7.5% strain.

Test	Cyclic load & count	Waveform & period	Post-shear	Notes
D-5	200no. 0-8 kPa	Haversine, 100s	N	Longer secondary consolidation period to reduce creep rates, for comparison to D-4. Stable strain accumulation.
D-6	200no. 0-15 kPa	Haversine, 100s	Y	Very slow stable strain accumulation. Final cyclic strain of 0.28%. Partial static liquefaction in post-shear as per intact tests. Failure at 6.4% strain.
D-7	50no. 0-8 kPa; 200no. 0-20 kPa	Haversine, 100s	Y	Longer secondary consolidation period to reduce creep rates. Stable strain accumulation. 8kPa regime produces final strain of 0.01%, 20kPa regime final strain of 0.54%. Increased strength and stiffness in post-shear, fails at 11.5% strain.
D-8	100no. 0-40kPa	Haversine, 100s	N	Cyclic liquefaction and recovery. Final cyclic strain of 9%. Terminated at 100no. Cycles to expedite testing, no post-shearing conducted.

Table 5.8: Series E tests (all anisotropically consolidated to p' = 210kPa, K = 0.45)

Test	Cyclic load & count	Waveform & period	Post-shear	Notes
E-1	1no. 0-40 kPa	Haversine, 100s	Y	Cyclic load above the liquefaction threshold, final strain of 0.2%, i.e. at or just above the initiation strain. Partial static liquefaction, failure at 10.5% strain.
E-2	7no. 0-40 kPa	Haversine, 10s	Y	Cyclic load above the liquefaction threshold, final strain of 0.4%. Fast relaxation in between end of cyclic and start of static. Partial static liquefaction, weaker than intact tests. Some dilatant recovery, fails at 5.5% strain.
E-3	200no. 0-20 kPa; 200no. 0-40 kPa	Haversine, 10s; 100s	N	Initial cyclic load below the liquefaction threshold, final strain of 0.3%. Strain under 40kPa cyclic load lower than usual, possible slight liquefaction followed by stabilisation.
E-4	8no. 0-20 kPa	Haversine, 100s	Y	Cyclic load below the liquefaction threshold, final strain of 0.1%. No liquefaction. Possibly disturbed - high iso. vol. change.
E-5	10no. 0-20 kPa	Haversine, 100s	Y	Cyclic load below the liquefaction threshold, final strain of 0.1%. Liquefaction.

Table 5.9: Series F tests (all anisotropically consolidated to p' = 210kPa, K = 0.45)

Test	Cyclic load	Cycle count	Waveform & period	Post-sheared	Notes
F-1	0-40kPa	200	Haversine, 10s	Y	Cyclic liquefaction and recovery. No stress correction.
F-2	±40kPa	200	Square wave, 100s	N	Cyclic liquefaction and recovery. No stress correction.
F-3	±40kPa	200	Sine wave, 100s	N	Cyclic liquefaction and recovery. No stress correction.
F-4	±40kPa	200	Sine wave, 10s	N	Cyclic liquefaction and recovery. No stress correction.
F-5	0-15kPa; 0-20kPa	670; 500	Haversine, 10s	Y	Stress-corrected: stable strain accumulation. 1% final strain, non-liquefying. Fails at 10% strain.
F-6	0-25kPa	840	Haversine, 10s	N	Stress-corrected: cyclic liquefaction and recovery.

Table 5.10: Series G tests (all anisotropically consolidated to p' = 210kPa, K = 0.45, 100s haversine waveforms)

Test: Cyclic load	Cycle count: Drainage	Post-sheared	Notes
G-1: 0-40kPa	1; 20; 200: 2hrs after each phase	Y	Anisotropic consolidation records lost. Drainage after 1st cycle and then every 1% plastic strain. Dissipation near-total (2kPa residual). No liquefaction, final cyclic strain 1.7%. Increased strength/ stiffness in post-shear. Fails at 9% strain.
G-2: 0-40kPa up to 0-201kPa (11no. Stages)	5no. each stage: 2hrs after large strains	Y	Drainage after 1st cycle and then if either liquefaction (accelerating strains) or >1% strain accumulation per stage, intending to determine upper limit to strength gain from consolidation. Halted at total axial strain of 9.6% - ultimate failure not reached. Increased strength and stiffness in post-shear, fails at 15% strain.
G-3: 0-40kPa	1; 13; 118: 5mins after each phase	Y	Drainage after 1st cycle and every 1% plastic strain. Small dissipation, increasing in each stage. No liquefaction, similar to test G-1 up to around 1% strain, then accumulation increases. Higher post-shear strength/stiffness, fails at 7.5% strain.

Test: Cyclic load	Cycle count: Drainage	Post-sheared	Notes
			PWP transducer faulty. Lower consolidation volume change and higher final consolidation creep rate than G-3. Drainage after 1st cycle and every 1% increment in plastic strain, no cyclic liquefaction, similar to G-3 during 1st 100no. cycles. Cyclic load incremented, with intermediate vol. change threshold tests and drainage. Fails at 14% strain.
G-4: 0-40kPa (first 3no. stages) to 0-124kPa (9no. Stages)	1; 13; 86; 6no. each stage: 5mins and 2hrs	Y	
G-5: 0-20kPa; 0-40kPa; to 0-150kPa (9no. Stages)	70; 100; Varies per stage: 5mins and 2hrs	N	Lubricated sample top to investigate end restraint effects. PWP transducer faulty. First two stages replicated test E-3, i.e. 70no. 100s cycles of 20kPa load followed by 40kPa. No liquefaction. Increasing strength with drainage during incremental load stages apparent.

Table 5.11: Series CL tests

Test	Conditions	Notes
CL-1	Anisotropic ($\sigma'3$ = 75kPa, K = 0.63), monotonic shear (1mm/hr)	Non-liquefying, contractant

Test	Conditions	Notes
CL-2	Anisotropic (*σ'3* = 150kPa, K = 0.63), monotonic shear (1mm/hr)	Non-liquefying, contractant, slight strain-softening at failure (> 8% strain)
CL-3	Anisotropic (*σ'3* = 150kPa, K = 0.63), cyclic (200no. 20kPa, 100s haversine)	Gradual strain accumulation, starting to accelerate after ~6% strain.
CL-4	Anisotropic (*σ'3* = 150kPa, K = 0.63), cyclic (200no. 15kPa, 100s haversine), post-shear	V. slow strain accumulation, stabilising, post-cyclic strength slightly below CL-2.
CL-5	Anisotropic (*σ'3* = 150kPa, K = 0.63), cyclic (200no. 17kPa, 100s haversine), post-shear	Stabilising strains, post-cyclic strength below CL-2 and CL-3. Shear banding failure at 10% strain.
CL-6	Anisotropic (*σ'3* = 150kPa, K = 0.63), cyclic (incrementing load, 100s haversine) with drainage, post-shear	Larger than usual load cell noise, hard to control. Tendency for increased strength from drainage intervals clear. Shear banding at failure.
CL-7	Anisotropic (*σ'3* = 150kPa, K = 0.63), cyclic (initially 17kPa @ 10s, then 20kPa @ 100s before incrementing load) with drainage, post-shear	Initial 17kPa stage seems to increase subsequent 20kPa strain accumulation. Drainage intervals effective in reducing strain accumulation and increasing post-cyclic strength. Shear banding at failure.

CHAPTER 6: RESULTS AND DISCUSSION

6.0. Introduction

This chapter presents and discusses the experimental results in the context of using cyclic load to improve subgrade soil and reduce degradation under a relatively small number of extremely large heavy haul vehicles. The focus of the testing was the liquefiable Silt Mix soil, as this type of soil presents the most serious hazard to heavy haul traffic, i.e. sudden large ground movements due to meta-stable liquefaction (see Chapters 3.3 and 4.1). It is demonstrated in this chapter that, if the necessary conditions which preserve such a soil's precarious initial fabric are maintained, a relatively small perturbation from traffic may be sufficient to trigger liquefaction. Conversely, if the fabric can be disrupted whilst maintaining stability, liquefaction can be averted and the soil improved. Different methods of treatment through application of transient load are tested and evaluated; a series of tests on stable, plastic clay (English China Clay) also are included as a control to determine to what extent improvement is dependent upon the soil having a liquefiable initial fabric.

In some graphs, 'static' is used to describe monotonic, constant strain rate tests, for reasons of brevity.

6.1. Triaxial Consolidation

6.1.1. Compression characteristics

The triaxial consolidation stage aims to achieve the anisotropically normally consolidated state expected of young alluvial deposits at depth. This process also

yields information on the compression characteristics, progression of consolidation over time and also whether disturbance from preparation procedures are likely to have significantly changed the sample behaviour. The characteristics of the accelerated, two-step consolidation process are compared to the longer zero lateral strain process to determine how well this reproduces the desired results.

The K-series tests determined $K_{0,NC}$ and virgin compression paths. For initial tests on the original sand mix (see Chapter 4.1.1 and 4.2.2.2) $K_{0,NC}$ = 0.38 to 0.55 (determined after Head, 1986); accordingly $K_{0,NC}$ = 0.45 was selected for the accelerated, two-stage anisotropically consolidated repeatability tests (R-series). As was apparent in Chapter 4.2.2.2, the shear behaviour changed dramatically when samples used the new sand. It was later determined, through tests K-5 and K-6, that compression characteristics also changed; $K_{0,NC}$ was found to be in the range 0.48 to 0.50, whilst water contents for a given p' were increased (Figure 6.1).

The preconsolidation pressure, determined using Casagrande's method, was approximately p' = 70kPa; assuming $K_{0,NC}$ = 0.50 during slurry consolidation indicates $\sigma'_1 \approx$ 105kPa. During slurry consolidation the maximum load was 1500N, equal to σ_1 = 190kPa, implying the difference, (45%) was lost to friction. It is difficult to precisely determine friction losses this way due to the subjective and approximate nature of this analysis; Peters (1988) suggests Casagrande's method to be a lower-bound approximation. However it suggests, even with the developments in Chapter 4.1.2.2, mould-to-soil friction was still significant. Pore pressure measurement by Valls-

Marquez et al. (2008) similarly indicated maximum slurry pore pressures of 40-80% of the applied load, i.e. significant friction losses.

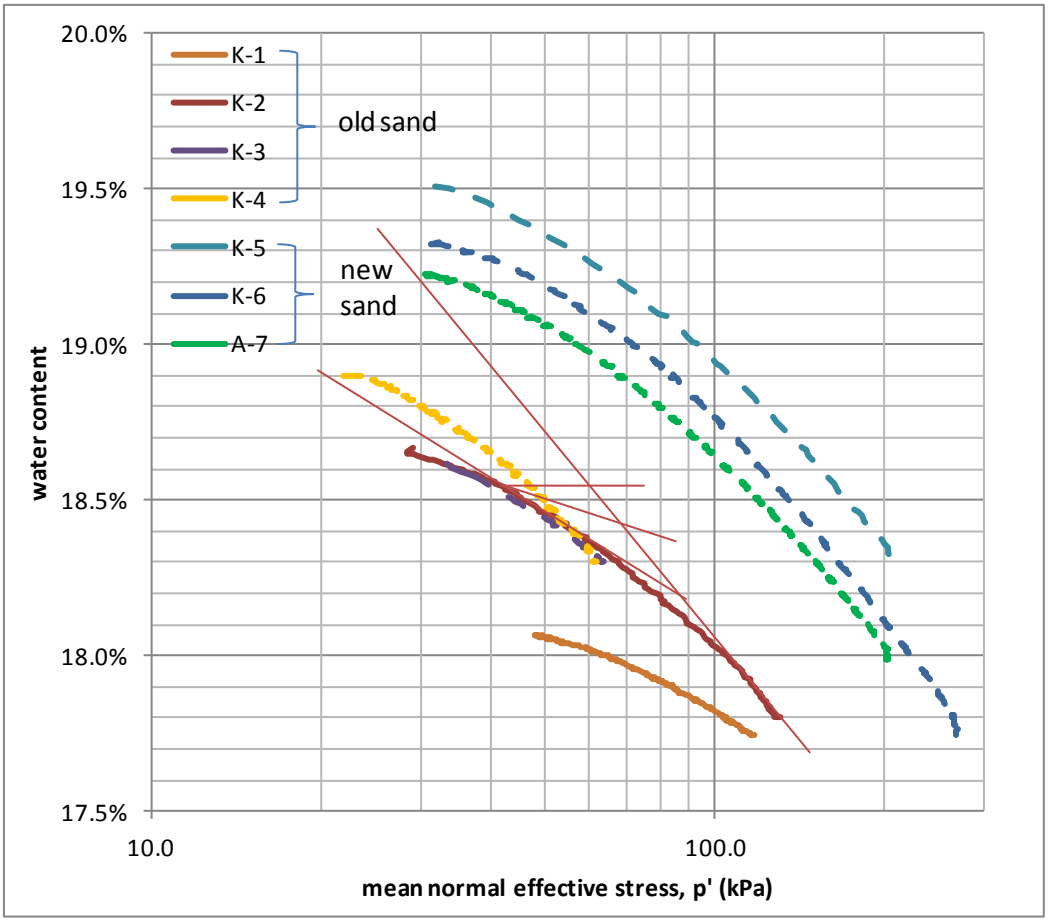

Figure 6.1: One-dimensional consolidation results for the different sand mixes. Initial water content of new sand samples inferred from volume change is 20.0-20.5%.

The relatively low volume change tendency of silt is apparent from the compression paths; the linear gradient of the K_0 Normal Compression Line (K_0-NCL) for the new sand mix (Figure 6.1) is 2.2% water content per log cycle of p' (±0.1%) or in Cam-Clay parameters, λ = 0.0282 (± 0.0013). From the volume change measurements during these tests, the total water content change from anisotropic consolidation to p' = 210kPa is 1.8% to 2.1%, whilst inherent variations in measured water content of 0.3% water content are apparent from the new sand tests in Figure 6.1, i.e. a significant source of error. Water content is not a good estimator for a sample's consolidation

pressure or strength, and estimates for the intercept of the K_0-NCL with p' = 1kPa are particularly prone to error, varying from 23.3% to 22.7% (void ratios of 0.627 to 0.610). A wider variation in water content is apparent when all two-step anisotropic results are plotted (Section 6.1.3): these samples use multiple batches of China Clay and Silica Flour from the stores, likely to increase variability (similarly to Figure 4.39). Despite mixing with the same initial water content, differences in slurry consistency were observed, particularly in hot weather: this may also affect the water content at the start of consolidation and subsequent compression paths. For comparison, overconsolidated tests indicate a swell-back gradient of 0.28% per log cycle (κ = 0.0035, i.e. $\lambda/8$). Such a low swell-back gradient similarly makes changes in water content a poor parameter for describing overconsolidation.

Test A-6 performed isotropic consolidation to p' = 190kPa slowly, which kept the base excess pore water pressure low to minimise the error arising from estimating the sample average excess pore water pressure. The Isotropic NCL is broadly parallel with the K_0 tests (Figure 6.2), with a gradient of 2.0% water content change per log cycle and water content change during consolidation of 2.0%.

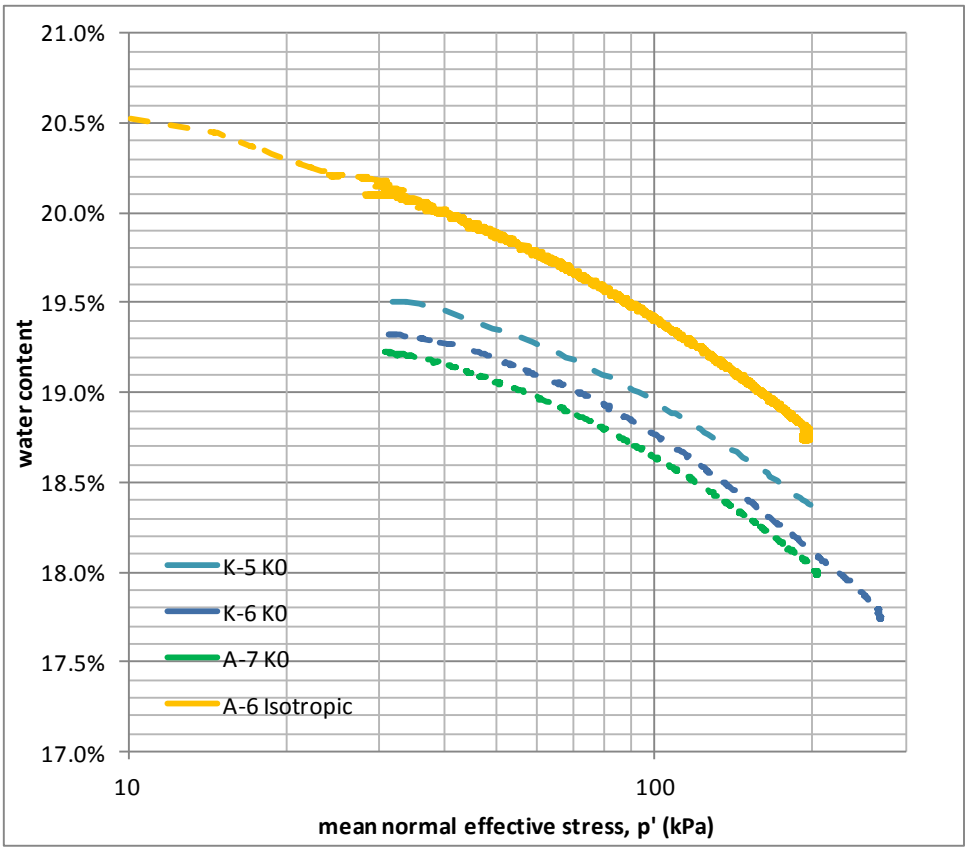

Figure 6.2: Comparison of 1-dimensional and isotropic compression paths

6.1.2. Consolidation characteristics

As sample trimming is avoided to minimise disturbance, slight differences in sample length arise (213mm to 244mm, with the median 50% in the range 232-238mm). There is a relatively wide scatter in first-stage (isotropic) consolidation time apparent in Figure 6.3, reduced by normalising with respect to drainage length. There is also some correlation between elevated volume change and increased consolidation time. Using Taylor's method for determining t_{90}, the median 50% of samples are in the range 140-210 mins, corresponding to c_{vi} = 4.1 to 5.9 x 10^{-6} m^2/s. These estimates compare well to pore pressure dissipation data (Figure 6.4): the median 50% of t_{90} is 140-200 mins. c_{vi} estimates based on Casagrade's method and 50% excess pore pressure dissipation are similar (3.7 to 7.4 10^{-6} m^2/s and 3.7 to 5.9 10^{-6} m^2/s respectively).

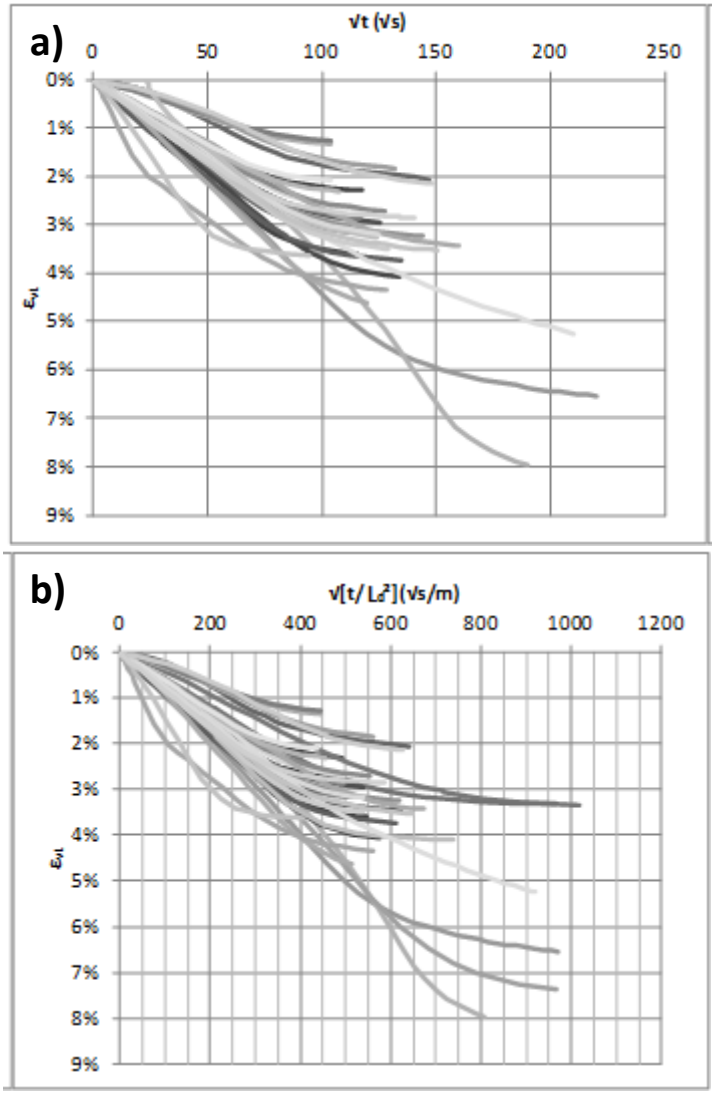

Figure 6.3: Consolidation relationships for samples with top-only drainage against square root time (a) and normalised by drainage length (b)

Some samples are consolidated from both the top and base to accelerate testing. As expected, consolidation is accelerated approximately fourfold; when normalised to drainage path, the difference appears small (Figure 6.5; some samples were consolidated for longer partly because the base pore pressure could not be used as an indicator for 95% of complete consolidation).

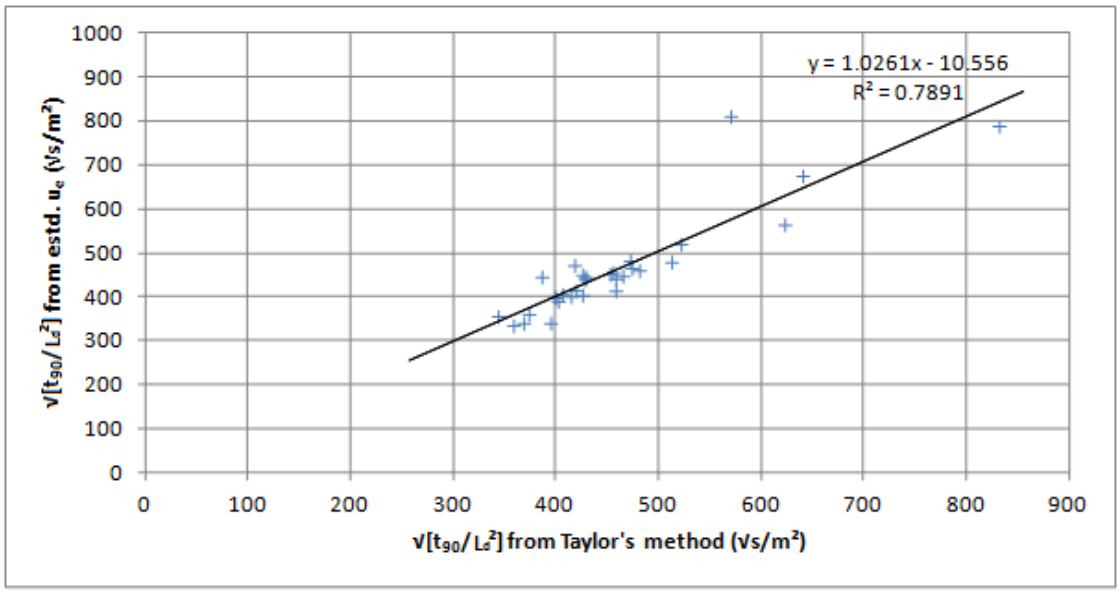

Figure 6.4: Correspondence of t_{90} from Taylor's method and from estimated average excess pore pressure dissipation (i.e. u_e, not u_{base}). Best fit indicates strong correlation and agreement (near 1:1); largest variations are in the outliers with longer than typical consolidation time.

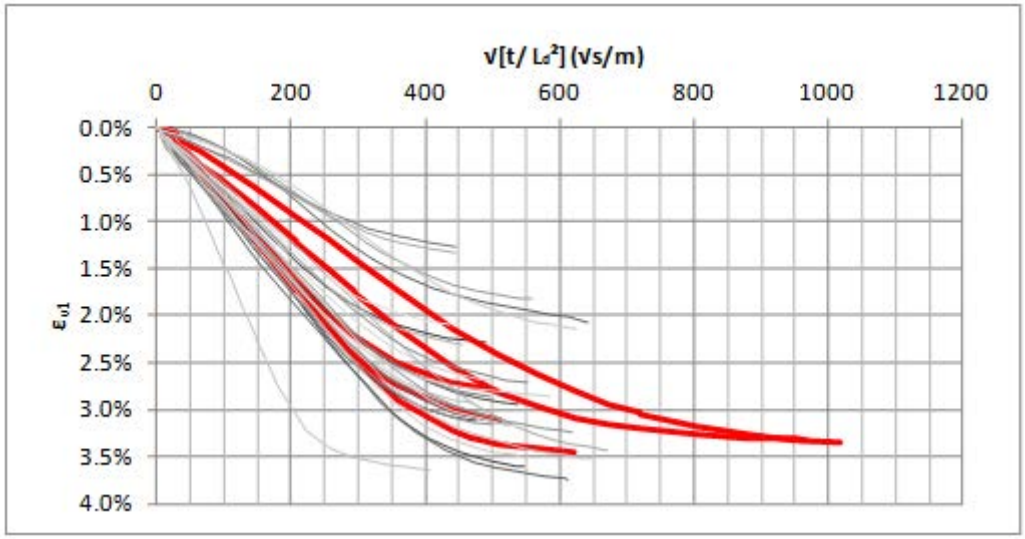

Figure 6.5: Comparison of consolidation volume change normalised by drainage path length for top-only drainage samples (thin lines) and top and base drainage samples (thick, red)

During the anisotropic consolidation stage the mean applied strain is 2.3%, resulting in a final mean sample length of 225mm. For 90% consolidation of cyclically-induced excess pore water pressures in Series G tests, this implies a consolidation period of

115-160 mins (following Head, 1986, c_{vi} is multiplied by a factor of 1.2 for K_0 conditions) and consolidation times of 2 hours are thus expected to result in 85-90% consolidation (following Terzaghi's consolidation theory). Base pore pressure measurements during these consolidation intervals show >95% consolidation (Figure 6.6), indicating faster consolidation, possibly from reduced compressibility. The assumption of zero lateral strain for estimating the anisotropic c_v is, however, not met; a more appropriate comparison is with the consolidation of excess pore water pressure after the final deviator stress is reached in anisotropic consolidation (Figure 6.6); axial strain from the first to last consolidation stage in G-1 is less than 1.5%, meaning a negligible change in L_d^2 of 3%. Whilst the initial pore pressures during drainage intervals are difficult to estimate due to initial equalisation over the first 5 minutes (implications of which are discussed in Chapter 6.6.1), it is still clear that during the 2-hour drainage intervals a greater proportion of excess pore pressure is dissipated than during the first 2 hours at the end of anisotropic consolidation (>90% c.f. 85%). A comparison of relative dissipation between 5 minutes and 2 hours in the two drainage intervals also indicates a slight increase in the second (92% c.f. 89%); the reducing compressibility (axial strain increments in the stages shown are 0.11%, 0.04% and 0.03% respectively) as this test progresses is expected to be responsible.

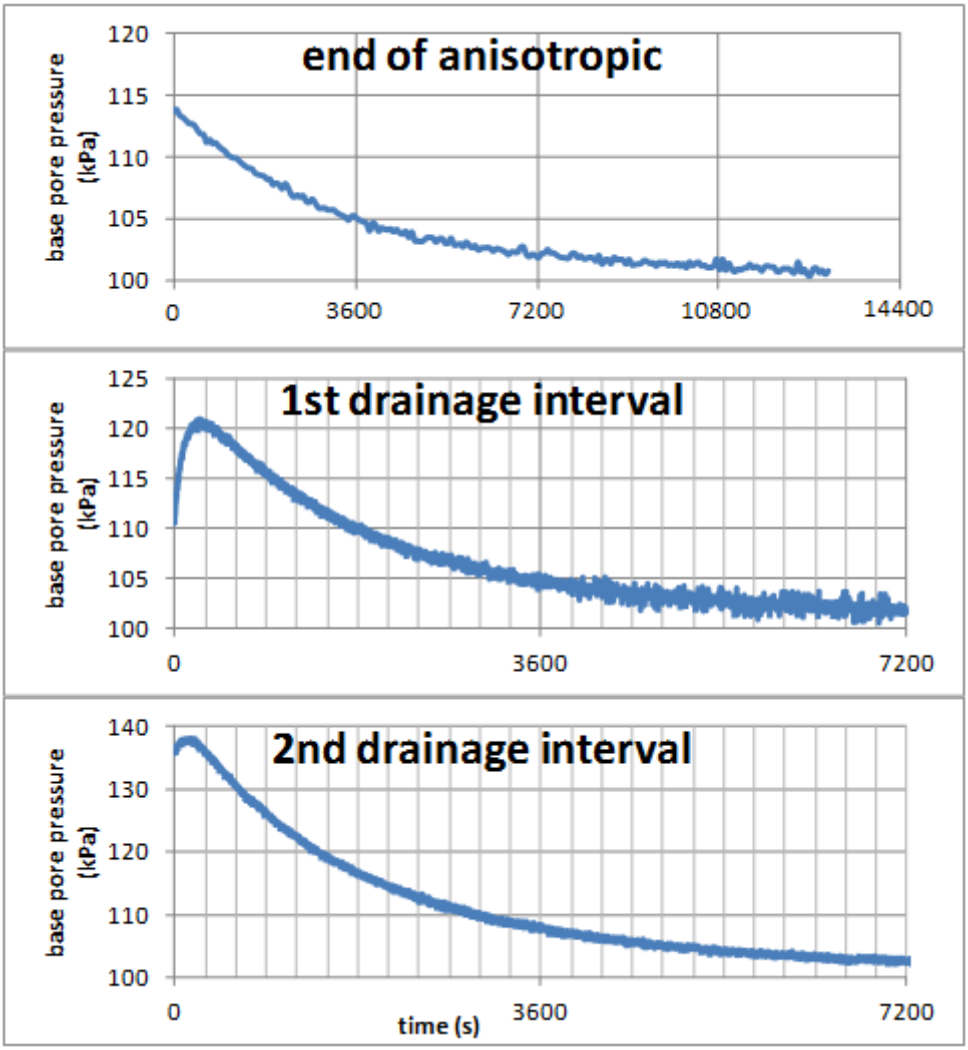

Figure 6.6: Comparison of excess pore pressure dissipation in test G-1 between the end of anisotropic consolidation (i.e. from when maximum deviator stress is reached) and drainage intervals between cyclic loading

6.1.3. Preparation-induced disturbance effects

As previously discussed, soft silt samples must be carefully handled during preparation to avoid disturbance and slumping. Even with refined careful handling procedures, some samples were still disturbed in preparation. Most samples with visually apparent disturbance were discarded, but some were tested to qualitatively determine possible disturbance effects. During consolidation, particularly the initial isotropic stage, disturbed samples tend to experience more volume change and reach lower final

water contents. Under static or cyclic undrained shear, the behavioural differences are greater; disturbed samples do not liquefy (Figure 6.7 and Figure 6.8).

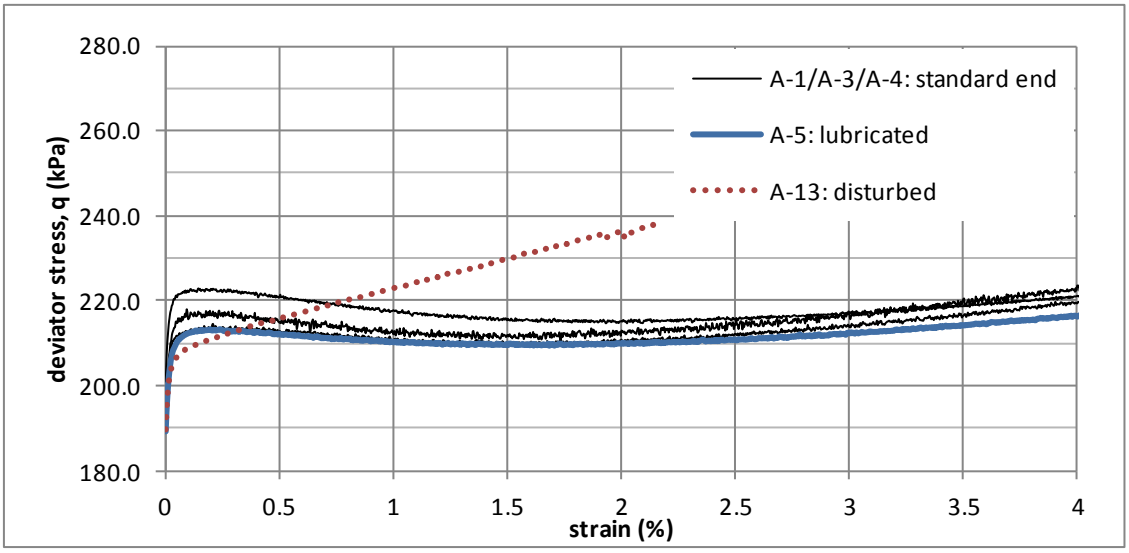

Figure 6.7: Sample A-13 with visually apparent disturbance and high volume change in initial isotropic stage (ε_{v1} = 6.5%) in undrained static shear: no liquefaction, poor sample verticality (from slumping) causes very early shear banding at ~2% strain.

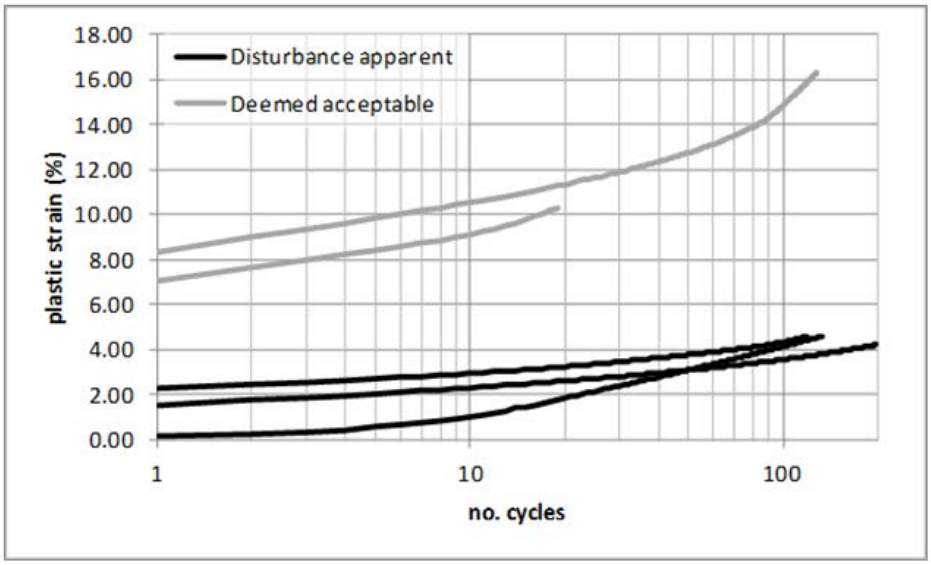

Figure 6.8: Comparison of samples with and without visually apparent disturbance, subject to 50kPa (approximately 2x liquefaction threshold) cyclic load. Undisturbed samples (ε_{v1} = 1.4% to 1.8%) experience first cycle liquefaction whilst disturbed ones (ε_{v1} = 4.1% to 7.4%) do not.

As expected, the diameter of the disturbed samples tends to be increased by slumping, although there is some overlap between 'undisturbed' (i.e. liquefying) and disturbed samples (Figure 6.9). It is possible that slight differences in the mould set-up could have resulted in a smaller than usual diameter before mould disassembly, meaning slump was not detected by measuring the diameter. Alternatively slump may have been localised and missed during diameter measurements.

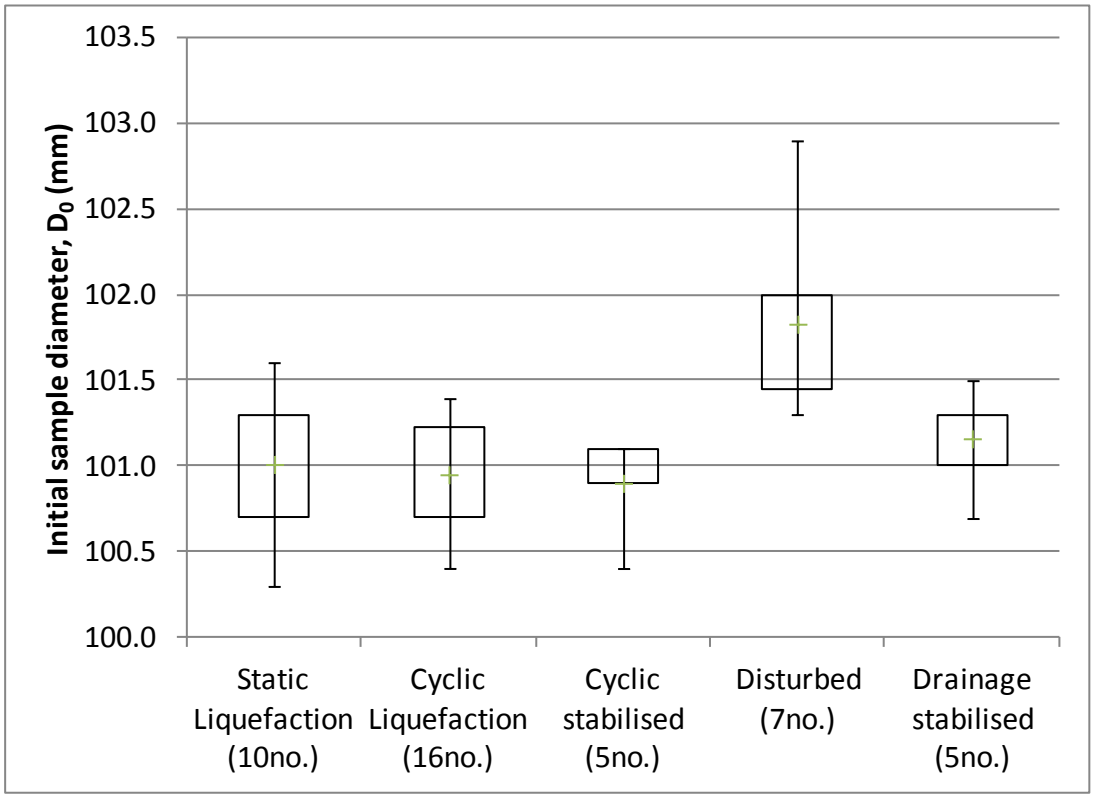

Figure 6.9: Link between slumping (increased diameter) and a disturbed, non-liquefying response. Below 101.3mm, disturbance is highly unlikely, whilst above 101.5mm, it is highly likely.

Whilst the greater consolidation volume change of disturbed samples tends to result in lower final water contents, the inherent variability in initial water content discussed previously makes it difficult to use this as a metric to assess risk of sample disturbance (Figure 6.10).

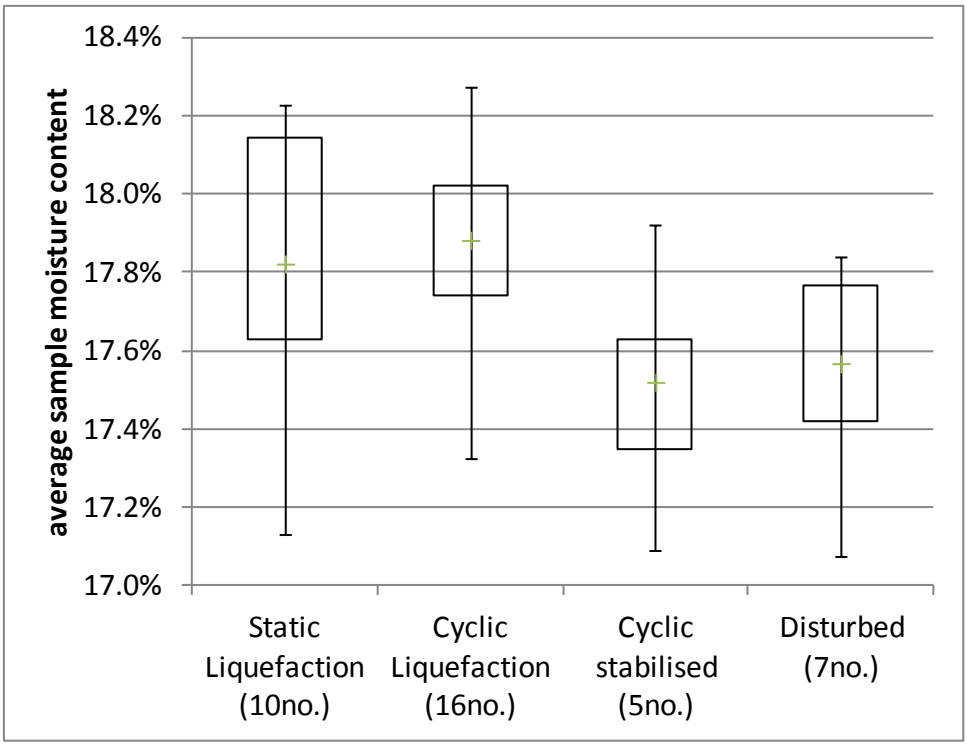

Figure 6.10: Final water content (whole sample mass) – there is some weak correlation between drier samples and disturbance during preparation but difficult to separate from inherent scatter. There is a very clear trend towards drier samples over time (cyclic stabilised tests are later).

In Figure 6.11 it is apparent that disturbed samples reach lower water contents through greater volume changes during consolidation, whilst the compression paths for liquefying samples are flatter with less variation in gradient. Handling-related damage may be similar to the sampling-related disturbance simulated by Santagata and Germaine (2005); a strain is imposed which sets up excess pore pressures. The volume change during reconsolidation to the in-situ pressure depends upon the magnitude of this imposed strain; normally consolidated samples are particularly prone to greater volume change once disturbed (Lunne et al., 1997, 2006; Santagata and Germaine, 2005). The preconsolidation pressure falls below the *p'* reached in the initial, isotropic stage and there is a clear difference in the volume change during this stage for disturbed samples (Figure 6.11, Figure 6.12).

Volume change during the second, anisotropic stage is not noticeably affected by sample preparation disturbance.

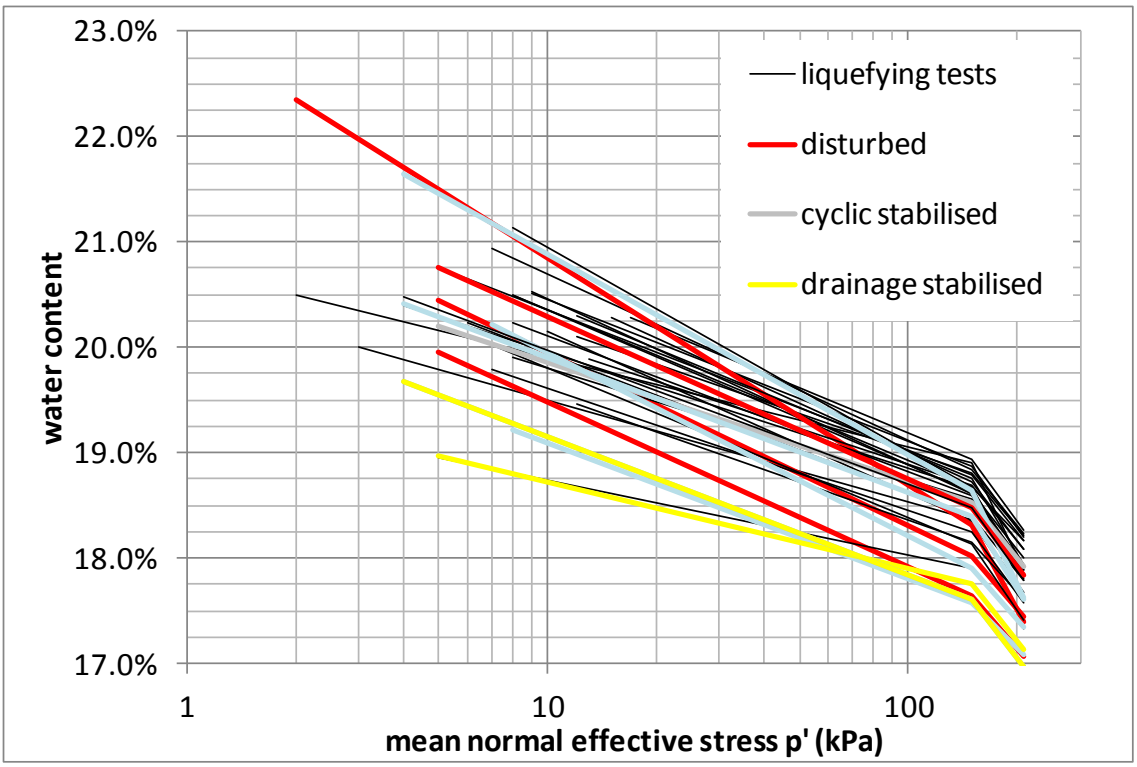

Figure 6.11: Simplified compression paths for all samples consolidated using two-step (isotropic to 150kPa, anisotropic to K = 0.45) process, highlighting differences in consolidation between liquefying and disturbed samples particularly.

The slumping from handling disturbance can be considered as analogous to the sampling strains applied by Santagata and Germaine (2005). The increased consolidation volume change indicates there is permanent rearrangement associated, which appears to have affected the precarious micro-structure and allowed some grains to move to more stable positions, reducing liquefiability.

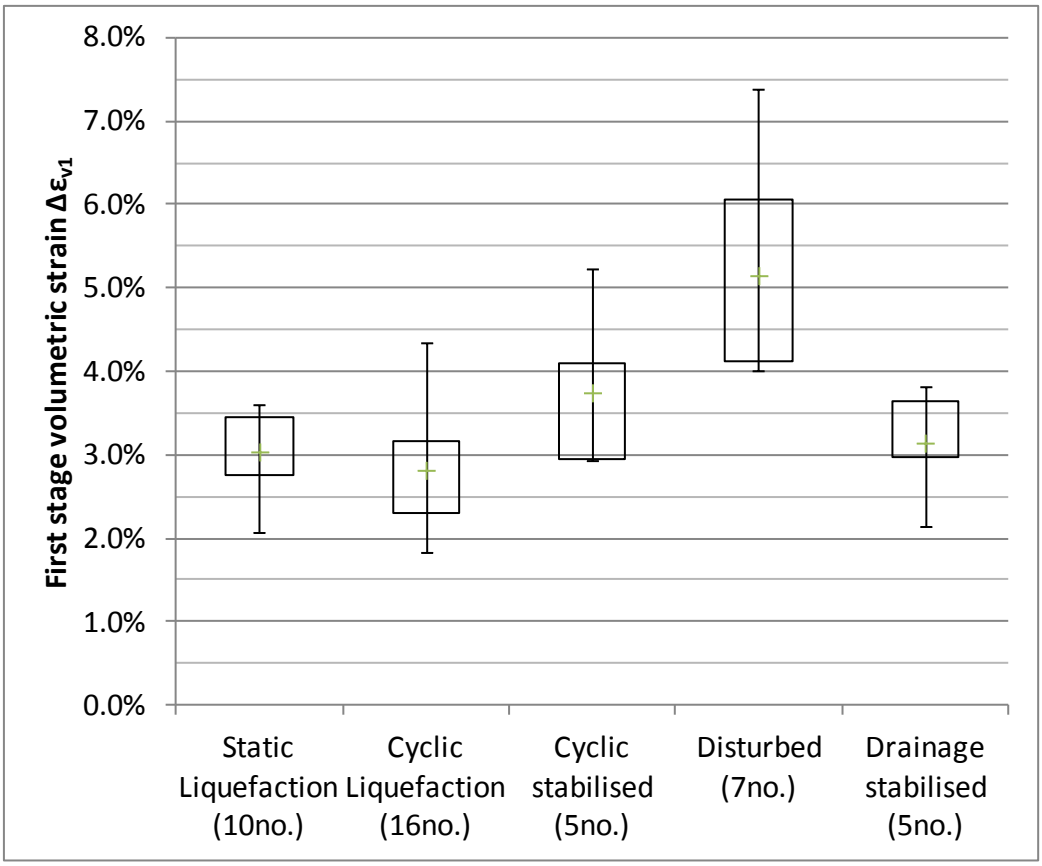

Figure 6.12: Volume strain in first stage of the two-stage consolidation. Some cyclic stabilised tests raise concerns – higher than the range observed for liquefying, i.e. >4.0-4.5%, (identified for repeat tests).

As a generalised metric for sampling disturbance, applicable to a range of clay soils, Lunne et al. (1997) recommend the use of relative change in void ratio, $\Delta e/e_0$, for a sample reconsolidated back to its in-situ stress. Applying this metric to the initial isotropic consolidation stage shows a similar pattern in terms of disturbance to Figure 6.12. Both ε_{v1} and $\Delta e/e_0$ identify the same tests, which behave as though stabilised by cyclic load, to be possibly disturbed and in need of repetition.

The samples were consolidated beyond their maximum previous stress, meaning results are not directly comparable to the sampling quality classes of Lunne et al. (1997, 2006). However Figure 6.2 indicates the volume change to p' = 150kPa is

approximately twice of the volume change to p' = 70kPa; if the sample disturbance class criteria from Lunne et al. (1997, 2006) are thus doubled, it implies liquefying samples are at the boundary of good ($\Delta e_1/e_0 < 0.08$) and good to fair ($0.08 \leq \Delta e_1/e_0 \leq 0.14$) quality. Samples within the poor ($\Delta e_1/e_0 > 0.14$) category are sufficiently disturbed for liquefaction to be disrupted (Figure 6.13).

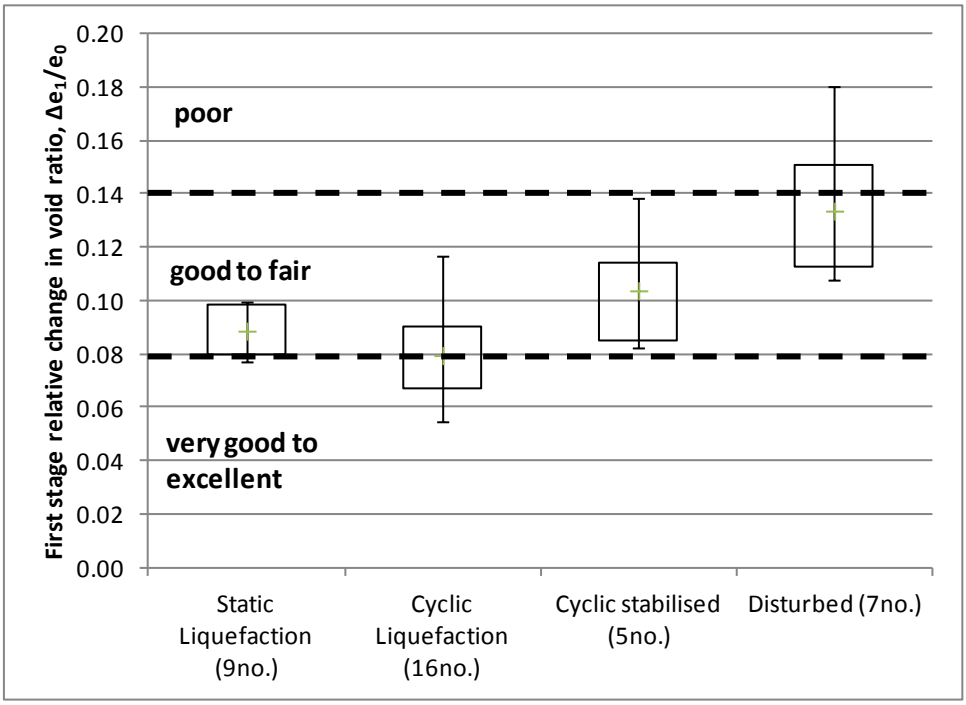

Figure 6.13: Relative change in void ratio in initial isotropic consolidation stage, used as a sample quality metric similarly to Lunne et al. (1997, 2006).

6.2. Static and cyclic liquefaction

No clear critical state is reached by the Silt Mix samples (see Chapters 4.2.2.1 and 4.2.2.3); tests are terminated before the critical state by strain localisation. Furthermore, water content/void ratio is not a good parameter for description of strength due to low volume change tendency and inherent variability of the mix. Instead liquefaction on the Instability Line is used as a reference state, i.e. cyclic stresses for the Silt Mix soil are described by:

Equation 6.1: $$\Psi = \Delta q_{cyc}/\Delta q_{peak}$$

Unlike the very large-strain, completely remoulded fabric attained upon reaching the Critical State Line, independent of fabric and applicable to all stress states of a given soil, the Instability Line only applies to normally consolidated soil and is heavily dependent upon fabric, i.e. can change with load history. However using Δq_{peak} for normalisation presents data in a clearer relation to the phenomenon of interest, i.e. meta-stable liquefaction.

Table 6.1 indicates that below σ'_3 = 150kPa, changes in *e* in response to effective stress are small, implying some memory of overconsolidation at σ'_3 < 150kPa.

Table 6.1: Pre-liquefaction Δq_{peak} and void ratio as a function of consolidation pressures in liquefying static tests

Test	Consolidation σ'_3 (kPa)	Consolidation σ'_1 (kPa)	Δq_{peak} (kPa)	Final void ratio, *e*	$e_c - e_0$
A-1	150	337	26	0.490	0.073
A-3	150	348	24	0.490	0.062
A-4	150	316	28	0.492	0.057
A-5	150	336	26	0.486	0.059
A-10	75	168	11	0.492	0.029
A-11	50	112	7	0.493	0.025
A-12	200	445	38	0.460	0.111

6.2.1. Dependence upon strain

As noted in Chapter 4.2.2.1, the anisotropically normally consolidated Silt Mix soil has an initial high-stiffness, strain-hardening undrained monotonic shear response followed by liquefaction. Liquefaction and post-liquefaction recovery are both experienced at consistent strain levels (0.1% to 0.3% and 1.5% to 2.0% respectively, Figure 6.14) when starting from a similar stress state. Table 6.1 indicates Δq_{peak} at σ'_3 = 150kPa varies from 24kPa to 28kPa, with a mean value of 26kPa (used in calculations of Ψ). When normalised by the consolidation σ'_1, this compares well with results from Doanh et al. (2012) previously discussed in Chapter 3.3.1 (i.e. 8% c.f. 2-10%). As discussed in Chapters 3.2 and 3.3, strain is an indicator of micro-structural rearrangement and a certain amount of particle movement is necessary to start a chain reaction collapse of the micro-structure. Static liquefaction also coincides with a specific effective stress state, i.e. reaching the Instability Line; under monotonic load there is a single relationship between applied strain and effective stress state.

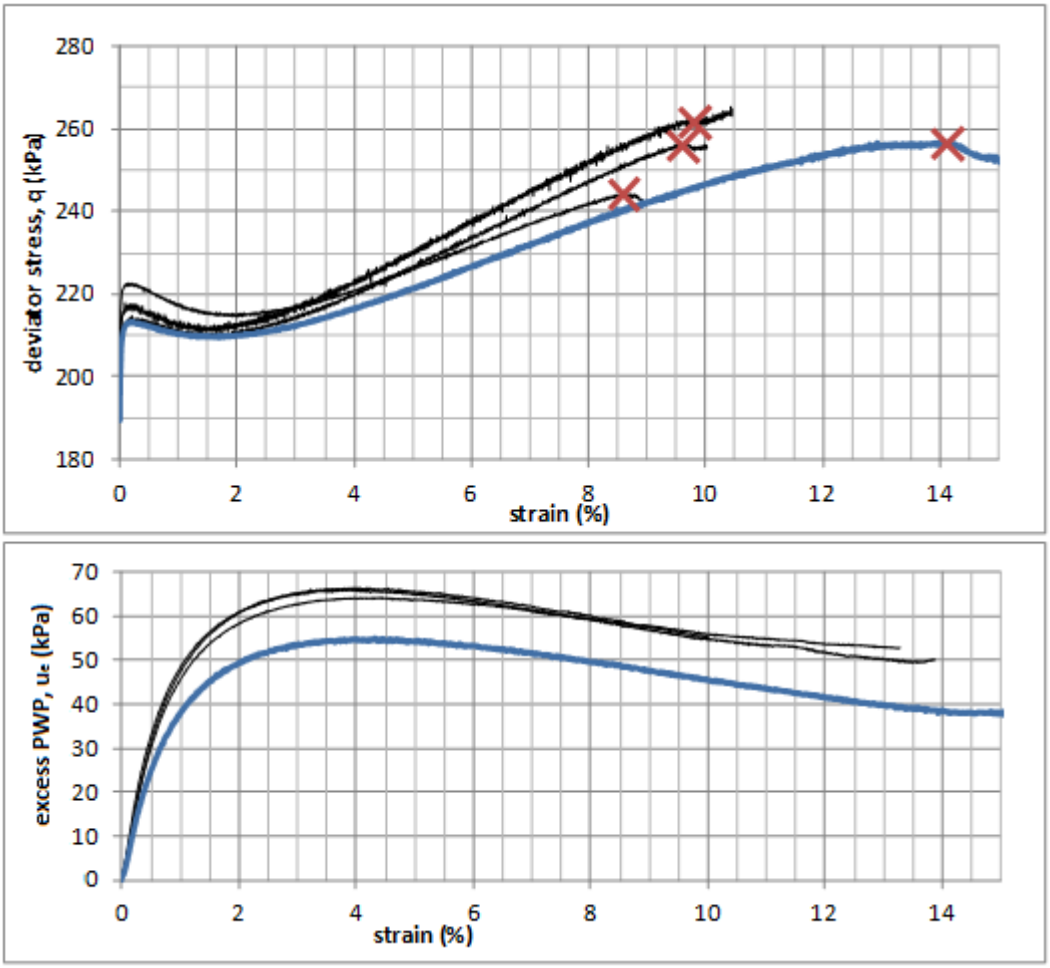

Figure 6.14: Strain-dependent meta-stable liquefaction under monotonic shear – initiated at 0.1% to 0.3%, recovers strength at 1.5% to 3.0%. 'X' indicates the onset of shear banding. Blue line – lubricated top cap.

Under load-controlled cyclic shear, liquefaction is similarly dependent upon strain: above the liquefaction threshold stress, increasing $\Delta\varepsilon_{pl}$ is apparent after 0.1% to 0.3% strain (Figure 6.15). The threshold stress bears a close resemblance to the pre-liquefaction peak; the lowest cyclic stress triggering liquefaction corresponds to Ψ = 0.96. The first application of a cyclic stress induces a smaller strain and excess pore water pressure than the same stress in monotonic loading; these accumulate with subsequent load cycles, so the cyclic q-ε-u_e relationship varies over time. Cumulative cyclic strain exceeding the initiation strain, ε_{tl}, is not sufficient to cause liquefaction;

test D-3 (Ψ = 0.77; Figure 6.15) reaches 0.72% strain. Similarly, relaxation of the peak stress in test C-12 (Ψ = 0.96; Figure 6.16) indicates cyclic load initially exceeding the threshold stress can avoid liquefaction if the peak cyclic stress reduces to below the threshold. This suggests triggering liquefaction depends upon the application of the threshold stress coinciding with reaching ε_{tl}. The effective stress state is also important (see Sections 6.2.2 and 6.3.2). Series E tests examined the necessary conditions for liquefaction further, as discussed in Section 6.5.2.

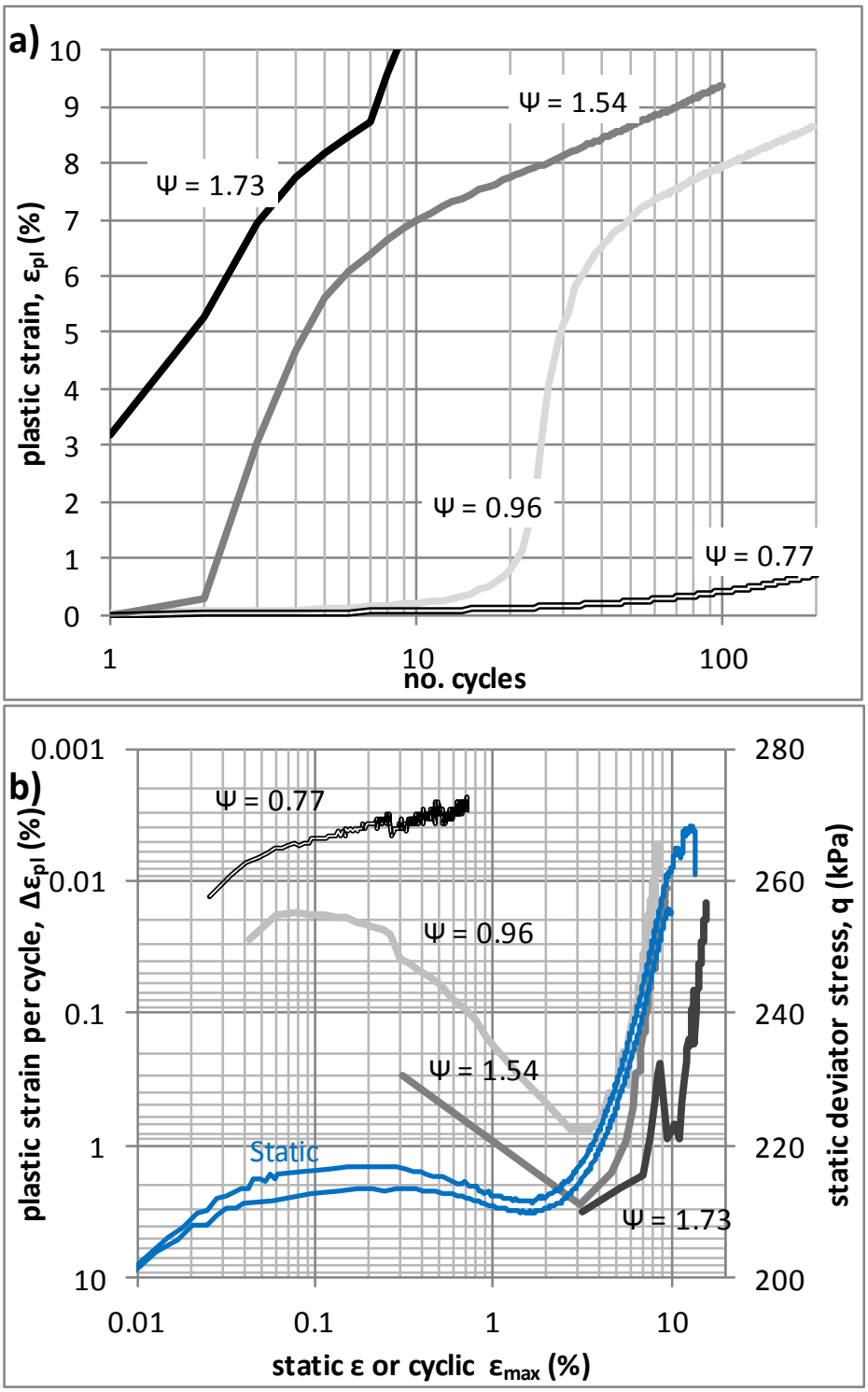

Figure 6.15: Liquefaction and threshold stress effect for Silt Mix samples under cyclic load (Series D tests). a) – accumulation of plastic strains. b) – plastic strain rate, $\Delta\varepsilon_{pl}$, (left axis, values in reverse order to show similarity between cyclic and monotonic liquefaction/recovery), compared to strain-softening and recovery behaviour in static tests to highlight similarity in initiation and recovery strains.

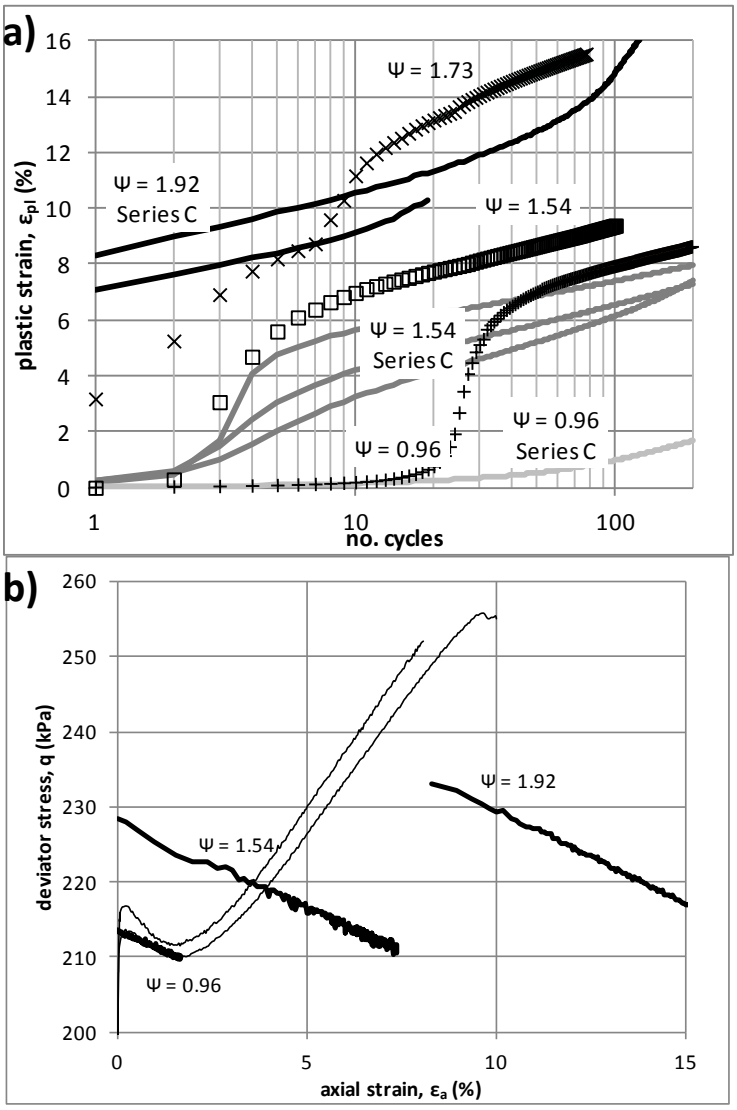

Figure 6.16: Series C cyclic tests at constant load with peak cyclic stress relaxation. a): changes to threshold stress and strain accumulation as a result of corrections. b): reduction in stress without relaxation corrections (static response shown for context).

6.2.2. Dependence upon stress state

As discussed in Section 6.1., a slight change in $K_{0,NC}$ is apparent with the change to the new sand. Initial static tests (A-1 to A-5) were performed using K = 0.45, i.e. slightly more anisotropic than true K_0 conditions, and found to behave similarly to A-7 (K_0 consolidation). Conversely, there is a greater change in behaviour for reduction of stress state anisotropy, i.e. K = 0.55 or 1.0 as opposed to 0.48 (Figure 6.17). The

isotropic test does not liquefy, whilst the *K* = 0.55 test shows a marked reduction in strain softening.

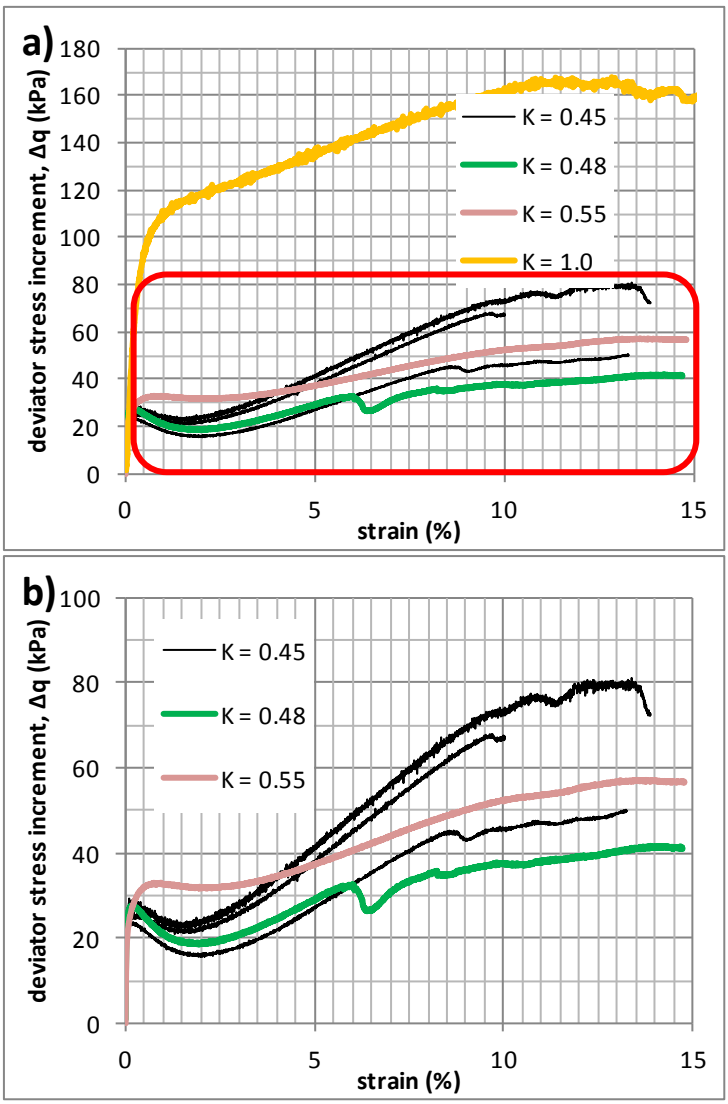

Figure 6.17: Effect of increasing *K* for normally consolidated samples: reduced strain softening is apparent. a) all tests, b) anisotropic samples only (tests outlined in red box in part a).

The effective stress paths indicate a common Instability Line (Figure 6.18) for all anisotropic tests. The effect of decreased stress anisotropy (higher *K*) is to increase the strain at which the stress path intercepts the Instability Line; for *K* = 0.55 it is at 0.8% strain whilst for *K* = 1.0 it is 1.6% strain (a similar effect was observed in Doanh et al.,

2012). As post-liquefaction recovery tends to occur from 1.5% to 2.0% strain, it is possible the isotropic monotonic test was able to achieve sufficient medium-strain fabric rearrangement for stability without first reaching a sufficiently anisotropic stress state for liquefaction. The reduction in strain-softening for the K = 0.55 test corroborates this: more strain and thus fabric rearrangement in the stable domain is performed before the Instability Line is reached, meaning less potential for collapse of the soil skeleton. In this context, liquefaction requires interception of the Instability Line and strain within the range associated with liquefaction, but below that associated with recovery. Similarly to observations of Yamamuro and Lade (1999), there appears to be a slight tendency for reduced post-liquefaction recovery at lower consolidation p'. As samples at these pressures may retain some memory of overconsolidation (A-11, at the lowest p', particularly), and also due to increased difficulty of cyclic load control (Chapter 4.2.1.3), cyclic testing under these conditions was not performed.

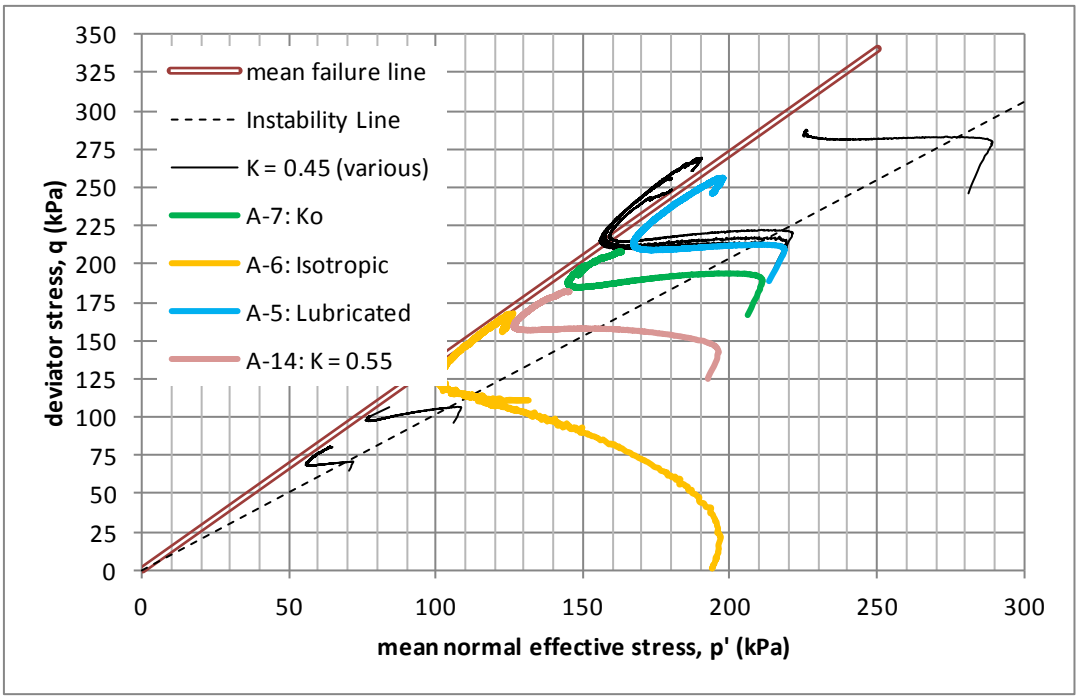

Figure 6.18: Effective stress paths in invariant (p', q) stress space for Silt Mix tests at various stress states.

Figure 6.18 indicates failure occurs along the line q/p' = 1.36, with liquefaction initiated along q/p' = 1.02 (equivalent to ϕ' = 33.7° and 25.8° respectively). As ultimate failure is dilatant, stress paths tend to follow the ultimate failure line until shear banding occurs (this is further discussed in Chapter 6.3.3).

6.3. Strain thresholds and behavioural transitions

6.3.1. Plasticity and modulus degradation

Hsu and Vucetic (2006) present a method for determining the strain threshold between small and medium strain regimes (the volume change threshold, ε_{tv}) using the NGI Direct Simple Shear apparatus. Cyclic strains are applied in increasing magnitude until the pore water pressure accumulates with cycling. Replication in a triaxial cell has limitations; comparison of base pore pressures to global strain means ε_{tv} is determined from the radially-restrained base, which is likely to experience lower localised strains

and a lesser contractant tendency. ε_{tv} may thus be overestimated due to inherent stress/strain non-uniformity.

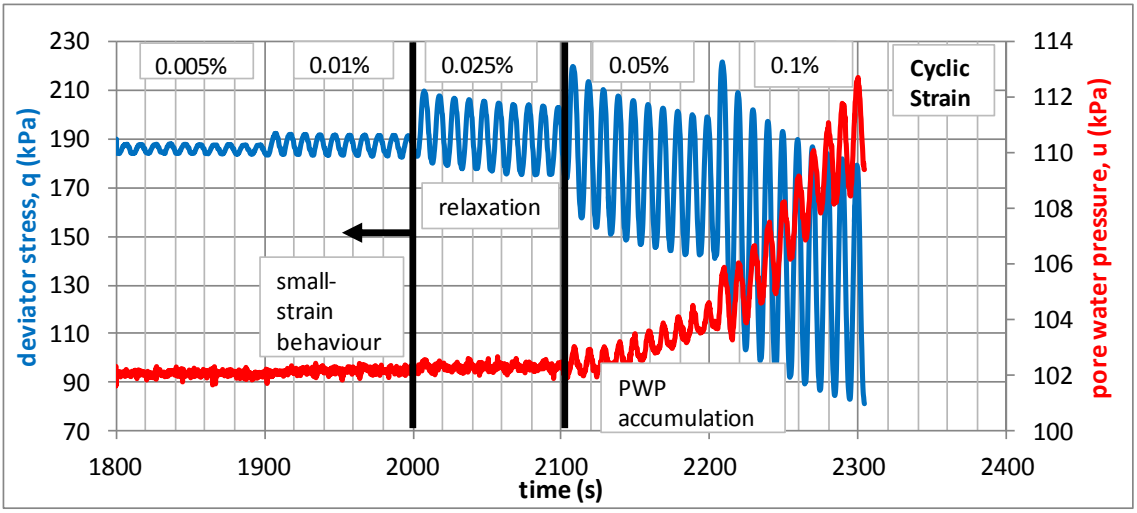

Figure 6.19: Accumulation of pore water pressure and relaxation of anisotropic consolidation stress in test B-2 when medium-strain, plastic behaviour is initiated – within the interval 0.01 to 0.025%.

During tests B-1 and B-2, a relaxation of post-consolidation deviator stress was apparent (Figure 6.19), implying plasticity (from a global sample measurement, to relate to global strain) and thus volume change tendencies not apparent at the base pore pressure transducer. For anisotropically consolidated triaxial samples, relaxation appears to be the better indicator of medium-strain behaviour. Tests B-1 and B-2 both indicate relaxation at 0.02% to 0.025% with no clear pore water pressure accumulation; this is only distinguishable from instrument noise in both tests at 0.05% (Figure 6.20). This threshold between 0.01% and 0.02% is in agreement with results for low plasticity silts and clays presented by Díaz-Rodríguez and López-Molina (2008). This medium-strain threshold coincides with a cyclic stress of 8-10kPa, i.e. 3% of consolidation σ'_1.

At small strains, monotonic shear tests indicate a significantly increased stiffness (Figure 6.21). As strains reduce, the instrument noise from the load cell starts to become significant; below 0.005% strain a reliable estimate is not possible, meaning the very small strain, constant modulus regime cannot be investigated with this triaxial setup. As established by Díaz-Rodríguez and López-Molina (2008), there is a hysteretic-elastic, small-strain region with decreasing modulus but no plasticity (below 0.01% strain).

Whilst strain-controlled cyclic load below the volume change threshold does not initiate significant relaxation (Figure 6.19), small-strain load-controlled cyclic tests slowly accumulate plastic strains. Creep strains due to anisotropic consolidation stresses continue after excess pore water pressures have dissipated and during subsequent shear stages.

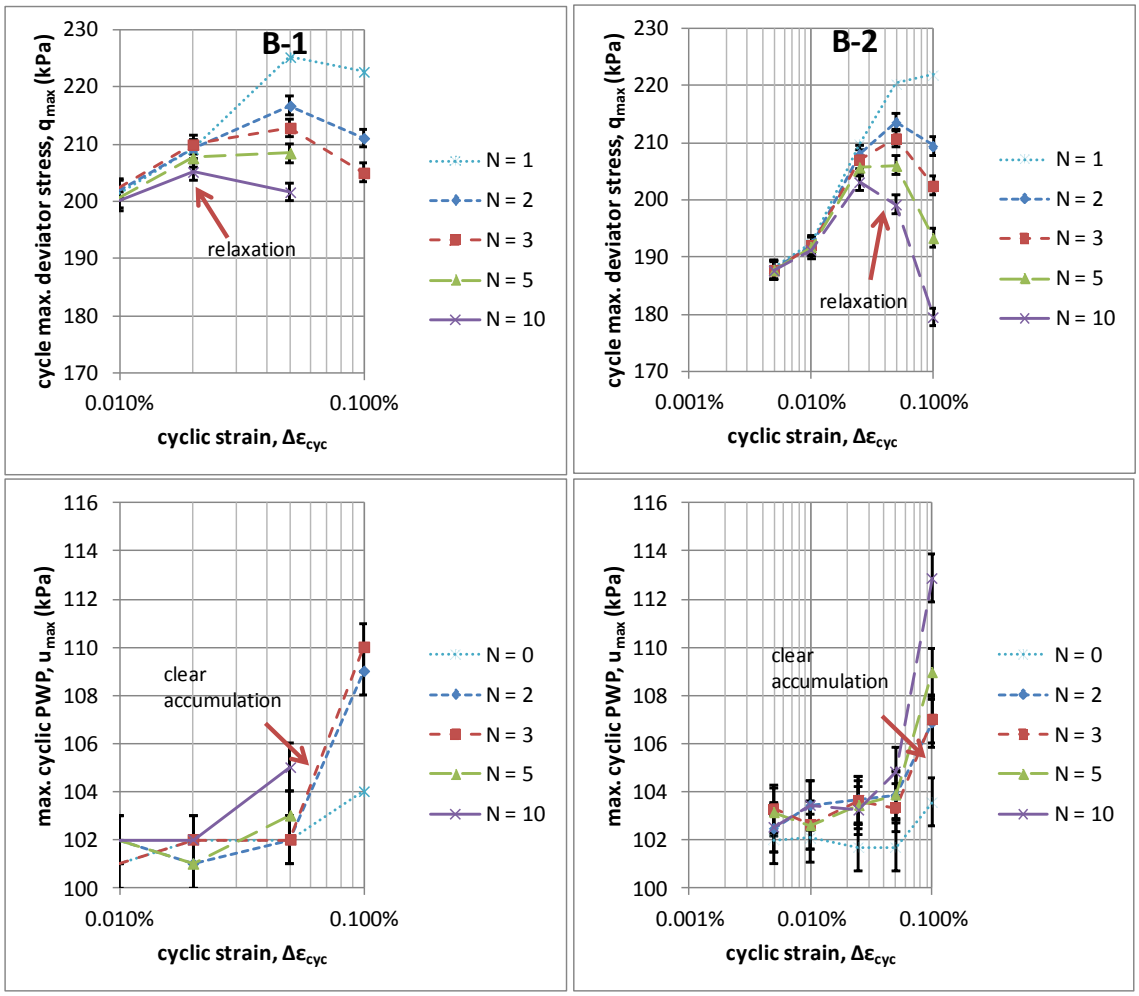

Figure 6.20: Cyclic relaxation and pore water pressure accumulation in tests B-1 and B-2, implying a volume change threshold between 0.01% and 0.02%.

For undrained monotonic tests, Santagata and Germaine (2005) suggest the strain rate should be selected to be 30-50 times faster than the final consolidation creep rate to avoid creep influencing the test. Transient strain rates in Figure 6.22 are sufficient to avoid interaction (cyclic strains of 0.008%, i.e. 0.58%/hr), however plastic strains accumulate only slightly faster than creep rates (i.e. 2.7-3.5 times faster) even when creep is reduced by extending consolidation times. Pore pressure accumulation is also highly dependent upon creep rates (Figure 6.22). It is likely the observed strain and pore pressure accumulation are entirely as a result of creep interaction. As samples are tested after a day of consolidation and creep rates, unlike primary consolidation, are

likely to be unaffected by drainage path (Joseph, 2014), this behaviour is unlikely to occur in the field. Laboratory estimates of strain accumulation under such low loads are therefore likely to be significantly overestimated.

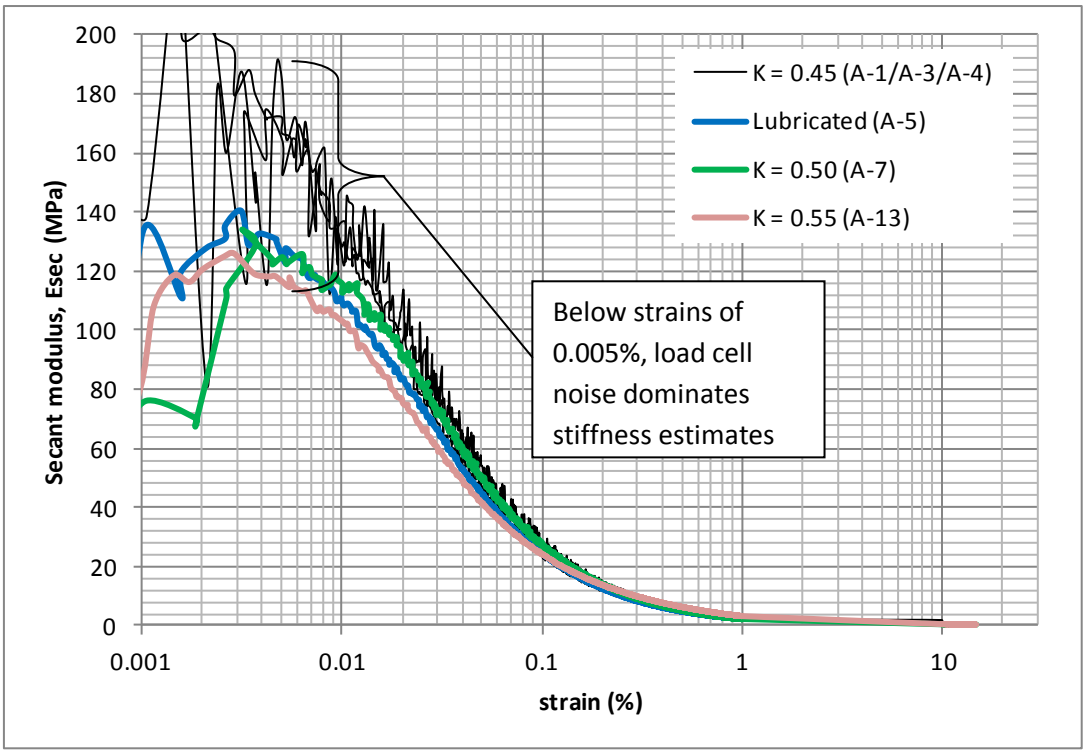

Figure 6.21: Small strain modulus degradation for anisotropically consolidated samples in static shear. Results are not smoothed by applying moving average, in order to show influence of load cell noise at very small strain.

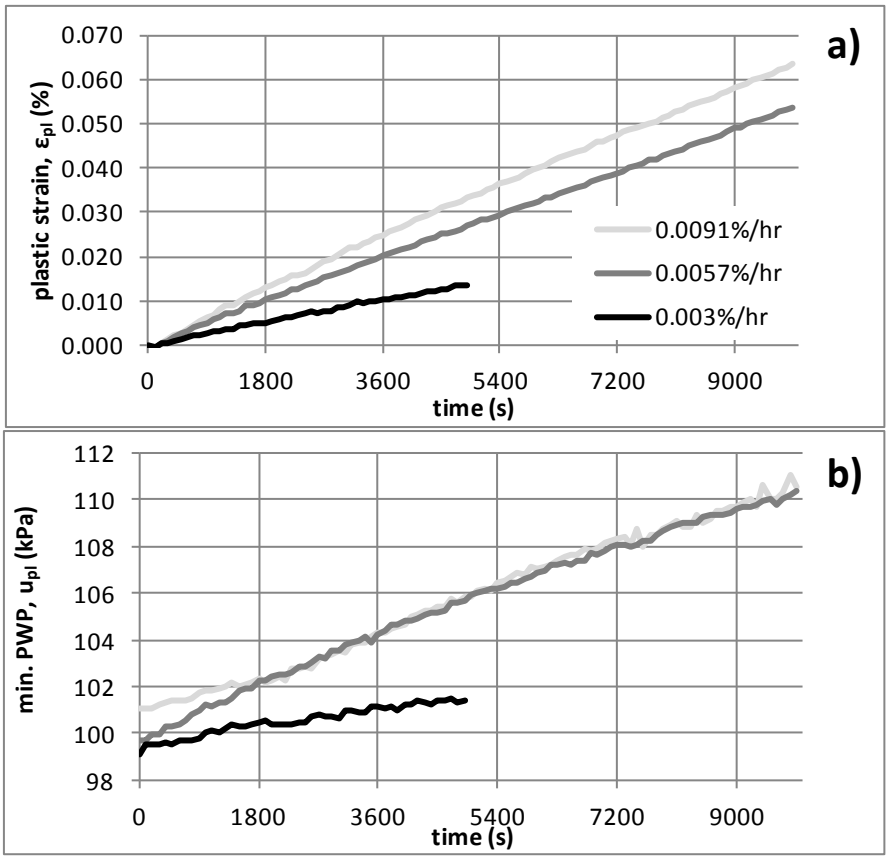

Figure 6.22: Influence of final consolidation creep rate (achieved by longer secondary consolidation periods) on plastic strain (a) and pore water pressure accumulation (b) in tests D-4, D-5 and D-7.

Tests D-3 and D-7 (second stage), loaded at Ψ = 0.77, experience initial cyclic strains of 0.022% to 0.026% (just above the volume change threshold strain) and become similarly influenced by creep rates later in the test as $\Delta\varepsilon_{pl}$ reduces (Figure 6.23, Figure 6.24). D-3, with the greater creep, reaches a near-constant plastic strain rate, suggesting creep interaction. Whilst the limit from Santagata and Germaine (2005) appears effective in describing the range over which creep interaction is negligible, the similarity of the two tests up to cyclic plastic strains of 0.003% (i.e. 15x D-3's creep rate) suggest it may be conservative in this case.

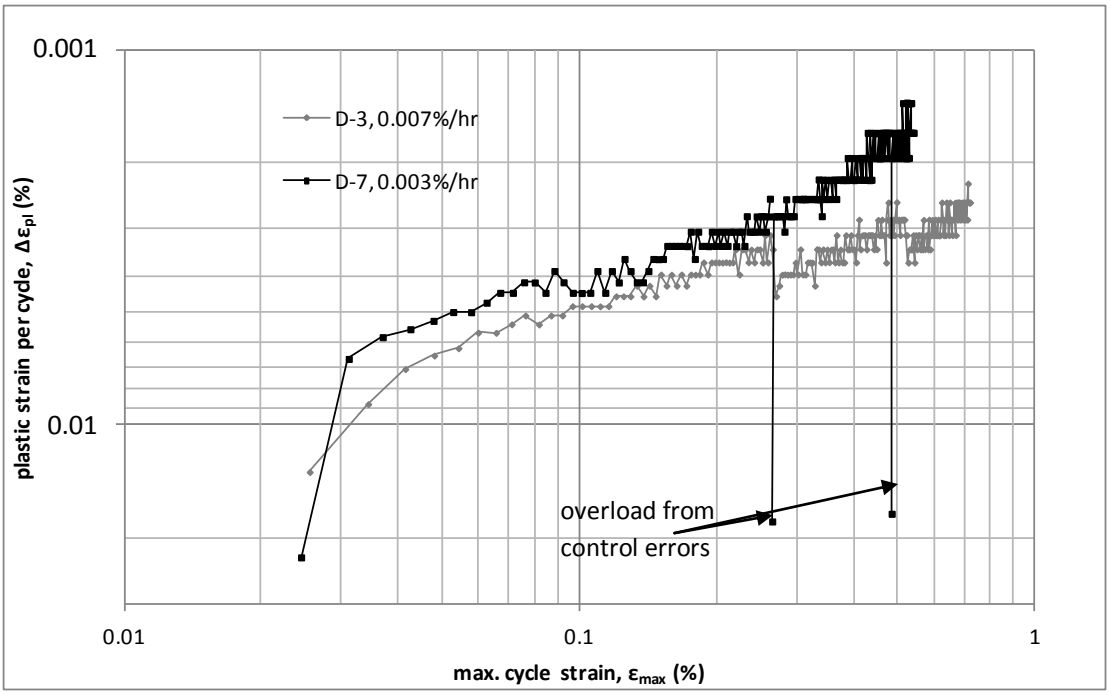

Figure 6.23: Comparison of Ψ = 0.77 cyclic tests (D-3 and D-7) with differing final consolidation creep rates. Creep strains per equivalent 100s cycle are 0.0002% and 0.00008% respectively.

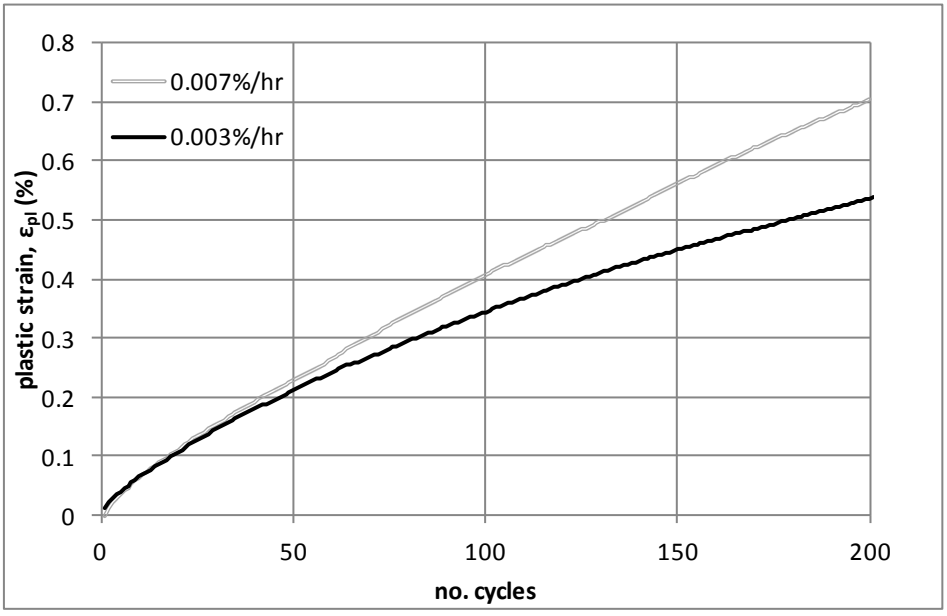

Figure 6.24: Differences in strain accumulation as a result of increased final consolidation creep rates for cyclic tests D-3 and D-7.

6.3.2. Pore water pressures and soil skeleton re-structuring

For the medium-strain cyclic tests (i.e. $\Psi \geq 0.77$), there is a common relationship between pore water pressure and strain. Up to approximately 0.5% strain, u_{max} follows the monotonic tests closely (Figure 6.25), after which liquefying tests diverge (achieving a lower pore water pressure than the monotonic tests). The apparent lag in pore pressure for $\Psi \geq 1.54$ tests occurs within the first few cycles (strain and pore pressure accumulation is rapid due to liquefaction) is not considered representative; pore pressure equilibration between the sample base and the centre in the first few cycles is unlikely.

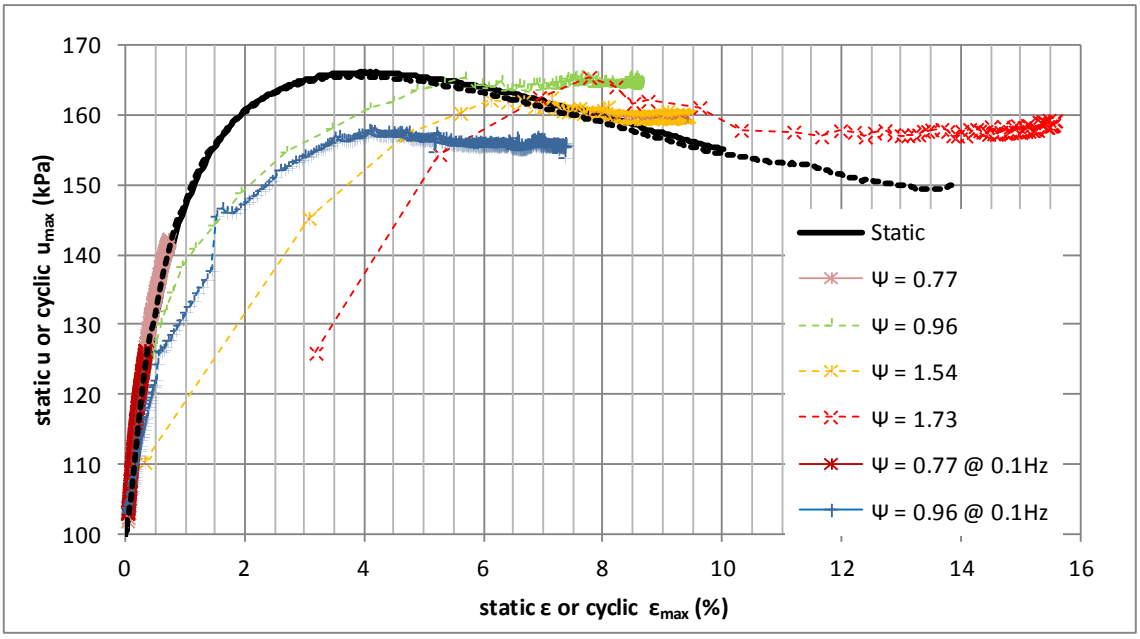

Figure 6.25: Correspondence of maximum cyclic pore water pressure as a function of strain to static pore pressure; particularly below the liquefaction threshold (Ψ < 0.96).

Rising pore water pressures and loss of mean effective stress during contractant cyclic loading can be represented by increasing deviator stress ratio (q/p'). The maximum and minimum deviator stress remain fixed throughout in Series D tests, so rising q/p'

indicates the stress state moving left on a *p'*-*q* plot towards the mean failure line. Initially the stress state at the cycle maximum follows the static curve closely (Figure 6.26), but after liquefaction is triggered the stress anisotropy remains lower than for the monotonic loading, although above the lower deviator stress ratios in the lubricated and K_0 consolidated tests.

Acceleration of $\Delta\varepsilon_{pl}$ coincides with crossing the Instability Line (i.e. cycle maximum $q/p' > 1.02$) and ε_{max} exceeding ε_{tl}. The largest cyclic strains then occur when the minimum cyclic *q/p'* exceeds the Instability Line. At and below the liquefaction initiation strain (<0.3%), the effective stress state (i.e. *q/p'*) at cycle maximum is a function of strain accumulated, so triggering cyclic liquefaction in effect requires simultaneously applying cyclic stress above the threshold and $\varepsilon_{max} > \varepsilon_{tl}$. The relationship between u_e and ε also allows prediction of one property from another, which may be useful for cross-checking in-situ monitoring results or estimating one from the other.

Ψ = 0.96 and 1.54 tests reach a stable *q/p'* range by approximately 6% strain; further strain accumulates but the *q/p'* maxima and minima do not change. This coincides with pore water pressure accumulation rates reducing to very small levels. Bearing in mind dilatant recovery behaviour in monotonic tests at these strains, it is possible that inter-particle 'locking' action is providing stability to the cyclic tests. There is a slight difference in the Ψ = 1.73 test (Figure 6.26), which attains a higher peak *q/p'* at approximately 8% strain and gradually drops to a stable value at 12%. Unlike other D-series tests this sample failed in shear banding during cyclic loading, as evidenced by

the sudden rise in $\Delta\varepsilon_{pl}$ from approximately 9% strain in Figure 6.15. It is possible the pore pressure dilation to resist the higher cyclic loads in this case was unsustainable and thus a shear band was initiated. Beyond 9% strain, global stress-strain and pore pressure relationships will not be representative of the zone controlling the sample behaviour, i.e. the shear band.

At high strains following liquefaction, the pore pressure waveforms change from 'lagging' the stress pulse (as expected when finite sample permeability is considered) to 'leading' the stress pulse (Figure 6.27), implying the maximum stress induces a negative, dilatant change in pore water pressure. As most of the strains accumulate at the peak cyclic stress and dilation, as a flow phenomenon, requires movement to generate resistance, it is likely that during recovery the Silt Mix soil reaches 'dilatant creep' behaviour similar to alternating plasticity described in shakedown theory: ongoing plasticity is required to mobilise dilatant resistance, giving a continued creep strain accumulation but no change in pore water pressure.

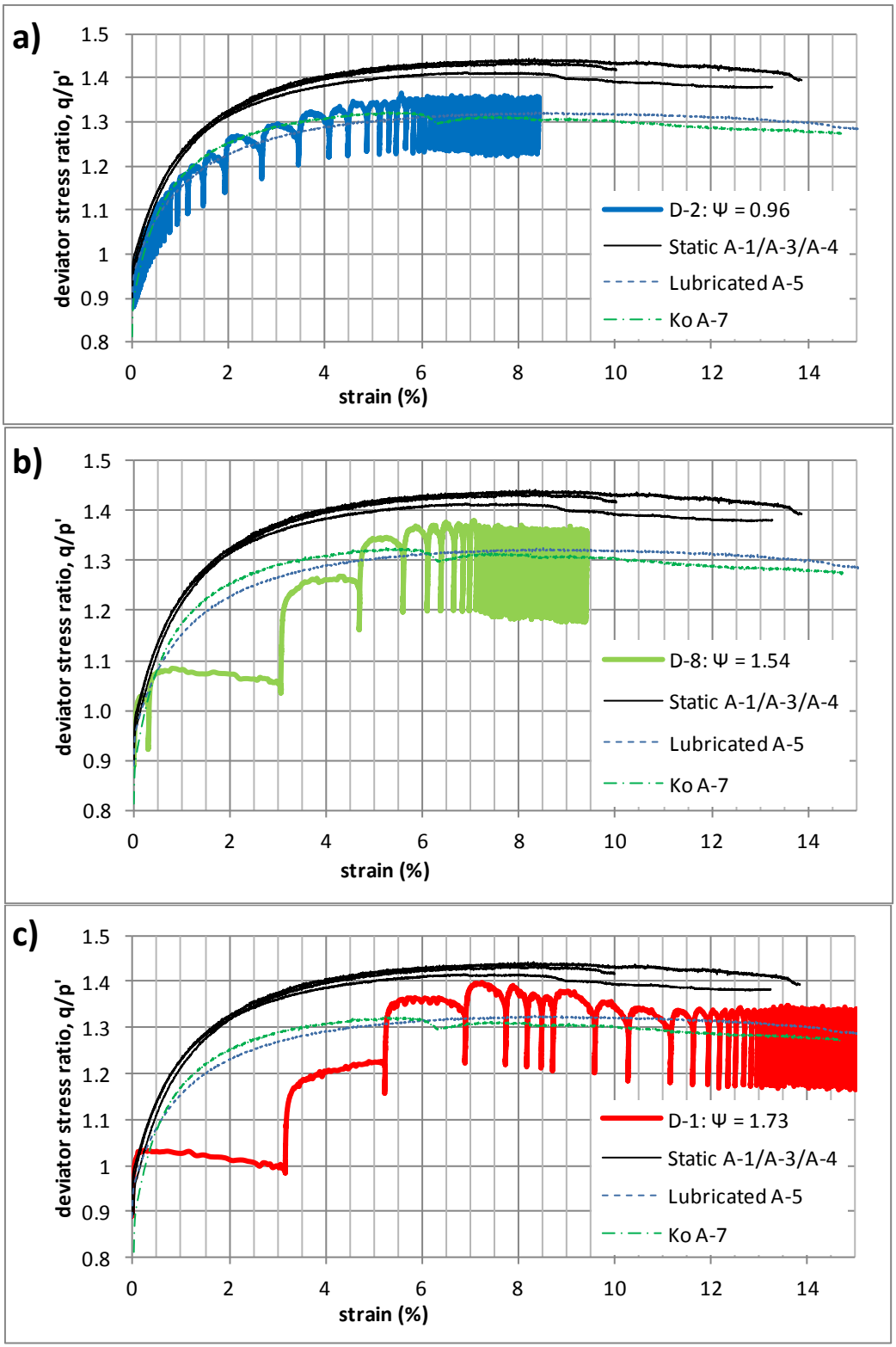

Figure 6.26: Comparison of stress ratio (i.e. stress anisotropy from pore pressure accumulation) for 25kPa (a), 40kPa (b) and 45kPa (c) cyclic tests.

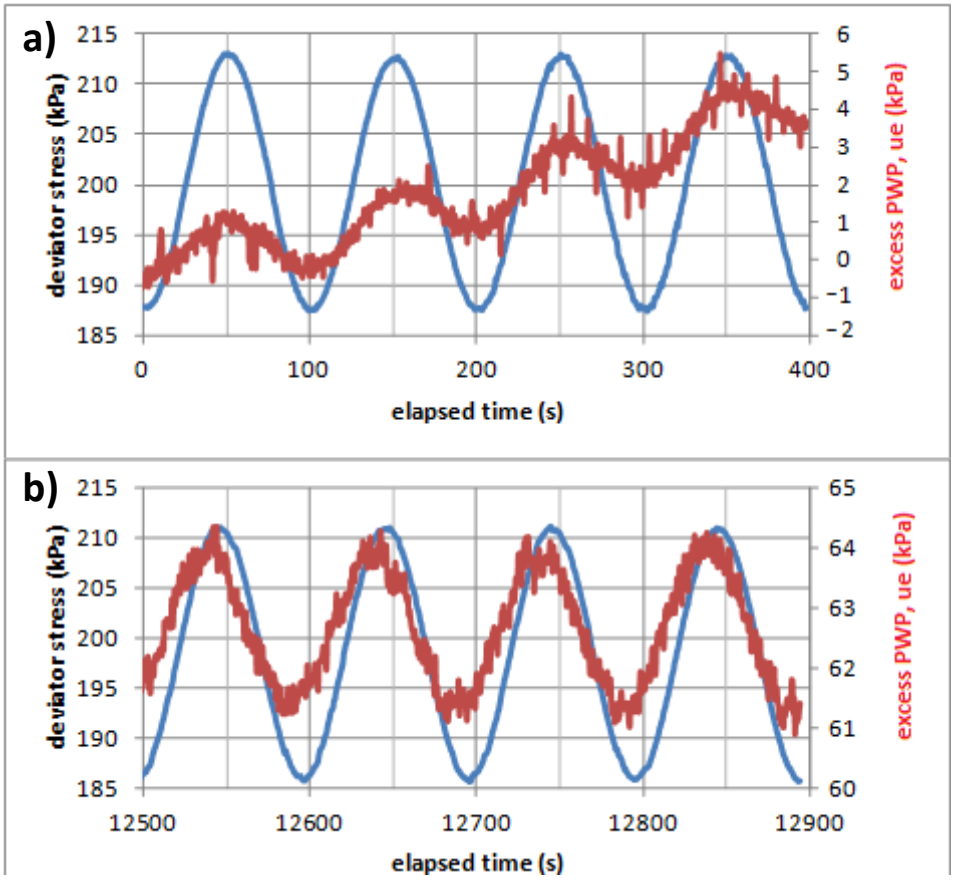

Figure 6.27: Change in pore pressure response in test D-2, from a slight lag at low strains (a: 0-0.1%) to leading the peak stress at large strains (b: 8.1-8.2%) indicating possible dilation.

6.3.3. Shear banding and ultimate failure

Liquefaction exhibited by the Silt Mix samples is not an ultimate failure state but a meta-stable initial state as discussed by Muhunthan and Worthen (2011); the mechanism is contractant and self-arresting, as is apparent from post-liquefaction recovery. The Silt Mix does not reach a critical state in monotonic shear due to premature shear banding failure at strains lower than that commonly associated with the critical state in silts; studies such as Wang and Luna (2012) and Yamamuro and Lade (1999) achieved these strains (>25%) through greater control of end restraint. After shear bands initiate, whilst the raw load cell data may indicate intermittent

increases in resistance, the corrected deviator stress accounting for membrane restraint (Head, 1986; La Rochelle et al., 1988) shows continual strain-softening. Dependence on strain uniformity for stable dilation, given the expected non-uniform stress fields and potentially heterogeneous soils in the field, indicates dilatant strength must be treated with caution.

Figure 6.26 indicates the maximum cyclic *q/p'* increases slightly with increasing cyclic stress – this is expected as u_e (responsible for reducing *p'*) as a function of strain is not significantly affected by changes to the cyclic q_{max}. Test D-1 reaches the highest *q/p'* (similar to the monotonic tests A-1, A-3, and A-4) and similarly undergoes shear banding (first identified at 9% strain and may coincide with the sudden increase in plastic strain). No D-series tests with lower cyclic stresses exhibited shear banding during cyclic loading and it may depend upon the combination of *q/p'* and strain achieved, as in test D-1. Similarly, tests C-6 and C-11 (Ψ = 1.92, but without area corrections to correct relaxation) experienced shear banding during cyclic loading.

Shear banding is expected to be accentuated by stress/strain localisations from increased end restraint and at large strains (see Chapters 3.1.1, 3.1.2, 3.3.3 and 4.2.2.3). If end restraint is reduced by lubricating the sample top, as in Figure 6.14, dilatant recovery and shear banding failure appears slightly delayed. Similarly in Figure 6.28, shear banding of the top-lubricated test C-9 is not apparent and strain accumulation is slower; test C-5 also shows lower strain accumulation at large strain, in this case diverging from 4% strain. Lee and Vernese (1978) similarly found end lubrication to reduce cyclic strain accumulation, particularly at large strains.

Divergence of strains for samples with end lubrication coincide with the initiation of dilation in static tests; it is likely that more evenly distributed dilatant strains are less damaging in terms of opening up a shear band. The observed differences in shear banding failure mode between lubricated and standard-ended samples (Chapter 4.2.2.3) support this.

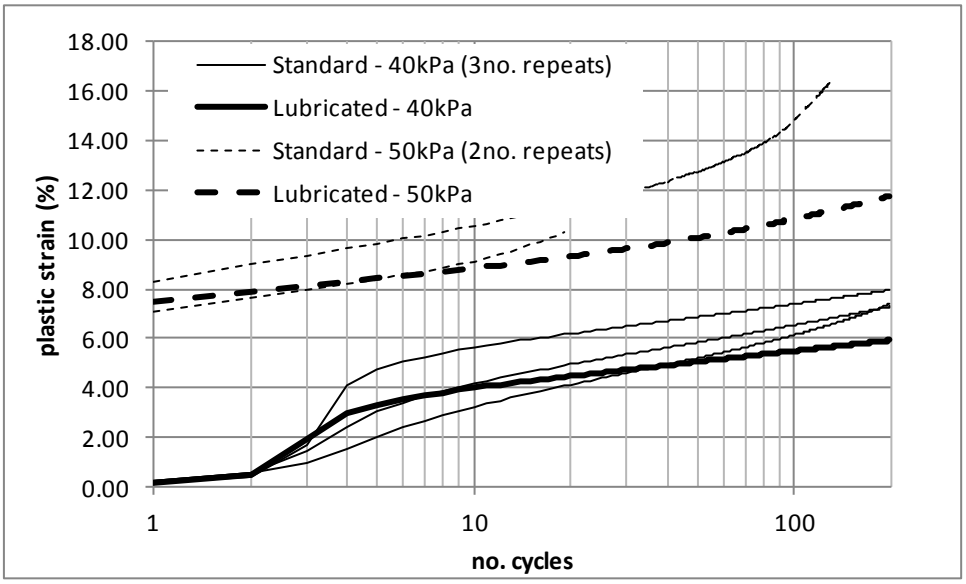

Figure 6.28: Reduction in very large-strain plasticity resulting from end lubrication for Series 'C' tests (i.e. without stress-correction).

Triaxial end restraint may be a major factor in developing post-liquefaction recovery, meaning it is unrepresentative of field behaviour (Zhang & Garga, 1997). Unlike Zhang and Garga (1997), who observed recovery at 10-20% strain, the Silt Mix soil displays recovery at much lower strains (1.5-3.0%). Stress non-uniformities in standard-ended samples particularly are likely to dominate behaviour at ε = 10-20%, however at ε = 1.5-3.0% non-uniformities should be minor (Bishop and Green, 1965; Sheng et al., 1997). As lubricated monotonic tests (Figure 6.14) and cyclic tests (Figure 6.28) follow standard-end tests closely up to ε = 3-4%, followed by gradual divergence, dilatant

recovery in Silt Mix appears to be inherent. The greater propensity for dilatant recovery and lower recovery strains may be due to the angularity and better grading of the Silt Mix soil compared to uniform sands.

6.4. Loading rate and duration influence

6.4.1. Plasticity and liquefaction

When comparing load waveforms of different periods, there are two linked effects to consider: the increased stress and strain rates for a shorter period and the shorter duration under load. Varying frequencies in the small-strain regime is found to have negligible effect upon the predominantly elastic strains (Figure 6.29); divergence is only apparent within the medium-strain regime, suggesting it is predominantly the duration of loads causing yield which are affected by changing cyclic frequencies and not the rate at which load is applied. This is further corroborated when comparing the stress-strain characteristics of the first cycle of load (Figure 6.30), for which stress and strain rates will vary depending on the waveform period and amplitude; below the volume change threshold, all tests are very similar. Additionally, as is apparent from Table 6.2, within the range Ψ = 0.96-1.54 (just above the threshold stress) a single load cycle is significantly stiffer than monotonic loading (up to 18x). This is likely as a result of reduced load duration within the liquefiable range. At higher loads (and so faster strain rates) this effect reduces; there may be additional fabric disruption and a greater collapse initiated by the significantly higher mechanical power input during these higher loads.

Below 0.01% strain all behaviour in Figure 6.30 is recoverable, regardless of period. Above this, most plastic strain occurs around the peak stress. In fact, during

liquefaction significant plastic strain occurs during unloading (Figure 6.31), implying a kinematically unstable mechanism and highly duration-dependent strain accumulation. Plastic work being done on the sample must arise from by a changing internal energy state and thus kinematic instability, rather than external load (Schofield and Wroth, 1968; Lade, 1994). The longer the conditions permitting collapse are maintained, the greater the strain accumulated. In Figure 6.32 a distinction is apparent between elastic strain, which reaches a peak at 50% of the cycle duration; plastic strain with some post-peak creep, which reaches a peak at 60% to 70%; and liquefaction, which accumulates strain rapidly during the unloading period (i.e. to >70% cycle duration). Similarity of strain accumulation between 0.1Hz and 0.01Hz tests in Figure 6.32 up to 0.01% strain and divergence after similarly suggests it is plastic strain which is most affected by changes in load period.

Table 6.2: Comparison of Silt Mix monotonic (mean of tests A-1, A-3, A-4) and cyclic (Series D) strains in response to various stress levels.

Δq (kPa)	Ψ	monotonic ε(%)	ε_{max} (%) (1st cycle @ 0.01Hz)	N for ε_{max} > monotonic ε	Mean strain rate (1st cycle) (%/hr^{-1})
15	0.57	0.013	0.014	1	0.91
20	0.77	0.025	0.026	1	1.70
25	0.96	0.108	0.044	5	6.48
40	1.54	5.75	0.31	5	15.9
45	1.73	7.16	3.18	3	143
50	1.92	8.63	7.66	2	345

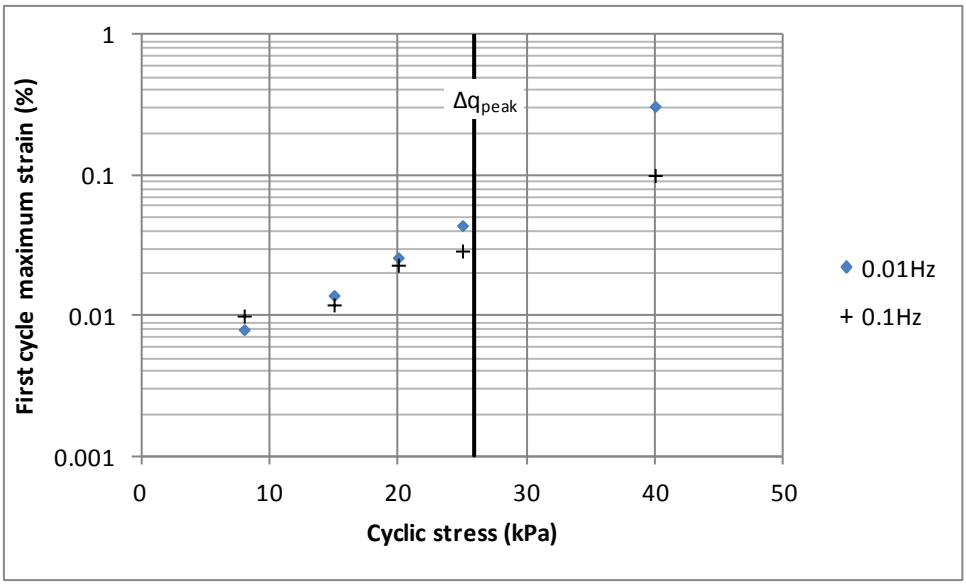

Figure 6.29: Time-dependent plasticity apparent from divergence of 0.01Hz and 0.1Hz frequency waveforms above 20kPa cyclic stress ($\Psi = 0.77$). The maximum strain under 20kPa stress is just above the volume change threshold.

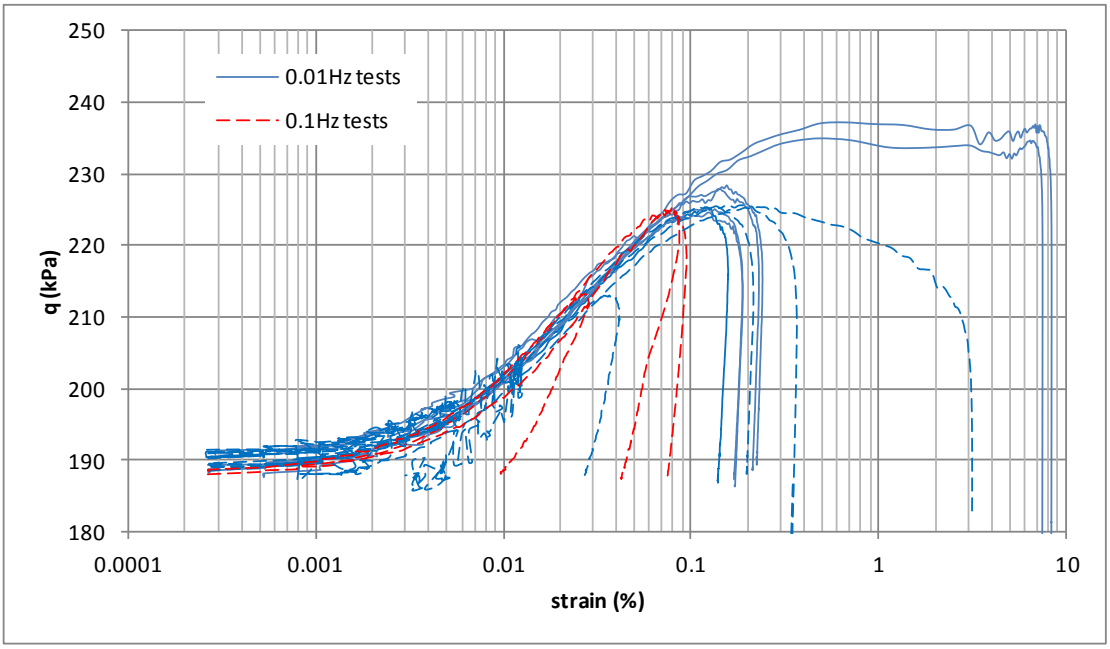

Figure 6.30: Stress-strain curves for the first load cycle, sine/haversine waveforms tests from series C, D, E, and F. An initially similar loading curve is apparent with divergence around q_{max}.

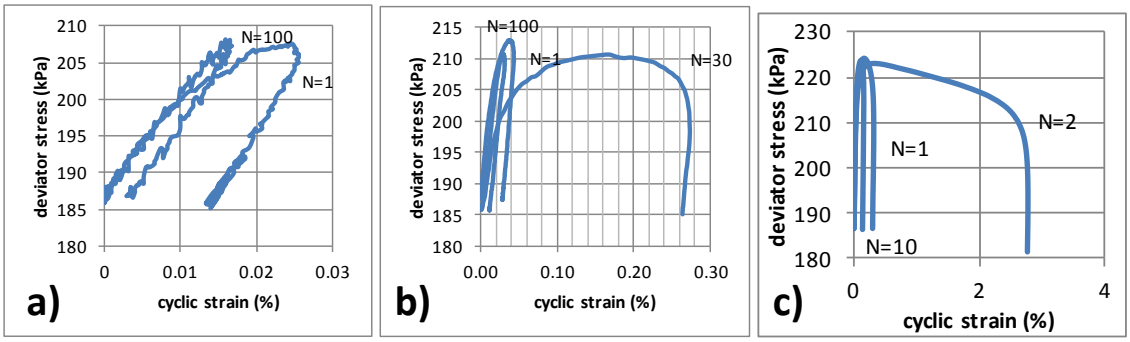

Figure 6.31: Comparison of strain-softening, time-dependent response apparent during liquefying load cycles to more stable response of non-liquefying or post-liquefied load cycles, from tests D-3 (a: Ψ = 0.77; non-liquefying), D-2 and D-8 (Ψ = 0.96 and 1.54; b and c respectively). Test D-8 liquefies in the second cycle and recovers subsequently, D-2 begins to liquefy from cycle 10 and begins recovery at cycle 25.

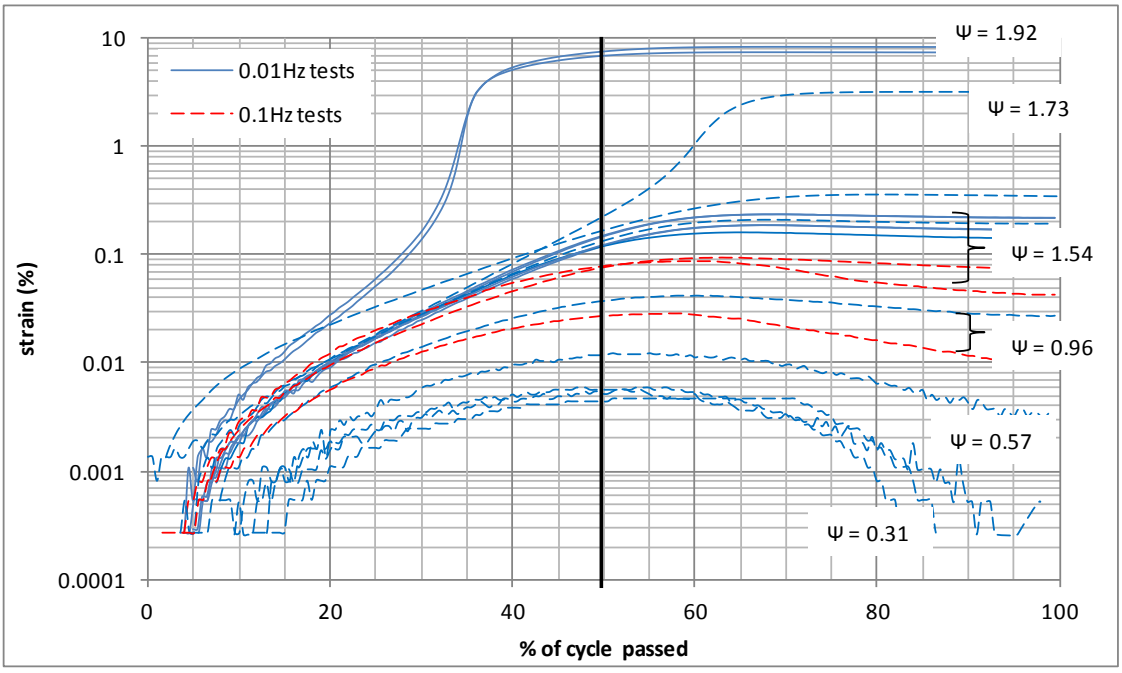

Figure 6.32: Accumulation of strain within first cycles of load for sine/haversine waveforms from Series C, D and E tests. Irrecoverable strain coincides with transition to plastic behaviour (0.01% strain).

A comparison of 0.1Hz and 0.01Hz loading indicates the slower test accumulates 6-10 times more strain per cycle (Figure 6.33), broadly in agreement with what would be expected if plastic strain was purely dependent upon the time spent above a certain yield stress. Where 0.1Hz loading accumulates more than 1/10 of 0.01Hz loading, it may suggest a lower yield stress at higher frequency. Figure 6.33 also indicates the

strain-dependent evolution of liquefaction and recovery previously noted is only affected slightly by loading rate (both phenomena initiated at slightly lower strains in the faster test).

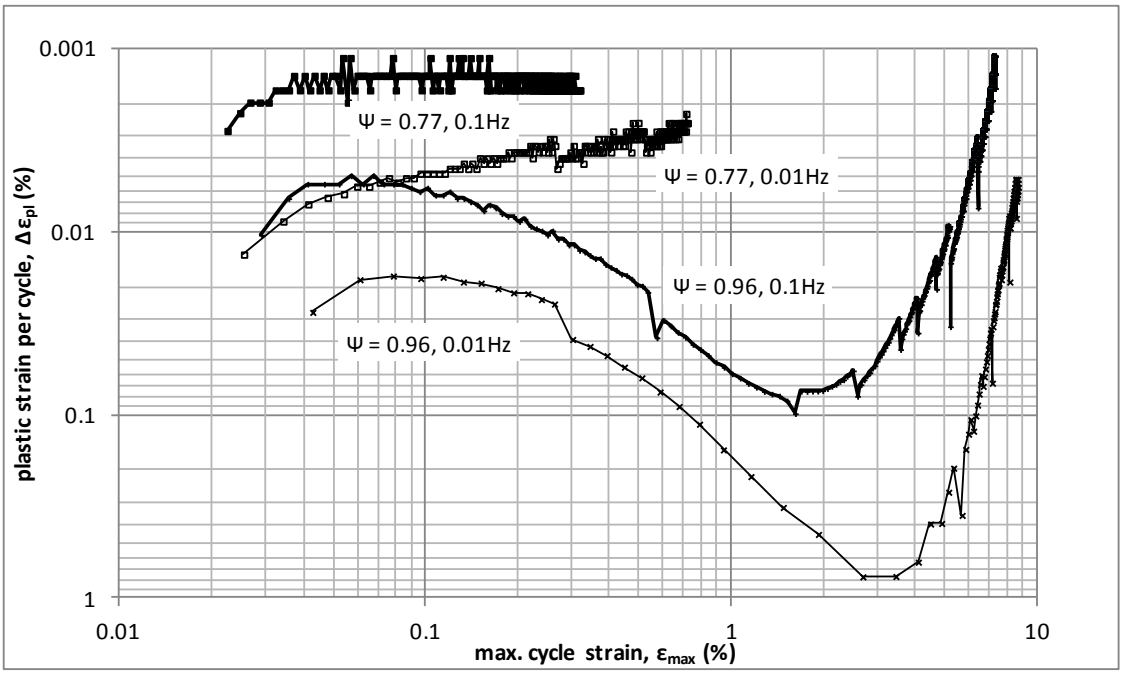

Figure 6.33: Comparison of plastic strain accumulation response for 0.01Hz and 0.1Hz frequency cyclic load for liquefying and non-liquefying tests.

In Figure 6.33, Ψ = 0.77 at 0.1Hz (1st stage of E-3) reaches a constant $\Delta\varepsilon_{pl}$ of 0.015%/cycle early in the test, equal to 50 times the final creep consolidation rate. Based on the results in Section 6.3.1., this is unlikely to be creep interaction; it is possible that, given the role of energy in meta-stable soils discussed in Chapter 3.3.4, the higher power input of a 10 second cycle is more destabilising. This may indicate small reductions to the threshold stress with waveforms of shorter periods but the same amplitude, however experimental evidence is insufficient to confirm this.

6.4.2. Modulus degradation

Under the faster strain rates applied by the various cyclic loads (up to 1000mm/hr for the Ψ = 1.92 or 50kPa cyclic tests, c.f. 2.856mm/hr for monotonic tests), the small-strain secant modulus remains similar to values from slow monotonic loads. Within the medium-strain, plastic regime, loading rate does appear to increase stiffness slightly (Figure 6.34).

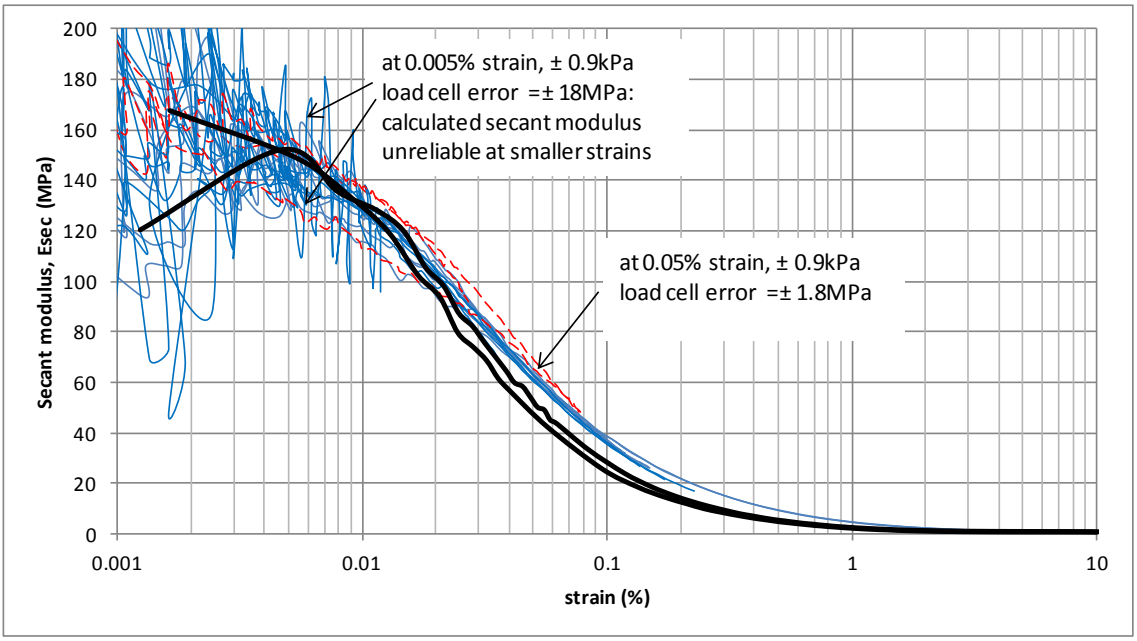

Figure 6.34: Small-strain secant modulus for first load cycle, compared to static curves. n.b. static points are averaged over 10no. results, cyclic are not.

The load modulus, E_L (= $\Delta q_{\varepsilon,max}/\Delta\varepsilon_{cyc}$) is the minimum secant modulus under a load cycle and can illustrate stiffening and softening trends over a number of cycles. In the first cycle for the tests in Figure 6.35, E_L is close to the monotonic secant modulus curve. For a given Δq_{cyc} value, there is a corresponding reciprocal curve of E_L vs $\Delta\varepsilon_{cyc}$ which cyclic tests must follow, hence tests in Figure 6.35 are sorted by cyclic stress level but not by frequency. The cyclic tests drop below the monotonic curve as the strain increases during liquefaction and rise above during stabilisation. In fact during

liquefaction, because $\Delta q_{\varepsilon,max}$ can be less than Δq_{cyc} due to strain-softening and creep (Figure 6.31), results lie slightly below the reciprocal curve. As the cyclic strains reduce during cyclic stabilisation (either post-liquefaction or for sub-threshold stress tests) the stiffness becomes increasingly improved relative to the intact monotonic curve. This suggests there may be some beneficial fabric re-arrangement attained from stable cyclic loading and post-liquefaction recovery.

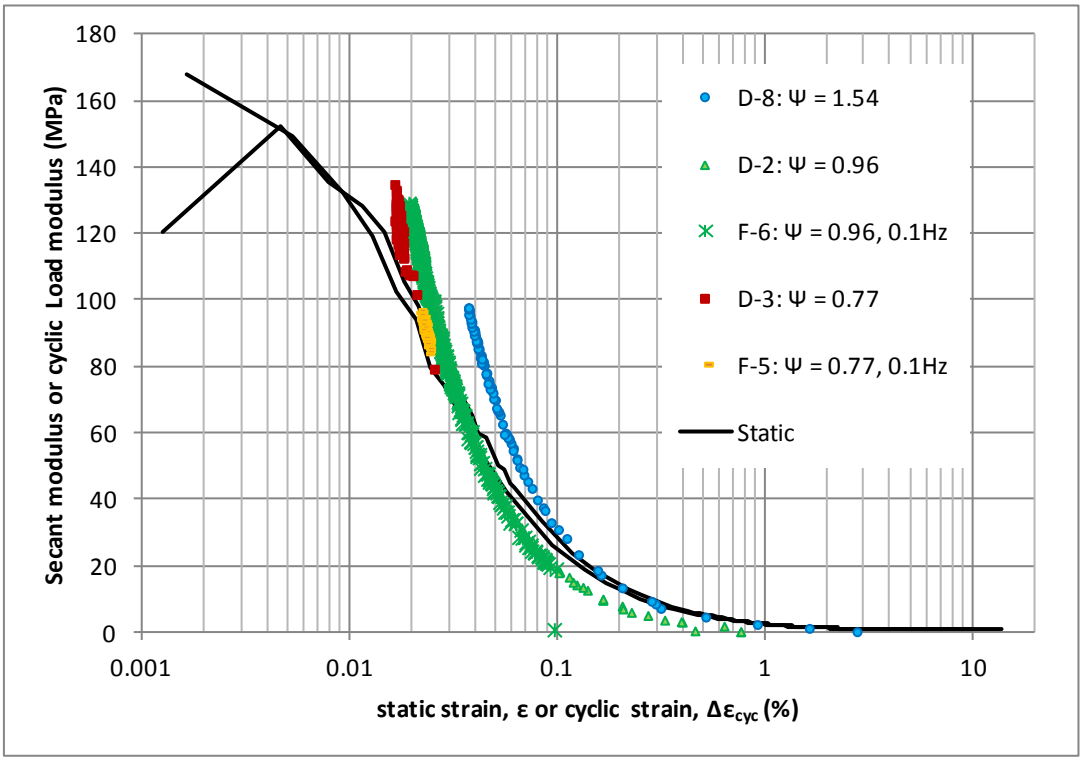

Figure 6.35: Cyclic load modulus results for all cycles of various tests. As the tests stabilise or reach post-liquefaction recovery, cyclic strains reduce and stiffness is increased relative to static or first-cycle (Figure 6.34) results.

6.5. Disruption of liquefaction

As discussed in Chapter 6.2., liquefaction requires specific external conditions to be maintained so that the precarious soil fabric can be preserved. Disruption of this fabric in unstable conditions (i.e. undrained shear) can cause a meta-stable collapse reaction.

Conversely, if disruption is effected whilst maintaining stable conditions, liquefaction can be reduced or even averted.

6.5.1. Changes to consolidation stresses

As observed by Wang and Luna (2012) and Santagata and Germaine (2005), overconsolidation can avert liquefaction. As is apparent in Figure 6.36, this can occur at lower overconsolidation ratio (OCR) than the aforementioned studies. Test A-9, with the lower OCR (1.1), is continuously strain-hardening but the formerly precarious fabric influence is still apparent through loss of stiffness between 0.1% and 2.0% strain, i.e. the strain range associated with liquefaction. This suggests the overconsolidation experienced is only just sufficient to avert liquefaction. Subsequent dilation (>3% strain) still causes stiffening. Overconsolidated ultimate strength is similar to normally consolidated samples, due to the low swell potential of silt.

Changes in these tests' stress states (reduction in cell pressure rather than maintaining K_0 conditions, to follow cyclically-induced overconsolidation) and the marginally-stable response of test A-9 suggests their stabilisation may be due to crossing of the Instability Line in stable, drained swell-back conditions (Figure 6.37).

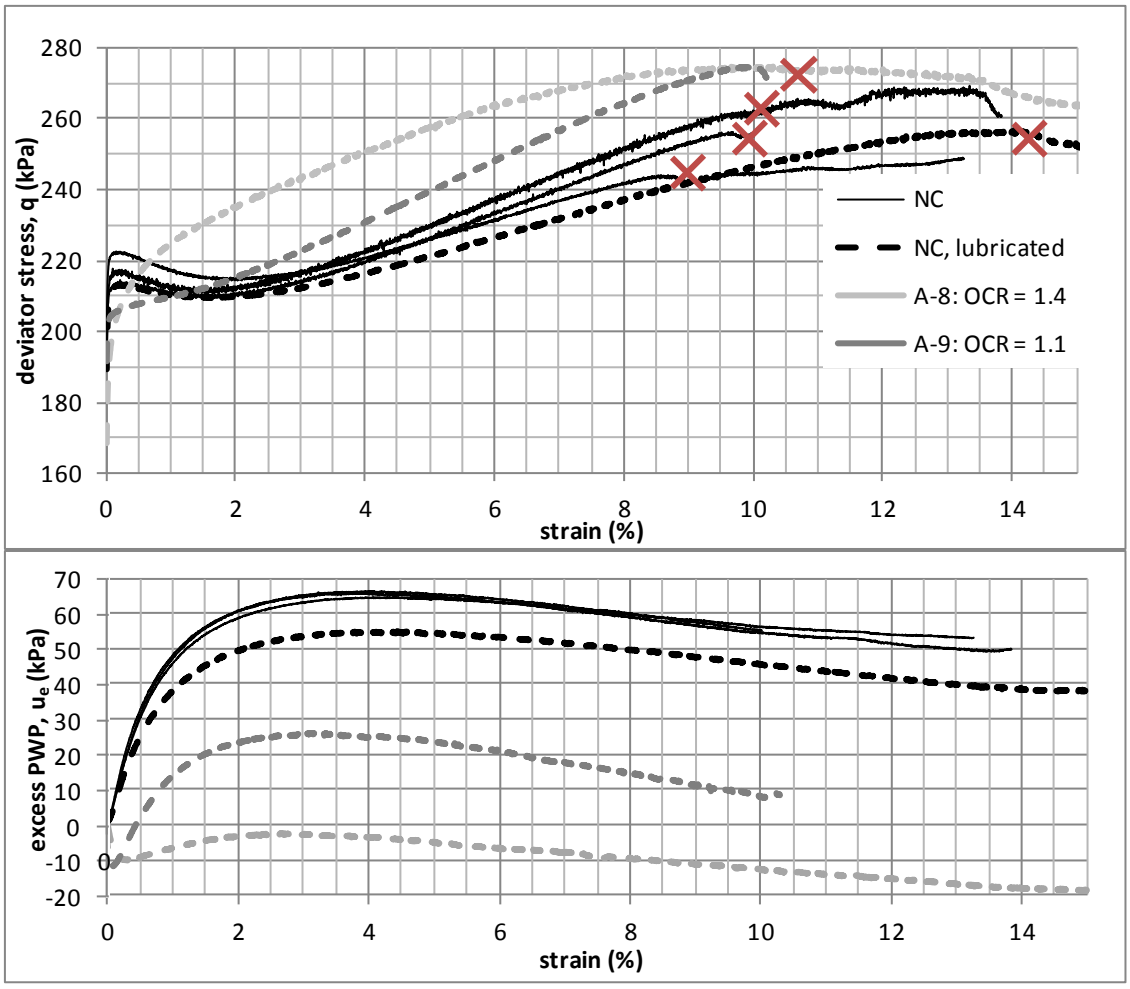

Figure 6.36: Reduction in liquefiability with increased OCR (achieved by reducing cell pressure with no change to ram) n.b. red 'X' indicates shear band initiation.

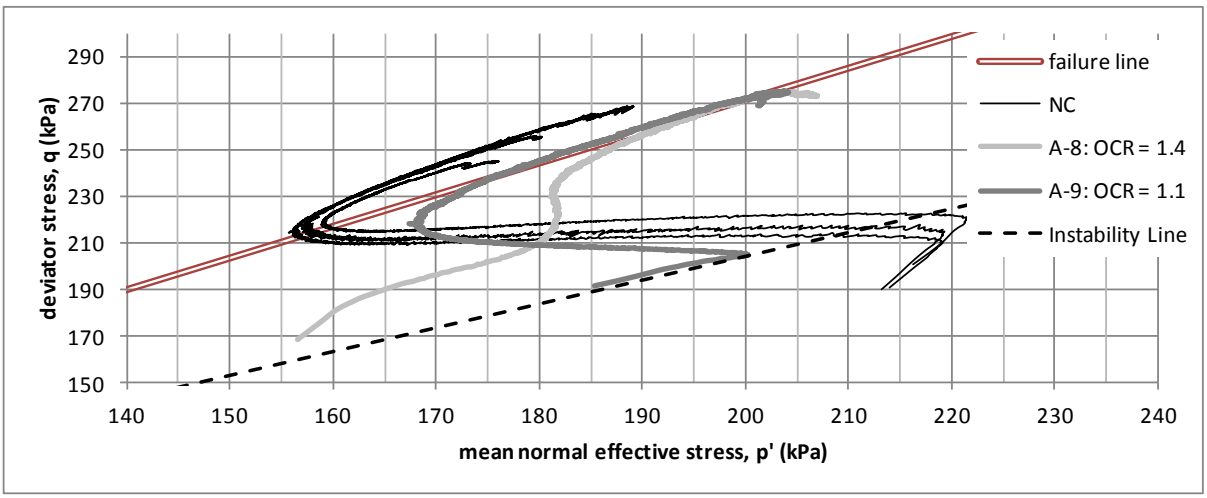

Figure 6.37: Effective stress paths of normally consolidated and overconsolidated Silt Mix samples. Both overconsolidated tests (thick grey lines) start from above the Instability Line and avoid liquefaction.

As is apparent in test C-13 (Figure 6.38), removal and reapplication of consolidation deviator stress can similarly avert cyclic liquefaction. During reapplication of anisotropic stress, a further small change in water content of 0.08% occurs (c.f. 2.7% total consolidation water content change and 0.6% during first application of anisotropic stress). It is possible this small additional consolidation is responsible for stabilisation. Additionally, as soils retain some 'memory' of overconsolidation up to 1.5 to 4 times the previous maximum stress (Ladd and Foott, 1977; Overy, 1982; Santagata and Germaine, 2005), this stress history may stabilise the structure, similarly to Doanh et al. (2012). These results highlight how sensitive this initially liquefiable fabric is to changes in stress history.

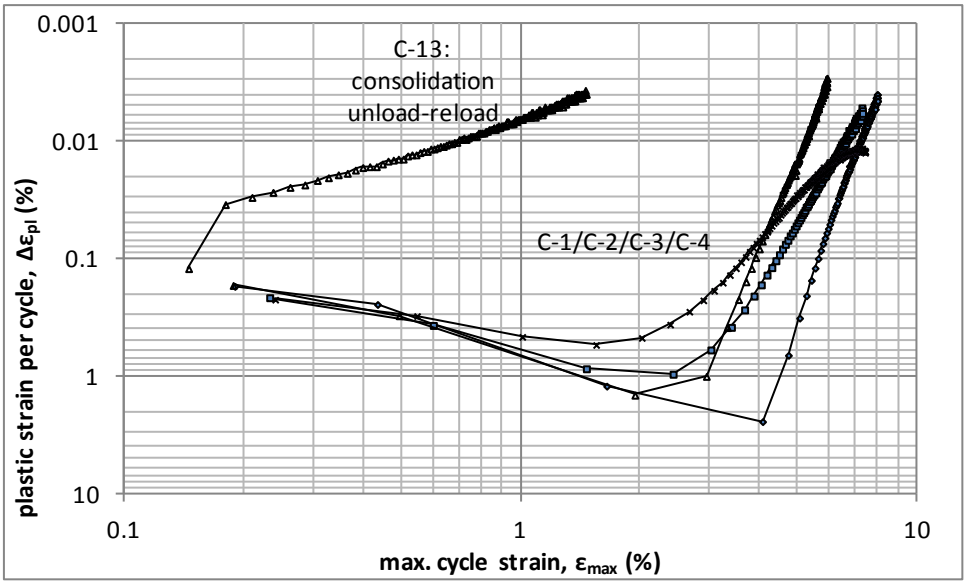

Figure 6.38: Test C-13, subject to full unloading and reloading of deviator stress (control error in 2nd stage of consolidation) compared to load controlled cyclic tests with the same parameters (C-1 to C-4; Ψ = 1.54). Handling disturbance for sample C-13 not considered likely cause of stabilisation; ε_{v1} = 3.7%.

6.5.2. Cyclically-induced plasticity – changes to monotonic response

As discussed in Section 6.4.2., samples subject to cyclic liquefaction subsequently display recovery behaviour, i.e. dilatant strain-hardening. Failure is much more brittle, with shear banding after much smaller strain increments. Behaviour is largely controlled by cumulative strain; the post-cyclic and intact stress-strain curves converge (Figure 6.39). For a dilating soil to fail, large localised movement of soil grains is required to allow a shear band to 'open-up'(Atkinson, 2000; Zhao and Guo, 2015). It is reasonable to assume cumulative strain is directly related to shear banding, and thus responsible for this strength reduction in the Silt Mix soil.

The data implies, although with large uncertainty given inherent experimental variation, that cyclic loading tends to slightly reduce the total cumulative strain required for shear banding. The rapid loading and lack of time for pore pressure equalisation across the sample may influence this effect. In the field, where pore pressures are likely to be more non-uniform across the vehicle's influence zone, the likelihood of early shear banding may therefore be increased.

The Instability Line is a function of sample fabric rather than a more intrinsic property of the soil, such as the Critical State or Mohr-Coulomb failure lines. When this fabric is rearranged by plastic strain, as has been seen by Doanh et al. (2012) for example, the Instability Line can also change. Large-strain restructuring, through initiating liquefaction, is not necessary for stabilisation. The soil can also be stabilised by cyclic load within stable limits, i.e. below the threshold stress, provided sufficient plastic strain is induced. The ultimate strength is increased without significant reduction of ductility (Figure 6.40). A portion of the strength increase is related to greater dilatancy,

evidenced by a lower peak pore pressure and larger dilation rates (from 3% strain onwards).

As was implied by the Load Modulus data in Figure 6.35, the post-cyclic shear stages suggest plastic strains re-structure the soil beneficially even when dilatant recovery is not initiated. Figure 6.40 also indicates there is a minimum cumulative strain, required to avert liquefaction, just in excess of ε_{tl} (0.1% to 0.3%). This suggests the degree of micro-structural rearrangement required to trigger liquefaction is similar to that required to stabilise a liquefiable soil. This supports the concept of meta-stable liquefaction arising from a soil's initial micro-structure: sufficient perturbation, applied either in a stable or unstable manner, will dislodge sufficient precarious inter-particle contacts so the potential energy is released (quickly in the former case, slowly in the latter). A more compact and less ordered structure is achieved. As cyclic plastic strain increases further beyond this minimum, strength reduces, expected to be as a result of rising pore water pressures.

Exceeding ε_{tl} and averting liquefaction in post-cyclic shear also coincides with the effective stress path crossing the Instability Line (Figure 6.41). This is expected as monotonic and cyclic pore pressures agree closely within this strain range (Figure 6.25). A certain plastic strain can thus be considered to impart a certain degree of fabric rearrangement, corresponding to a certain contraction of the soil skeleton (rising pore pressure). Crossing the Instability Line in stable or unstable circumstances represents the same phenomenon: sufficient disturbance to rearrange a soil from a precarious to a compact state.

Post-cyclic strength and stiffness exceeding the overconsolidated samples (Figure 6.40 c.f. Figure 6.36) suggests stress state changes are not the only cause of strengthening; some beneficial fabric rearrangement is taking place. This effect is also apparent from secant modulus results of post-cyclic shear stages (Figure 6.42). Whilst the small-strain modulus appears slightly reduced by cyclic load (although load cell noise at these low strains makes distinction difficult), stiffness in the medium-strain regime appears slightly increased, even for tests which have experienced insufficient cyclic strain to avoid subsequent large-strain liquefaction (test D-6; $\Psi = 0.57$).

Figure 6.42 also implies extended strain thresholds; the constant stiffness region appears extended. The medium-strain part of the post-cyclic secant modulus curve is improved to match or even exceed the cyclic (constant stress) curve; the soil has become 'conditioned' to resist the cyclic load within a decreased cyclic strain range. Improvement beyond this reciprocal curve is also apparent at large strains for stabilised/post-liquefied tests, due to remediation of liquefaction.

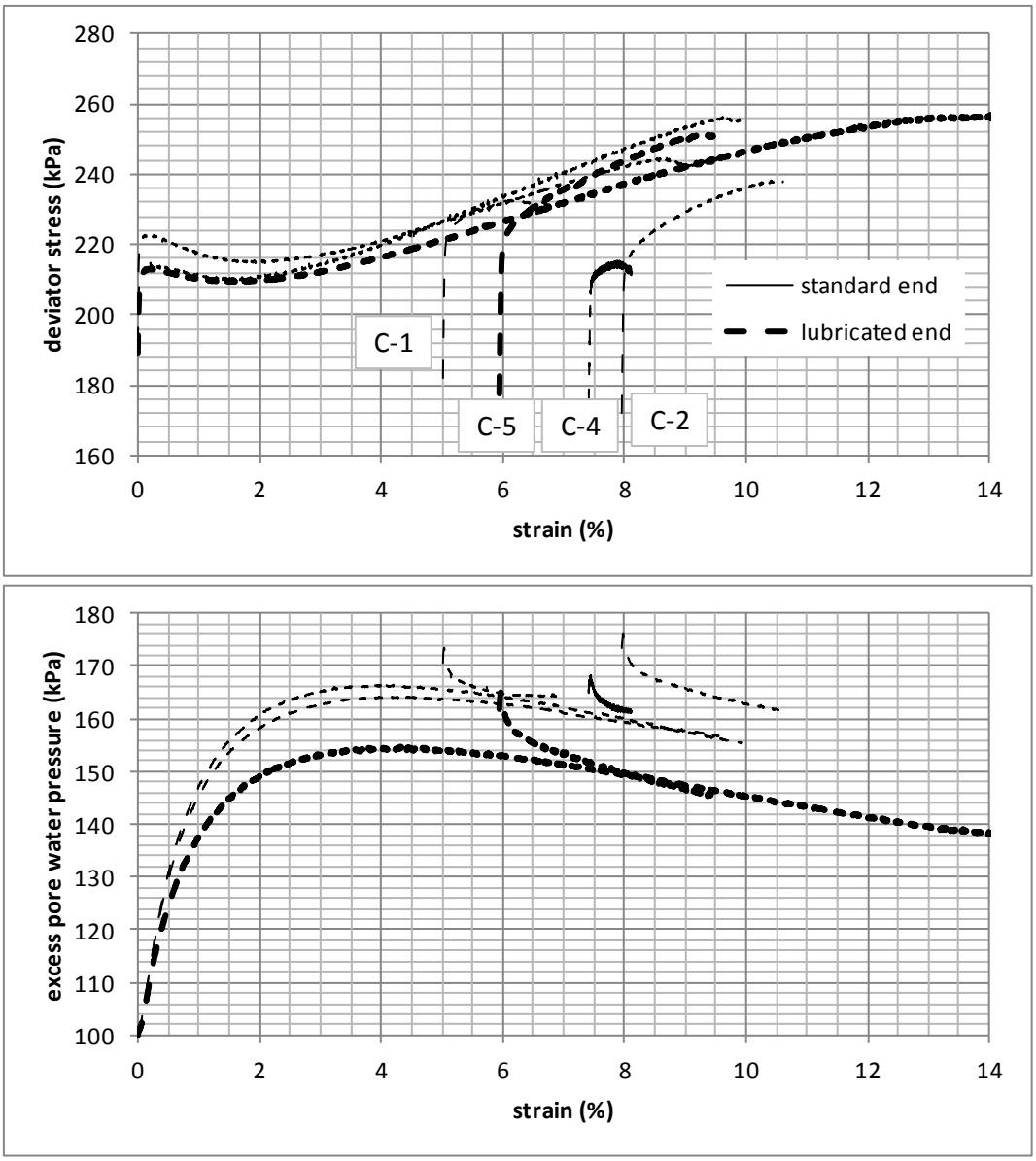

Figure 6.39: Post-cyclic monotonic shear response of liquefying Series 'C' tests with varying accumulated cyclic ε_{pl}; *u* and *q* of cycled samples converge to the intact curve but can trigger shear banding at lower strengths.

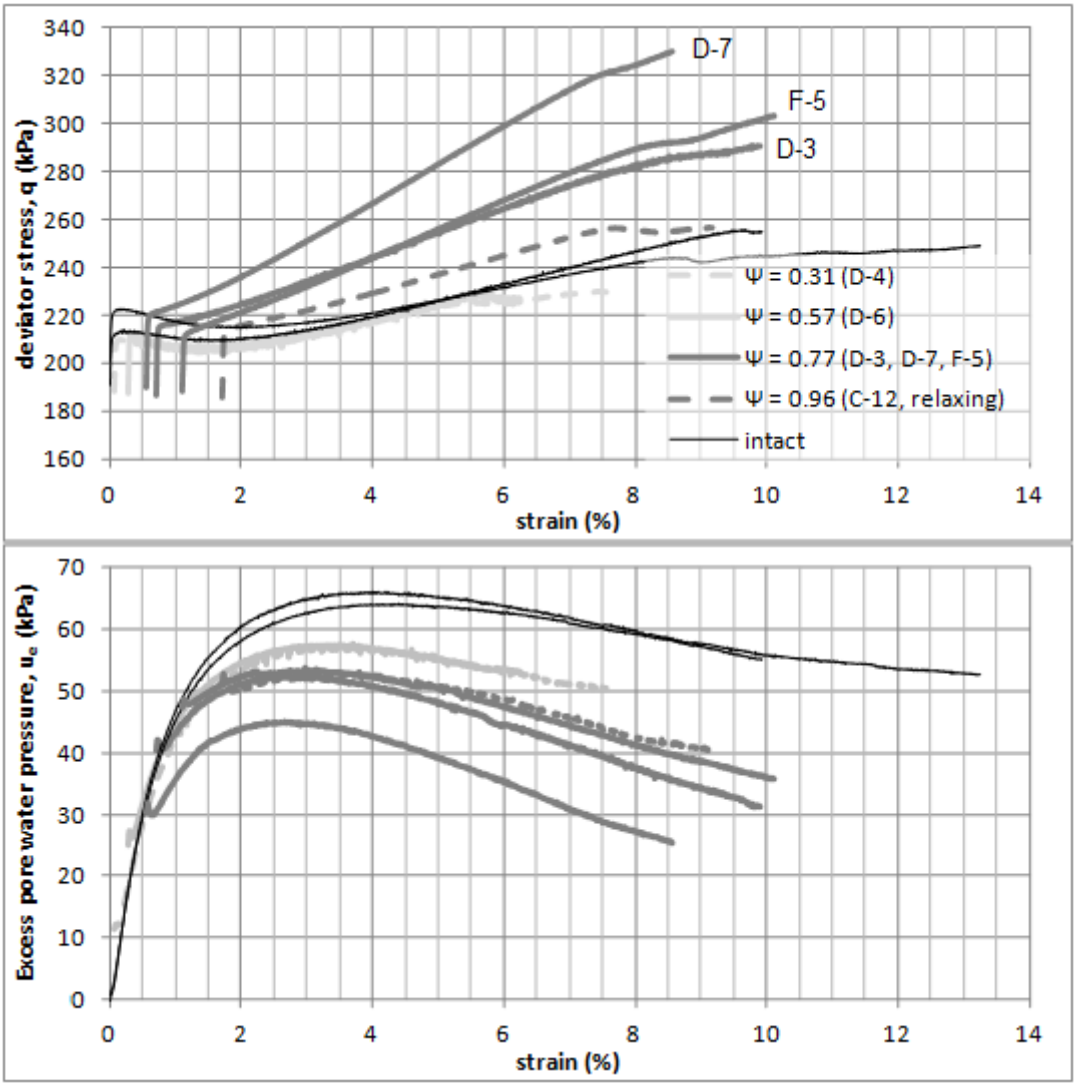

Figure 6.40: Post-cyclic monotonic shear response of non-liquefying samples; above ε_{pl} = 0.5% show no liquefaction, others remain as per intact. Tests C-12, D-3, and F-5 are not expected to be subject to handling disturbance (ε_{v1} = 2.9% to 3.5%) whilst D-7 is marginal (ε_{v1} = 4.1%).

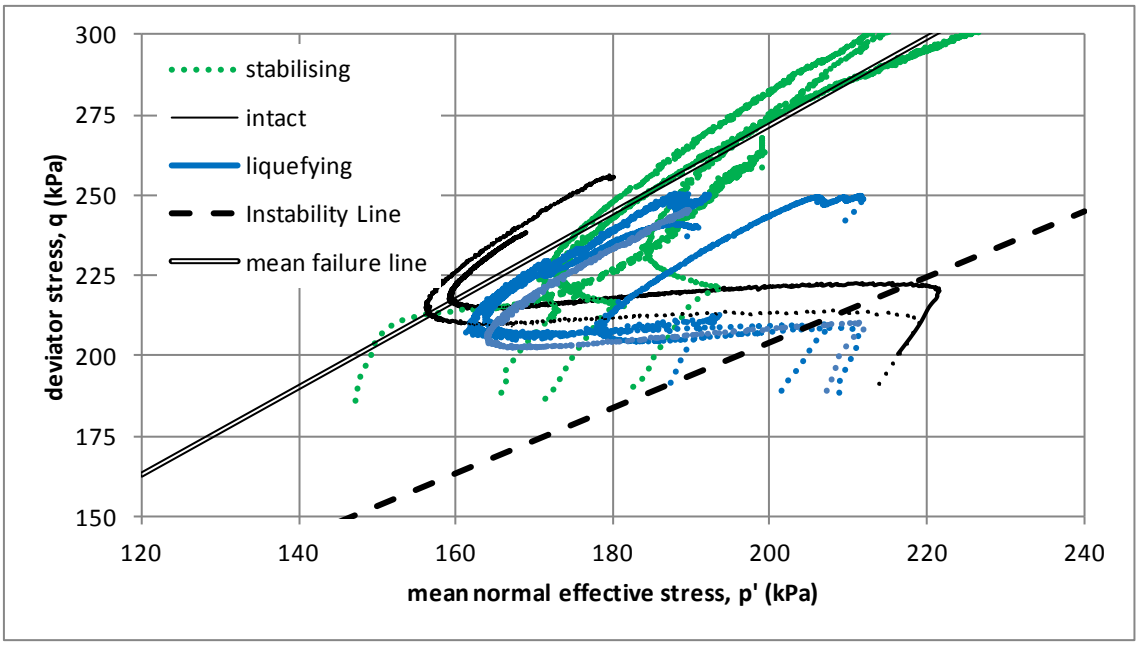

Figure 6.41: Effective stress paths of post-cyclic static shear: samples starting to the left of the Instability Line (also exceeding ε_{tl}) are stable, whilst those on the right liquefy.

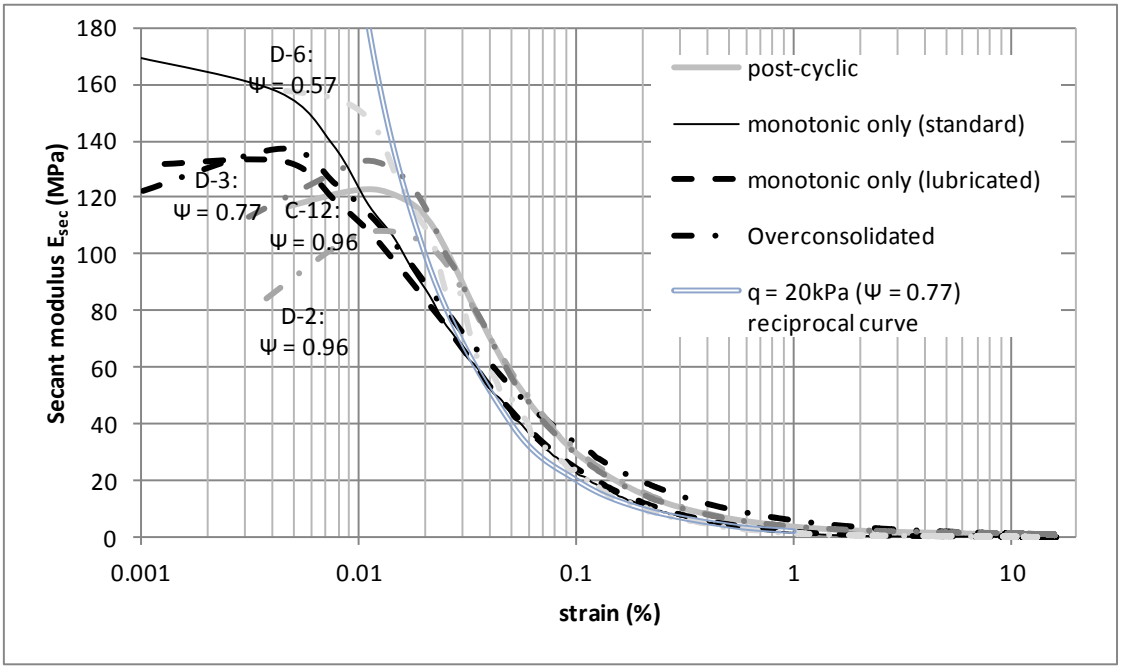

Figure 6.42: Secant modulus degradation curves of post-cyclic static shear stages implying increased medium-strain stiffness for all post-cyclic tests and increased large-strain stiffness (i.e. no liquefaction) for cyclic stabilised (D-3), post liquefied (D-2) and overconsolidated (A-8) tests. For comparison, a curve corresponding to Δq_{cyc} = 20kPa (Ψ = 0.77) is superimposed.

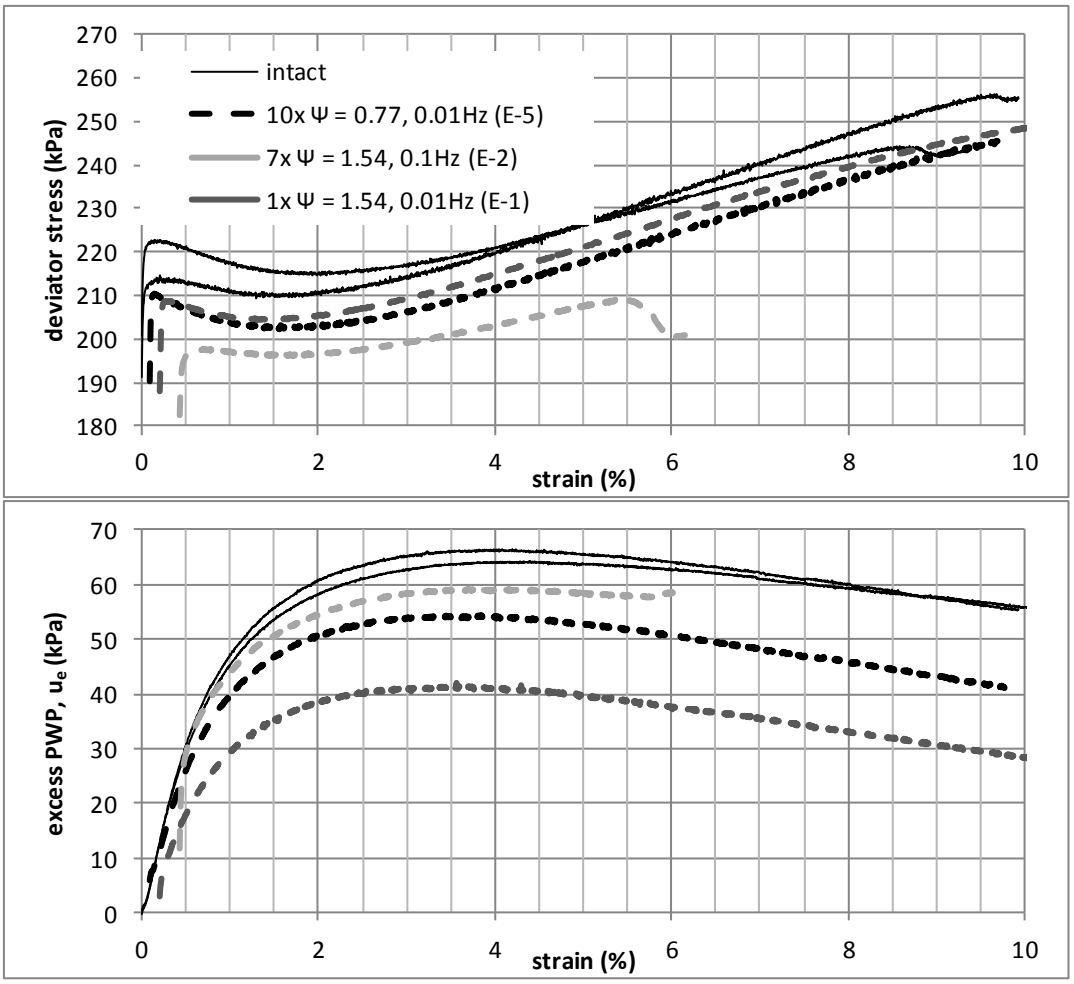

Figure 6.43: Post-cyclic monotonic shear response for samples maintaining liquefiable conditions.

Figure 6.43 shows cyclically-induced stabilisation is not controlled by cyclic stress, but by plastic strain and how strain is achieved. Test E-1 and E-5, which apply Ψ = 1.54 and 0.77 but do not exceed ε_{tl}, liquefy with a reduced strength but a less contractant response than intact tests. Test E-2 had begun to experience accelerating cyclic plastic strains, indicating ongoing liquefaction, and ε_{pl} exceeded ε_{tl}. During the small pause (several seconds) between halting the cyclic stage and initiating monotonic shear, liquefaction continued and the axial ram, maintaining a constant position, was unloaded (as is apparent from the lower starting stress in Figure 6.43). Therefore for

cyclically-induced stabilisation, a medium-strain, sub-threshold cyclic stress is required and the necessary plastic strain (and attending pore pressure) must be exceeded, but only in stable conditions. If liquefaction is initiated, stabilisation will only occur when large dilatant recovery strains are reached, which increases the risk of shear banding failure.

The main difference between a liquefying and stable cyclic response appears to be the mechanical power used to achieve the initial plasticity, i.e. whether the strain is imposed as a single action or through multiple small actions; this may relate to whether loss of particle redundancy is in localised clusters or a globally connected mechanism. Comparison of the diverging strain rates of tests D-2 and C-12 particularly (Ψ = 0.96, relaxing over time for C-12) in Figure 6.44 suggest a limiting stable cyclic strain, which may relate to power input: $\Delta\varepsilon_{cyc} \approx 0.03\%$ within the range ε_{max} = 0.1% to 1.5% (i.e. the domain of liquefiable behaviour) separates stable and liquefying stress-controlled tests.

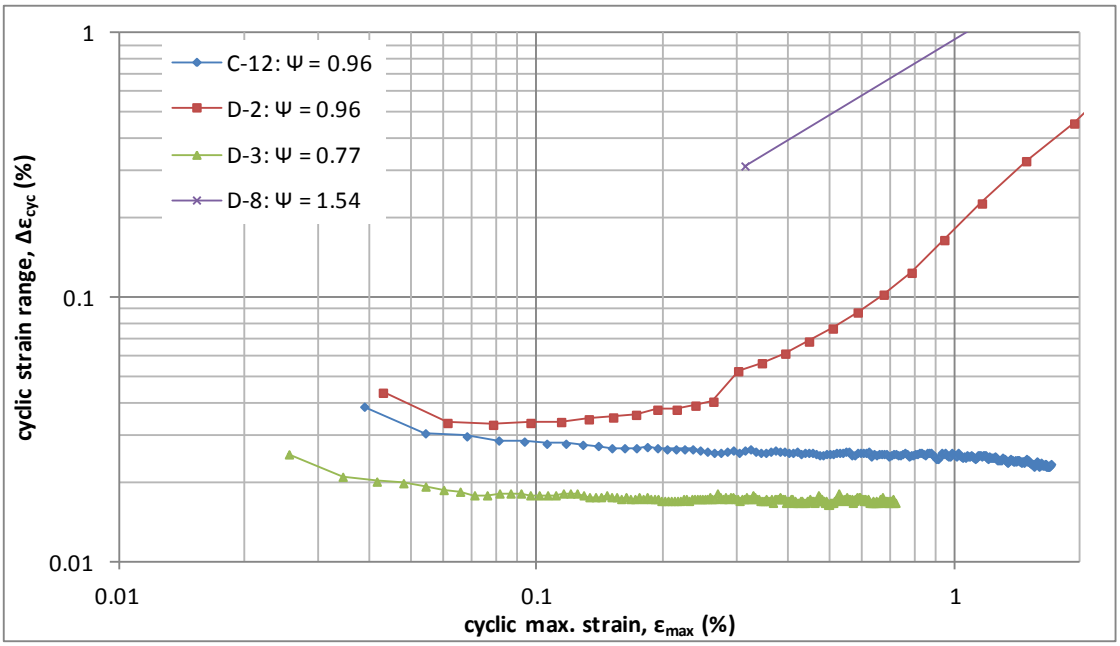

Figure 6.44: Divergence of $\Delta\varepsilon_{cyc}$ for stabilising and liquefying tests. C-12 stabilises due to uncorrected relaxation.

6.5.3. Cyclically-induced plasticity – changes to cyclic response

Similarly to post-cyclic monotonic results, cyclic loading which is predominantly small-strain (i.e. Ψ = 0.31 – 0.57) does not appear to have significant impact upon strain accumulation in subsequent medium-strain (Ψ = 0.77) cyclic tests (Figure 6.45). For a cyclic load of single magnitude, or one preceded only by small-strain loads, the plots of plastic strain against maximum cycle strain are therefore useful tools in predicting cumulative deformations.

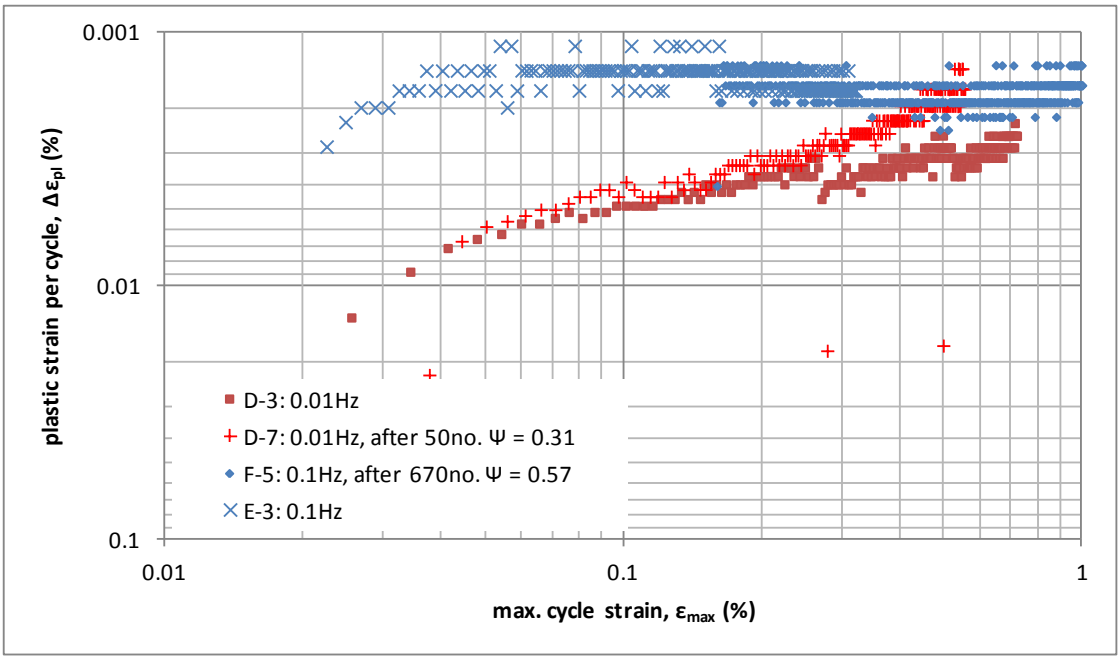

Figure 6.45: Similarity between response of Ψ = 0.77 cyclic tests with no preceding cyclic regime and following small-strain cyclic tests (Ψ = 0.31 – 0.57). n.b. The differing response of later cycles in tests D-3 and D-7 is expected to arise from varying consolidation creep rates, as discussed in Section 6.3.1.

By applying medium-strain cyclic loading below the threshold stress, shown to be effective in improving monotonic shear response, it may also be possible to change cyclic strain accumulation characteristics and avert cyclic liquefaction. Test E-3 applied 200no. cycles at Ψ = 0.77 (10 second period for speed of testing), which accumulated a plastic strain of 0.305%, i.e. just above ε_{tl}. Subsequent plastic strain under Ψ = 1.57 was significantly lower than the test without pre-loading (Figure 6.46), although a smaller liquefaction is still present as more strain accumulates in the second cycle than the first. Recovery and reducing plastic strain accumulation occurs from the third cycle onwards (a strain of 1.8% onwards).

Consolidation data for test E-3 (ε_{v1} = 5.2%) suggests sampling disturbance; strengthening effects may depend entirely upon disturbance and not cyclic pre-

loading. Furthermore, as a result of analysis of rate and duration-dependent effects, doubts were cast upon the assertion that strains achieved by fast loading had the same effect as the same strain achieved by slow loading. Therefore the first stage of test G-5 comprised 70no. cycles of Ψ = 0.77 to accumulate a plastic strain of 0.311%. The lower consolidation volume change (ε_{v1} = 3.8%) and good comparison with other Ψ = 0.77 cyclic tests (0.307% after 70no. cycles in D-3) suggest lower risk of disturbance. Strain accumulation is significantly reduced following cyclic pre-load in test G-5: sub-threshold cyclic load therefore appears to be an effective treatment. At the strains concerned (close to the upper bound of ε_{tl}, 0.3%) faster cyclic loading appears much less effective, potentially having little or no benefit; changes to liquefiability in test E-3 may be entirely due to disturbance. Fast loading in test F-5 is noted to have achieved stabilisation (Figure 6.40), however this test accumulated more strain (0.7%). It is possible that the higher power input in faster load cycles is more disruptive: in addition to causing more plastic strain over a given time period, faster loading may require larger cyclic strains for stabilisation.

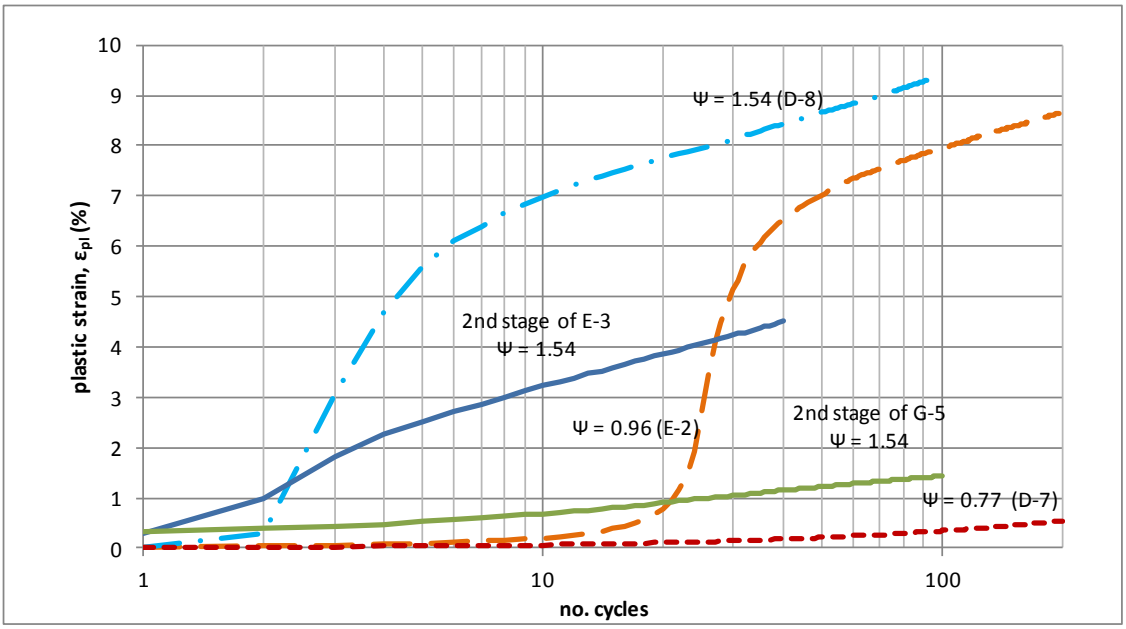

Figure 6.46: Reduction in cyclic plastic strains following initial sub-threshold cyclic load (200x Ψ = 0.77 @ 0.1Hz and 70x Ψ = 0.77 @ 0.01Hz respectively). Test E-3 is likely to be influenced by sampling disturbance (ε_{v1} = 5.2%) whilst for G-5 (ε_{v1} = 3.8%) this is unlikely.

Strain accumulation in test G-5 (Figure 6.47) indicates cyclic pre-loading can produce improved performance (lower $\Delta\varepsilon_{pl}$) to that seen in the recovery stage of liquefied tests. By averting liquefaction, cyclic pre-loading not only avoids sudden ground movements and excessive strains, but also has much lesser risk of brittle shear banding failure.

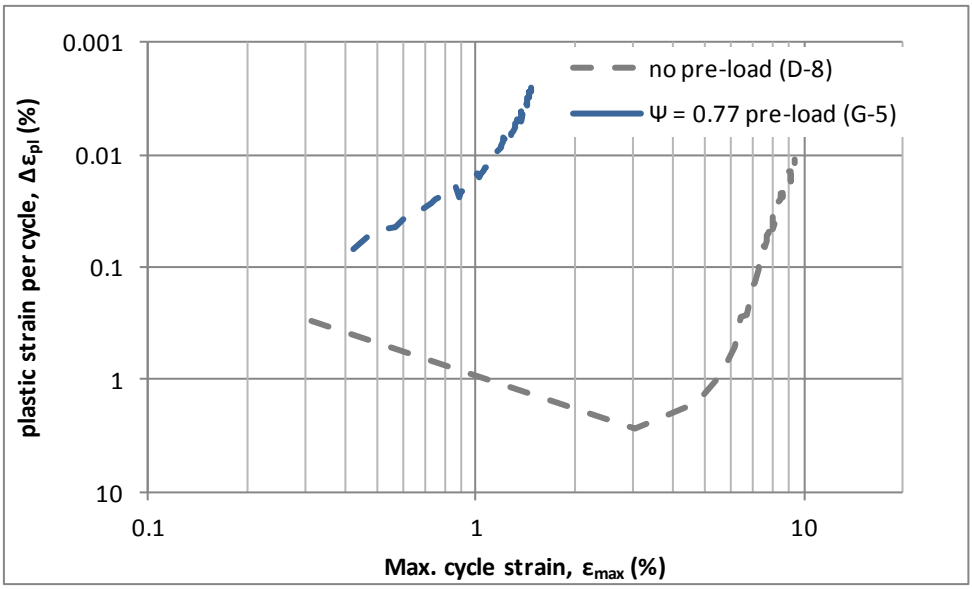

Figure 6.47: Reduction of cyclic plastic strain rates for Ψ = 1.54 from cyclic pre-load of Ψ = 0.77.

6.6. Intermediate drainage effects

6.6.1. Averting liquefaction

As liquefaction progresses, a rapid increase in pore water pressure is apparent (Figure 6.25) which corresponds to collapse of the soil skeleton and shedding of load to incompressible pore fluid. By including rest periods with opportunity for drainage between load cycles, pore pressures can dissipate and effective stresses are restored. Liquefaction is averted and cyclic strain accumulation significantly reduced if drainage is permitted after the first cycle in Ψ = 1.54 tests, i.e. at just below ε_{tl} (Figure 6.48, Figure 6.49).

Comparison of tests G-1 and G-3 suggest the reduction in liquefiability due to drainage intervals is not affected by reducing consolidation time from near-complete (2 hours) to only a small fraction (5 minutes). Whilst other authors have demonstrated that liquefaction depends upon undrained conditions, it is surprising that such a small quantity of drainage has this effect. It was suspected that behaviour may be influenced

by sample disturbance; whilst test G-3 is not within the ε_{v1} range associated with disturbance, it is higher than that for G-1 (3.6% c.f. 2.1%). Differences in the first cycle plastic strain (0.36% in G-1, 0.12% in G-3) suggest factors other than drainage duration are influential here. The first stages of test G-4 (ε_{v1} = 3.0%) therefore repeated the sequence of Ψ = 1.54 and 5 minute drainage intervals. Similarity of the two tests (Figure 6.49) improves confidence in the hypothesis that even short drainage periods are effective in averting liquefaction in the Silt Mix soil. It should be noted the first cycle strain differences are similar to those observed in the first cycle of Series C Ψ = 1.54 cyclic tests (Figure 6.30), all of which subsequently liquefied; such variation appears to be inherent to this particular soil and preparation methods but the fundamental behaviour of interest, liquefaction, is not affected by this variation.

Liquefaction depends upon formation of a mechanism in the micro-structure through contractant breaking of inter-particle contacts; re-forming of contacts during consolidation reverses this action. The small reversal of contraction from the short drainage periods are sufficient to stop a mechanism forming, highlighting that the Silt Mix soil only needs a relatively small change to the fabric to stabilise. It may also indicate Silt Mix to be less liquefiable than other soils in the literature (e.g. uniform sands), which may require more substantial rearrangement to stabilise. However experiments on uniform sand by Lade (1994) indicate similar high sensitivity to volume change; by closing the valve on a sample in a state of drained stress but above the Instability Line, creep strains and contraction led to liquefaction.

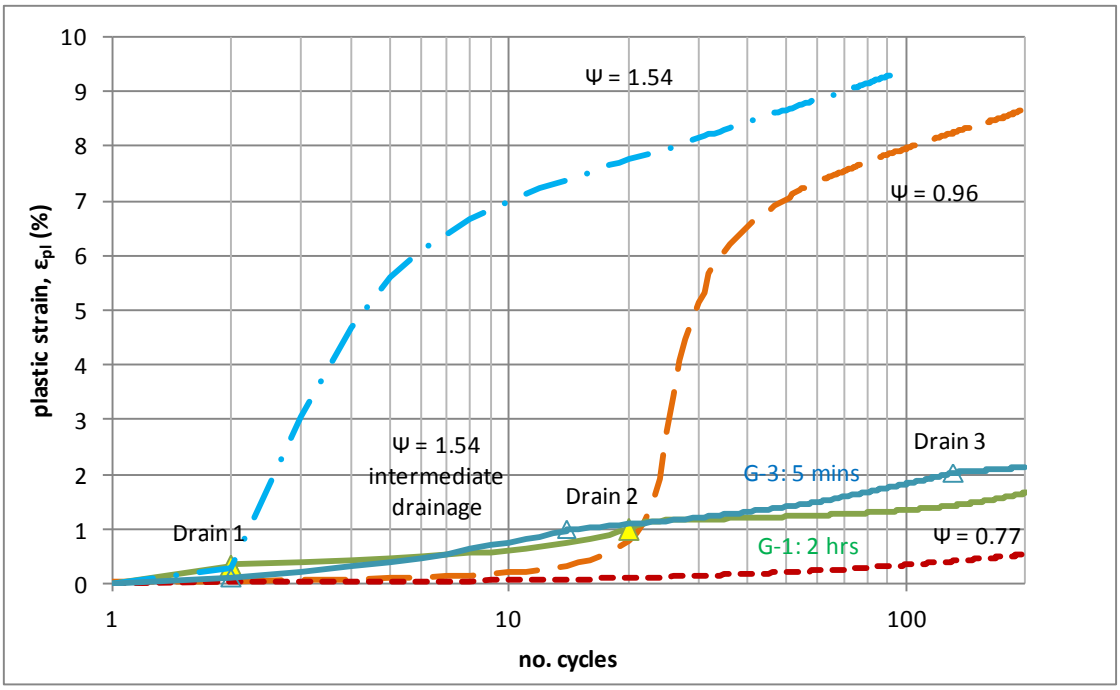

Figure 6.48: Stabilising effect of rest periods with drainage (solid lines, c.f. undrained tests, dashed lines). Timing of drainage periods is indicated by triangles – solid for 2 hour duration (G-1, ε_{v1} = 2.1%) and open for 5 minutes duration (G-3, ε_{v1} = 3.6%).

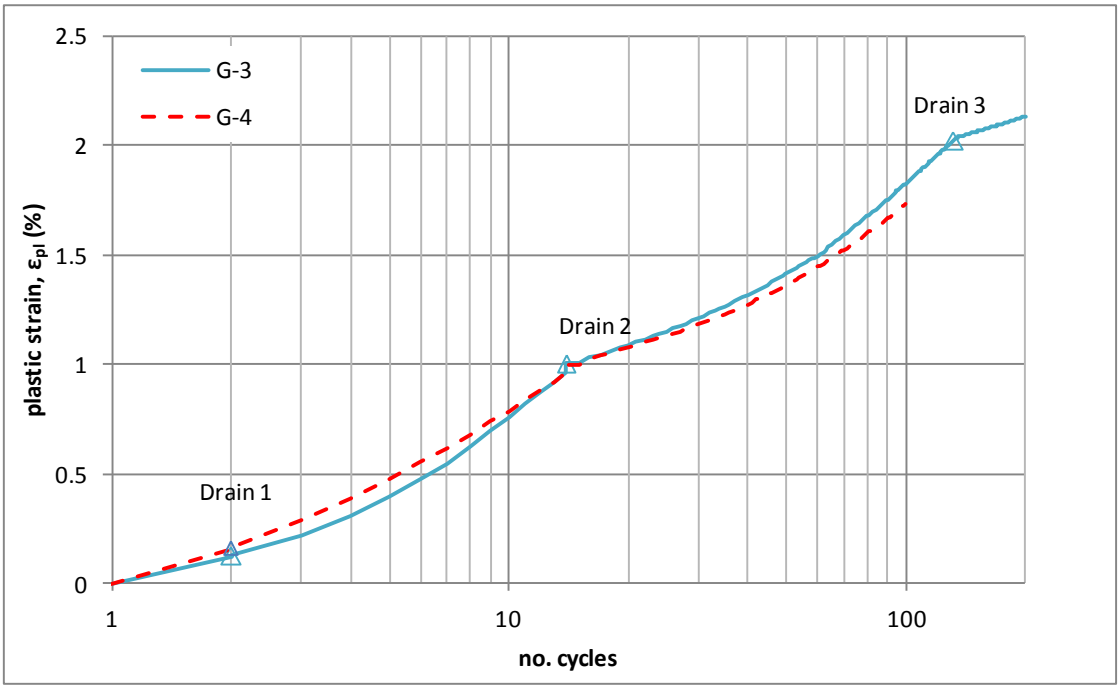

Figure 6.49: Similar strain accumulation in tests G-3 and G-4 (Ψ = 1.54 with 5 minute drainage periods, ε_{v1} = 3.6% and 3.0% respectively) suggesting sample disturbance as cause of stabilisation is unlikely.

During the later stages of cyclic testing, strain in G-3 and G-4 (5 minute drainage intervals) accumulates much faster than G-1 (2 hours). This suggests dissipation of pore pressures becomes increasingly important as strains increase; as discussed in Chapters 3.2.1 and 3.3.2, the large-strain regime is expected to be dominated by changes in effective stress rather than initial micro-fabric, as the soil becomes increasingly re-structured. The influence of different drainage durations is shown in Figure 6.50; the first short duration period (G-3) makes little difference to subsequent pore pressure accumulation as a function of strain, whereas for the longer duration (G-1) the relationship is fundamentally altered.

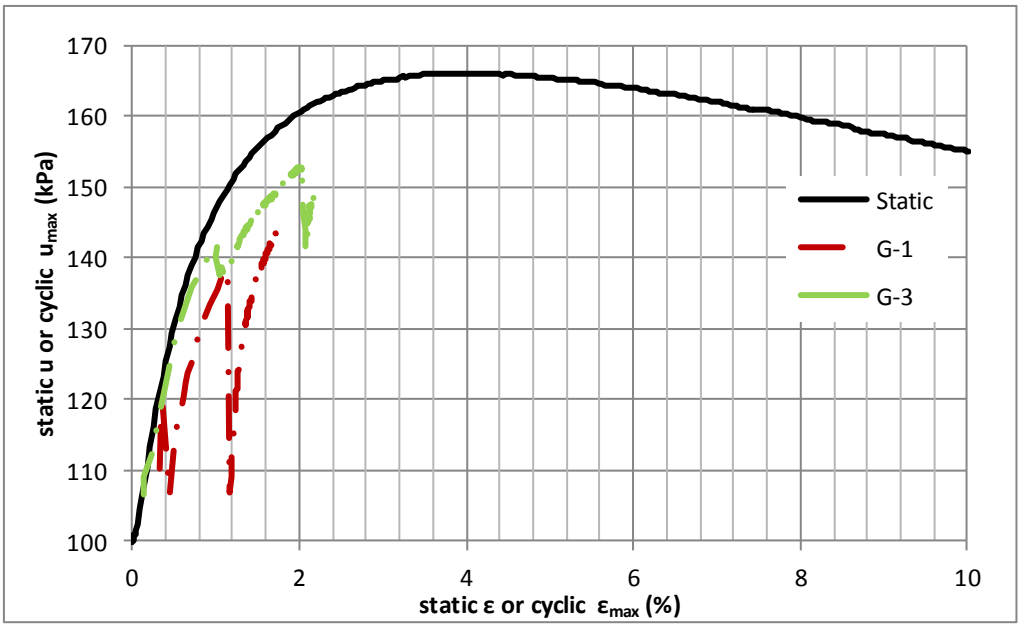

Figure 6.50: Development of pore water pressure with cyclic strains during tests with drainage rest intervals (2 hours for G-1; 5 minutes for G-3).

As test G-3 progresses, the larger pore pressures result in greater dissipation and volume change (Table 6.3). Comparing tests G-3 and G-4, volume change after the first cycle appears to be very sensitive to strain; as these strains are approaching ε_{tl}, rapid

divergence in terms of soil skeleton contraction is expected. Close agreement between volume change results at the second interval (1% strain) indicates the observed initial divergence is likely to be primarily influenced by differences in first cycle strain. Considering differences in strain accumulation in Figure 6.49 and volume change in Table 6.3, short drainage durations appear most effective at medium strains; as strains increase, larger excess pore pressures and greater consequent consolidation volume changes become increasingly beneficial.

Table 6.3: Volume change during drainage intervals in series G tests with Ψ = 1.54 cyclic load

	Volume change during drainage interval (ml)			Cumulative strain at start of interval (%)		
Test (drainage duration)	Interval 1	Interval 2	Interval 3	Interval 1	Interval 2	Interval 3
G-1 (2 hours)	1.68	2.94	-	0.36	1.11	-
G-3 (5 minutes)	0.11	0.71	1.23	0.12	1.00	2.03
G-4 (5 minutes)	0.59	0.75	-	0.16	1.00	-

During the first drainage interval in test G-1 (after the first cycle, with a strain of 0.32%), excess pore pressures were observed to initially rise from 10kPa, to a peak of 21kPa after 4 minutes, before dropping. This may be as a result of the base pore pressure transducer lagging behind the sample centre (an effect implied by pore pressure accumulation in Figure 6.25) combined with the impermeable base boundary condition. Alternatively it could indicate ongoing soil skeleton contraction initiated by the first cycle, similar to that seen in test E-2 (Figure 6.43). As rapid relaxation during liquefaction continued after the final cycle in test E-2, a similar effect (i.e. initially rapid strain under maintained load) should be expected if the first cycle of G-1 had initiated

a collapse. However the total strain over the first drainage period was 0.05%, suggesting that either no collapse was initiated or that it was quickly halted by the volume change.

6.6.2. Strength and stiffness improvement: medium-strain loading

By reducing plastic strains, a stiffer response is achieved in tests G-1, G-3 and G-4. Similar stiffness is only achieved after liquefaction in undrained tests of similar load magnitude, or is associated with stable cyclic load (Figure 6.51). By preventing micro-structural collapse, drainage intervals maintain stability and keep cyclic strains and corresponding stiffness to medium-strain levels.

Post-cyclic monotonic shear suggests improvements from drainage during tests G-1, G-3 and G-4 are primarily medium-strain and related to re-structuring rather than noticeably increased density; at large strains there is little difference between the ultimate strength of these tests and post-cyclic tests with no intermediate drainage (Figure 6.52). The principal difference between the post-cyclic tests appears to be the Δq at which stress-strain curve reaches a constant, low gradient; for $\Psi = 0.77$ (20kPa) this is 27kPa whilst for $\Psi = 1.54$ (40kPa) it increases to 43-46kPa. As was implied by Figure 6.42, cyclic load conditions the soil to resist the maximum load level with significantly reduced plasticity, implying a preferentially aligned particle contact network within the secondary plasticity ($q < q_{max}$) domain; the effect of intermediate drainage in this case is primarily to allow the soil to sustain higher cyclic loads without liquefying.

Volume change and pore pressure dissipation during consolidation can be compared to the K_0-compression line. u_e is estimated from the base transducer readings assuming a sine curve profile (see Chapter 4.2.1.5). For test G-1, as residual pore water pressures at the end of drainage intervals are low (2kPa); spatial variation assumptions make little difference to the analysis. For test G-3 this assumption has more influence on the analysis. The short interval duration also means the initial, unknown spatial pressure distribution in the sample is more important. However, as base pore pressures are observed to start to reduce before the 5 minute drainage periods end, the same assumption of a sine curve profile is thought to be sufficiently representative as internal pressure equalisation and flow towards the top cap should be established.

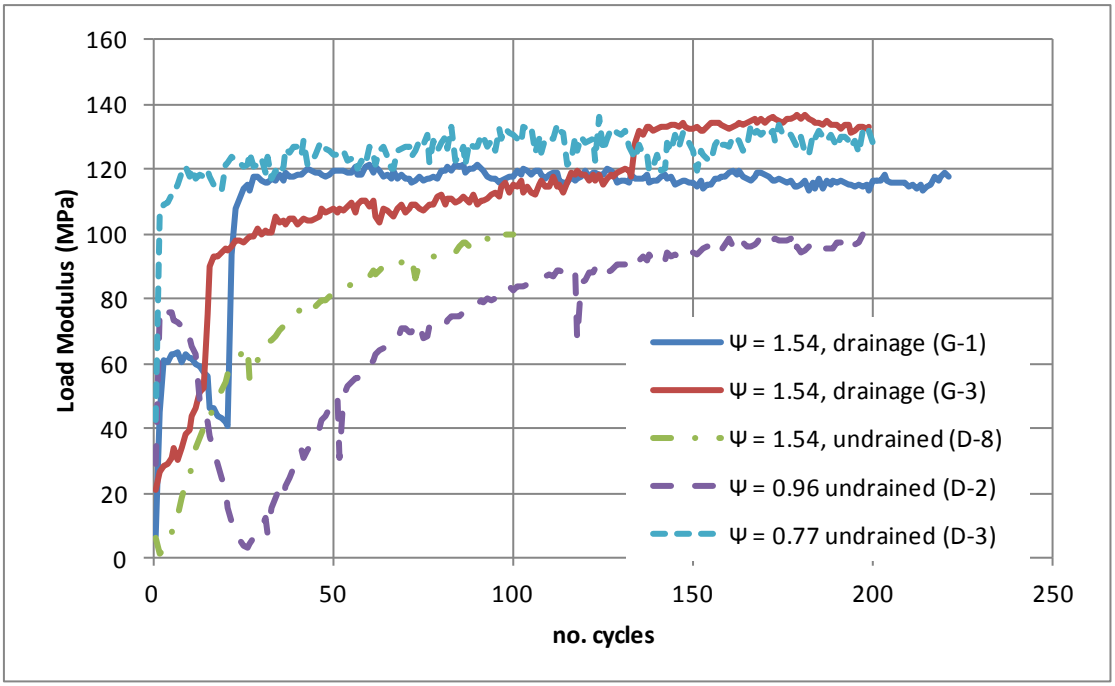

Figure 6.51: Development of cyclic load modulus results for undrained tests and tests with drainage rest periods. n.b. Ψ = 0.77 (D-3) is stable in undrained cyclic loading whilst other undrained tests liquefy and recover.

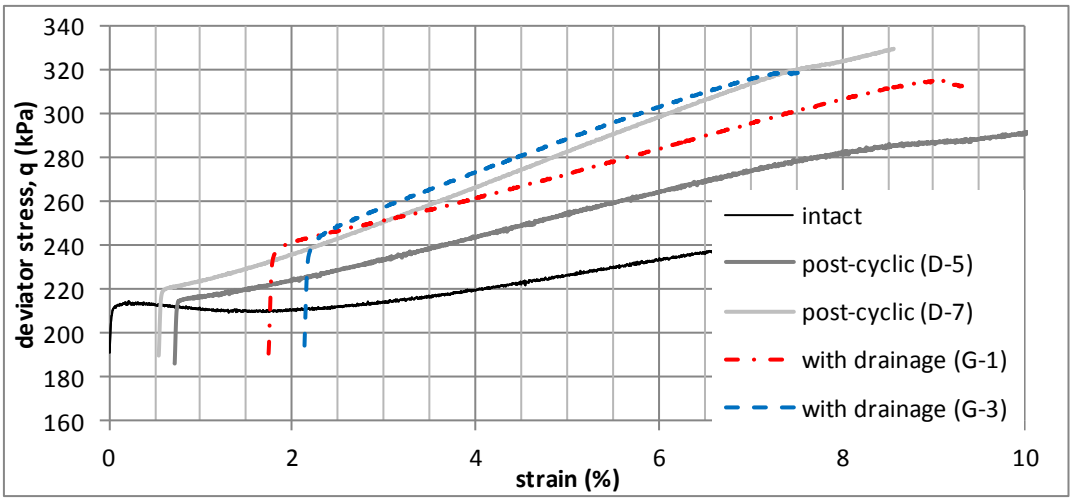

Figure 6.52: Post-cyclic monotonic shear for undrained sub-threshold cyclic load (Ψ = 0.77) and super-threshold cyclic load (Ψ = 1.54) with intermediate drainage, indicating minimal influence of consolidation on strength increase.

Figure 6.53 shows the volume change gradients of tests G-1 and G-3 are shallower than that of the K_0 compression line (mean gradients of 51% and 23% of the K_0 line respectively), implying a partial but not full rearrangement of the structure and a greater micro-structural disruption than static overconsolidation (swell-back gradient is 13% of the K_0 line). As test G-3 progresses and excess pore water pressures build up, the volume change gradient also becomes steeper, implying the higher pore pressures permit greater re-structuring. In the context of the K_0 line, it is apparent that volume changes during test G-1 and G-3 are small. The equivalent *p'* at the final water content is 245kPa and 225kPa respectively, which explains why ultimate strength is not noticeably increased; increased brittleness from induced overconsolidation is likely to counteract any strength improvement from densification.

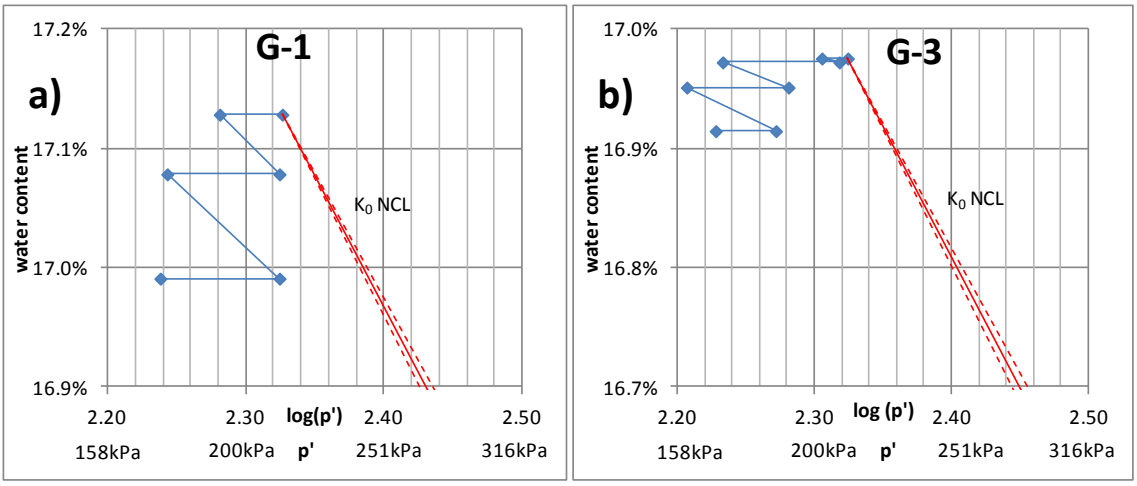

Figure 6.53: Compression characteristics of intermediate drainage during Ψ = 1.54 tests, with 2 hour drainage intervals (G-1, a) and 5 minute drainage intervals (G-3, b). A projection of the gradient of the mean K_0-NCL, with upper and lower bounds as stated in Section 6.1.1., is provided for comparison.

6.6.3. Strength and stiffness improvement: large-strain loading

Test G-2 includes 2 hour drainage intervals but also applies incrementally increasing loads. The first drainage interval is effective at preventing liquefaction under Ψ = 1.54 cyclic load, however when the load is increased to Ψ = 2.11 (starting from a cumulative strain of 0.35%) large strains and liquefaction (i.e. increasing $\Delta\varepsilon_{pl}$) are apparent. This implies some risk of meta-stability persists at these strains; the initially precarious micro-structure has not been completely rearranged into a stable form and larger cyclic stresses, which cause greater strains, are able to trigger liquefaction. The plastic strains experienced, compared to the first cycle of Series C Ψ = 1.92 tests (0.9%, c.f. 7.1% to 8.3%), are still a significant improvement but this highlights the need for caution when transporting increasingly heavy loads over liquefiable soil.

An improved resistance to plastic strain is apparent after each drainage interval, particularly following liquefaction under Ψ = 2.11 (Figure 6.54); a maximum cyclic stress of Ψ = 7.73 (i.e. 59% of consolidation σ'_1) is resisted, albeit after accumulation of

very large (8.7%) strain. As Ψ increases, drainage-related improvement reduces; this may be because the accumulated pore pressure and corresponding volume changes are smaller. The pore pressure response to load also becomes increasingly dilatant as Ψ increases, reaching a lower maximum in each stage (Figure 6.55). Whilst dilatancy in undrained conditions provides additional strength, subsequent consolidation of excess pore pressures is reduced. Dilatancy is likely to provide a limit to how much intermediate drainage intervals can increase strength – beyond a certain point, strain will weaken soil by the formation of shear planes. Dilatant pore pressures, particularly those localised to a shear band, cause swelling and weakening rather than strengthening during consolidation. Large-strain consolidation may improve resistance to dilatant failure; in Figure 6.56, the *q/p'* ratio after consolidation is able to increasingly exceed that of the monotonic tests. Unlike previous cyclic tests which reached large post-liquefaction strains, no shear banding was apparent during cyclic loading for test G-2.

Figure 6.53 indicates overconsolidation is accumulated in tests G-1 and G-3; drainage intervals partially counteract this but the relatively steep volume change gradient means some overconsolidation is retained. Following liquefaction in test G-2, large volume changes occur in the drainage interval (Figure 6.57), suggesting large-strain re-structuring; during this consolidation stage overconsolidation is maintained (the volume change gradient is 95% of the K_0-NCL). As discussed in Chapter 3.5.1, this implies complete re-structuring; compression characteristics are like a freshly-deposited soil.

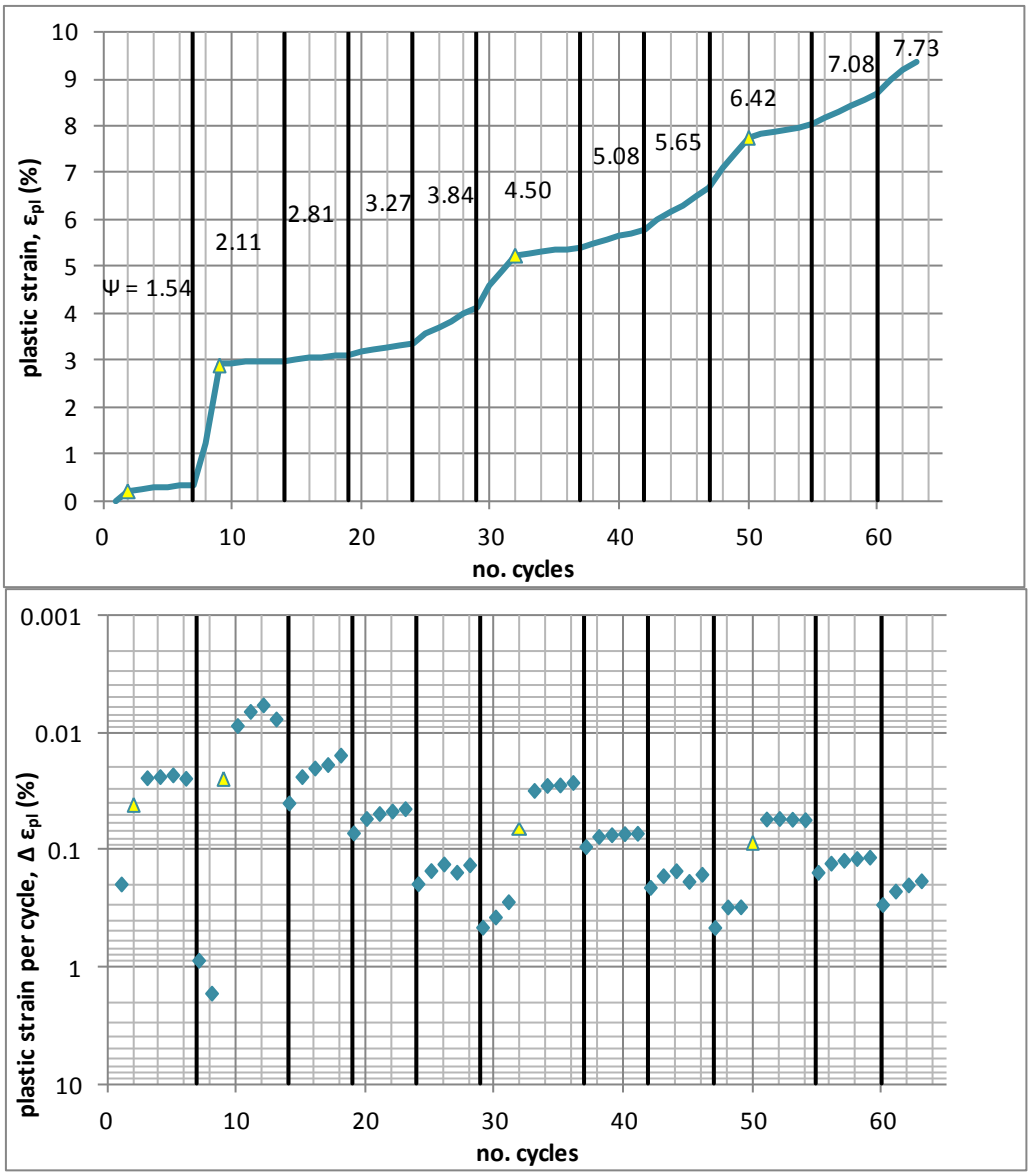

Figure 6.54: Strain accumulation in test G-2 with incrementally increasing cyclic load. Yellow triangles indicate 2-hour drainage intervals before that load cycle; after each drainage increment plastic strain accumulation is reduced.

For subsequent drainage intervals, the volume change gradient reduces. Strain increments between intervals are similar (2% to 3%) so it is clear that volume change gradient depends on factors other than strain. The actual relationship is likely to be complex and depend upon fabric and stress history, however from Figure 6.57 it

appears pore water pressure, indicating skeleton contraction, may be a good descriptor.

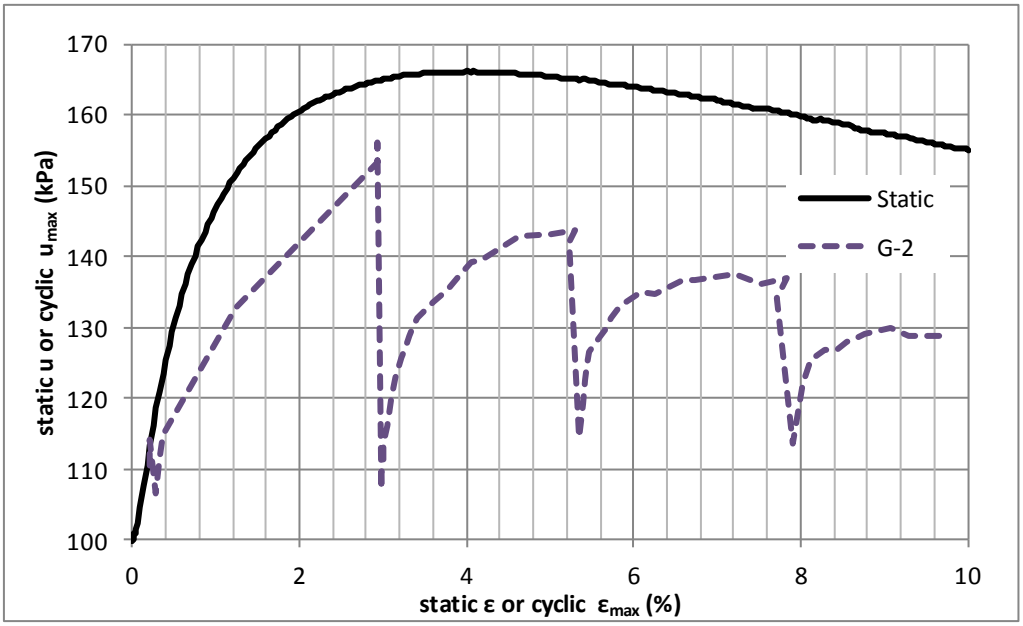

Figure 6.55: Pore pressure accumulation under cyclic load and dissipation during drainage for test G-2.

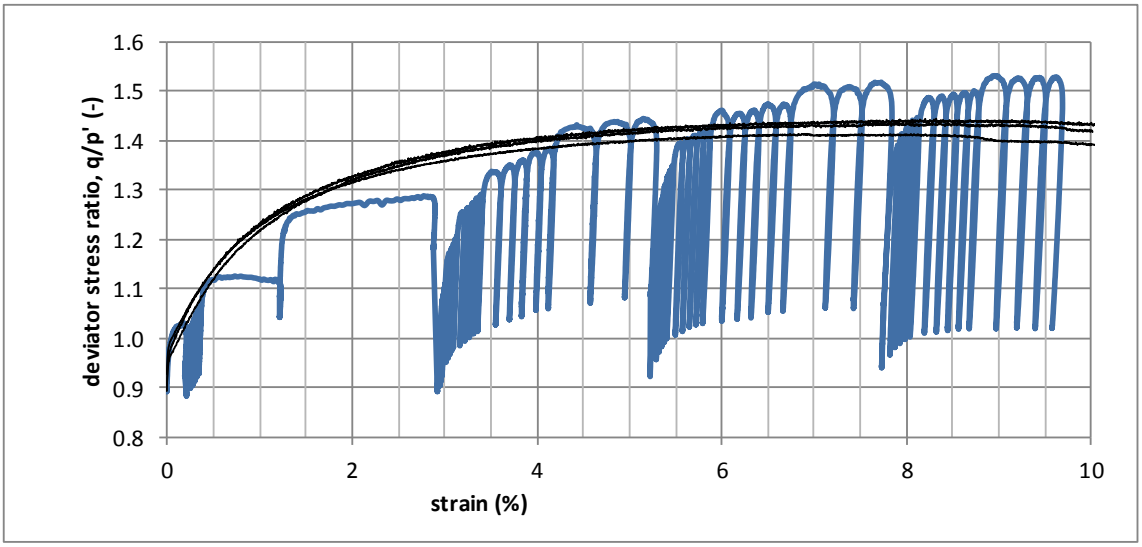

Figure 6.56: Increasing stress ratio under incrementally increasing cyclic stresses in test G-2 – cyclic *q/p'* exceeds the maximum experienced during monotonic shear.

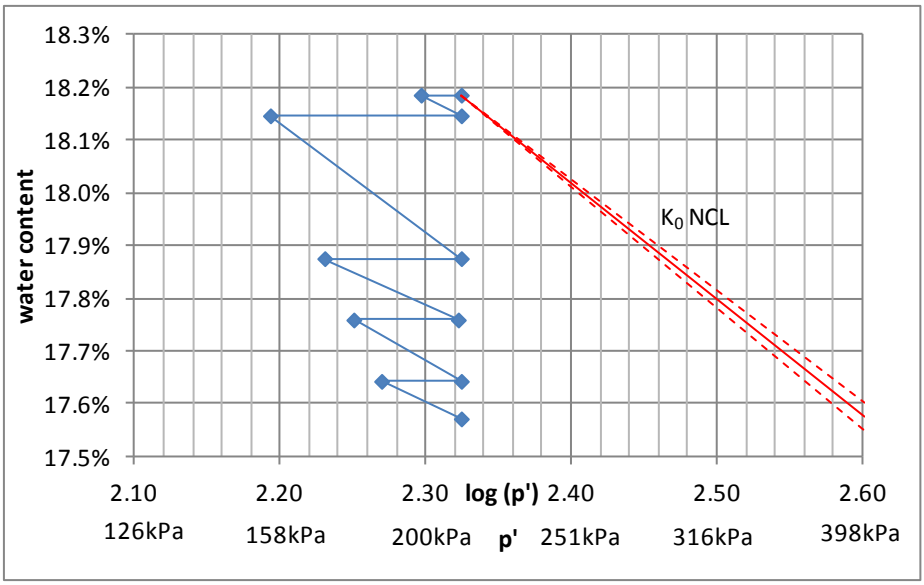

Figure 6.57: Compression characteristics of intermediate drainage during test G-2 (incrementally increasing cyclic load). Final equivalent p' on K_0-NCL is 400kPa.

The change in water content for test G-2 is much more significant and the equivalent *p'* on the K_0 compression line is much higher than tests G-1 and G-3; accordingly a higher ultimate strength is reached (Figure 6.58). The effect of intermediate drainage in reducing brittleness is apparent: G-2 fails at larger strains than the intact monotonic tests, as opposed to post-cyclic undrained tests in Figure 6.39 which fail at or below the monotonic failure strain.

There is a close correspondence between the cyclic q_{max} and ultimate post-cyclic q in test G-2 (both 385kPa, equivalent to Ψ = 7.50), although unlike tests G-1 and G-3 the stiffness begins to reduce dramatically above q = 330kPa (Ψ = 4.23), i.e. well below the cyclic q_{max}. The lower numbers of cycles at maximum load in G-2 may mean lesser conditioning was achieved, or alternatively the more damaging dilatant response under the larger loads may mean similar conditioning cannot be achieved.

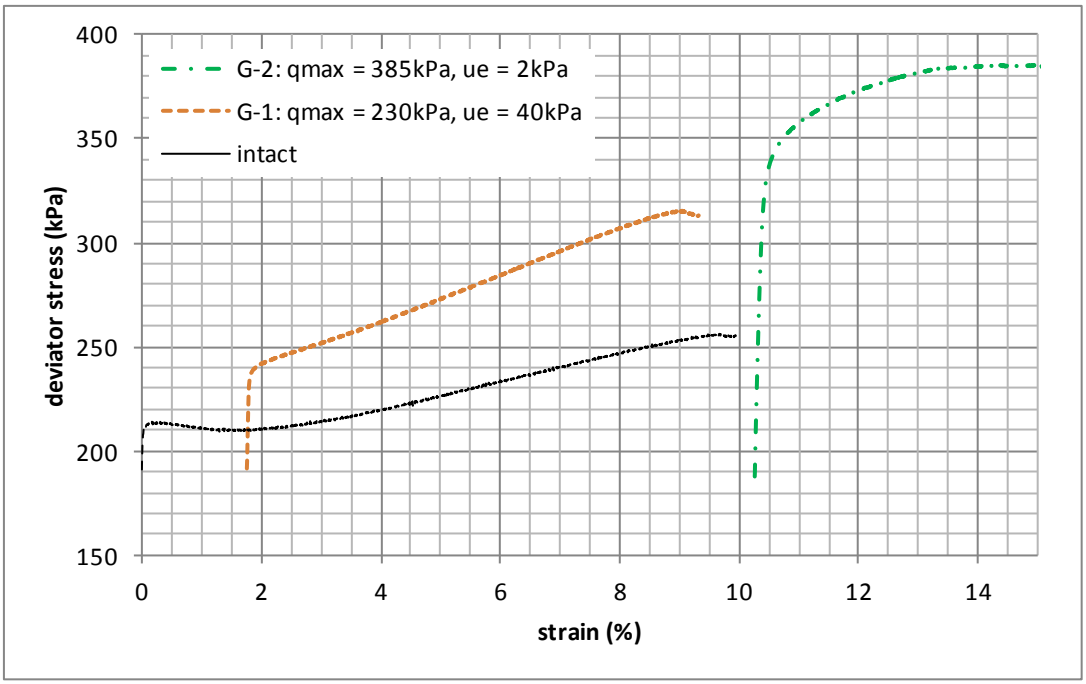

Figure 6.58: Improvement in post-cyclic strength for tests with intermediate drainage subject to partial re-structuring (G-1) and full post-liquefaction re-structuring (G-2).

The cause of liquefaction in test G-2 under the Ψ = 2.11 cyclic loading is unclear. It is possible the micro-structure was rearranged sufficiently to remain stable under loads already experienced but still retained sufficient initial fabric to liquefy under higher loads. If this is the case, a similar combination of gradual straining in the stable regime and dissipation of excess pore pressures may be effective in averting liquefaction. In test G-4, ε_{pl} = 1.74% from 100no. cycles of Ψ = 1.54 (Figure 6.49) was found to provide stabilisation under increasing cyclic loads (Figure 6.59). Applying stable cyclic loading until plastic strain is beyond that associated with liquefaction may be effective in completely averting liquefaction under any stress level. With an incrementally increasing load sequence, caution and gradual increments of load are thus advised whilst strains remain within the range associated with liquefaction. Rest periods for

consolidation both before and after transit of a new maximum load are also considered sensible to minimise liquefaction risk.

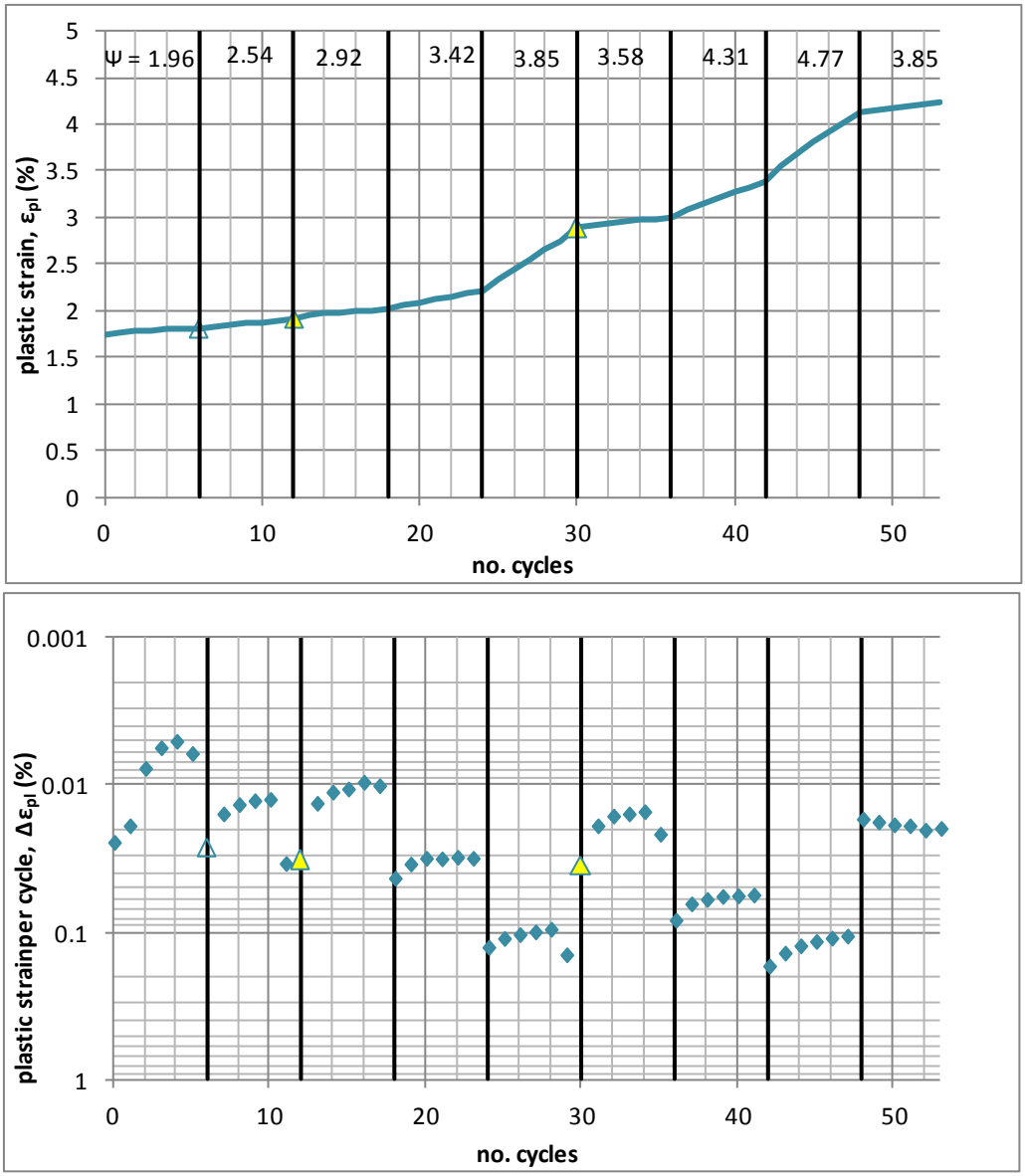

Figure 6.59: Strain accumulation in test G-4 with incrementally increasing cyclic load. Yellow triangles indicate 2-hour drainage intervals before that load cycle whilst hollow triangles indicate a 5 minute drainage interval.

As test G-2 developed very large strains from liquefaction, it is unclear whether the strength gain observed arises primarily from barrelling of the sample and end/membrane restraint. Test G-4 results (Figure 6.59) seem to indicate barrelling

effects have only a small influence: similar cyclic strengthening is observed (Ψ = 4.77, 36% of consolidation σ'_1) with much smaller strains (up to 4.25%). In post-cyclic monotonic shear, an improvement in strength is also apparent, although as the sample experienced a lower q_{max} (312kPa c.f. 386kPa for G-2) and smaller volume changes (0.2% change in water content c.f. 0.6% for G-2) a lower ultimate strength was reached (in both cases, corresponding closely with cyclic q_{max}; Figure 6.60). Unlike test G-2, which was subject to a 2-hour drainage interval before monotonic shear, test G-4 was subject to monotonic shear directly after cyclic stages. The greater proximity to the failure line in effective stress space, similarly to tests G-1 and G-3, is expected to be responsible for the more brittle failure.

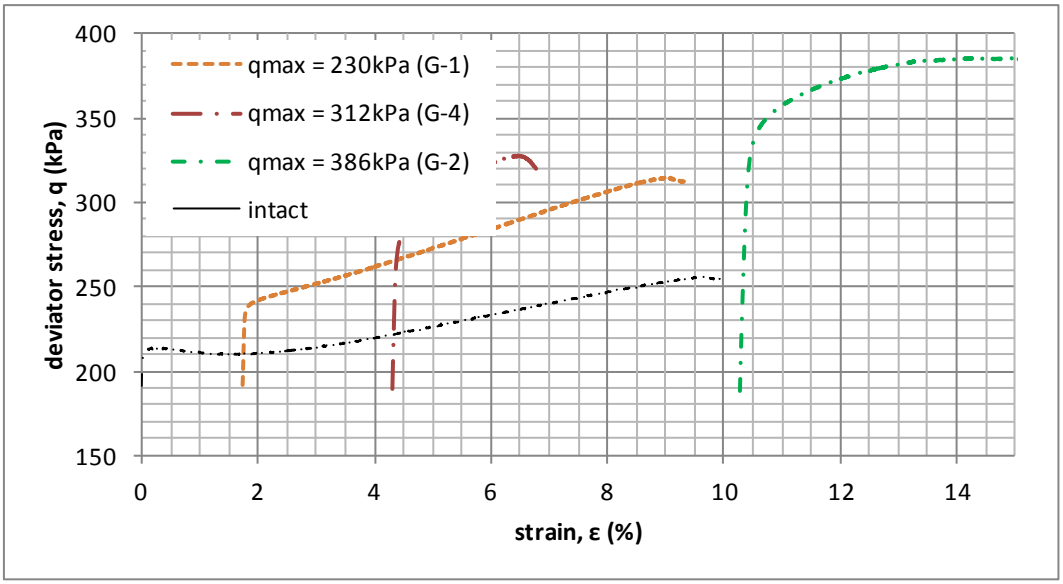

Figure 6.60: Improvement in post-cyclic strength for samples with intermediate drainage intervals and varying degrees of cyclic strain

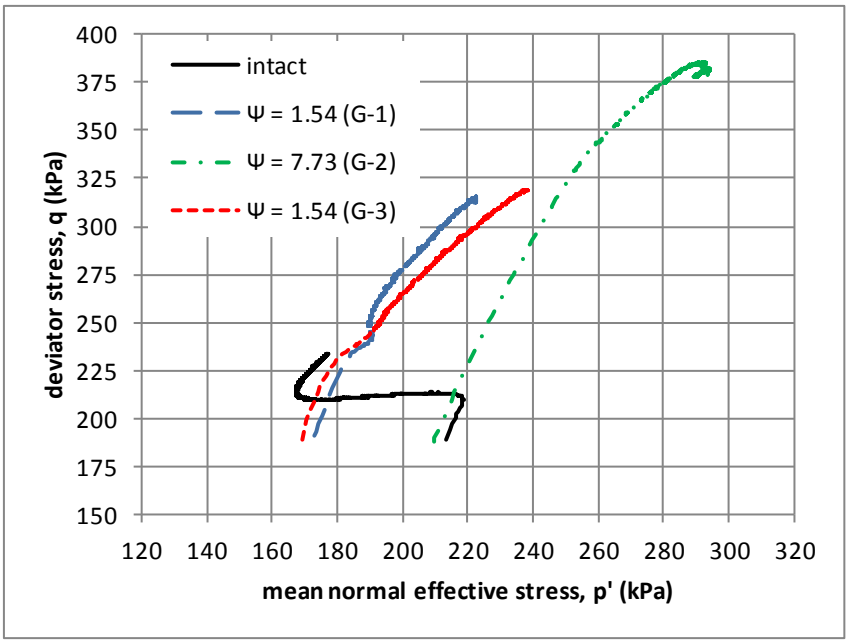

Figure 6.61: Effective stress paths for tests G-1 and G-3 (tested with full residual PWP) compared to test G-2 (tested after a 2-hour drainage interval). All tests are dilatant, test G-2 reaches the failure line at higher values of *q*. n.b. effective stress path for test G-4 is not available due to pressure transducer problems.

Test G-5, which used lubricated ends to reduce restraint, was similarly able to resist cyclic stresses of $\Psi = 5.77$ (44% of consolidation σ'_1) through incrementally increasing load and including drainage intervals, with a final strain of 4.3% (Figure 6.62). This further suggests the effects of end restraint on observed strengthening are low; it is reasonable to assume cyclic load and drainage intervals are the primary cause of observed strengthening. Furthermore, significant strength improvements achieved through cyclic loading and drainage intervals do not necessarily need very large strains to mobilise: if liquefaction is avoided through appropriate caution, strengthening should be achievable with manageable cumulative strains.

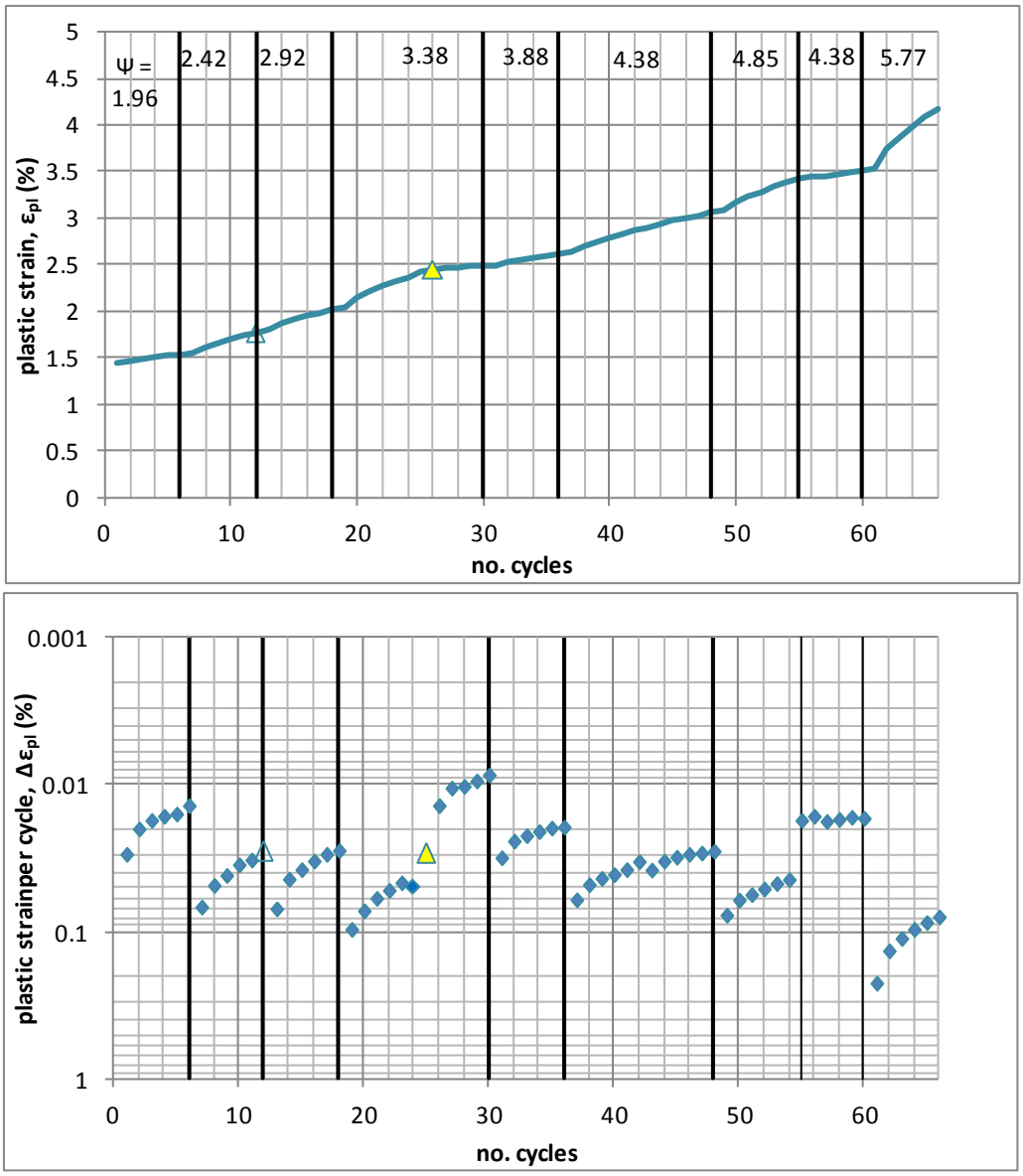

Figure 6.62: Strain accumulation in test G-5 (lubricated top), indicating observed strengthening under cyclic load is not significantly affected by end restraint. Yellow triangles indicate 2-hour drainage intervals before that load cycle, hollow triangles indicate a 5 minute drainage interval.

6.6.4. Changes to strain thresholds

Similarly to Figure 6.42, monotonic stages following cyclic loading with intermediate drainage show an increased constant-stiffness regime (normally associated with elastic small-strain behaviour). For higher q_{max}, this regime extends to even greater strains (Figure 6.63). As previously discussed, this suggests conditioning of the soil to resist a

previously experienced load level with reduced plasticity. If the elastic strain range increases until it matches $\Delta\varepsilon_{cyc}$ (which reduces gradually), this preferential restructuring provides a credible mechanism for shakedown.

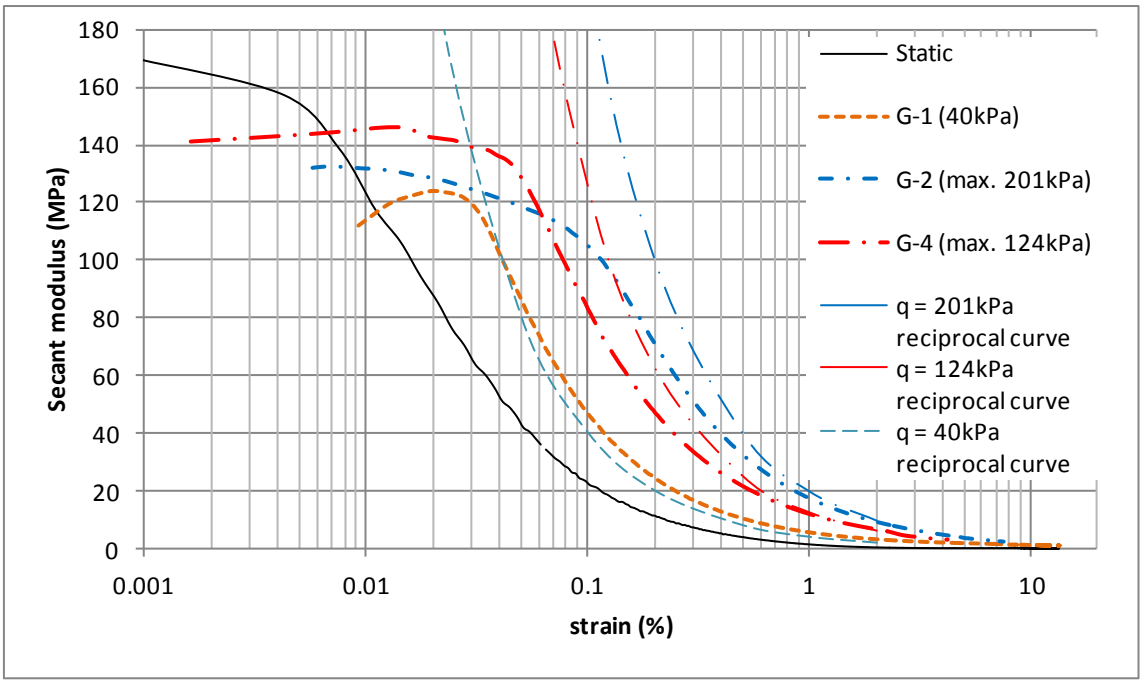

Figure 6.63: Secant modulus degradation curves of post-cyclic static shear stages of series G tests showing greatly increased regions of constant, high stiffness and improvement extending to the large-strain regime.

A series of volume change threshold tests (as described in Section 6.3.1.) were included at various points between incrementally increasing cyclic stages of test G-4 (Table 6.4) and after drainage intervals. These tests investigated whether changes in secant modulus degradation corresponded with increased elastic behaviour and the effect of drainage intervals. A volume change threshold test was not performed directly after consolidation due to concerns of disrupting the precarious initial state.

From Figure 6.64 an increase in the elastic strain range is clear: compared to the intact state (Figure 6.20), which found ε_{tv} = 0.01% to 0.02%, the first test finds ε_{tv} in the range

0.02% to 0.05%. As the test progresses, the plasticity implied by relaxation during the 0.05% cyclic strain stage reduces, until in test 4 the response is almost completely elastic. This reinforces the assertion that cyclic load extends the elastic strain range. Figure 6.64 also indicates increasing cyclic stress levels, rather than the drainage intervals, are responsible for this effect: relaxation in tests 2 and 3 (before and after a drainage interval) is practically the same, whilst it varies significantly between tests 3 and 4 (increasing cyclic load applied but no drainage interval). Despite drainage intervals allowing densification, there are only minor changes to small-strain stiffness throughout this test. Consolidation appears to primarily influence the stress state and large-strain behaviour.

Table 6.4: Timing of volume change threshold tests within the incrementally increasing cyclic stress stages in test G-4.

V.C. Threshold test no.	Preceding cyclic Ψ	After drainage interval?
1	2.54	N
2	1st 3.85	N
3	1st 3.85	Y
4	2nd 3.85 (final)	N/A

A comparison of stiffness modulus from the different test stages (Figure 6.65) further illustrates this tendency of extending the small and very small-strain ranges. By connecting the results from volume change threshold test 1 and Ψ = 2.54, or test 4 and subsequent Ψ =3.58-4.77 cyclic stages, the translation of the modulus degradation curve towards higher strain is clear, particularly the strain at which modulus degradation starts. The cyclic Load Modulus results (which use the actual $\Delta q_{\varepsilon,max}$ and so account for creep post-peak stress) also provide a better fit to the post-cyclic secant modulus curve than the constant stress curve in Figure 6.63.

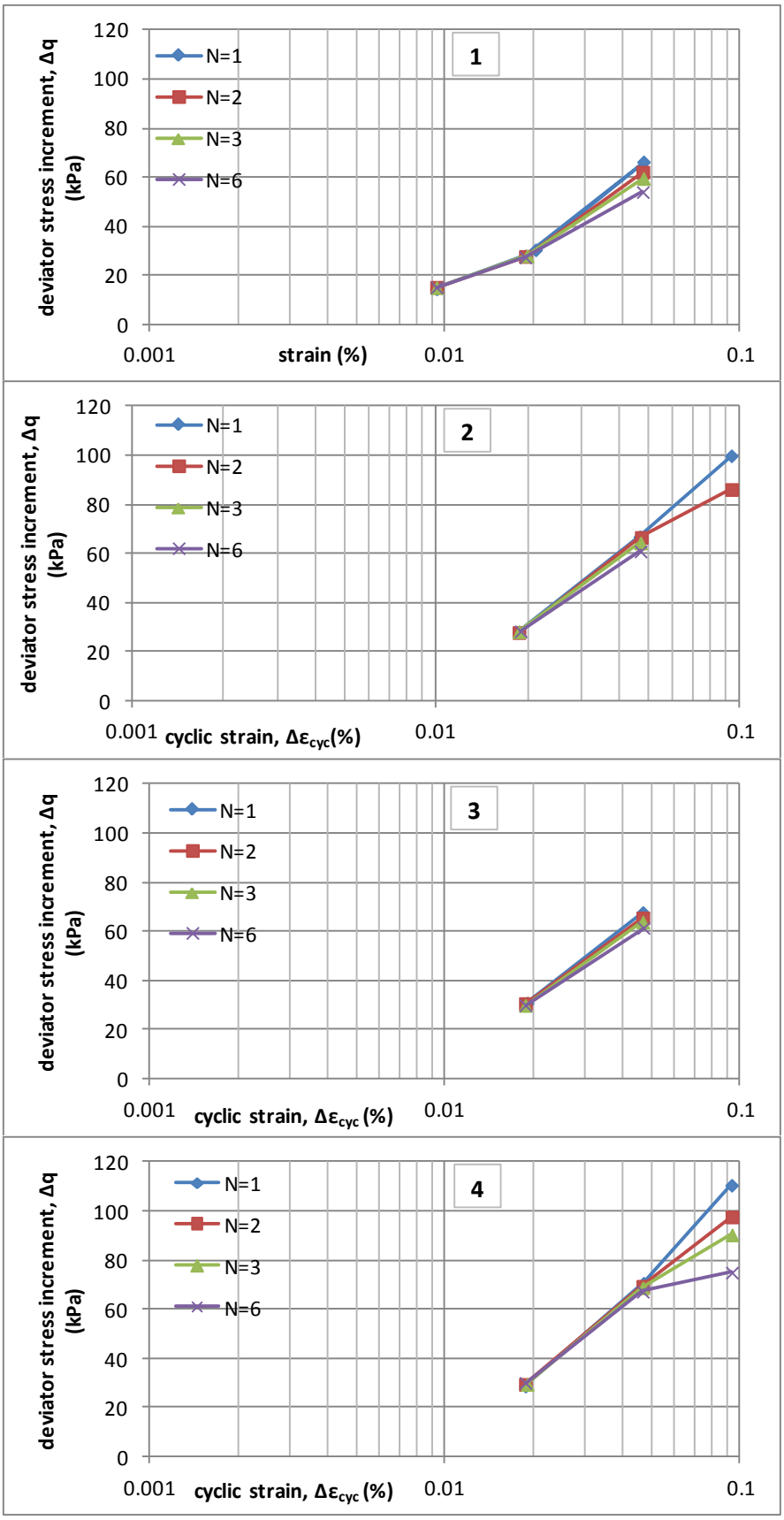

Figure 6.64: Relaxation of stresses in volume change threshold tests throughout test G-4 (interval timing described in Table 6.4)

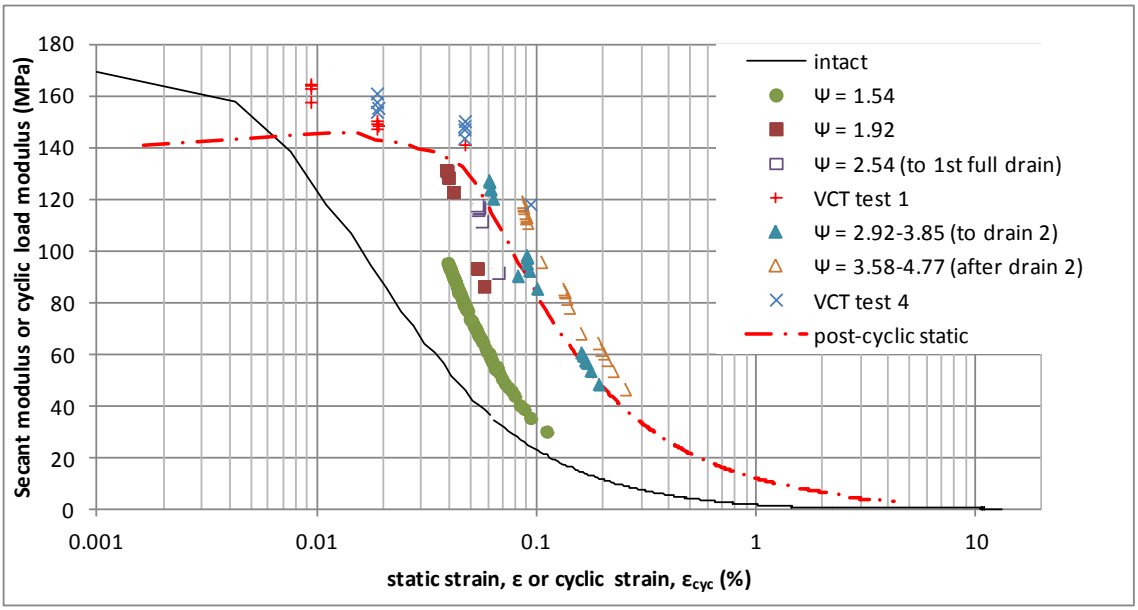

Figure 6.65: All strain-dependent stiffness modulus results for test G-4: cyclic load modulus, volume change threshold (VCT) tests and post-cyclic secant modulus.

Further investigation into how the modulus degradation curve is apparently conditioned over time could be useful for predicting when fully stable, resilient conditions under cyclic load are reached.

From these results, stiffness improvement and increased elasticity can be seen as a phenomenon principally dependent upon the magnitude of cyclic stresses and strains applied to the soil; in order to resist these increasing stresses in a stable manner, drainage intervals are required. The impact of drainage intervals following large-strain cyclic load is to increase the ultimate strength and also to reduce brittleness by reducing overconsolidation. The extent to which overconsolidation is reduced depends upon the nature of preceding loading; large cumulative pore pressures and liquefaction in particular are likely to result in greater densification but more retained overconsolidation. Maintaining stability through gradual increases in load and inclusion of rest periods is thus not only important in terms of minimising operational risks and

maintenance activity, but also in terms of future performance and risk of brittle shear banding failure. Test G-4 in particular demonstrates the feasibility of using sequenced traffic load and drainage intervals to dramatically increase the capacity of a heavy haul road subgrade whilst incurring only moderate plastic strains.

6.7. Control tests (English China Clay)

The majority of tests used the liquefiable Silt Mix soil to investigate how heavy haul traffic loads could initiate or avert liquefaction. To gain a more general understanding of how treatments which stabilised Silt Mix tests could apply to non-liquefiable soils, a small number of similar tests were performed on English China Clay. Index tests in Chapter 4.1.1 indicate English China Clay is a plastic clay soil, which is expected to strain-harden until a perfectly plastic critical state is reached.

Monotonic shear tests (at a strain rate of 0.47%/hr) indicate a general strain-hardening tendency, with a peak stress reached at 8 to 10% strain. As samples are anisotropically consolidated and the deviator stress increment to failure is small in relation to the consolidation deviator stress, results are highly sensitive to assumptions made on changes to area with strain. If the equivalent right cylinder method is assumed, as used for Silt Mix tests, the increasing area at large strains produces a slight loss of stress, coinciding with pore water pressure reaching a constant value. This implies a critical state is not reached but rather a strain-softening failure (Figure 6.66). If a constant cross-sectional area is assumed however, the peak deviator stress and pore water pressures coincide, and a perfectly plastic critical state is reached. It is unlikely the latter assumption is more representative than the former, as the clay samples are

close to saturation (B > 0.95) and unlikely to exhibit volume changes in undrained shear. As changes in area with strain are likely, even if they do not faithfully follow the equivalent right cylinder approximations, it is reasonable to describe the observed failure in monotonic clay tests as slightly strain-softening. In any case, behaviour is approximately plastic and contractant at failure with no shear bands observed in these tests, i.e. sufficiently different from the liquefiable Silt Mix which ultimately fails by dilatant shear banding. The ultimate stress, Δq = 17kPa, is therefore treated as the critical state strength for use in normalisation, i.e.:

Equation 6.2 $$\chi = \Delta q_{cyc} / \Delta q_c$$

Effective stress paths for the monotonic clay tests indicate a mean critical state line/failure line of q/p' = 0.87, equivalent to ϕ' = 22.3° (Figure 6.67). The higher consolidation stress (σ'_3 = 150kPa) was chosen for the remainder of tests, partly because the samples are less likely to retain any memory of overconsolidation at these higher pressures but also because the relatively small stress increments for the lower consolidation stresses mean load cell instrument error is relatively large.

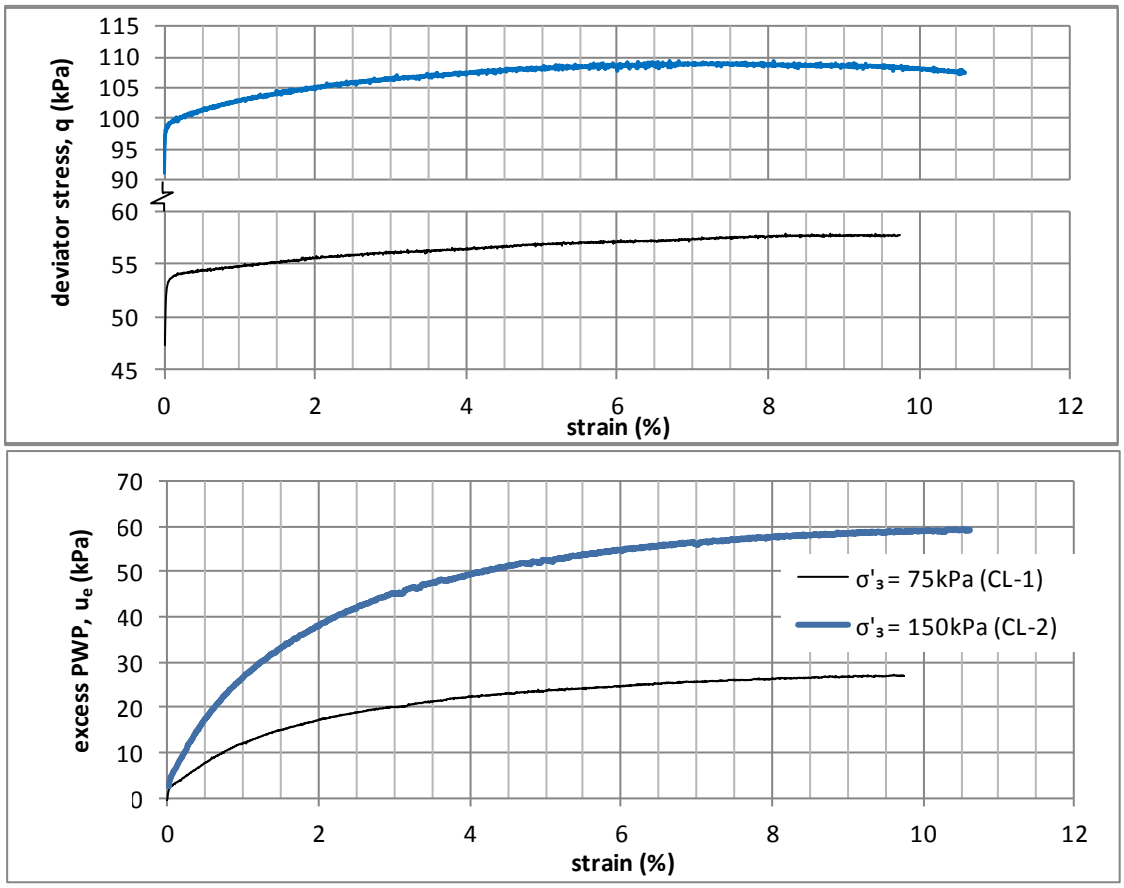

Figure 6.66: Monotonic shear response of anisotropically consolidated English China Clay at varying effective confining pressures.

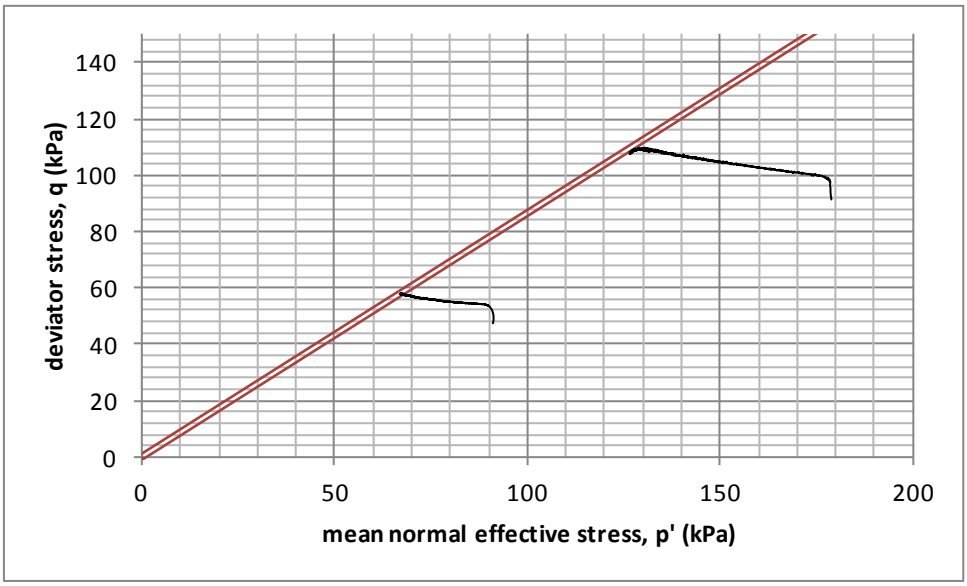

Figure 6.67: Effective stress paths for anisotropically normally consolidated English China Clay tests

Under cyclic load, the clay tests show a gradual accumulation of load in all cases (Figure 6.68). Even when loaded above Δq_c (χ = 1.18), strain rates only begin to accelerate after 6% strain, which corroborates the observation of slight strain-softening in monotonic tests. The ability of clays particularly to withstand fast, transient loading above the static strength is documented by Houlsby and Burd (1999) and is likely to be related to their more viscous behaviour; cyclic strains are much smaller as a proportion of monotonic strain (Table 6.5) than in the Silt Mix soil.

Table 6.5: Comparison of clay monotonic and cyclic strains in response to various stress levels.

***Δq* (kPa)**	***χ***	**monotonic *ε(%)***	**ε_{max} (%) (1st cycle @ 0.01Hz)**	***N* for ε_{max} > monotonic *ε***	**Mean strain rate (1st cycle) (%/hr^{-1})**
15	0.88	2.71	0.08	N/A	4.24
17	1.00	7.32	0.09	136	4.63
20	1.18	7.32 (peak)	0.19	113	9.91

As is extensively found in the literature (Chapter 3.1), the principal hazard for cyclically-loaded plastic clays appears to be gradual softening rather than sudden liquefaction. The divergence of these tests with relatively small differences in cyclic stress, and also the near-linear trend in strain accumulation, suggest all of these tests exceed the threshold stress in the conventional sense of runaway strains over large numbers of cycles. In the sense of temporary heavy haul road traffic however, the strains experienced may be manageable. In common with the Silt Mix cyclic tests, there is a reasonably strong agreement between the cyclic and static relationships between pore water pressures and strain (Figure 6.69). This is not a common phenomenon in the literature and so is not expected to be a general rule, but it may be widely applicable to a range of similar soils in an anisotropic stress state and subject

primarily to one-way cyclic loading. More research on a wider range of soils will be useful in determining necessary conditions for this behaviour to apply; a strong correlation between pore pressures and strain could be attractive in using pore pressure monitoring data to estimate strains, and vice versa.

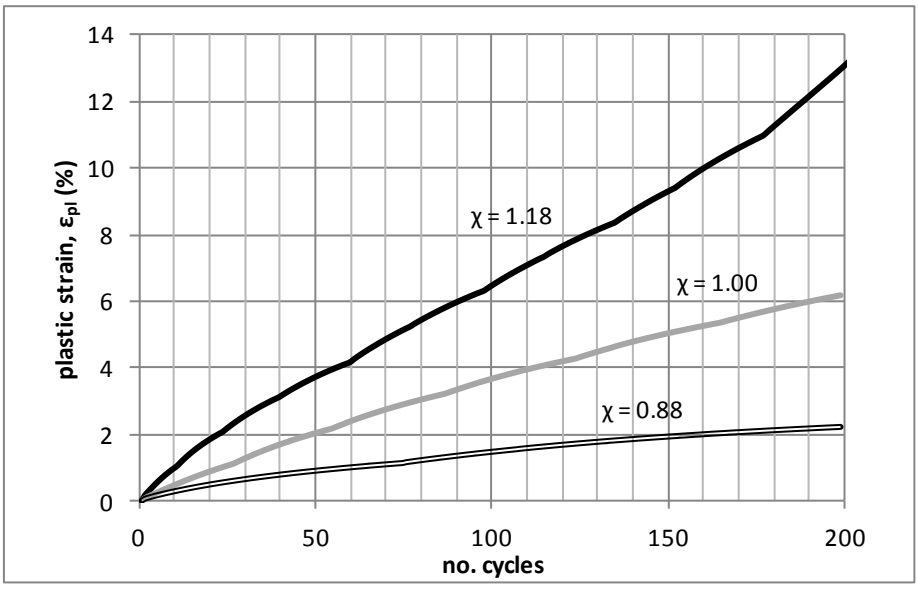

Figure 6.68: Cyclic strain accumulation for English China Clay tests subject to varying cyclic stresses.

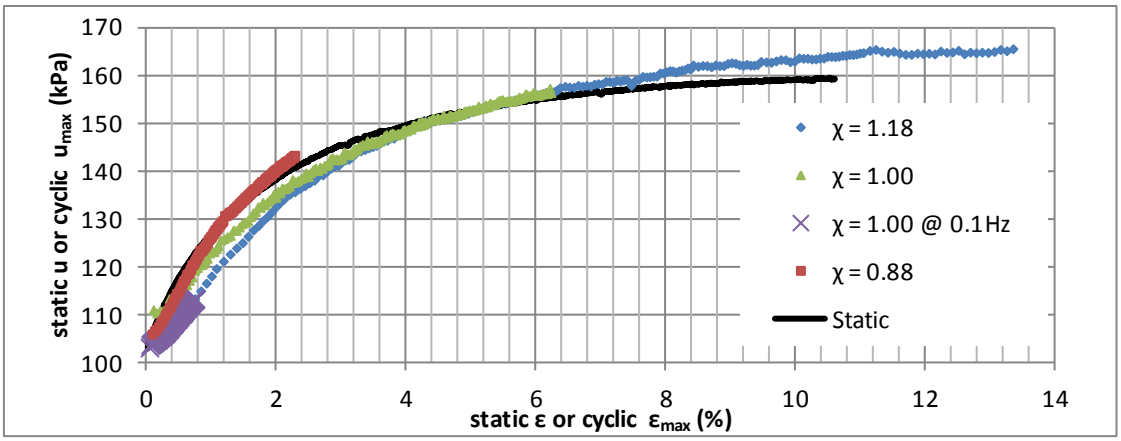

Figure 6.69: Pore pressure accumulation as a function of strain for cyclic and static English China Clay tests.

Unlike the remediation of liquefiable Silt Mix soil, cyclic loading of English China Clay is only observed to reduce the post-cyclic strength, with the strength reduction increasing as cumulative strain increases (Figure 6.70). This is in agreement with the vast majority of studies on clays (Chapter 3.1.2), although it is possible that under lower cyclic stresses and smaller cumulative cyclic strains, a small strengthening effect may be observed, as for Brown et al. (1977). This further corroborates the assertion that strengthening from stable undrained cyclic loading in the Silt Mix soil is as a result of rearrangement of the initially precarious fabric: the clay samples have no such fabric and so obtain no such benefit. Instead, the most important factor is the accumulation of pore water pressures, which tend to induce overconsolidation. Effective stress paths from post-cyclic monotonic tests show this effect (Figure 6.71), as does the brittle shear banding failure observed in test CL-5.

In the case of test CL-4 there may be an improvement in effective strength parameters, as has been observed by Brown et al. (1977). Further tests at lower cyclic stresses will be necessary to determine whether this is significant or simply a function of inherent variation, and whether an optimal strain or stress range for undrained cyclic improvement, as seen for the Silt Mix tests, also exists for clays.

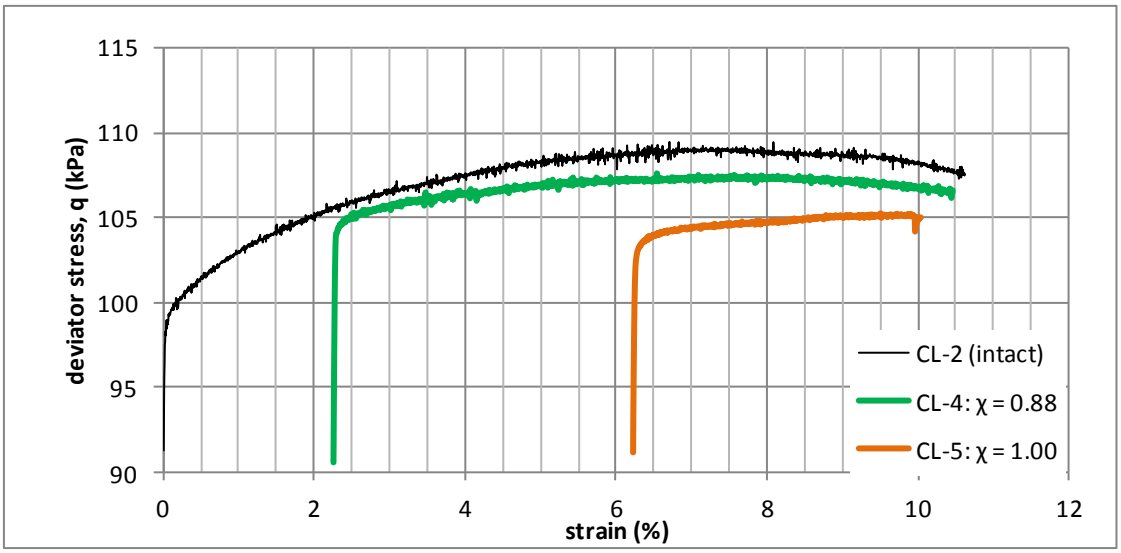

Figure 6.70: Post-cyclic monotonic shear tests indicating strength reduction for English China Clay tests.

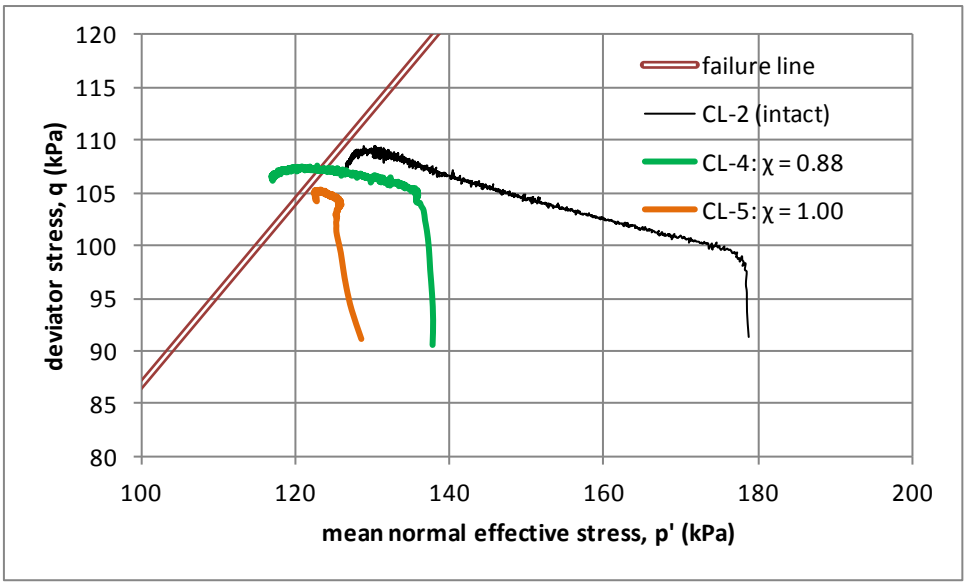

Figure 6.71: Effective stress paths for post-cyclic monotonic tests, indicating increasingly overconsolidated-like behaviour with increasing cyclic excess pore pressure.

Similarly to the Silt Mix tests, cyclic loading tends to increase the strain-dependent stiffness, possibly with an increased elastic strain range as cycling progresses (although no volume change threshold tests were performed to explicitly verify this). The post-cyclic monotonic secant modulus is translated towards the cyclic Load Modulus curve,

similarly to Silt Mix tests, although for clays the match between the two is less clear (Figure 6.72). Clays may be less amenable than silts to conditioning under load due to their plasticity; greater strains may be necessary to cause the same micro-structural rearrangement effects, similar to their response to large-strain consolidation improvement noted by Wang et al. (2015b). Furthermore, clay stiffness is more sensitive to loading rate and so should be reduced in slow monotonic tests.

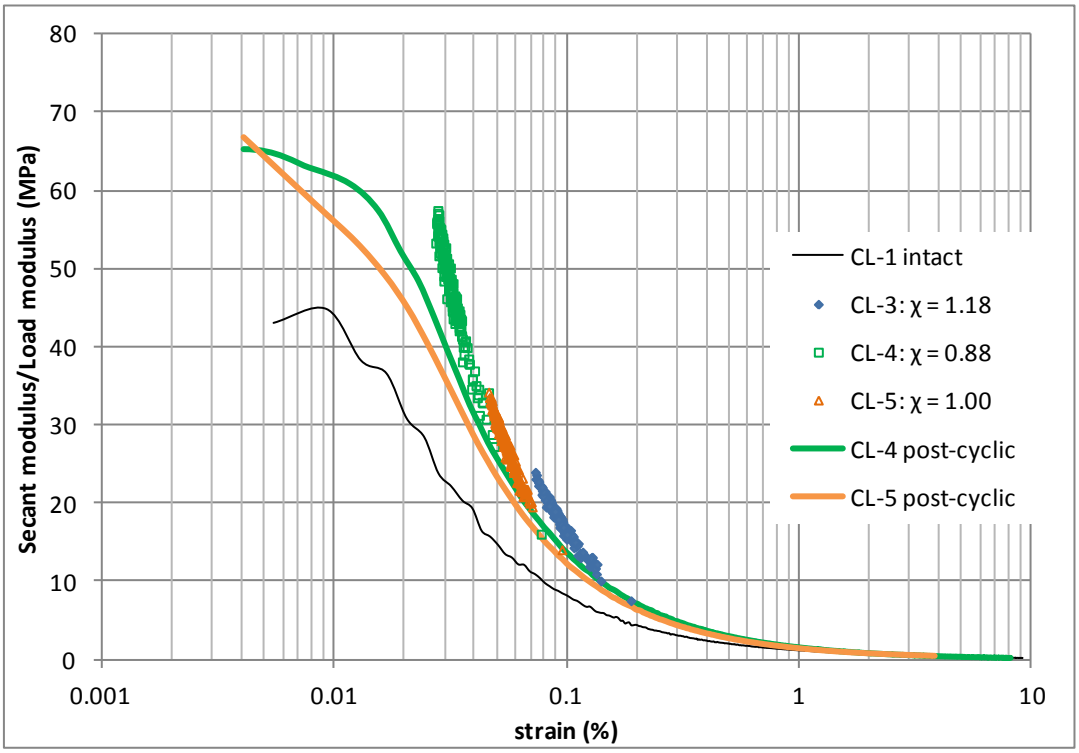

Figure 6.72: Cyclic load modulus and monotonic secant modulus degradation curves for English China Clay

Test CL-7 applied a higher-frequency χ = 0.85 cyclic load to compare the effects of faster rates and shorter durations in clay. The more plastic behaviour and lesser importance of initial fabric of the clay is apparent; plastic strain rates are reduced by approximately 10 times compared to CL-5 (Figure 6.73), indicating the material to be dominated by load duration, similarly to findings of Li et al. (2011). However plastic

strain rates appear to reach a minimum at much lower strain (0.10% to 0.25%) and show a slight tendency to accelerate beyond this point; similarly to the Silt Mix, this may indicate the more damaging effects of higher-frequency load. In subsequent χ = 1.0 cyclic load at 0.01Hz (i.e. the same as test CL-3) plastic strain rates are higher (by a factor of 2-3 times). As no repeat was performed, it is unclear how much of this difference is due to inherent sample variation and how much is due to the initial fast loads. There is a possibility of a general tendency in soils for faster load to be more damaging and less amenable to providing load-induced strengthening; testing on a wider range of soils could better inform how such treatments are effected in practice and also could help develop methods to limit construction damage to road subgrades.

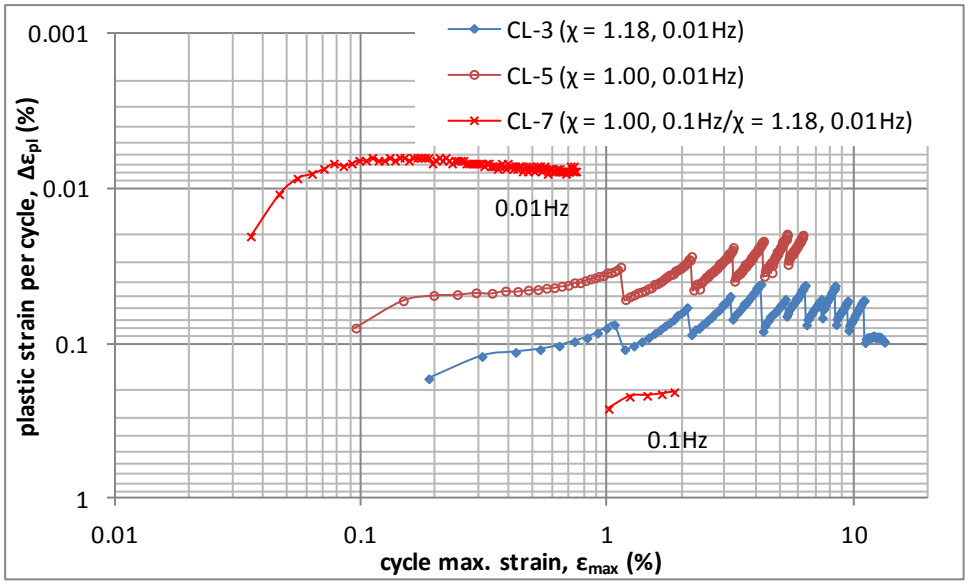

Figure 6.73: Cyclic strain accumulation rates at varying frequency and accelerating plastic strain rates observed in 0.1Hz cyclic test

From the limited number of tests done, cyclic pre-loading alone does not appear effective in improving strength; there is some medium-strain stiffness improvement but this coincides with reduced ductility (failure occurs at very similar total cumulative

strains). Clays can gain strength when cyclically-induced pore pressures are permitted to drain, as in test CL-6 (Figure 6.74). Elevated load cell instrument noise made it difficult to apply well-controlled cyclic load regimes; however a tendency to reduce cumulative strains and resist increased load levels in a stable manner is apparent. Drainage is more effective at early stages, similarly to Silt Mix tests. Test CL-7, for which better cyclic load control was achieved, shows similar strengthening effects of drainage intervals (Figure 6.75), even those which only achieve partial dissipation (2 hours c.f. 14-18 hours).

Strength increase is proportionally smaller than for Silt Mix tests and it is easy to trigger rapid large strains when applying a load increase (e.g. χ = 2.24 for CL-6, χ = 1.76 for CL-7). It is likely that, as seen by Wang et al. (2015b), clays require larger strains to achieve similar proportional strength gains to silts. Therefore whilst clay soils present a lesser risk of catastrophic, sudden failure, the risk of gradual softening and strain accumulation is harder to mitigate through cyclic load-induced strengthening. This will be further exacerbated by longer consolidation times; in test CL-7 it is clear that partial drainage is less effective in reducing plastic strains, particularly later in the test.

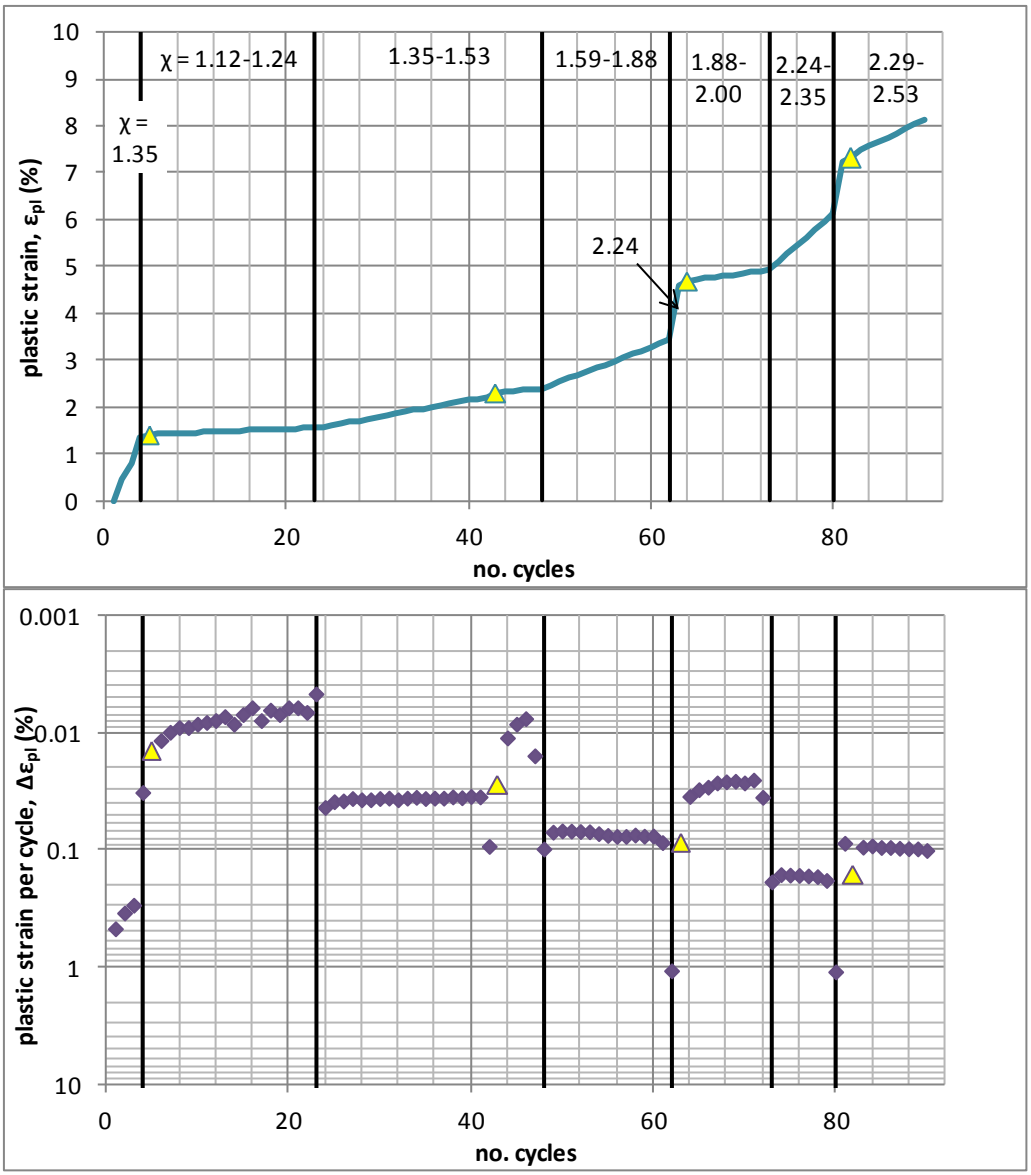

Figure 6.74: Strain accumulation in test CL-6; reduced plasticity as a result of drainage is apparent, although variations in stress from cycle to cycle make it difficult to see clear trends over cyclic stress regimes. Yellow triangles indicate drainage intervals of minimum 14hrs.

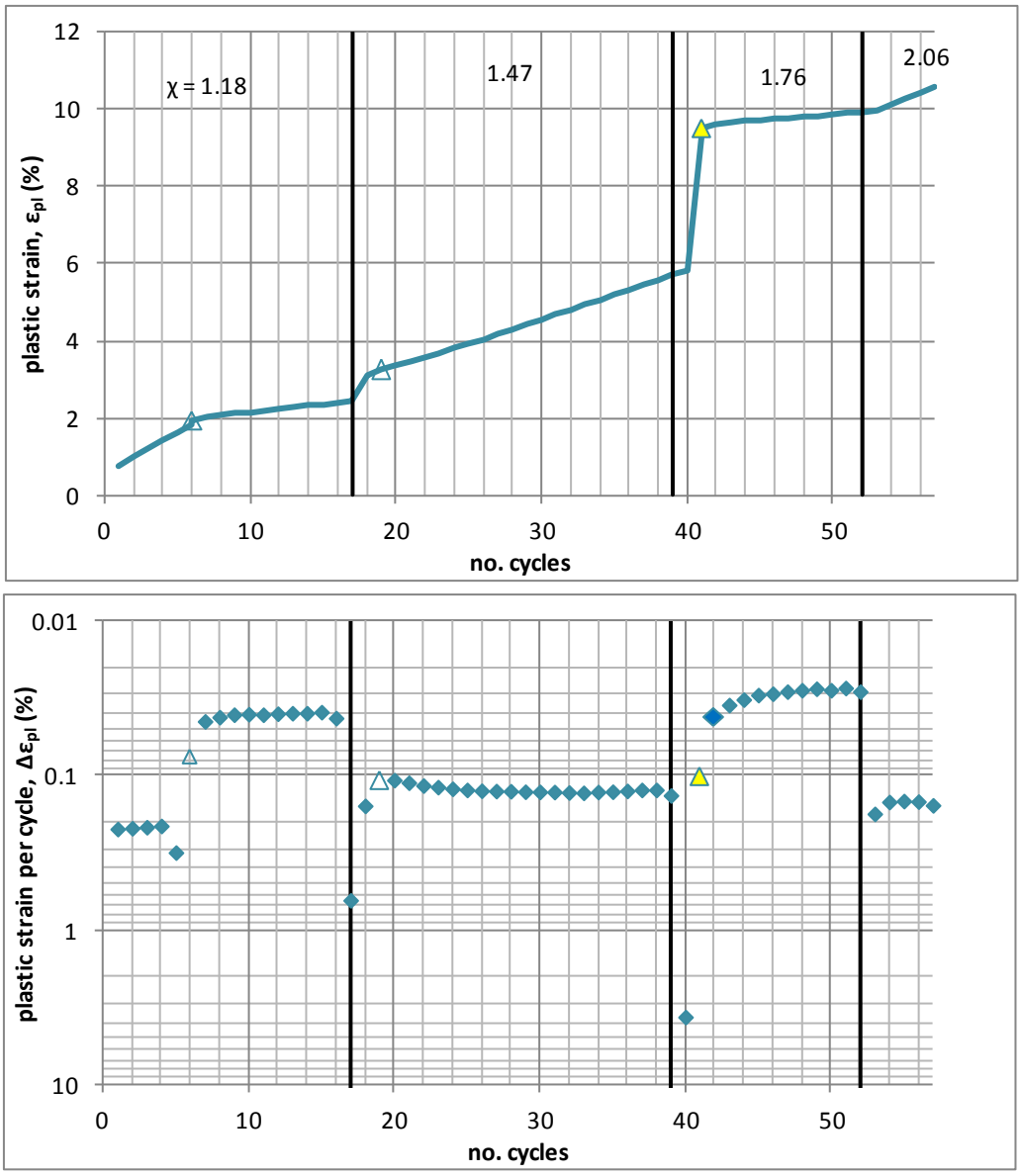

Figure 6.75: Strain accumulation in test CL-7; partial drainage (2 hours) is effective at reducing plasticity initially but becomes less effective at larger strains. Open triangles indicate 2 hour drainage intervals, yellow triangles indicate minimum 14hrs.

As with the Silt Mix tests, large-strain cyclic loading with drainage intervals can increase monotonic strength (Figure 6.76). As observed in the cyclic stages, changes in strength are proportionally smaller than for the Silt Mix tests; even after large strains (>8%), strengths are 150% of the intact, as compared to 300% of intact in test G-2. Much of the strength increase in test G-2 comes from the medium-strain re-structuring

and mitigation of liquefiability; if compared to tests stabilised by cyclic load without drainage intervals, G-2 reaches 145% to 195% of tests D-3/D-7/F-5.

As is apparent in the Silt Mix tests and also Figure 6.76, drainage intervals are not fully effective at reducing brittleness induced by overconsolidation. As opposed to the intact, normally consolidated monotonic clay tests, CL-6 and CL-7 monotonic tests both failed with clear shear banding, in agreement with Silt Mix tests and concepts in the literature (Chapter 3.1.2) that link brittleness and loss of post-cyclic strength in clays with increasing induced overconsolidation. These conceptual models appear highly effective in describing changes induced to soils from accumulation and dissipation of cyclically-induced excess pore water pressures.

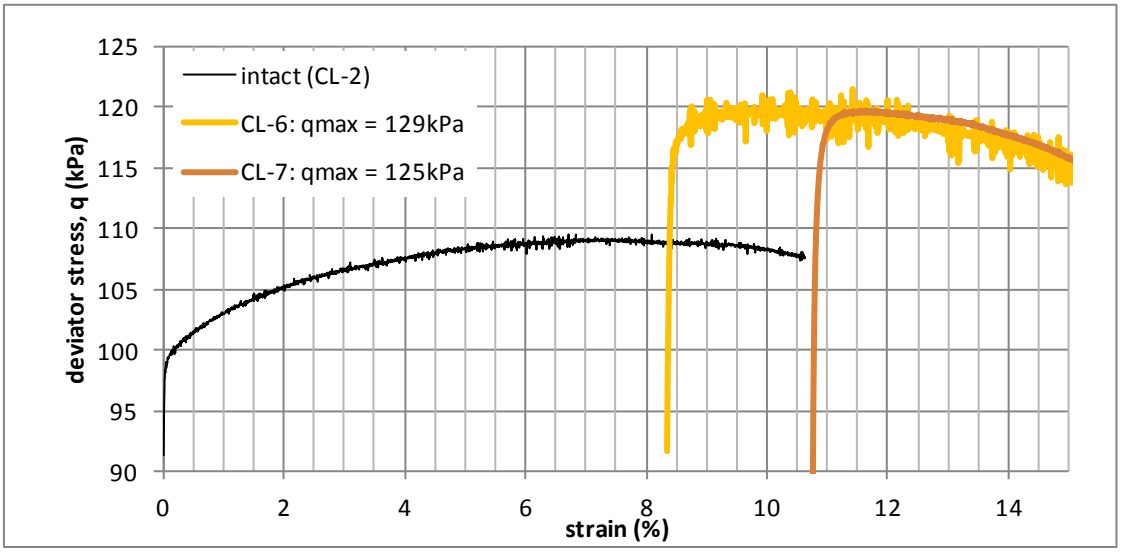

Figure 6.76: Increased post-cyclic monotonic strength of clay samples subject to incrementally increasing load and drainage intervals

During dissipation of excess pore pressures in drainage intervals, the clay samples showed a similar sensitivity of the volume change gradient to the induced excess pore pressure (Figure 6.77), with greater re-structuring following greater excess pore

pressure accumulation (particularly CL-7, which varied from 2.6% to 3.3% water content per log cycle for u_e < 30kPa and 5.0% per log cycle for u_e = 43kPa). This effect may be part of a general link between undrained re-structuring and volume change; if this increased retention of overconsolidation following large strains is fundamental to a wide range of soils, careful control of strains for temporary heavy traffic routes will in general result in reduced maintenance and reduced risk of a brittle ultimate failure during service.

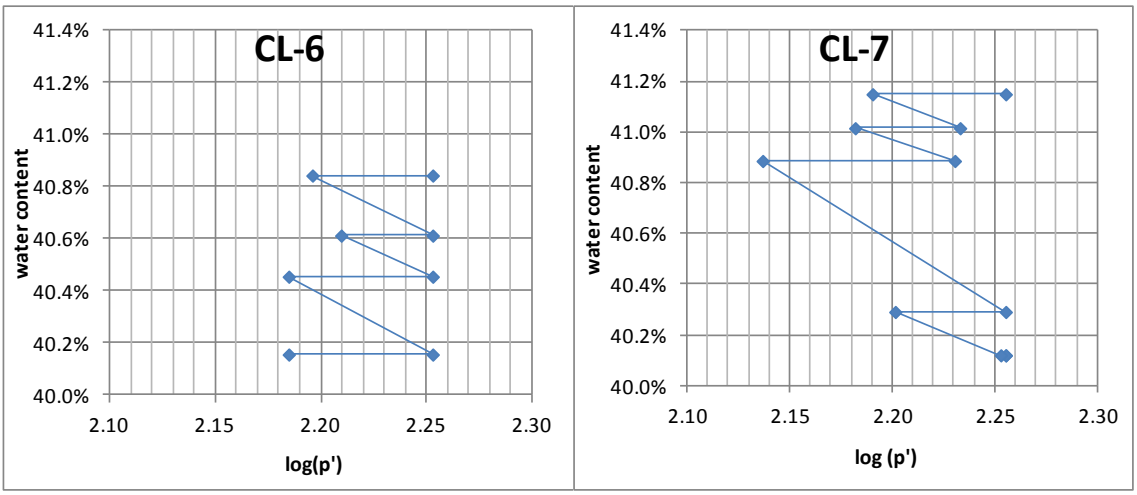

Figure 6.77: Volume change characteristics of clay tests with intermediate drainage intervals, showing a trend towards steeper volume change gradients for higher excess pore pressures.

Similarly to Silt Mix tests, tests CL-6 and CL-7 show the secant modulus degradation curve to be translated to higher strains towards the cyclic Load Modulus curve (Figure 6.78), implying an extension of the very small-strain constant modulus regime and a similar extension of the small-strain elastic strain range. As with Silt Mix tests, the conditioning towards the cyclic curve is less complete for these tests, which applied a smaller number of high-magnitude load cycles. The mechanism for shakedown suggested herein, i.e. micro-structural rearrangement which increases the elastic strain

range until it reaches the cyclic strain range, may thus be applicable to a wide range of soils and could prove a useful conceptual model for analysing and predicting how a fully resilient response may be reached under cyclic load.

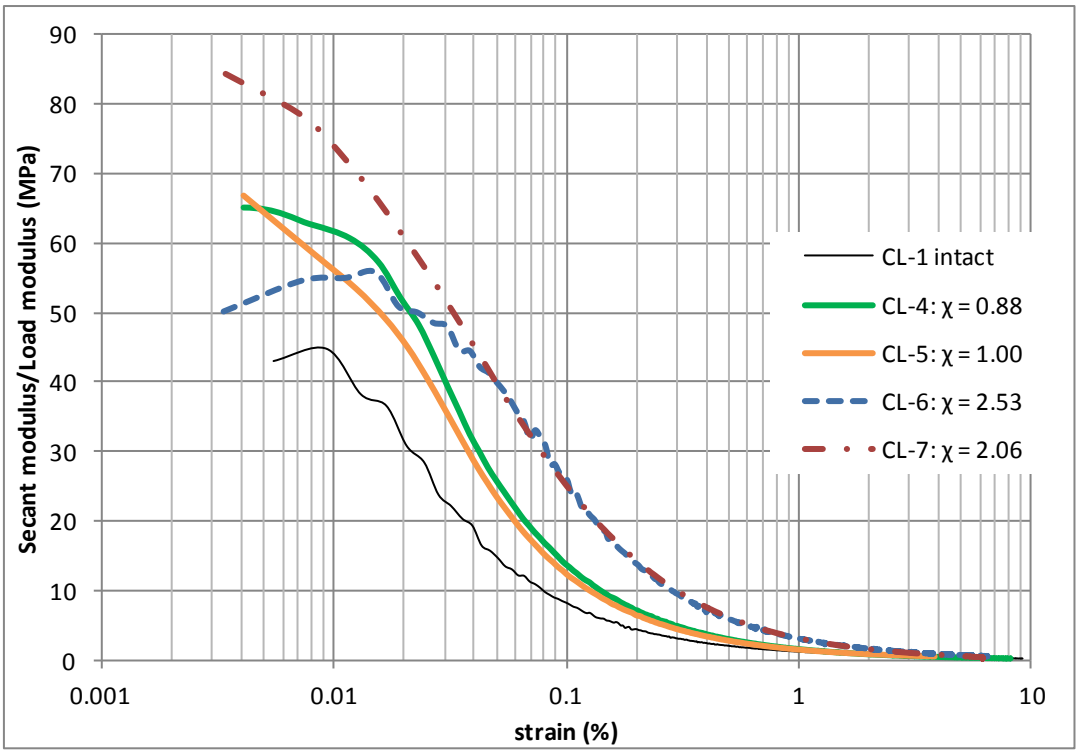

Figure 6.78: Post-cyclic secant modulus results comparing intact tests, undrained tests and incrementally increasing cyclic load tests with drainage intervals (CL-6 and CL-7). An increased elastic strain range in the later tests is implied.

6.8. Conclusions

Experimental cyclic triaxial testing has demonstrated it is possible to use cyclic load to remediate and improve soft subgrade soils, particularly silty soils prone to meta-stable liquefaction. As liquefiable soils present the greatest danger to heavy haul traffic, efforts have been concentrated upon understanding more fully this phenomenon and means of averting it. The following key observations have arisen from the research conducted in this chapter:

- The concept of meta-stable liquefaction arising due to a precarious micro-structure has been corroborated by determining more precisely the necessary conditions to maintain liquefiability and trigger liquefaction and dependence on the initial fabric.
- Strain, which correlates with rearrangements on a micro-scale, is central to liquefaction. Strain is also linked with contraction of the soil skeleton, which causes progression of collapse of the precarious micro-structure and is measured by increasing pore water pressure.
- Liquefaction can only be triggered by sufficient medium-strain (i.e. plastic) perturbation applied in unstable (undrained) conditions. A liquefaction initiation strain (ε_{tl} = 0.1%-0.3% for the Silt Mix soil) must be exceeded, which causes the effective stress state to cross the Instability Line, whilst the threshold stress, close to the static q_{peak} for Silt Mix soil, is simultaneously exceeded.
- The Instability Line is dependent upon the initial fabric and, unlike large-strain properties, can be altered by applying plastic strain. Applying strains > ε_{tl} in a stable manner, such as by allowing drainage during or after loading, or lowering the mechanical power input through low-amplitude cyclic loading, effects the necessary re-arrangement of the structure to a more compact, stable state without collapse of the soil skeleton. Experiments indicate that under medium strains, relatively small proportions of full consolidation can be effective in averting meta-stable liquefaction.

- If larger cyclic loads are applied which produce large strains and corresponding high excess pore pressures, providing drainage intervals can produce significant strength improvement. However steeper volume change gradients are associated with large-strain deformations; retained overconsolidation and consequent brittle behaviour is expected. A more careful control of strains and gradual increases in cyclic load magnitude is considered preferable to retain more ductile behaviour.
- Meta-stable soils are able to benefit from medium-strain cyclic loading because their behaviour is heavily dependent upon the initial fabric and this tends to be beneficially rearranged by this treatment. More stable soils, such as English China Clay, do not benefit from medium-strain cyclic load and may in fact be weakened by accumulation of excess pore water pressures. Dissipation of pore water pressures in these soils is expected to produce benefits, although the strains necessary to induce noticeable water content changes are expected to be larger and consolidation times longer. Accordingly, although clays can resist transient loads with significantly reduced strains compared to static loading, progressive softening and settlements in clay soils are expected to remain significant hazards.

Additionally, a number of findings in this chapter, whilst not of primary importance to the heavy haul road problem, may be useful in extending the understanding of cyclic loading:

- **Physical mechanisms for shakedown:** It appears shakedown arises as a result of the elastic strain range increasing until it matches the cyclic strain range; this appears dependent upon both the cyclic stress magnitude and duration of cycling. The exact mechanism remains unknown; however it is likely to relate to preferential re-structuring of the soil's fabric.
- **Damaging effects of faster loading:** Results suggest faster loading causes liquefaction more easily, is less effective at providing improvement and can accumulate more strain over time. The testing presented in this chapter is insufficient to reach a strong conclusion.
- **Correspondence between strain and pore pressure:** Cyclic tests on silt and clay indicate similar pore water pressures are reached regardless of the cyclic loading regime. Stronger experimental evidence for a link between two fundamental soil properties would be valuable for in-situ monitoring schemes.

CHAPTER 7: APPLICATIONS IN PRACTICE

7.0. Introduction

Based on experimental findings in Chapter 6, this chapter considers where the hazards identified are likely to be found, how to investigate them and how phenomena identified experimentally can be used as treatment for problematic soil resisting heavy haul traffic loads. The conventional approach to this problem is to ensure the soil can resist the maximum loads without significant degradation as soon as construction is complete, through either limiting sub-soil strains by spreading load through earthworks, or ground improvement. This chapter presents a practical approach for using cyclic traffic load to gradually develop the necessary resistance to support the largest loads safely; careful application of plastic strain to re-arrange soil fabric and consolidation to allow reduction in water content are the mechanisms by which this is achieved. The proposed observational approach, similar to that used by Peck (1969) for transporting Saturn rockets, could result in significant reduction in the cost of temporary access, which may result in the use of modular construction more widely on projects with problematic ground.

7.1. Hazard identification

Soft, weak and easily deformable soils are the principal geohazards jeopardising successful operation of heavy haul roads; early identification is key to successful risk management. In particular, meta-stable soils which can undergo collapse and strain-softening present the greatest risk: this type of failure is sudden with no prior signs of

distress. As previously discussed, liquefiable, normally consolidated silt soils are considered a worst-case soil as they combine 'sand-like' liquefiable behaviour (Boulanger and Idriss, 2006) with sufficiently low permeability to remain undrained under slow traffic load. There are other soils, not tested experimentally in this study, which may present a similar hazard:

- Quick clays prone to significant strength loss upon remoulding (Åhnberg and Larsson, 2012).
- Loess soils predominantly formed from wind-blown silt (Assallay et al., 1998)

These soils all share similar open, precarious initial micro-structures: this is the cause of catastrophic loss of strength once disturbed. Other problematic soils prone to sudden collapse such as desert sabkhas (Waltham, 2002) pose a similar risk, but may require a different treatment approach. At the initial stages of a heavy haul road project it is therefore of utmost importance to identify whether the route crosses meta-stable soils and the nature of these deposits.

Bearing in mind the extreme consequences of inadvertently triggering meta-stable liquefaction through overload (e.g. damage to equipment, delays, injuries or fatalities to personnel), it is crucial the risk posed by potentially problematic soils be investigated thoroughly. Expenses incurred and effort expended during ground investigation, laboratory testing and in-situ monitoring recommended in this chapter can thus be easily justified. The sensitivity of meta-stable soils to disturbance displayed in this study demonstrates a need for special care in planning and executing investigation and testing works.

7.1.1. Desk study

Identification of geohazards must start at an early stage and desk study can provide a valuable and inexpensive source of information to inform later on-site stages (Waltham, 2002). This section does not intend to provide definitive, detailed models for formation mechanisms of meta-stable soils but instead offers simplified and generalised context for consideration of relative risk for a haul road crossing varied terrain.

Sedimentary silts and clays are typically transported and laid down by water (Waltham, 2002; Åhnberg and Larsson, 2012), although these can also form aeolian deposits such as loess (primarily transported from its origin by air, or a combination of air and water; Assallay et al., 1998). Silts and clays suspended in rivers are only deposited in very slow-moving flows (Waltham, 2002) or areas of flow speed deceleration (Bell, 2007). Soft alluvial silts and clays are thus associated with deltas, lake deposits and slow-moving, non-turbulent features of lowland, 'plain' stage rivers, e.g. old channels, oxbow lakes, and flood plains (Bell, 2007). A haul road near to current or former rivers, lakes and deltas is likely to encounter such soils.

Soft alluvial clays may present a hazard through low strength and high deformability, but arguably alluvial silts (and possibly silty alluvial sands) present a greater geohazard, i.e. liquefaction. The correct deposition environment is necessary to lay down these soils but there must also be a source of silt available to deposit. Assallay et al. (1998) describe silt production as a high energy process to shatter quartz crystals into silt flakes; glacial grinding, fluvial abrasion and frost shattering are identified as processes which can yield large quantities of silt (Assallay et al., 1998; Soreghan et al., 2016).

Rivers are themselves a source of new silt; if they also encounter glacial, post-glacial or peri-glacial areas, silt yields are likely to be increased. Silt may also be eroded from parent rocks formed of smaller, more elongated grains, such as siltstones and mudstones or foliated shales and slates (Assallay et al., 1998). An assessment of current and historic river systems is thus necessary to assess liquefaction risk.

Sub-glacial soils are likely to be rich in silt and inactive rock flour, however the glacial overburden stresses are expected to have induced overconsolidation and so liquefaction risk is likely to be low. Glacial outwash and re-deposition of these soils is of greater concern, particularly glacio-lacustrine deposits which can combine high deposited silt content with recent fluvial deposition (i.e. normal consolidation). Upper soil strata, particularly those above the water table, are likely to have experienced fluctuating effective stresses and so be lightly overconsolidated; the soils at risk of liquefaction and/or localised yield are closer to normal consolidation, at depth.

Other meta-stable soils, e.g. loess and quick clays, have environments where their formation is more likely. For example, quick clays, typically being initially deposited in saline water, exhibit open, flocculated structures: to become quick, the pore fluid is then leached by rainfall, removing salt and bonding (Waltham, 2002). Locations subject to reducing salinity, e.g. marine regression, post-glacially uplifted coastlines, are therefore at risk. Loess can often form where wind transports silts and clays; close downwind proximity to glacial environments or flood plains and deltas are thus likely locations for loess (Assallay et al., 1998). For example alluvial silts of the Mississippi river valley (studied for liquefiability by Wang et al., 2014; 2015a; 2015b) are posited

by Assalay et al. (1998) to be the source for loess in the Midwestern USA. Unlike alluvium, loess is unsaturated and often collapses when saturated (Waltham, 2002); meta-stability is often confined to upper, unsaturated layers, although these can still extend to great depths in arid or upland environments. Rapidly deposited and then desiccated alluvial silts (i.e. from flooding of lowland basins) can also form open structures prone to collapse, similar to loess (Waltham, 2002).

This simplified picture represents just some of the circumstances surrounding meta-stable soil deposition; it is recognised many alternative environments can give similarly problematic soils and a sound understanding of local geology is critical for successful risk evaluation.

7.1.2. Ground investigation

A carefully researched desk study should allow a risk-based ground investigation which specifically targets the geo-hazards of greatest concern. The increased influence of deep soil strata (Chapters 2.4 and 2.5) will require a different investigation, design and monitoring approach for roads carrying very large, heavy, multi-wheeled vehicles. More conventional surface tests, such as CBR, dynamic probing or in-situ surface stiffness tests (Frost, 2000), will still be useful in understanding resistance to rutting on the scale of a single wheel but less useful in understanding the behaviour of deeper soils when exposed to large vehicle passages, which requires investigation to greater depths using investigation techniques more common to design of large foundations.

In soft ground, Cone Penetration Tests (CPTs) are effective in classifying strata and determining depths and basic strength properties (Barnes, 2000) whilst achieving good

production rates. An initial stage of high-volume investigation, based on CPTs targeting areas identified in desk study, can determine more precisely the extents and nature of soft ground. This initial stage can then inform where to take soil samples for laboratory testing, particularly if high-quality samples with minimal disturbance are desired.

CPTs, when compared to more basic penetration tests (e.g. SPT, DCP) yield more information. In sand-like soils (encompassing non-plastic silts) Boulanger and Idriss (2006) present methods for determining liquefaction risk from CPT data; these are useful for corroborating liquefaction risk profiles, however these tests will not indicate the stresses/strains at which liquefaction occurs, which requires laboratory testing. The greater dependence upon electronic technology and large volumes of data from CPTs also requires skilled operation and interpretation for results to be meaningful.

Recovery of bulk/disturbed soil samples for index testing can provide valuable information to refine estimated risk levels. Liquefiability of soft soils depends upon whether they are 'sand-like' or 'clay-like' (Boulanger and Idriss, 2006) and much of the work involved in classifying liquefiable soils uses index properties. Andrews and Martin (2000) relate liquefiability to the Liquid Limit ($LL < 35$) and clay-sized particle content (<10% finer than 2μm), whilst Boulanger and Idriss (2006) recommend using Plasticity Index ($PI < 7$) to determine whether a soil exhibits 'sand-like' liquefaction. When assessing marginal cases (i.e. PI = 3-8 or only fulfilling one of the criteria of Andrews and Martin (2000), as was the case for the Silt Mix soil (Chapter 4.1.1), deeper consideration of the mineralogy and weathering history (i.e. are fine particles likely to be high or low activity?) should also be considered in defining the risk levels.

Quick clays can be identified by water content as they typically exist at well above the Liquid Limit, hence their low remoulded (large-strain) strength (Åhnberg and Larsson, 2012). Loess collapse risk is commonly assessed by load-collapse tests, either in-situ or in the laboratory. There is also potential to combine this with geophysical methods, such as the use of seismic surveys to measure density and changes induced by dynamic compaction (Evans et al., 2004).

The above stages (desk study, CPTs or loess collapse tests, bulk samples for index tests) provide a relatively good picture of risk to heavy haul roads from soft and meta-stable ground and the most problematic areas identified. The highest-risk areas are likely to require laboratory-based stress testing on recovered samples; parameters such as the liquefaction threshold stress and initiation strain (ε_{tl}) are crucial in managing risk through design and ongoing monitoring of heavy haul roads. The complexity of testing will depend upon the level of risk presented and the amount of strengthening through cyclic load treatment required.

It has been established in this study and by others (Lunne et al, 1997; 2006; Santagata and Germaine, 2005) that meta-stable, liquefying soils in particular can fundamentally change if subject to high sampling disturbance strains; field sampling can thus significantly underestimate liquefaction risk. Lunne et al. (2006) found samples from a Sherbrooke block sampler liquefied at medium-strain whist samples extracted using the NGI 54mm piston sampler did not; only samples within the 'very good' sampling quality category consistently retained liquefiability (also observed in Chapter 6.1.3). If

in-situ samples are to be taken for stress testing, it is only worthwhile to take samples of the best quality.

Santagata and Germaine (2005) and Lunne et al. (2006) found that reconsolidating to well above the in-situ stress and normalising results following SHANSEP (Ladd and Foott, 1977) is effective for regaining intact liquefiable behaviour. However this virgin compression also re-structures the soil; if cementation is present, which tends to increase initial strength but also brittleness, this will be destroyed (Lunne et al., 2006; Zapata-Medina et al., 2014). For this reason, Lunne et al. (2006) suggest it is a less reliable measure of in-situ strength than block samples tested at in-situ stresses. SHANSEP is still useful for extracting more useful information from lower-quality samples, particularly regarding liquefaction risk. Bearing in mind SHANSEP reconsolidation de-structures the in-situ fabric, reconstituting samples from bulk soil following the method outlined in Chapter 4.1.2.2 may represent a cost-effective way to create liquefiable, soft soil samples to obtain equally representative data.

Laboratory stress testing of liquefiable soil should aim to derive the following information: for medium-strain treatment, the liquefaction threshold stress and strain thresholds for volume change and liquefaction respectively (ε_{tl} and ε_{tv}); additionally for large-strain treatment, an understanding of safe load and drainage sequences. The following tests are recommended:

- **Anisotropically consolidated undrained monotonic shear** – as demonstrated in Chapter 6.2.2, anisotropic consolidation is important as isotropically consolidated samples may not liquefy. Peak pre-liquefaction stress (which may

have a strong link with threshold stress for cyclic liquefaction), ε_{tl}, dilatant recovery strains and ultimate strength values can be derived from this test. These may also be used to inform stress selection for cyclic tests. Dilatant strength from triaxial tests must be treated with caution as these represent an element under (nearly) uniform stress. In the field, a non-uniform stress field is expected and localised pore water movement from a contractant area to a dilatant one could soften the dilatant soil, preventing it from reaching the maximum strength under true zero volume change conditions.

- **Undrained cyclic shear** – direct determination of the threshold stress for liquefaction, safe limits on $\Delta\varepsilon_{cyc}$, and ε_{tv} to inform the design of cyclic load treatments, such that stable plastic strain accumulation can be achieved. Post-cyclic monotonic stages are essential to confirm the efficacy of sub-threshold cyclic load in providing strengthening.
- **Cyclic load with intermediate drainage –** if significant large-strain strengthening is desired, a series of these tests are necessary to allow an informed choice of load increments and drainage intervals: as is apparent in Chapter 6.6.3, it is easy to cause large ground movements by applying too large an increment to a soil with high residual excess pore water pressures. It is also essential that treatments intended to achieve large-strain strengthening are supplemented by ongoing monitoring during operations.

As discussed in Chapters 3.3.1, 4.1.2.2, 4.3 and 5.0, it is considered more important to regain normally consolidated behaviour than test at the appropriate stress level, as the former condition has a much greater effect on liquefaction behaviour. Therefore it is

recommended that samples for the above tests are consolidated to above their *in-situ* stresses, preferably at least 3 times, and then results normalised by the consolidation stress as per Ladd and Foott (1977). It is recognised that the higher confining pressures can change the post-liquefaction recovery behaviour, potentially overestimating ultimate strength (Chapters 3.3.3 and 6.2.2). Designers should therefore be wary of relying on dilatant post-liquefaction strength.

If an investigation of large-strain consolidation strengthening is considered necessary for the stability of the temporary heavy haul road, it may be advisable to also conduct in-situ permeability tests; large-scale phenomena are not identified by testing small samples. In alluvial areas particularly, heterogeneity and thin permeable layers are likely to control movement of water. Higher in-situ permeability, whilst beneficial to consolidation, may limit the mobilisation of dilatant strength: local flows of water under load could soften dilatant zones.

7.2. Risk mitigation

7.2.1. Design stage

Whilst it is likely to be uneconomical to produce a conventional, yield-limiting design for the whole-vehicle stress bulb demonstrated in Chapter 2.4.1, this design approach is recommended when considering either individual wheels or adjacent sets of wheels to avoid localised rutting and deterioration of upper, non-liquefiable strata.

For consideration of the whole-vehicle response, finite element models which are updated to match in-situ monitoring data will be extremely valuable in analysing the response of the ground to load passages and developing assessment of risk. Depending

on the level of ground investigation and laboratory testing undertaken, many parameters are likely to be little more than intelligent estimates; instead of a single model, it may be more productive to describe upper and lower bounds as this will be more useful to compare to monitoring data. Constitutive models of sufficient simplicity to be useable with the data anticipated are unlikely to capture complex effects such as the response to rotating principal stresses, which could significantly impact progression of cyclic degradation. This is why an observational approach is so important in managing risks: by comparison of best-guess models to in-situ monitoring data, anomalies and modelling inaccuracies can be identified. A key outcome of the design stage should be a series of in-operation contingency mitigation measures, such as rest periods or placement of lateral bunds, and a series of observable triggers to inform when these are necessary. Such indicators could comprise settlement, heave or pore water pressure measurements (discussed further in Chapter 7.2.3).

The evolving understanding of risk throughout the infrastructure's life and its criticality to success in these projects necessitates a close relationship between design, construction and operation personnel. An observational design approach which involves the designer in the construction and operation stages is key; similarly, the design stage must progress collaboratively with those involved in construction and operation if monitoring regimes and treatments are to be applied effectively.

7.2.2. Construction stage

During construction of the road it is possible to remedy shallow-seated, partially saturated meta-stable soils (such as loess) by compaction. Air void space can be reduced by compaction and Evans et al. (2004) were able to effect an improvement to

3m depth in loess through use of Rapid Impact Compaction equipment. Monitoring of surface movement during this process or the compaction of road fill layers is also recommended as this will help refine assumed ground profiles and risk assessments. However this approach is not effective on saturated deposits and may in fact weaken the soil through zones of local shear.

Where soft, low permeability deposits are encountered, operational requirements may dictate a need for accelerated consolidation if this is necessary for stabilisation; this is likely to be the case for thick soft clay strata. Installing vertical wick drains will be an effective method to speed up consolidation (e.g. Barnes, 2000) and so ensure safe and efficient operation of the road without excessive construction costs.

It may be possible to use construction traffic as a cyclic pre-load treatment on completed sections of road. The influence depth of treatment needs to be considered; a construction vehicle with a width that is small relative to the large, heavy vehicles will not stress the full influence depth. In order to effect medium-strain rearrangement, ε_{tv} must be exceeded (for the Silt Mix soil, this occurred at a strain of 0.01-0.02%, coincident with a cyclic stress of 3% of the effective overburden stress). Smaller vehicles disperse stresses (and so strains) more quickly with depth; as demonstrated in Figure 7.1, improvement is much shallower, even if higher surface loads are applied. Conversely, the risk of liquefaction for smaller construction vehicles, even with high bearing pressures, is likely to be significantly lower due to the rapid dispersal of stress. The top of the normally consolidated soil layer (i.e. 6.5m depth in Chapter 2.5) is expected to require the most strengthening; under heavy vehicle

passages it will experience the highest stress relative to its effective overburden stress (Chapter 2.5). If construction traffic is expected to apply strains between ε_{tv} and ε_{tl} (transient stresses of 3-8% of effective overburden in the case of the Silt Mix soil; Chapters 6.2.1 and 6.3.1), it can be used to remediate the upper part of the normally consolidated soil. However the effective depth of treatment is expected to be limited by the vehicle size (Figure 7.1) and additional treatment of deeper layers is likely to be required.

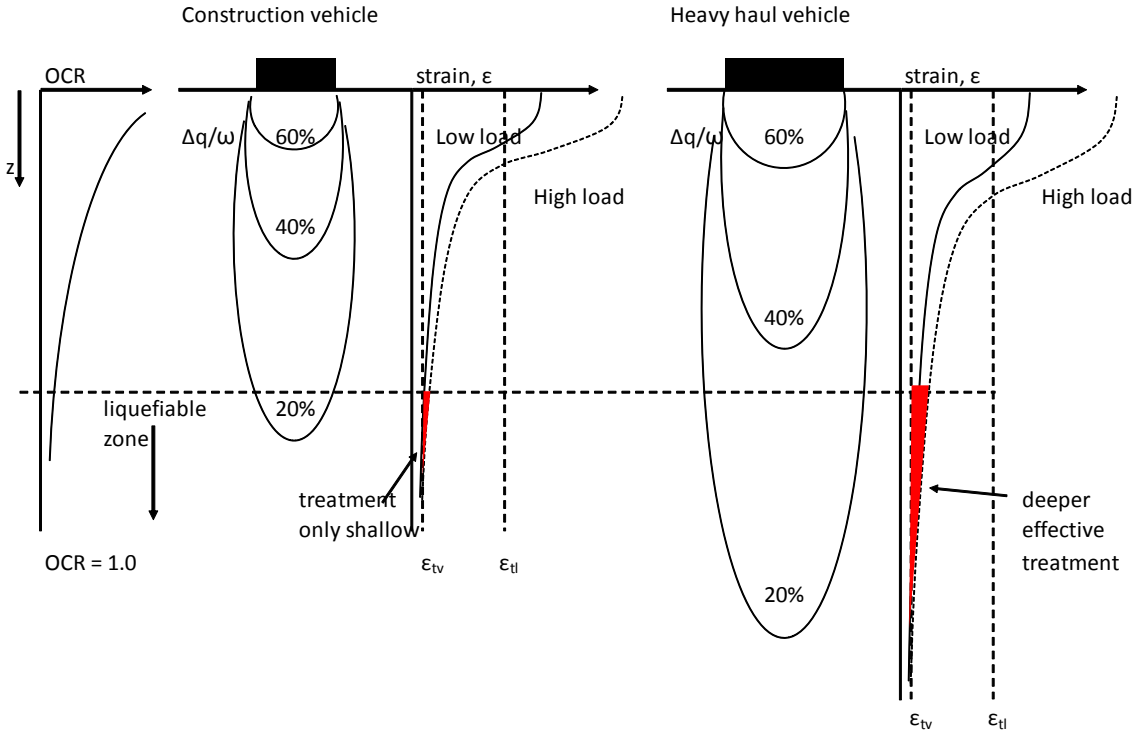

Figure 7.1: Reduced influence depths and effective treatment for construction traffic compared to heavy haul vehicles (assuming a Boussinesq stress distribution); cyclic strain limits for safe cyclic load treatment between ε_{tv} and ε_{tl}.

During construction, the passage of a heavy haul vehicle (of the same dimensions and hence a similar stress bulb to those carrying heavy loads) which is not fully laden (carrying road construction materials, for example) will be useful in identifying unexpected soft spots at a time when remediation is cheaper and easier to apply. This

loading must avoid liquefaction in the uppermost (untreated) part of the normally consolidated soil, e.g. based on Chapter 2.5 a 300 tonne (or lighter) vehicle is required to apply stresses below the liquefaction threshold (8% effective overburden stress; Chapter 6.2) at 6.5m. A 300-400 tonne vehicle load may not treat soil at 12m depth (transient stress in Chapter 2.5 is close to the Silt Mix medium-strain threshold in Chapter 6.3.1); once the upper layer is stabilised, deeper treatment can be applied by cautious increases in vehicle weight. In-situ monitoring (discussed in Chapter 7.2.3 and 7.3) will be required to confirm treatment and control residual risk during this medium-strain improvement.

7.2.3. Operational stage

The operation of the heavy haul road is the most critical stage: this is when liquefaction risk is highest and the majority of treatment is applied. Risk in this stage can be controlled in three ways: ongoing monitoring throughout operations, carefully controlling heavy vehicle passage and contingency measures to rectify any dangerous defects. The strategy presented herein is that a combination of these measures can be used not only to control degradation but also to effect gradual improvement in strength.

Monitoring is the most important part of cyclic load treatment; the resistance to load is developed over time and initially the ground may be unsafe to support the maximum loads. Monitoring needs to check the cyclic load treatment is applied as planned and identify unanticipated hazards as soon as possible.

The results in Chapter 6.5.2 demonstrate that the progression of cyclic stabilisation of liquefiable soil is manifested in cumulative irrecoverable strains and pore water pressures, which are strongly linked: measuring these can indicate levels of risk and progression of treatment. Liquefaction can be described by a certain pore pressure increment (to take the effective stress to the Instability Line) or alternatively a certain plastic strain (ε_{tl}).

In-situ pore pressure measurement is expected to give a good indication of strain within a layer and in soft strata has the additional advantage of monitoring consolidation between loads (Peck, 1969); vertical settlements during intermediate consolidation (Chapter 6.6 and Appendix 1) were found to be low and may not be visible in settlement monitoring. At low strains particularly, (i.e. close to ε_{tv}, 0.01%-0.02% for the Silt Mix soil) the resolution of settlement monitoring data is likely to be insufficient; however corresponding transient excess pore water pressures are likely to be captured by vibrating wire piezometers (providing their data can be sampled regularly). This improved resolution will be of particular importance when monitoring a liquefiable soil, to see that medium-strain treatment is progressing satisfactorily. A piezometer is however only a point measurement and may miss features in between locations; they are most useful in identified problem areas. Installation of piezometers beneath the road could also carry significant expense.

Monitoring of ground movements (settlement/heave) along the road may be cheaper and yields richer spatial information, allowing previously unidentified problems to be noticed and remedied earlier. It is therefore recommended during all heavy haul road

operations. During operation, it may be possible to perform rapid, real-time measurement of ground movement by using laser scanners mounted on the heavy vehicle itself, referenced to targets sufficiently remote from the road to not be affected by induced movements. Localised rutting along wheel tracks, governed by shallow soils, will give an unrealistic indication of strains at depth, which are critical to the evolving liquefaction risk assessment. Settlement monitoring should focus on a spatial average taken across the entire road width as this is more likely to be influenced by a deep-seated settlement 'dish'. Monitoring of the ground adjacent to the road is also important to identify heave, which could indicate deep-seated bearing failure. Ground surface movements in response to weather need to be taken into account; a set of baseline readings will be necessary before operation starts.

Significant heave adjacent to the road may suggest mobilisation of strength in the passive zone; modelling (see Chapters 2.4.3 and 2.4.5) links this to near-complete yield of the compression zone, redistribution of stresses and significant principal stress rotation (which can accelerate cyclic degradation). Heave may therefore indicate the start of rapid propagation of a failure mechanism. Halting traffic is recommended to allow consolidation of excess pore pressures, which are expected to become large as the compression zone yields. Soil response to rotation of principal stress is difficult to investigate and even more difficult to predict, particularly for the complex stress field and heterogeneous soils beneath a heavy haul vehicle. A berm laterally adjacent to the road will increase vertical overburden stresses in the passive zones, improving the strength of the passive wedge and also reduce the tendency for principal stresses

rotation. This can be used as a contingency measure or even constructed in advance in identified trouble spots.

Central to safe operation are the trigger levels for intervention and contingency measures. Upper and lower bound predictions for cumulative settlements and pore water pressures will be useful in determining the expected range for normal operation. An example of a set of triggers and associated actions, from 'green' (normal operation) to 'amber' (geotechnical engineer alerted) and red (halt operations, apply contingency measure), are shown in Table 7.1. These triggers will need to reflect site-specific hazards and there may be a number of separate triggers applicable to different areas of a project. As back-analysis and refinement of predictions is envisaged to be a central part of this treatment, trigger levels are likely to also evolve over time.

Table 7.1: Example trigger levels for intervention in operation of heavy haul road

Monitoring data shows:	Level	Action
Settlement/pore pressure data within predicted bounds	Green	None required – continue operations and monitoring
Settlement/pore pressure data exceeds upper bound	Amber	Risk of deterioration - refer to geotechnical engineer, back-analyse data and refine predictions
Settlement/pore pressure data below lower bound	Amber	Treatment may not be effective – refer to geotechnical engineer, back-analyse, refine.
Pore pressure close to Instability Line (strains below initiation strain)	Red	Liquefaction risk – halt operations, allow time for consolidation
Settlement per load passage increasing for 2no. passages	Red	Liquefaction/softening risk – halt operations, allow time for consolidation
Heave data exceeds upper bound prediction	Red	Risk of progressive bearing failure – halt operations, allow consolidation, place lateral berm

7.3. Cyclic load treatments

Chapters 6.5 and 6.6 demonstrate cyclic load can effect different improvements dependent upon the levels of strain induced: at medium strains, an initially meta-stable micro-structure can be remediated but large strains are necessary to induce meaningful densification from consolidation. The type of treatment required and testing/monitoring necessary will depend upon the loads transported and time between vehicle passages for consolidation (Figure 7.2) but can also vary along the route with different soil types and strengths.

7.3.1. Alluvial silt: Stabilisation through medium-strain treatment

In cases where the maximum load causes liquefaction but only gradually after several cycles (e.g. results for Ψ = 0.96 in Chapter 6.2), the aim will be to avert liquefaction but not necessarily to densify the soil. Accordingly, operational risks in these circumstances are lower and monitoring requirements may be reduced (Figure 7.2). For the stresses associated with vehicle loads of 390 tonnes in Table 2.5 (3-9% effective overburden, i.e. just exceeding the liquefaction threshold at the top of the liquefiable stratum), a combination of pre-loading with smaller vehicles (e.g. 200-300 tonnes, similarly to tests in Chapter 6.5.2) and rest periods between heavier vehicles (as per results in Chapter 6.6.1) is expected to produce stable strain response. Monitoring then only needs to confirm strain accumulation remains stable. The results in Chapter 6.6.1 indicate complete consolidation is not necessary for stabilisation and so monitoring of consolidation is of lesser importance if rest periods err on the side of caution.

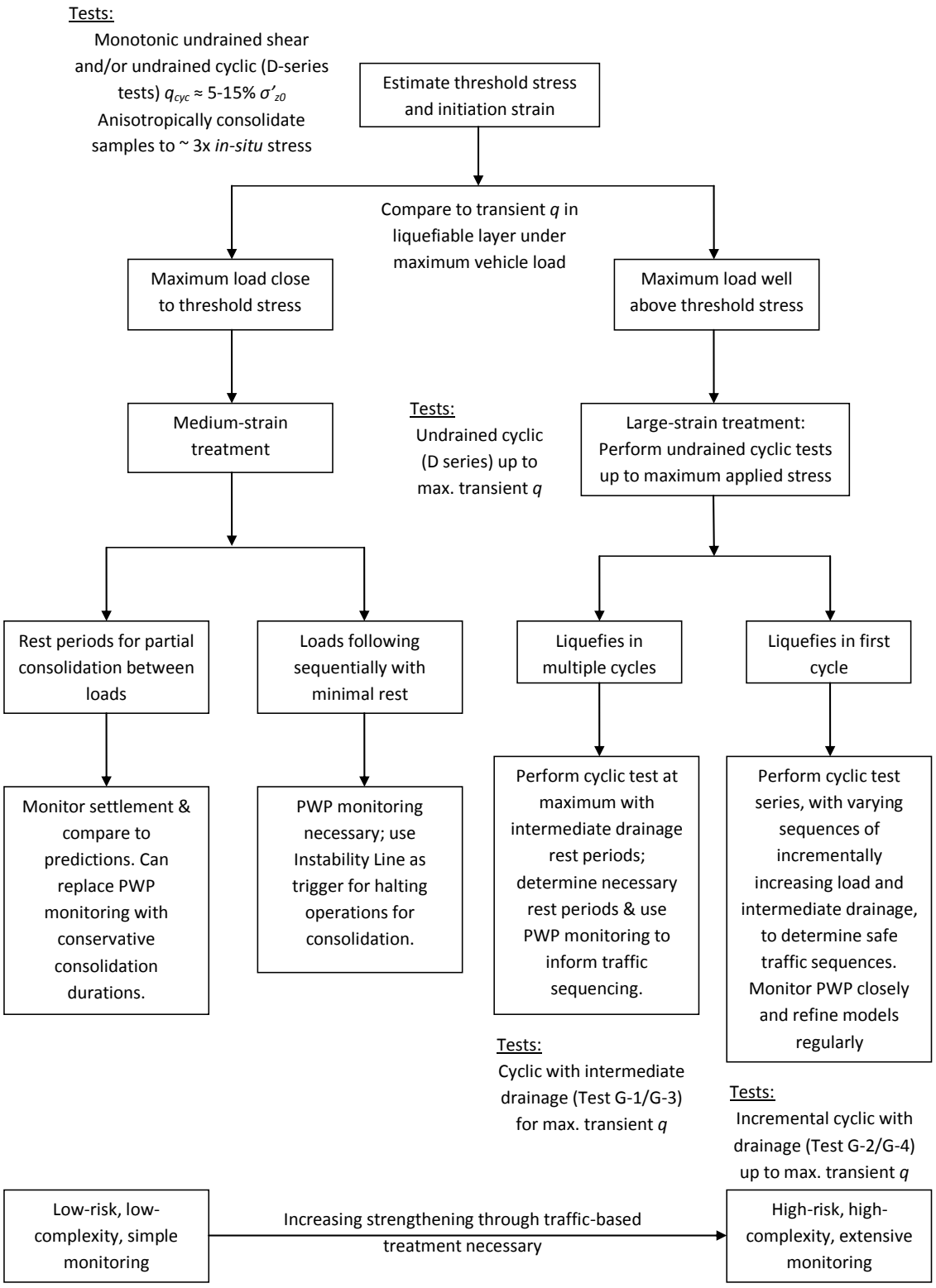

Figure 7.2: Simplified decision tree for selection of treatments and corresponding testing and monitoring requirements in meta-stable soil

For heavier vehicles (e.g. 1000 tonnes, applying transient stresses of 5-25% effective overburden), it will be necessary to take more care over the sequence of loads and work upwards to the maximum; there is also greater need for validation of medium-strain treatment. If logistics and programme permits, it will be highly beneficial to run a series of sub-liquefaction threshold loads until settlements indicate ε_{tl} is exceeded. These loads should be applied using vehicles of similar size to heavy haul vehicles, carrying kentledge (e.g. earth, water, road materials). This cautious approach reduces the need to monitor consolidation; undrained tests in these circumstances (D-3/D-7/F-5/G-2) remained stable. For treatment of the uppermost liquefiable strata it is recommended to provide rest periods for at least partial consolidation before incrementing; Tests G-4 and G-5 (Chapter 6.6.3) indicate it is possible for the Silt Mix soil to resist super-threshold stresses in a stable manner through gradual load incrementing and partial consolidation rest periods (up to 19-22% of effective overburden with approximately 2% cumulative strain). Tests G-3 and G-4 (Chapter 6.6.1) indicate it is possible to stabilise a test which liquefies in the second cycle using a short intermediate drainage interval after the first cycle. However, bearing in mind the uncertainties of estimating liquefaction thresholds in the field and the catastrophic ground movements associated with overload, applying such loads without first using gentler loads for conditioning is not recommended.

If possible, super-threshold stress loads should be transited cautiously, allowing time for partial consolidation between passages until settlements associated with recovery strains are reached. As a rough guide, based on scaling up experimental consolidation of the Silt Mix soil results from Chapter 6.1.2 to a 3m thick layer, 18 hour rest periods

should achieve sufficient partial consolidation for stabilisation, although clearly the efficacy of partial consolidation on averting liquefaction needs to be experimentally confirmed for a wider range of soils to be applicable generally. Based on experimental results in Chapters 6.2.1, 6.5.2 and 6.5.3, and findings in the literature (Chapter 2; Wang et al., 2014; Yamamuro and Lade, 1999) medium-strain treatment on silty soils can be expected to require strains of 0.3% to 1.0% to be effective, i.e. exceed ε_{tl}.

If project logistics demand an accelerated programme with little time for gentle pre-loading, the greater risks implied require a better understanding of the ground, which can be achieved by monitoring in-situ pore water pressures. The Instability Line provides a useful (and conservative) limit for pore water pressures (as done by Peck, 1969, for Saturn rockets); liquefaction cannot progress, even in undrained conditions, in these stress states.

The medium-strain options are expected to be the most attractive to a contractor: monitoring is simple but controls residual risk. The relevant soil properties, i.e. the liquefaction threshold stress and threshold strains (ε_{tv} and ε_{tl}) can be estimated from monotonic tests (Chapter 6.2) and the literature (e.g. Díaz-Rodriguez, and López-Molina, 2008) or more accurately determined via a series of simple undrained cyclic tests (Series D tests in Chapter 5.4). However there may be certain circumstances where very large modules cannot be sub-divided and the additional cost of testing and monitoring is favourable in comparison to the cost of additional fill for a conventional (stress-limiting) design. Additional strength from large-strain (consolidation) treatment

will need to be mobilised, requiring a site-specific understanding of the soil's response to large-strain cyclic load and consolidation.

7.3.2. Alluvial silt: Strengthening through large-strain treatment

If loads well in excess of the liquefaction threshold (e.g. 2000-3000 tonne loads, applying transient stresses of 9-45% and 15-75% effective overburden in Table 2.5 respectively), possibly even exceeding the ultimate strength, are expected, greater risk is introduced. Regularly-spaced piezometers are recommended in areas of liquefiable soil subject to large-strain treatment; accumulation and dissipation of pore water pressures are critical to the evolution of risk (Chapter 6.6.3; Peck, 1969). Strain measurement alone is unlikely to be sufficient; the relationship between pore water pressure and strain during large-strain treatment also depends upon consolidation. In the case of 3000 tonne loads particularly, it is expected that very large localised strain will occur at the top of the normally consolidated stratum: test G-2 experienced a maximum cyclic stress of 59% of the effective overburden stress and final ε_{pl} = 9.6% (Chapter 6.6.3). Such strains present a high residual risk of brittle shear band failure (from induced overconsolidation); adding 1-2m additional earthwork height in the worst-case locations (i.e. the softest ground, with the liquefiable deposits closest to surface) to further distribute transient stresses may be preferable.

It is recommended that large-strain treatment is only applied once medium-strain treatment has achieved full stability, i.e. reached recovery strains, > 1.5% in this study, 3-6% from other studies of silty soils (Yamamuro and Lade, 1999; Wang and Luna, 2012). Test G-2 (Chapter 6.6.3) demonstrates that incrementing load before recovery strains are reached can induce liquefaction, even if medium-strain treatment has

achieved stability under lower loads. If logistics dictates this is not possible, increases in load should be as gradual as possible and incorporate rest periods before and after. In-depth laboratory testing for areas requiring large-strain improvement is recommended (Figure 7.2).

Large-strain improvement is much more dependent upon full consolidation as the stress state, rather than the initial fabric, increasingly governs behaviour. There may be significant programme benefits from installing vertical wick drains in large-strain treatment areas to accelerate consolidation.

7.3.3. Commentary on application of treatment to clay

Although only a minor part of the testing, experiments on clay soil have highlighted significant differences in transient load response to silts (corroborated in the literature). Firstly, clays tend to require larger strains to achieve similar micro-structural changes but also produce a much stiffer response under transient load. Secondly, significantly lower permeability greatly extends rest durations necessary for consolidation. Thirdly, the increased plasticity tends to reduce liquefiability (with the exception of quick clays mentioned previously) and as such, medium-strain cyclic load treatment is not effective in providing improvement. Gradual softening and settlement, rather than catastrophic sudden collapse, is thus the principal hazard for clays.

As clays accumulate strain and soften more gradually under transient loads, and can withstand a limited number of cyclic loads above their static strength (see Chapter 6.7), clays present lower risk; testing/monitoring requirements may be reduced,

depending on the load magnitude, acceptable settlements (Figure 7.3) and available consolidation time. Test CL-7 indicates partial consolidation can be effective in reducing plastic strain rates at low cumulative strains.

When significant large-strain consolidation strengthening is required, monitoring of pore water pressures is of increased value. As stated previously, loads should be incremented as gradually as possible, with consolidation periods before and after the first passage of a new maximum load; tests CL-6 and CL-7 (Chapter 6.7) demonstrate it is still possible to induce large and rapid strains in clays if overload occurs. As greater strains may be required to achieve necessary strengthening, more road re-profiling must be anticipated.

The combination of lower permeability, larger strains necessary and the dependence of large-strain behaviour on the effective stress state, will mean large-strain improvements are slow to develop in clays. Where increases in strength are necessary for safe operation, vertical wick drains should be seriously considered; full consolidation without them may take several weeks. In such cases it is also important to obtain representative in-situ permeability estimates rather than rely on laboratory data, particularly in alluvial clays; varying river speeds change the type of sediment deposition (Waltham, 2002) and lenses and bands of sand in such soils are common. If these layers are able to transmit water perpendicularly away from the line of the road rapidly, effective layer thicknesses may be significantly reduced and consolidation accelerated by orders of magnitude compared to a homogeneous deposit, meaning wick drains are in fact not necessary.

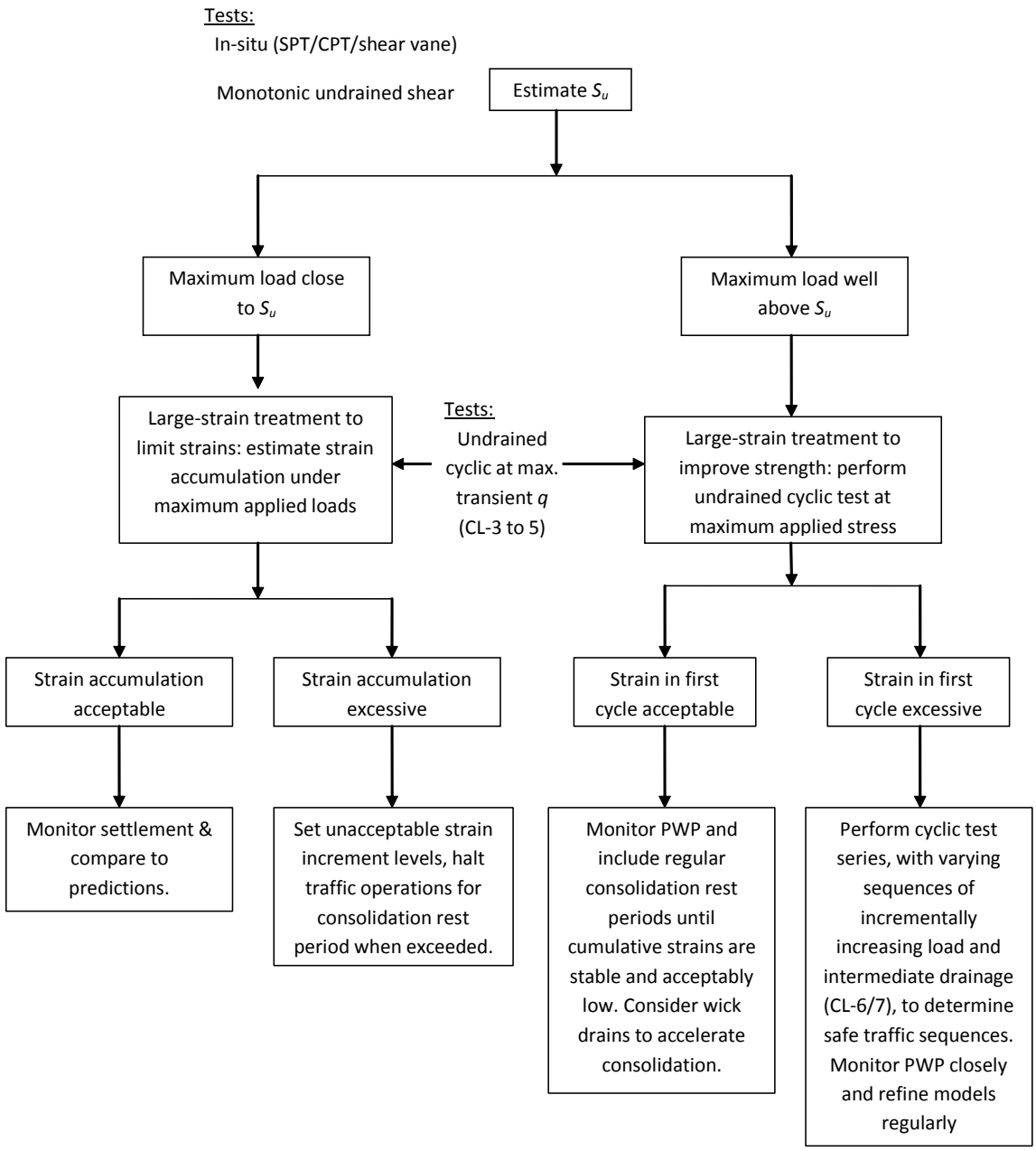

Figure 7.3: Simplified decision tree for selection of treatments and corresponding testing and monitoring requirements in stable (clay) soil

7.3.4. Commentary on treatment of cemented or bonded soils

The samples tested in this study are, by virtue of slurry consolidation, 'young' and expected to be uncemented. In the field, meta-stable soils may have tension-transmitting inter-particle connections (e.g. cementation or water suction from partial saturation). This could cause initially stiffer behaviour and a higher ε_{tv} (i.e. a greater

elastic strain range), but ultimately could be more brittle, with a greater strength drop when these bonds are broken, as in research by Lunne et al. (2006). Cyclic load treatments may be applicable to these soils, however the strain range for effective and safe treatment ($<\varepsilon_{tl}$ and $>\varepsilon_{tv}$) may be much narrower. Collapse risk levels are higher; investigation, monitoring and cautious operation will all need to reflect this. Reconstituted samples will not behave in the same way as cemented/bonded in-situ soils and high-quality sample recovery may be necessary.

7.3.5. Risk map example

To aid visualisation of how cyclic load treatment might be applied over a heavy haul route comprising various ground conditions, an example geotechnical risk map sketch is provided (Figure 7.4).

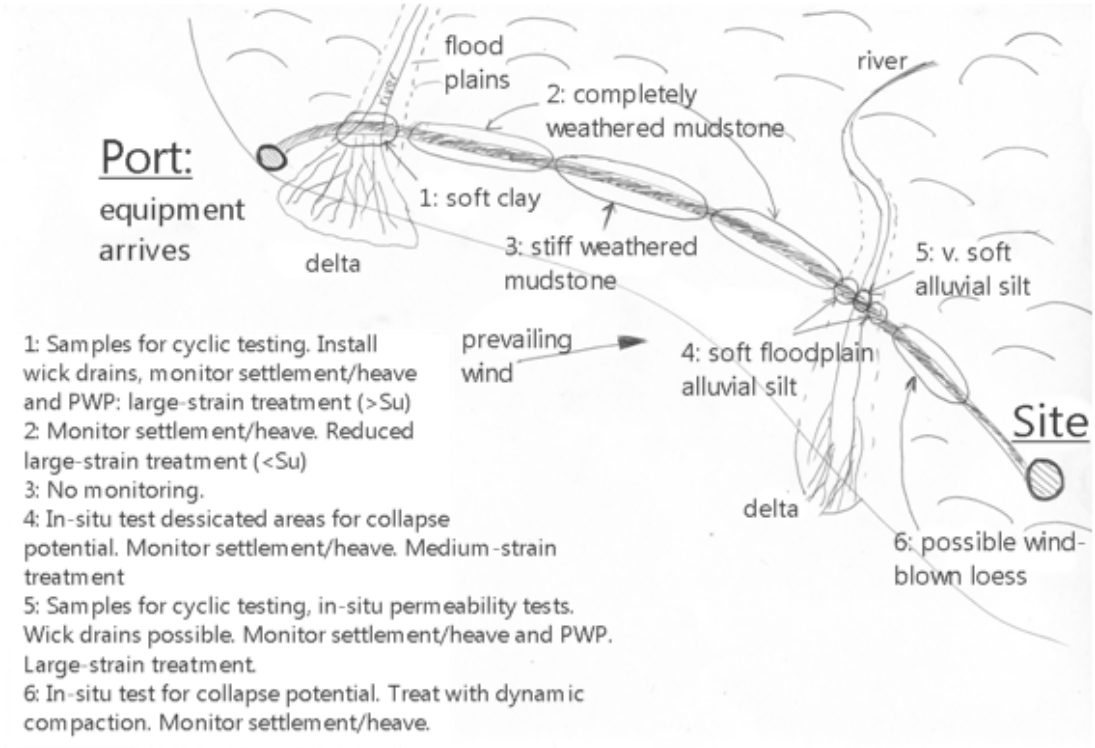

Figure 7.4: Example of a geotechnical risk map outlining requirements for investigation, testing, monitoring and cyclic load treatments for different areas and geohazards.

7.4. Conclusions

Using heavy haul traffic to improve the ground, in lieu of more expensive earthworks or ground improvement options, has potential to reduce fill quantities by a factor of two or more (i.e. from a 3.5-5.5m to a 1.5-2.5m earthwork; see Chapters 2.5, 3.3.1 and 7.3). The associated reduction in access works costs, particularly in areas where transportation of large fill quantities is difficult, could allow modular construction to reach a wider range of sites. Instead of building large earthworks to 'cushion' the problematic sub-soil, an observational design approach is proposed which allows reduced road construction depths and adapts to conditions as they develop on site, to accumulate strength in the sub-soil from cumulative passes of large, heavy vehicles.

As the size of the vehicle determines the stress bulb size, ground investigation must consider deep soils, similar to the approach for large shallow foundations. Similarly, cyclic load treatment must use the same large vehicles (possibly carrying smaller loads) to induce strains over the same stress bulb.

Ground investigation, sampling for laboratory testing and in-situ monitoring need to be targeted on problem areas, identified during a thorough desk study, where the greatest strength improvements are necessary for safe operation under maximum loads, i.e. areas of soft or collapsible soils. It may be necessary to recover samples for in-depth laboratory testing and install sophisticated instruments for monitoring, such as vibrating wire piezometers, to provide a risk-managed strategy for strengthening without catastrophic ground movement.

Liquefiable silts, studied in detail herein, are considered the worst-case scenario as they combine 'sand-like' liquefiable behaviour with sufficiently low permeability to remain undrained under slow application of heavy haul traffic load. Treatment for these soils depends on the improvement necessary for safe operation and can be subdivided into medium-strain and large-strain, the former remoulding liquefiable fabric gently until it is stable and the latter effecting greater strength improvements through large strains and consolidation. Testing for the former may simply incorporate anisotropically consolidated monotonic tests, to estimate stresses and strains which trigger liquefaction; for the latter a series of cyclic tests to determine stable sequences of cyclic load, cumulative plastic strain and consolidation intervals may be required. Medium-strain treatment is expected to present an optimal balance of improved subgrade strength and simple testing and monitoring, whilst covering a good range of vehicle weights (i.e. up to 1000 tonnes, based on Chapters 2.5, 6.5 and 6.6). For the heaviest loads, savings on earthworks quantities may justify the extensive testing and monitoring required for large-strain treatment. In both cases, the improved control of residual risk from *in-situ* monitoring may make an observational design more attractive even if there is no cost benefit.

Pore water pressure monitoring is expected to provide better data resolution on soil behaviour at medium strains and during consolidation, but is likely to be more expensive than settlement monitoring and only representative of a point (or small area). A combination of the two methods, with piezometers clustered in problem areas and settlement measured on a wide grid, is recommended for optimal value and understanding of risk. As strain and excess pore water pressure have common

relationships in the soils tested, monitoring both properties allows cross-checks between data sets.

Dilatant strength in the field is unreliable, particularly considering the more complex stress conditions encountered and potential for movement of pore water through localised bands/lenses/fissures. Gradual improvement as opposed to rapid straining and consolidation is recommended; although the latter achieves high strengths in the laboratory, it retains dilatant behaviour and is at greater risk of brittle shear banding.

Bearing in mind the influence of sample disturbance on liquefiable soils particularly, samples for testing must be either of very good quality (e.g. Sherbrooke block samples) or reconstituted from bulk soil slurry to provide an approximation of 'young' soil behaviour without ageing or bonding. Cemented/bonded soils may have a narrower 'safe strain range' between elastic behaviour and liquefaction (0.01% to 0.3% in the Silt mix soil) and cyclic load treatment could be harder to effect safely: this behaviour must be assessed by testing high-quality in-situ samples.

Clay soils tend not to liquefy as silts do, but instead progressively soften. Clays are expected to require greater strains to effect similar levels of treatment and undergo consolidation much more slowly. The risk of ongoing settlement and associated maintenance must be considered; wick drains to accelerate consolidation in clays may be valuable from a programme perspective.

CHAPTER 8: CONCLUSIONS

This study has combined finite element modelling, a systematic literature review and experimental testing of a liquefiable silty soil (the Silt Mix soil, as defined in Chapter 4.1.1) in order to investigate how deep, normally consolidated deposits respond to unusually large (1000 to 3000 tonnes) heavy haul vehicle loads, and how these large loads can be used to strengthen this soil. Comparison to experiments on English China Clay is also included to highlight the influence of the silt's meta-stability. Recommendations have been made on how experimentally identified phenomena can be used to improve road design efficiency and control residual risk through an observational approach. The Aims and Objective of this study, stated in Chapter 1.3, have therefore been met.

A completely new approach for the design and operation of temporary heavy haul road foundations is possible; in fact, along routes where poor ground is encountered frequently, this approach may be necessary for modularised construction projects to be economically feasible. Formerly, this infrastructure would be designed to limit strains in problematic soil, requiring either deep ground improvement or substantial earthworks (up to 5m high) to spread the load. This foundation design approach would achieve, from the start of traffic operations, the strength necessary to support the maximum loads with minimal strength degradation. Such excessive robustness is difficult to justify economically for a temporary asset.

This study has demonstrated that heavy haul road foundations do not necessarily have to be designed to protect the soil in its initial condition from degradation under the

maximum traffic load. If carefully managed, the action of smaller repeated traffic loads can stabilise a meta-stable soil, whilst rest periods for consolidation between loads can improve shear strength during use; the necessary strength is gradually achieved. Unlike permanent road foundations, plastic yield does not need to be kept to minimal levels through use of deeper or more robust foundations; this plasticity can be used to rearrange the soil fabric and provide increased resistance to plastic deformation. Surface reprofiling will be necessary to maintain alignment. In-situ monitoring to estimate induced changes to the soil and warn of unacceptable failure risk levels is necessary as part of such treatment.

The consideration of behaviour of saturated, anisotropically normally consolidated and potentially liquefiable soil in pavement engineering is entirely new to the field. Whilst similar phenomena have been investigated experimentally in earthquake and foundation engineering, the unusual circumstances of temporary heavy haul roads, i.e. short design life, tolerance of large strain and potential for consolidation rest periods between loads, have required experimental testing to determine the influence of these factors and to develop guidelines for how phenomena identified could form a novel approach for using cyclic load to strengthen poor soil.

The central findings relevant to this new method which this study has revealed are summarised in Figure 8.1 and described below:

1. Deep soils must be considered

The scale of loading from multi-wheeled heavy haul vehicles is important: modelling in Chapter 2 shows interaction between multiple wheels stresses deep, normally consolidated deposits in the compression zone which are more prone to localised large-strain yielding, even at low utilisation. Deep soils, particularly soft silts and loose silty sands, carry a risk of catastrophic meta-stable liquefaction which overconsolidated surface soils do not (Chapter 6.5.1; Wang and Luna, 2012); the larger stress bulb therefore increases liquefaction risk. Deep investigation is therefore a necessity for heavy haul road projects.

2. Liquefaction is dependent upon disruption of a meta-stable fabric in unstable conditions

Undrained cyclic and static tests (Chapter 6.2) indicate initiation of meta-stable liquefaction under cyclic load requires the threshold stress and initiation strain to be simultaneously exceeded with no volume change permitted (i.e. undrained conditions). Meta-stable silts are thus at higher-risk than sands due to their lower permeability. As cyclic pore water pressures (i.e. soil skeleton contraction) and cumulative strains are found to be strongly linked in undrained conditions, inducing sufficient strain and corresponding pore pressure to cross the Instability Line, as described by Lade (1994), results in liquefaction if the conditions above are violated, but remains stable if not. Cyclic tests also indicate rearrangement of the initially meta-stable fabric through plastic strain can stabilise a liquefiable soil. Conversely, experimental testing must take care to retain meta-stable soil fabric by

minimising disturbance of samples; disturbance can fundamentally change soil response to load (Chapter 6.1.3) and may dangerously underestimate liquefiability. Reconstitution from slurry (Chapter 4.1.2.2) may be effective in replicating 'young', uncemented soils but cemented soils carry very different risks which may require high-quality in-situ sampling (e.g. Sherbrooke block sampling) to fully understand.

3. Soil response to load varies depending on levels of strain experienced

Localised yielding and large strains in deep normally consolidated deposits results in very different behaviour to surface soils subject to conventional traffic loading (predominantly small to medium-strain). The degree of relative inter-particle movement, as described by strain thresholds, governs macro-behaviour. Emergent phenomena of elasticity and plasticity, stability and liquefaction, and dilatant flow thus arise. Controlled medium-strain accumulation is key to achieving stability; cyclic load tests (Chapter 6.5.2) suggest a 'safe strain range' whereby cyclic strains are sufficient to remould a meta-stable fabric but insufficient to trigger liquefaction. In the plastic (medium to large-strain) region, the Silt Mix soil displays some sensitivity to changes in load frequency and duration (Chapter 6.4). Frequency-dependence in clay (Chapter 6.7) is much stronger.

The stress state is found to govern soil response in the large-strain (fully remoulded) regime. During cyclic loading, overconsolidation induced by rising pore water pressures changes the soil behaviour. Post-cyclic static shear tests (Chapter 6.5.2) show the tendency to contract in shear to be reduced but the risk of brittleness and shear banding failure increased. Dilatancy is found to be a large

component of ultimate strength in silt soils particularly, however complex stress fields and heterogeneous site soils are likely to increase the risk of brittle failure and caution against relying on dilatant strength is advised.

A thermodynamic treatment of soil (Edwards et al., 2004; Blumenfeld, 2010) suggests a mechanism for cyclic stabilisation: the initially precariously arranged particles, once liberated by medium-strain plasticity, seek out a denser configuration. Gradual particle liberation and restructuring under gentle repeat loads, rather than simultaneous liberation under higher load, may be the reason the Instability Line can be crossed in these conditions without liquefaction; insufficient work is done in any cycle to start a chain reaction collapse. Faster, higher-frequency loading, which applies work to the sample at a higher rate, may be more damaging, although this remains to be confirmed.

4. Problematic soils can be strengthened by traffic loading, followed by consolidation: greater straining achieves greater strengthening but requires more intense engineering scrutiny

Medium-strain fabric rearrangement in stable circumstances, by sub-threshold cyclic loading or permitting consolidation rest periods, can remove the initially meta-stable structure (Chapters 6.5.2 and 6.6.1). Medium-strain treatment is only applicable to meta-stable soils and results in negligible reduction in void ratio; large-strain rearrangement is necessary to cause noticeable strength improvement through consolidation (Chapter 6.6.3; Wang et al., 2014). Plastic clays may require greater strains to achieve similar levels of consolidation strengthening to silts.

Cyclic tests with drainage rest periods (Chapters 6.6.2 and 6.6.3) show that the type of undrained straining experienced, i.e. medium-strain rearrangement or large-strain total restructuring, determines the volume change gradient (in *p'-e* space) in subsequent consolidation. Strengthening is thus greater but induced overconsolidation and brittleness are more fully retained following large strains. A gradual, cautious approach, particularly when load magnitudes are increased, is recommended to retain ductility in case of accidental overload.

The nature of the ground investigation, predictive modelling and monitoring during operations is likely to depend upon how much strengthening is required and how quickly. For significant consolidation strengthening, laboratory stress testing of soil samples, more advanced modelling and in-depth back-analysis of monitoring data, including pore water pressure monitoring, may be necessary. The effort expended in obtaining and testing representative samples for testing should also be proportional to the amount of strengthening desired. Different treatments may be necessary at different points along a route, with large-strain treatment and corresponding clustering of ground investigation and monitoring localised to 'problem areas'. Piezometers, whilst more expensive, are expected to provide better data resolution and information more fundamental to soil behaviour; a wide grid of settlement monitoring supplemented by piezometers in problem areas is considered optimal for risk management.

Figure 8.1: Mapping of chapter conclusions to key points of thesis conclusions

8.1. Further work

Using cyclic load to strengthen road foundations is currently at an embryonic stage and this study primarily presents a proof-of-concept rather than a complete theory which could be routinely used in practice. To advance this concept to something practically useful, the following is suggested:

Consideration of the complex real stress conditions: Assessing the simplest case of pure compression is a key limitation of results in Chapter 6; principal stress rotation is known to accelerate cyclic degradation and can worsen liquefiability but may also cause increased consolidation. Cyclic testing in direct shear, triaxial extension or Hollow Cylinder Apparatus could give insight into how the various 'zones' subject to different stresses behave under cyclic traffic load. However these tests are limited to a single non-interacting element. Model or even full-scale testing may provide more useful information on the response of a half-space to non-uniform stress field, how various zones interact, the effect of localised water flows between zones (particularly in relation to localised water-softening of dilatant zones) and the efficacy of cyclic load treatment on different zones subject to different actions.

Linking retained overconsolidation and consolidation strengthening: Consolidation rest periods appear to achieve smaller reductions in moisture content with each interval, i.e. strengthening may asymptotically reach a limit. Under higher loads, more volume change is apparent but more overconsolidation is retained; an inverse relationship between ductility and strengthening is implied. Further investigation of

these limits may inform engineers on the acceptable trade-off between these factors for reliable designs.

Linking partial consolidation and stability in meta-stable soil: Testing herein indicates partial consolidation is effective for medium-strain cyclic load treatment, even at relatively low proportions of full consolidation. Better quantification of exactly how much consolidation is necessary to avert liquefaction and the factors affecting this would be highly advantageous for efficient operation of heavy haul roads crossing meta-stable soils. This could be investigated through undrained cyclic triaxial testing with drainage between cycles, or even through tests with drainage permitted; varying the drainage length through side filter papers etc. would allow control of the degree of consolidation without requiring changes to cycle frequency and duration.

More representative pore pressure measurement: It was not possible to develop a method to measure mid-height pore pressures in the soft samples without inducing disturbance; for laboratory testing of site soils, determination of more representative pore pressures will be critical in accurately estimating strains and liquefaction risk from in-situ monitoring data. Mid-height pore pressure measurement will also allow better investigation of partial consolidation as discussed above. Development of such a pore pressure monitoring system will need to consider minimising the weight applied from the probe to the sample whilst remaining able to move freely under large strains.

Testing a wider range of soils: Principles developed here strictly only apply to the soils tested, i.e. very young, normally consolidated and uncemented soils. The Silt Mix soil used is also noted to be relatively clayey compared to many silts studied in the

literature and this may be the reason for its more stable response, i.e. not liquefying from an isotropically consolidated state, and indeed the reason for it stabilising under cyclic load treatment. Applying similar tests to a range of silts and silty sands would provide more confidence that cyclic load treatment can be applied successfully on a range of projects. Testing cemented/bonded meta-stable soils will also be particularly valuable; it is expected these soils will have a narrower 'safe strain range' between initiation of plasticity and collapse; these potentially present a greater hazard to heavy haul routes. Similarly, the correspondence between the static pre-liquefaction peak stress and threshold stress should be investigated in other meta-stable soils; this could provide a useful approximation in practice and reduce dependence on laboratory testing. Development of straightforward sample preparation and consolidation procedures to allow testing on normally consolidated site-derived samples at lower consolidation stresses, which may develop lower post-liquefaction strength and thus be a better descriptor of the *in-situ* behaviour is also recommended.

Reproduction of experiments in DEM (Discrete Element Modelling) : This study has used findings from DEM modelling (Chapters 3.1.3 and 3.3.2) to construct a theoretical framework to explain experimental results; by simulating these tests in DEM, whereby individual particle energies can be tracked, assertions made herein on mechanisms controlling cyclic liquefaction and stabilisation can be tested. This work could also lead to a thermodynamics and energy-led analytical framework which may be more successful in describing how and when cyclic load can stabilise a meta-stable soil. Similarly, DEM simulation may provide insight into how the increasing elastic strain

range develops under cyclic load and provide predictions of strains necessary to achieve resilient conditions.

Whilst this study concentrates on a highly specialist area, there may be applications for the findings in other fields. Minimising construction work on temporary foundations, instead strengthening them in service through monitored loading and consolidation, may be beneficial for temporary crane foundations, spudcans for jack-up offshore rigs and piling platforms for bridge construction, for example. A modified form of cyclic loading, e.g. low frequency vibration, may be viable as a means for treating meta-stable slopes at risk of flowslide.

REFERENCES

Åhnberg, H., and Larsson, R. (2012). *Strength degradation of clay due to cyclic loadings and enforced deformation.* Swedish Geotechnical Institute Report No. 75, Swedish Geotechnical Institute, Linkoping.

Amini, F., Qi, G. Z. (2000). *Liquefaction testing of stratified silty sands.* ASCE Journal of Geotechnical and Geoenvironmental Engineering 126(3), 208-217.

Anandarajah, A. (2000). *On influence of fabric anisotropy on the stress/strain behavior of clays.* Computers and Geotechnics 27: 1-17.

Andersen, K. H. (2009). *Bearing capacity under cyclic loading - offshore, along the coast and on land*. The 21st Bjerrum Lecture presented in Oslo, 23 November 2007. Canadian Geotechnical Journal, 46(5): 513-535.

Andersen, K. H., Kleven, A., and Heien, D. (1988). *Cyclic Soil Data for Design of Gravity Structures.* ASCE Journal of Geotechnical Engineering, 114(5): 517–539.

Andrews, D. C. A., Martin, G. R. (2000). *Criteria for Liquefaction of Silty Soils*. Proceedings of 12th World Conference on Earthquake Engineering, Auckland, New Zealand, 30th January - 4th February 2000.

Arthur, J. R., Rodriguez, J. I., Dunstan, T., and Chua, K. S. (1980). *Principal Stress Rotation: A Missing Parameter*. ASCE Journal of the Geotechnical Engineering Division 106(4): 419-433.

Assallay, A.M., Rogers, C.D.F., Smalley, I.J., Jefferson, I.F. (1998). *Silt: 2–62 μm, 9–4φ.* Earth-Science Reviews Volume 45, Issues 1–2, November 1998, Pages 61-88

Atkinson, J. H. (2000). *Non-linear soil stiffness in routine design*. Geotechnique 50(5), 487-508.

Atkinson, J. H. (2007). *The mechanics of soils and foundations* (2nd Ed). Taylor and Francis.

Barnes, G. (2000). Soil mechanics: principles and practice (2nd Ed.). Palgrave Macmillan, London.

Been, K., Jefferies, M.G. (1985). *A state parameter for sand*. Geotechnique 35(2), 99-122.

Bell, F. G. (2007). *Engineering Geology (2nd Ed)*. Elsevier Science, Oxford, UK. ISBN 9780750680776

Berardi, R., Lancellotta, R. (2002). *Yielding from Field Behaviour and its Influence on Oil Tank Settlements*. ASCE Journal of Geotechnical and Geoenvironmental Engineering 128(5) 404-415.

Bishop, A.W., Green, G.E. (1965). *The influence of end restraint on the compression strength of a cohesionless soil.* Géotechnique, 15(3): 243-266.

Blumenfeld, R. (2010). *Stress transmission and incipient yield flow in dense granular materials.* AIP Conference Proceedings 1227, 167.

Boulanger, R.W., Idriss, I. M. (2006). *Evaluating the Potential for Liquefaction of Cyclic Failure of Silts and Clays*. Report No. UCD/CGM-04/01. . University of California at Davis.

Boulbibane, M., Collins, I.F., Ponter, A.R.S., Weichert, D. (2005). *Shakedown of Unbound Pavements*. Road Materials and Pavement Design, 6(1): 81-96.

Bradshaw, A. S., Baxter, C. D. P. (2007). *Sample Preparation of Silts for Liquefaction testing.* Geotechnical Testing Journal 30(4), Paper ID GTJ00206.

Brinch Hansen, J. (1970). *A revised and extended formula for bearing capacity*. Bulletin No. 28, Danish Geotechnical Institute: 5-11.

Brooker, E.W., Ireland, H.O. (1965). *Earth pressures at rest related to stress history*. Canadian Geotechnical Journal 2(1): 1-15.

Brown, S. F. (1996). *Soil mechanics in pavement engineering*. Geotechnique 46(3): 383-426.

Brown, S. F. (2004). *Application of Soil Mechanics Principles to Design and Testing of Pavement Foundations*. Proceedings of the 8th Conference on Asphalt Pavements for Southern Africa. Sun City, South Africa.

Brown, S. F., Andersen, K. H., and McElvaney, J. (1977). *The Effect of Drainage on Cyclic Loading of Clay*. In Proceedings of the 9th International Conference of Soil Mechanics and Foundation Engineering, Tokyo, July 11-15 July 1977, pp. 195-200.

Brown, S. F., Lashine, A. K. F., and Hyde, A. F. L. (1975). *Repeated load triaxial testing of a silty clay*. Geotechnique 25(1): 95-114.

Brown, S. F., Selig, E. T. (1991). *The design of pavement and rail track foundations.* Cyclic Loading of Soils: from theory to design, Ed. M. P. O'Reilly, S. F. Brown, pp 249-305 ISBN 0216928982. Blackie and Son Ltd, Glasgow and London.

BSI (British Standards Institution) (2015a). *BS 8002:2015 - Code of practice for earth retaining structures*. BSI, London, UK.

BSI (British Standards Institution). (1986). *BS 8004:1986 Code of practice for foundations.*

BSI (British Standards Institution). (1990a). *BS 1377-2:1990 - Methods of test for soils for civil engineering purposes — Part 2: Classification tests*

BSI (British Standards Institution). (1990b). *BS 1377-2:1990 - Methods of test for soils for civil engineering purposes — Part 4: Compaction-related tests*

BSI (British Standards Institution). (2015b). *BS 5930:2015 - Code of practice for ground investigations*.

Burd, H.J., Frydman, S. (1997). *Bearing capacity of plane-strain footings on layered soils.* Canadian Geotechnical Journal, 34: 241-253. NRC Canada.

Carter, J.P., Booker, J. R., Wroth, C. P. (1982). *A Critical State Soil Model for Cyclic Loading.* In Soil Mechanics - Transient and Cyclic Loads, Edited by G. N. Pande & O. C. Zienkiewicz. John Wiley & Sons Ltd. pp 219-252.

Chu, J., Wanatowski, D., Leong, W. K., Loke, W. L., He, J. (2015). *Instability of dilative sand.* Geotechnical Research 2 (1), 35-48.

Collins, K., McGown, A. (1974). *The form and function of microfabric features in a variety of natural soils*. Geotechnique 24(2), 223-254.

Cronin, B. (2015). *Prefab Progression.* New Civil Engineer 10.09.15: 28-30.

D'Appolonia, D. J., Poulos H. G., and Ladd C. C. (1971). *Initial Settlement of Structures on Clay*. ASCE Journal of the Soil Mechanics and Foundations Division 97(10): 1359-1377.

Davis, E. H., and Poulos, H. G. (1972). *Rate of settlement under two-and three dimensional conditions*. Geotechnique 22(1): 95-114.

Dewhurst, D. N., Brown, K. M., Clennell, M. B., Westbrook, G. K. (1996). *A comparison of the fabric and permeability anisotropy of consolidated and sheared silty clay*. Engineering Geology 42: 253-267.

Díaz-Rodriguez, J. A., López-Molina, J. A. (2008). *Strain thresholds in soil dynamics.* 14th World Conference on Earthquake Engineering. October 12-17th 2008, Beijing, China.

Díaz-Rodríguez, J. A., Santamarina, J. C. (2001). *Mexico city soil behavior at different strains:Observations and physical interpretation.* Journal of Geotechnical and Geoenvironmental Engineering 127 (9).

Doanh, T., Finge, Z., and Boucq, S. (2012). *Effects of Previous Deviatoric Strain Histories on the Undrained Behaviour of Hostun RF Loose Sand*. ASCE Journal of Geotechnical and Geological Engineering 30: 697-712.

Edwards, S. F., Brujić, J., Makse, H. A. (2004). *A basis for the statistical mechanics of granular systems*. Unifying concepts in Granular Media and Glasses. Elsevier, Amserdam.

Erken, A., Ulker, B. M. C. (2007). *Effect of cyclic loading on monotonic shear strength of fine-grained soils*. Engineering Geology 89: 243–257.

Evans, R.D., Jefferson, I., Northmore, K. J., Synac, O., Serridge, C. J. (2004) *Geophysical Investigation and Treatment of Collapsible Soils.* In ASCE GSP 126: Geotechnical Engineering for Transportation Projects 2004 p.1848 - 1857

Foye, K.C., Basu, P., Prezzi, M. (2008). *Immediate Settlement of Shallow Foundations Bearing on Clay*. ASCE International Journal of Geomechanics 8(5): 300-310

Frost, M. W. (2000). *The performance of pavement foundations during construction.* Loughborough University.

Frost, M.W, Fleming, P.R, and Rogers, C. D. F. (2004). *Cyclic triaxial tests on clay subgrades for analytical pavement design.* ASCE Journal of Transportation Engineering 130(3): 378-386.

Gong G. (2008). *DEM Simulations of Drained and Undrained Behaviour*. Ph.D thesis, University of Birmingham Department of Civil Engineering, Birmingham, U.K.

Gräbe, P. J., and Clayton, C. R. I. (2009). *Effects of Principal Stress Rotation on Permanent Deformation in Rail Track Foundations.* ASCE Journal of Geotechnical and Geoenvironmental Engineering 135(4) pp.555-566.

Gratchev, I. B., Sassa, K., Osipov, V. I., and Sokolov, V. N. (2006). *The liquefaction of clayey soils under cyclic loading*. Engineering Geology 86: 70-84.

Greeuw, G., den Adel, H., Chapers, A. L., den Haan, E. J. (2000). *Reduction of Axial Resistance Due to Membrane and Side Drains in The Triaxial Test.* Soft Ground Technology Conference GSP 112, Noordwijkerhout, the Netherlands May 28 - June 2, 2000.

Gu, X., Huang, M. Qian, J. (2014). *DEM investigation on the evolution of microstructure in granular soils under shearing.* Granular Matter 16, 91-106.

Head, K. H. (1986). *Manual of Soil Laboratory Testing Volume 3: Effective Stress Tests.* ELE International Ltd. Pentech Press, London.

Heath, D. L., Shenton, M. J., Sparrow, R. W., Waters, J. M. (1972). *Design of Conventional Rail Track Foundations.* ICE Proceedings 51(2): 251-267.

Houlsby G.T., Burd H. (1999). *Understanding the behaviour of unpaved roads on soft clay.* In Proceedings of the 12th European Conference on Soil Mechanics and Foundation Engineering, Amsterdam, June 1999, 31-44.

Hsu, C., Vucetic, M. (2006). *Threshold shear strain for cyclic pore water pressure in cohesive soils*. ASCE Journal of Geotechnical and Geoenvironmental Engineering 132: 1325-1335.

Hu, M., O'Sullivan, C., Jardine, R.R., Jiang, M. (2010). *Stress-induced anisotropy in sand under cyclic loading*. Granular Matter 12, 369-476. Springer-Verlag.

Hyde, A. F. L. (1974). *Repeated load triaxial testing of soils*. PhD thesis, University of Nottingham Department of Civil Engineering, Nottingham. U.K.

Ishihara, K., Towhata, I. (1982). *Dynamic Response Analysis of Level Ground based on the Effective Stress Method In Soil Mechanics.* In Transient and Cyclic Loads, Edited by G. N. Pande & O. C. Zienkiewicz. John Wiley & Sons Ltd. pp 133-172.

Ismail Ibrahim, K.M.H. (2016). *Bearing capacity of circular footing resting on granular soil overlying soft clay*. HBRC Journal 12(1):71-77

Jaky J. (1948). *Pressure in silos*. In Proceedings of the 2nd International Conference in Soil Mechanics and Foundation Engineering, Rotterdam.

Jamiolkowski M., Lancellotta R., Pasqualini E., Marchetti S., Nova R. (1979). *Design Parameters for Soft Clays*. General Report, In Proceedings of the 7th European Conference on Soil Mechanics and Foundation Engineering 1: 103-107.

Jefferies M., Shuttle D., Been K. (2015). *Principal stress rotation as cause of cyclic mobility.* Geotechnical Research 2(2): 66-96.

Joseph, P. G. (2014). *Viscosity and secondary consolidation in one-dimensional loading*. Geotechnical Research 1 (3), 90-98.

Juspi, S. (2007). *Experimental Validation of the Shakedown Concept for Pavement Analysis and Design* (PhD thesis). University of Nottingham, UK.

Kirkpatrick, W. M., Belshaw, D. J. (1968). *On the Interpretation of the Triaxial Test.* Geotechnique 18: 336-350.

Kirkpatrick, W. M., Rennie, I. A. (1972). *Directional properties of consolidated Kaolin.* Geotechnique 22(1), 166-169.

Knodel, P. C., Kuerbis, R.H., Vaid, Y. P. (1990). *Corrections for Membrane Strength in the Triaxial Test*. Geotechnical Testing Journal 13(4): 361-369.

Krizek, R. J., Chawla, K. S., Edil, T. B. (1977). *Directional creep response of anisotropic clays.* Geotechnique 27(1), 37-51.

Kruyt, N. P. (2010). *Micromechanical study of plasticity of granular materials*. Comptes Rendus Mecanique 338, 596-603. Elsevier.

Kruyt, N.P., Rothenburg, L. (2006). *Shear strength, dilatancy, energy and dissipation in quasi-static deformation of granular materials*. Journal of Statistical Mechanics: Theory and Experiment. doi:10.1088/1742-5468/2006/07/P07021.

La Rochelle, P., Leroueil, S., Trak, B., Blais-Leroux, L., Tavenas, F. (1988). *Observational approach to membrane and area corrections in triaxial tests*. Advanced Triaxial Testing of Soil and Rock, ASTM STP 977: 715-731. ASTM, Philadelphia.

Ladd , C.C., Foott, R. (1977). *New design procedure for stability of soft clays.* Journal of the Geotechnical Engineering Division of the ASCE 100 (GT4): 763–779

Ladd, C.C., Foott, R., Ishihara, K., Poulos, H.G., Schlosser F (1977). *Stress-deformation and strength characteristics*. State Of The Art Report In Session 1, In Proceedings of the 11th International Conference on Soil Mechanics and Foundation Engineering, Tokyo.

Ladd, R. S. (1978). *Preparing test specimens using undercompaction*. Geotechnical Testing Journal 1(1), 16-23.

Lade, P. V. (1994). *Instability and Liquefaction of Granular Materials*. Computers and Geotechnics 16, 123-151. Elsevier.

Laman, M., Yildiz, A., Ornek, M., Demi,r A. (2012). *Field Test of Circular Footings on Reinforced Granular Fill Layer Overlying a Clay Bed*. Geotechincal Testing Journal 35 (4), Paper ID GTJ103512.

Lee, K. L. (1978). *End restraint effects on undrained static triaxial strength of sand*. Journal of the Geotechnical Engineering Division of the ASCE 104(GT6):687–704

Lee, K. L., Vernese, F. J. (1978). *End restraint effects on cyclic triaxial strength of sand.* Journal of the Geotechnical Engineering Division of the ASCE 104(GT6): 705–719

Levenburg, E., Garg, N. (2014). E*stimating the coefficient of at-rest earth pressure in granular pavement layers.* Transportation Geotechnics 1(1): 21-30

Li, L., Dan, H., Wang, L. (2011). *Undrained behavior of natural marine clay under cyclic loading*. Ocean Engineering 38, 1792-1805. Elsevier.

Li, S., Huang, M. (2010). *Undrained Long-Term Cyclic Degradation Characteristics of Offshore Soft Clay.* Soil Dynamics and Earthquake Engineering: Proceedings of sessions of GeoShanghai 2010; Shanghai, China, June 3-5, 2010.

Lin, H., Penumadu, D. (2005). *Experimental Investigation on Principal Stress Rotation in Kaolin Clay*. ASCE Journal of Geotechnical and Geoenvironmental Engineering 131(5), 633-642.

Little, P. H. (1992). *The design of unsurfaced roads using geosynthetics*. University of Nottingham Department of Civil Engineering.

Lunne, T., Berre T., Andersen, K. H., Strandvik S., Sjursen, M. (2006). *Effects of sample disturbance and consolidation procedures on measured shear strength of soft marine Norwegian clays*. Canadian Geotechnical Journal 43: 726-750.

Lunne, T., Berre, T., Strandvik, S. (1997) *Sample disturbance effects in soft low plastic Norwegian clay*. In Proceedings of the Conference on recent developments in soil and pavement mechanics, Rio de Janeiro, Brazil, 25-17 June 1997 pp. 81-102.

Madabhushi, S.S.C., Haigh, S.K. (2015). *Investigating the changing deformation mechanism beneath shallow foundations*. Géotechnique 65(8): 684–693

Maleki, M., Ezzarkhah, A., Bayat, M., Mousivand, M. (2011). *Effect of physical parameters on static undrained resistance of sandy soil with low silt content*. Soil Dynamics and Earthquake Engineering 31: 1324-1331. Elsevier.

Mammoet Europe B.V, (2017a). *Case Studies* [online]. Available from http://www.mammoet.com/en/cases (accessed 21/07/2017)

Mammoet Europe B.V, (2017b). *Industrial Transport Solutions - SPMTs* [online]. Available from http://www.mammoet.com/en/equipment/transport/self-propelled-modular-transporter/spmt/ (accessed 21/07/2017).

Marto, A. (1998). *Pore Pressure Response of Undrained Two-Way Loading of Silt*. Jurnal kejuruteraan (Journal of Engineering) 11(1): 35-63, Malaysia.

Mayne, P.W., Kulhawy, F.H. (1982). *K0-OCR relationships in soil*. ASCE Journal of Geotechnical Engineering 108 (GT6): 851-872.

Meyerhof, G.G. (1974). *Ultimate bearing capacity of footings on sand layer overlying clay.* Canadian Geotechnical Journal11: 223-229.

MIDAS (2016) *GTS NX software Online Manual.* http://manual.midasuser.com/en_common/GTS%20NX/150/GTX.htm (accessed 29/06/2016)

Muhunthan, B.,and Worthen, D. L. (2011). *Critical state framework for liquefaction of fine grained soils*. Engineering Geology 117: 2-11.

Network Rail. (2005). *Business Process Document NR/SP/TRK/9039 Issue 1: Formation Treatments*.

Network Rail. (2011). *Standard NR/L3/CIV/071 Issue 4: Geotechnical Design.*

Ng, C. W. W., Zhou, C. (2014). *Cyclic behaviour of an unsaturated silt at various suctions and temperatures*. Geotechnique 64(9): 709-720.

Nicot, F., Darve, F. (2010). *Multiscale analysis of failure*. In Micromechanics of Failure in Granular Geomaterials, Edited by F. Nicot & R. Wan., ISTE and John Wiley & Sons. pp. 1-34.

Nouguier-Lehon, C. (2010). *Effect of the grain elongation on the behaviour of granular materials in biaxial compression*. Comptes Rendus Mecanique 338: 587-595.

Nova, R. (2010). *Controllability of Geotechnical Tests and their Relationship to the Instability of Soils*. Micromechanics of Failure in Granular Geomaterials, Ed. F. Nicot & R. Wan, 1-34. ISTE and John Wiley & Sons.

Okur, D. V., Ansal, A. (2007). *Stiffness degradation of natural fine grained soils during cyclic loading*. Soil Dynamics and Earthquake Engineering 27, 843–854.

O'Reilly, M.P., Brown, S.F., and Austin, G. (1988). *Some Observations on the Creep Behaviour of a Silty Clay*. In Proceedings of the International Conference on Rheology and Soil Mechanics Edited by M. J. Keedwell, Coventry, 12-16 Sept 1988, Elsevier Applied Science. pp. 44-58.

O'Riordan, N. J. (1991). *Effects of cyclic loading on the long term settlement of structures.* In Cyclic Loading of Soils: from theory to design Edited by M. P. O'Reilly, S. F. Brown, Blackie and Son Ltd, Glasgow and London pp 411-430.

Osman, A. S., Boulton, M. D. (2005). *Simple plasticity-based prediction of the undrained settlement of shallow circular foundations on clay*. Geotechnique 55(6), 435-447.

Overy, R. F. (1982). *The Behaviour of Anisotropically Consolidated Silty Clay Under Cyclic Loading*. Ph.D Thesis, University of Nottingham Department of Civil Engineering, Nottingham, U.K.

Pande G.N. (1982). *Shakedown of foundations subjected to cyclic loads*. In Soil Mechanics - Transient and Cyclic Loads, Ed. G. N. Pande & O. C. Zienkiewicz, pp 219-252. ISBN 0471100463. John Wiley & Sons Ltd.

Peck R.B. (1969). *Advantages and Limitations of the Observational Method in Applied Soil Mechanics*. Geotechnique 19 (2), 171-187.

Pender, M. J. (1982). *A model for the cyclic loading of overconsolidated soil.* In Soil Mechanics - Transient and Cyclic Loads, Edited by. G. N. Pande & O. C. Zienkiewicz, John Wiley & Sons Ltd.pp 283-311.

Peters, J. F. (1988). *Determination of undrained shear strength of low plasticity clays.* Advanced Triaxial Testing of Soil and Rock, ASTM STP 977, 460-474. American Society for Testing and Materials.

Ponter A.R.S., Hearle A.D., Johnson K.L. (1985). *Application of the Kinematical Shakedown Theorem to Rolling and Sliding Point Contacts*. Journal of the Mechanics and Physics of Solids 33(4): 339-362.

Qi, J., Luan, M., Feng, X., Ma, T., Nie, Y. (2007). *Cyclic Shearing Deformation Behavior of Saturated Clays*. Journal of Ocean University of China (Oceanic and Coastal Sea Research) 6(4), 413-420.

Ravi, K., Dash, S., Vogt, S., and Braeu, G. (2014). *Behaviour of Geosynthetic Reinforced Unpaved Roads Under Cyclic Loading*. Indian Geotechnical Journal 44(1): 77-85.

Roscoe K.H. and Burland J.B. (1968). *On the generalised stress-strain behaviour of 'wet' clay*, Eng. plasticity, Cambridge Univ. Press, 535-609

Rothenburg, L., and Kruyt, N.P. (2004). *Critical state and evolution of coordination number in simulated granular materials*. International Journal of Solids and Structures 41: 5763-5774.

Santagata, M., Germaine, J. T. (2005). *Effect of OCR on sampling disturbance of cohesive soils and evaluation of laboratory reconsolidation procedures*. Canadian Geotechincal Journal 42: 459-474. NRC Canada.

Sazzad, M., and Suzuki, K. (2010). *Micromechanical behavior of granular materials with inherent anisotropy under cyclic loading using 2D DEM*. Granular Matter 12: 597-605.

Schofield, A., Wroth, P. (1968). *Critical State Soil Mechanics*. McGraw Hill. London.

Selig, E. T., and Chang, C. S. (1981). *Soil failure modes in undrained cyclic loading.* ASCE Journal of Geotechnical Engineering Division 107 (5): 539-551.

Sharp, R.W., Booker, J. R. (1984). *Shakedown of pavements under moving surface loads.* ASCE Journal of Transportation Engineering 110(1), 1-14.

Sheng, D., Westerburg, B., Mattsson, H., Axelsson, K. (1997). *Effects of End Restraint and Strain Rate in Triaxial Tests*. Computers and Geotechnics 21(3): 163-182.

Singh, A., and Mitchell, J. K. (1968). *General Stress-Strain-Time Function for Soils.* ASCE Journal of the Soil Mechanics and Foundations Division 94(1): 21-46.

Sitharam, T. G., Vinod, J. S. (2009). *Critical state behaviour of granular materials from isotropic and rebounded paths: DEM simulations*. Granular Matter 11:33–42

Soreghan, G.S., Joo, Y.J., Elwood Madden M.E., Van Deventer, S.C. (2016). *Silt production as a function of climate and lithology under simulated comminution*. Quaternary International Volume 399, 18 April 2016, Pages 218–227

Soroush, A., and Ferdowsi, B. (2011). *Three dimensional discrete element modeling of granular media under cyclic constant volume loading: A micromechanical perspective*. Powder Technology 212: 1-16.

Southern, J. (2016). *Smart construction: How offsite manufacturing can transform our industry*. KPMG UK,

https://assets.kpmg.com/content/dam/kpmg/pdf/2016/04/SmartConstructionReport.pdf accessed 21/07/2017.

Tannant, D.D., Regensburg, B. (2001). *Guidelines for Mine Haul Road Design*. University of British Columbia, Okanagan, Canada.

Teachavorasinskun, S., Thongchim, P., Lukkunaprasit, P. (2002). *Stress rate effect on the stiffness of a soft clay from cyclic, compression and extension triaxial tests*. Geotechnique 52(1), 51-54.

Thom, N. (2014). *Principles of Pavement Engineering (2nd Ed.).* ICE Publishing, Thomas Telford, London.

Thornton, C. (2000). *Numerical simulations of deviatoric shear deformation of granular media*. Geotechnique 50(1): 43-53.

Togrol, E., Güler, E. (1984). *Effect of repeated loading on the strength of clay*. Soil Dynamics and Earthquake Engineering 3(4): 184-190.

Vaid, Y. P. (1988). *Time Dependent Shear Deformation of Clay*. In Proceedings of the International Conference on Rheology and Soil Mechanics Edited by M. J. Keedwell, Coventry, 12-16 Sept 1988, Elsevier Applied Science. pp. 123-129.

Valls-Marquez, M. (2009). *Evaluating the capabilities of some constitutive models in reproducing the experimental behaviour of stiff clay subjected to tunnelling stress paths.* Ph.D Thesis, University of Birmingham Department of Civil Engineering, Birmingham, U.K.

Valls-Marquez, M., Chapman, D. N., Ghataora, G. S. (2008). Preparation of K0-consolidated reconstituted samples in the laboratory. International Journal of Geotechnical Engineering 2: 343-354.

Walker, L. K. (1969). Undrained Creep in a Sensitive Clay. Geotechnique 19(4), 515-529.

Waltham, T. (2002). Foundations of Engineering Geology (2nd Ed.). Taylor and Francis, Oxon.

Wang, S., Luna, R. (2012). *Monotonic behavior of Mississippi River Valley Silt in Triaxial Compression*. Journal of Geotechnical and Geoenvironmental Engineering 138 (4): 516–525.

Wang, S., Luna, R., and Onyejekwe, S. (2015a). *Postliquefaction behavior of low-plasticity silt at various degrees of reconsolidation*. Soil Dynamics and Earthquake Engineering 75, 259-264.

Wang, S., Luna, R., Stephenson, R. W. (2011). *A slurry consolidation approach to reconstitute low-plasticity silt specimens for laboratory triaxial testing*. Geotechnical Testing Journal 34(4), Paper ID GTJ103529.

Wang, S., Luna, R., Zhao, H. (2015b). *Cyclic and post-cyclic shear behavior of low-plasticity silt with varying clay content*. Soil Dynamics and Earthquake Engineering 75: 112–120.

Wang, S., Onyejekwe, S., Yang, J. (2014). *Threshold Strain for Postcyclic Shear Strength Change of Mississippi River Valley Silt Due to Cyclic Triaxial Loading*. Journal of Testing and Evaluation 42(1): 1-9.

Ward, S. J. (1983). *The stability of a silty clay under repeated loading*. Ph.D thesis, Loughborough University, Loughborough, U.K.

Wei, L. M., and Yang, J. (2014). *On the role of grain shape in static liquefaction of sand–fines mixtures*. Geotechnique 64(9): 740-745.

Xiao, J., Juang, C. H., Wei, K., and Xu, S. (2014). *Effects of Principal Stress Rotation on the Cumulative Deformation of Normally Consolidated Soft Clay under Subway Traffic Loading*. ASCE Journal of Geotechnical and Geoenvironmental Engineering 140(4): 04013046.

Xu, X. M., Ling, D. S., Ghen, Y. P., and Chen, Y. M. (2015). *Correlation between liquefaction resistance and shear wave velocity of granular soils: a micromechanical perspective.* Geotechnique 65(5), 337-348.

Yamamuro, J. A., Lade, P. V. (1999). *Experiments and modelling of silty sands susceptible to static liquefaction*. Mechanics of Cohesive-Frictional Materials 4, 545-564. John Wiley & Sons Ltd.

Yasuhara, K., Murakami, S., Song, B., Yokokawa, S., Hyde, A. F. L. (2003). *Postcyclic Degradation of Strength and Stiffness for Low Plasticity Silt.* ASCE Journal of Geotechnical and Geoenvironmental Engineering. ASCE Publishing.

Zapata-Medina, D. G., Finno, R. J., Vega-Posada, C. A. (2014). *Stress history and sampling disturbance effects on monotonic and cyclic responses of overconsolidated Bootlegger Cove clays*. Canadian Geotechnical Journal 51. 599-609.

Zhang, H., Garga, V. K. (1997). *Quasi-steady state: a real behaviour?* Canadian Geotechnical Journal 34: 749–761

Zhao, J. Guo, N. (2015). *The interplay between anisotropy and strain localisation in granular soils: a multiscale insight*. Géotechnique 65(8), 642–656.

Zhao, J., Sloan, S. W., Lyamin, A. V., and Krabbenhøft, K. (2008). *Bounds for shakedown of cohesive-frictional materials under moving surface loads*. International Journal of Solids and Structures 45, 3290-3312.

Zhao, X., Evans, T. M. (2011). *Numerical analysis of critical state behaviors of granular soils under different loading conditions*. Granular Matter 13: 751-764

Appendix 1

Supplementary cyclic test data

This appendix details water content and consolidation data (presented graphically and statistically in Section 6.1) and detailed descriptions of stresses, strains, pore water pressures and consolidation intervals during the complex incrementally loaded cyclic tests, to facilitate understanding.

Table A-1: Water content and consolidation data for cyclic tests

Test	Final water content	Estd. initial water content (from ΔV)	ε_{v1}
C-1	18.3%	20.8%	3.1%
C-2	18.2%	20.5%	3.2%
C-3	17.6%	20.2%	3.2%
C-4	18.3%	20.8%	2.3%
C-5	17.9%	20.5%	3.4%
C-6	17.9%	20.5%	2.8%
C-7	17.7%	21.0%	4.8%
C-8	17.4%	22.4%	7.4%
C-9	18.0%	20.5%	3.3%
C-10	17.1%	19.9%	4.1%
C-11	17.9%	20.4%	3.0%
C-12	17.9%	20.2%	2.9%
C-13	17.0%	19.7%	3.7%
D-1	17.6%	19.5%	2.3%
D-2	17.9%	19.9%	2.3%
D-3	17.1%	19.2%	2.9%
D-4	17.8%	20.2%	3.2%
D-5	17.9%	20.3%	2.7%
D-6	17.6%	19.8%	2.7%
D-7	17.3%	20.2%	4.1%
D-8	17.3%	18.9%	1.8%

Test	Final water content	Estd. initial water content (from ΔV)	ε_{v1}
E-1	17.8%	20.2%	2.9%
E-2	17.4%	20.1%	3.4%
E-3	17.6%	21.6%	5.2%
E-4	17.8%	21.9%	4.6%
E-5	17.8%	20.5%	3.5%
F-1	18.3%	20.3%	2.3%
F-2	17.8%	21.1%	4.3%
F-3	17.7%	20.0%	2.9%
F-4	18.1%	19.9%	2.1%
F-5	17.6%	20.4%	3.5%
F-6	17.8%	20.3%	3.2%
G-1	17.0%	19.0%	2.1%
G-2	17.6%	not known	3.2%
G-3	16.9%	19.7%	3.6%
G-4	17.3%	19.8%	3.0%
G-5	17.8%	20.6%	3.7%

Table A-2: Specifics of test G-2

Cycle count	q_{min}	q_{max}	u_{min}	u_{max}	ε_{min}	ε_{max}	$q_{\varepsilon,max}$
	(kPa)	(kPa)	(kPa)	(kPa)	(%)	(%)	(kPa)
1	184	223	102	111	0.00	0.21	213
Drain 1: 2hrs, ΔV = 1.32ml			111	114	0.19	0.21	
2	184	222	102	107	0.21	0.28	219
3	184	222	105	109	0.25	0.30	220
4	184	222	107	111	0.28	0.32	220
5	184	222	109	114	0.30	0.35	220
6	184	222	111	115	0.32	0.37	220
7	187	238	114	133	0.35	1.24	215
8	187	239	133	153	1.22	2.92	219
Drain 2: 14hrs, ΔV = 9.10ml			153	156	2.88	2.92	
9	188	240	101	107	2.92	2.98	239
10	188	240	104	109	2.95	2.99	240
11	188	240	106	111	2.96	3.00	240
12	188	240	108	112	2.96	3.00	240
13	188	240	109	114	2.97	3.01	240
14	192	257	111	116	2.98	3.06	255
15	192	257	112	118	3.02	3.08	254
16	192	257	114	120	3.04	3.10	255
17	192	257	116	121	3.06	3.12	255
18	191	257	117	123	3.08	3.14	256
19	191	269	119	126	3.10	3.22	263
20	190	269	120	127	3.17	3.27	264
21	191	269	122	129	3.22	3.32	264
22	190	269	123	130	3.27	3.37	264
23	190	269	125	131	3.32	3.41	264
24	191	283	126	133	3.36	3.61	272
25	191	283	127	135	3.55	3.76	273
26	191	283	129	137	3.70	3.89	273
27	193	285	131	139	3.83	4.05	276
28	193	285	132	139	3.99	4.18	276
29	193	299	133	143	4.12	4.64	283
30	194	300	134	143	4.58	5.01	286
31	194	300	135	144	4.95	5.30	287
Drain 3: 2hrs, ΔV = 3.91ml			136	142	5.22	5.22	
32	194	301	103	114	5.22	5.36	298
33	195	301	110	119	5.29	5.39	299
34	194	302	114	123	5.32	5.42	299
35	194	301	116	125	5.35	5.45	299

Cycle count	q_{min}	q_{max}	u_{min}	u_{max}	ε_{min}	ε_{max}	$q_{\varepsilon,max}$
36	194	302	117	127	5.38	5.47	299
37	195	316	119	129	5.40	5.57	310
38	196	316	120	130	5.50	5.65	310
39	196	316	121	131	5.57	5.73	310
40	196	316	122	132	5.65	5.80	310
41	196	316	123	133	5.72	5.87	310
42	197	330	123	135	5.79	6.08	318
43	198	330	124	135	6.00	6.25	320
44	198	330	124	136	6.16	6.40	316
45	200	333	124	137	6.31	6.58	322
46	201	334	124	137	6.50	6.74	323
47	202	350	123	138	6.66	7.21	330
48	203	350	123	136	7.12	7.51	333
49	202	354	122	137	7.42	7.84	337
Drain 4: 2hrs, ΔV = 3.13ml			124	134	7.73	7.73	
50	201	352	102	114	7.73	7.91	346
51	203	352	107	119	7.81	7.97	347
52	203	352	110	122	7.87	8.02	346
53	203	352	112	124	7.92	8.08	346
54	203	352	113	125	7.98	8.13	347
55	204	368	113	127	8.03	8.29	354
56	206	368	114	127	8.19	8.42	358
57	205	368	114	128	8.32	8.54	359
58	205	368	114	128	8.44	8.66	359
59	205	368	115	129	8.56	8.78	359
60	206	385	113	130	8.67	9.07	366
61	208	385	113	129	8.96	9.30	372
62	208	386	113	129	9.19	9.50	370
63	208	385	113	129	9.38	9.68	373
Drain 5: 2hrs, ΔV = 2.39ml							

Table A-3: Specifics of incremental stages of test G-4, following 100no. cycles of 40kPa with 5 minute drainage intervals (PWP transducer faulty, no *u* readings)

Cycle count	q_{min}	q_{max}	ε_{min}	ε_{max}	$q_{\varepsilon,max}$
	(kPa)	(kPa)	(%)	(%)	(kPa)
0	187	239	1.74	1.80	237
1	188	238	1.76	1.82	238
2	187	238	1.78	1.83	238
3	187	239	1.79	1.83	238
4	187	238	1.80	1.84	238
5	187	238	1.80	1.84	238
Drain 1: 5 mins, ΔV = 0.71ml					
6	189	254	1.81	1.87	250
7	190	254	1.83	1.89	252
8	189	253	1.85	1.90	253
9	190	253	1.86	1.92	253
10	189	253	1.88	1.93	252
11	189	253	1.89	1.94	252
12	188	264	1.92	2.00	261
Drain 2: 16 hrs, ΔV = 0.2.56ml					
13	187	264	1.96	2.02	263
14	187	264	1.97	2.03	263
15	187	264	1.98	2.04	263
16	187	264	1.99	2.05	264
17	187	264	2.00	2.06	264
18	188	277	2.01	2.11	273
19	187	276	2.05	2.14	272
20	187	276	2.09	2.18	273
21	187	276	2.12	2.21	275
22	187	276	2.15	2.24	275
23	187	276	2.18	2.27	275
24	188	289	2.21	2.40	281
25	187	289	2.34	2.51	281
26	187	289	2.45	2.61	283
27	187	288	2.55	2.71	282
28	187	288	2.65	2.81	283
29	187	288	2.74	2.90	283
30	179	281	2.88	2.99	279
Drain 3: 2 hrs, ΔV = 2.04ml					
31	179	281	2.92	3.01	279
32	179	281	2.94	3.02	280
33	180	281	2.95	3.04	280

Cycle count	q_{min}	q_{max}	ε_{min}	ε_{max}	$q_{\varepsilon,max}$
34	179	281	2.97	3.05	280
35	179	281	2.98	3.07	280
36	186	300	3.01	3.16	293
37	185	299	3.09	3.23	295
38	185	300	3.15	3.29	296
39	186	299	3.21	3.34	298
40	185	299	3.27	3.40	297
41	185	299	3.32	3.45	297
42	186	312	3.38	3.63	303
43	185	312	3.55	3.77	304
44	185	311	3.68	3.89	305
45	185	311	3.81	4.01	306
46	185	310	3.92	4.12	305
47	185	310	4.03	4.22	307
48	187	288	4.14	4.22	287
49	187	288	4.15	4.24	287
50	187	289	4.17	4.26	286
51	187	288	4.19	4.28	287
52	187	288	4.21	4.30	287
53	187	288	4.23	4.32	288

Table A-4: Specifics of incremental stages of test G-5, following 70no. cycles of 20kPa (PWP transducer faulty, no *u* readings)

Cycle count	q_{min}	q_{max}	ε_{min}	ε_{max}
(-)	(kPa)	(kPa)	(%)	(%)
1	189	240	1.44	1.51
2	189	239	1.47	1.53
3	189	239	1.49	1.55
4	189	239	1.50	1.56
5	189	239	1.52	1.58
6	189	239	1.53	1.59
7	188	252	1.55	1.67
8	188	252	1.62	1.72
9	188	252	1.66	1.76
10	188	251	1.71	1.79
11	188	251	1.74	1.82
12	188	251	1.77	1.85
Drain 1: 5 mins, ΔV = 0.39ml				
13	189	265	1.80	1.93
14	189	264	1.87	1.97
15	189	264	1.91	2.01
16	189	264	1.95	2.04
17	188	264	1.99	2.07
18	189	264	2.01	2.10
19	189	277	2.04	2.20
20	189	277	2.14	2.27
21	189	277	2.21	2.34
22	188	276	2.27	2.39
23	188	276	2.32	2.43
24	188	276	2.37	2.48
Drain 2: 2hrs, , ΔV = 1.33ml				
25	188	276	2.42	2.51
26	188	276	2.45	2.53
27	188	276	2.46	2.54
28	188	276	2.47	2.55
29	188	276	2.48	2.56
30	188	276	2.49	2.57
31	188	289	2.50	2.61
32	188	289	2.53	2.63
33	188	289	2.55	2.65
34	188	289	2.58	2.67
35	188	289	2.60	2.69

Cycle count	q_{min}	q_{max}	ε_{min}	ε_{max}
36	188	288	2.62	2.71
37	188	302	2.64	2.78
38	188	302	2.70	2.83
39	188	302	2.74	2.87
40	188	301	2.79	2.91
41	188	301	2.83	2.95
42	188	301	2.86	2.98
43	188	301	2.90	3.02
44	188	301	2.94	3.05
45	188	301	2.97	3.08
46	188	301	3.00	3.11
47	187	301	3.03	3.14
48	187	301	3.06	3.17
49	188	314	3.09	3.25
50	188	314	3.16	3.32
51	188	314	3.22	3.37
52	188	314	3.28	3.42
53	187	313	3.33	3.47
54	187	313	3.38	3.51
55	188	301	3.42	3.52
56	188	301	3.44	3.54
57	188	301	3.45	3.56
58	188	301	3.47	3.57
59	188	301	3.49	3.59
60	188	300	3.51	3.61
61	188	339	3.52	3.85
62	188	339	3.74	3.99
63	187	338	3.88	4.10
64	187	338	3.99	4.19
65	187	337	4.08	4.28
66	187	337	4.17	4.36

Table A-5: Specifics of test CL-6

Cycle count	q_{min}	q_{max}	u_{min}	u_{max}	ε_{min}	ε_{max}
(-)	(kPa)	(kPa)	(kPa)	(kPa)	(%)	(%)
1	86	110	100	112	0.00	0.48
2	86	109	104	115	0.47	0.83
3	85	109	107	119	0.81	1.12
Drain 1: 14 hrs, ΔV = 5.00ml						
4	83	107	100	111	1.37	1.43
5	83	107	101	111	1.41	1.44
6	83	108	102	112	1.42	1.46
7	83	107	102	112	1.43	1.47
8	83	107	103	112	1.44	1.48
9	83	107	103	113	1.45	1.49
10	83	107	103	113	1.46	1.49
11	83	105	104	113	1.47	1.50
12	83	107	104	114	1.48	1.51
13	83	106	105	114	1.48	1.52
14	85	107	105	114	1.49	1.53
15	83	107	105	115	1.50	1.53
16	83	107	105	115	1.51	1.54
17	83	107	105	115	1.51	1.55
18	83	107	106	116	1.52	1.55
19	83	107	106	116	1.53	1.56
20	83	107	106	116	1.53	1.57
21	83	107	106	116	1.54	1.57
22	83	107	106	116	1.55	1.58
23	83	107	107	117	1.55	1.59
24	82	112	106	119	1.56	1.64
25	82	111	106	119	1.60	1.68
26	83	112	107	120	1.64	1.72
27	82	112	107	121	1.68	1.75
28	82	112	108	121	1.71	1.79
29	82	112	108	122	1.75	1.83
30	82	112	109	123	1.79	1.87
31	82	111	110	123	1.82	1.90
32	82	112	110	124	1.86	1.94
33	82	112	111	124	1.90	1.97
34	82	107	111	125	1.93	2.01
35	82	111	112	125	1.97	2.05
36	82	111	113	126	2.01	2.08
37	82	111	113	126	2.04	2.12

Cycle count	q_{min}	q_{max}	u_{min}	u_{max}	ε_{min}	ε_{max}
38	82	111	113	127	2.08	2.15
39	81	111	114	128	2.11	2.19
40	83	111	115	128	2.15	2.23
41	83	111	115	128	2.18	2.26
42	81	111	115	129	2.22	2.30
Drain 2: 14 hrs, ΔV = 3.42ml						
43	82	109	100	114	2.31	2.38
44	83	106	102	114	2.34	2.39
45	82	109	102	115	2.35	2.40
46	80	110	103	116	2.36	2.41
47	80	107	103	116	2.37	2.41
48	83	117	105	122	2.38	2.53
49	83	117	106	122	2.48	2.60
50	83	118	107	123	2.55	2.67
51	84	117	108	124	2.62	2.74
52	83	117	108	125	2.69	2.81
53	84	114	110	126	2.76	2.88
54	83	116	110	126	2.83	2.95
55	83	113	111	127	2.90	3.03
56	82	117	112	128	2.97	3.10
57	82	117	112	129	3.05	3.18
58	82	115	113	129	3.13	3.26
59	84	114	114	130	3.20	3.33
60	82	117	115	131	3.28	3.41
61	82	117	115	132	3.35	3.48
62	86	124	117	136	3.44	4.55
Drain 3: 14 hrs, ΔV = 6.48ml						
63	81	119	100	122	4.59	4.74
64	80	120	103	122	4.68	4.78
65	81	119	104	123	4.71	4.81
66	80	120	105	124	4.74	4.84
67	81	120	106	125	4.77	4.86
68	82	120	106	126	4.80	4.89
69	80	120	107	126	4.82	4.92
70	80	119	108	127	4.85	4.94
71	81	119	108	127	4.88	4.97
72	82	118	109	128	4.90	4.99
73	83	126	110	132	4.94	5.20
74	82	126	110	132	5.12	5.37
75	82	126	111	134	5.29	5.53
76	82	126	112	134	5.45	5.70

Cycle count	q_{min}	q_{max}	u_{min}	u_{max}	ε_{min}	ε_{max}
77	82	126	113	135	5.61	5.87
78	82	124	114	137	5.78	6.04
79	82	125	115	138	5.95	6.21
80	83	128	117	141	6.13	7.31
Drain 4: 7 hrs, ΔV = 5.55ml						
81	86	106	119	128	7.22	7.25
82	86	129	104	130	7.31	7.55
83	87	129	108	131	7.47	7.65
84	85	129	109	133	7.57	7.75
85	85	128	111	134	7.66	7.84
86	86	128	112	135	7.76	7.94
87	85	128	113	136	7.85	8.03
88	85	128	113	137	7.95	8.13
89	85	129	114	137	8.04	8.23
90	85	129	115	138	8.14	8.33
91	85	125	116	139	8.24	8.43

Table A-6: Specifics of incremental stages of test CL-7

Cycle count	q_{min}	q_{max}	u_{min}	u_{max}	ε_{min}	ε_{max}
1	91	110	116	126	0.77	1.01
2	90	109	120	128	0.99	1.23
3	90	109	121	129	1.21	1.45
4	90	109	122	131	1.43	1.66
5	90	109	123	132	1.64	1.87
Drain 1: 2 hrs, ΔV = 2.9ml						
6	90	109	115	122	1.95	2.06
7	90	109	117	123	2.03	2.10
8	90	109	118	124	2.08	2.14
9	90	109	119	125	2.12	2.19
10	90	109	119	126	2.16	2.23
11	90	109	120	126	2.20	2.27
12	90	109	121	127	2.24	2.31
13	89	109	121	127	2.28	2.35
14	89	108	122	128	2.32	2.39
15	89	108	122	128	2.36	2.42
16	89	108	123	129	2.40	2.46
Drain 2: 2 hrs, ΔV = 2.8ml						
17	90	116	124	132	2.44	3.04
18	89	114	116	126	3.08	3.28
19	89	114	120	128	3.24	3.39
20	89	114	121	129	3.35	3.50
21	89	114	122	131	3.45	3.61
22	89	114	123	132	3.57	3.72
23	88	114	124	133	3.68	3.84
24	88	114	125	133	3.80	3.97
25	88	114	126	135	3.92	4.09
26	88	113	127	135	4.05	4.22
27	88	113	127	136	4.17	4.34
28	88	113	128	137	4.30	4.47
29	88	113	129	138	4.43	4.60
30	88	113	130	138	4.55	4.73
31	88	113	130	139	4.68	4.86
32	87	113	131	140	4.81	4.99
33	87	112	132	140	4.94	5.12
34	87	112	132	141	5.07	5.24
35	87	112	133	141	5.20	5.37
36	87	112	133	142	5.33	5.50
37	87	112	134	142	5.45	5.62

Cycle count	q_{min}	q_{max}	u_{min}	u_{max}	ε_{min}	ε_{max}
38	87	111	134	143	5.58	5.75
39	87	111	135	143	5.70	5.87
40	89	119	135	147	5.83	9.22
Drain 3: 14 hrs, ΔV = 12.9ml						
41	88	119	101	113	9.50	9.65
42	88	119	105	115	9.60	9.70
43	88	119	107	116	9.64	9.73
44	88	119	107	117	9.68	9.77
45	88	119	109	118	9.71	9.80
46	88	119	109	119	9.74	9.83
47	88	119	110	120	9.77	9.86
48	88	118	111	121	9.80	9.88
49	88	118	112	121	9.83	9.91
50	88	118	112	122	9.85	9.94
51	88	118	113	122	9.88	9.97
52	88	118	113	123	9.91	10.00
53	89	125	116	126	9.94	10.19
54	89	124	120	128	10.12	10.34
55	89	124	121	129	10.27	10.49
56	89	124	122	131	10.41	10.63
57	89	124	123	132	10.56	10.79

Appendix 2

Derivation of normally consolidated shear strength and Young's modulus gradient with depth (m_1)

The shape of the yield surface is assumed to follow Modified Cam Clay, after Roscoe and Burland (1968).

Based on an assumed friction angle φ = 30° and effective unit weight γ' = 7.19kN/m^3:

$$K_0 = 0.95 - \sin(\varphi)$$

K_0 = 0.45

$$M = \frac{6 \cdot \sin(\varphi)}{3 - \sin(\varphi)}$$

M = 1.2

Insitu stresses can be expressed as:

$p' = \frac{1}{3} \cdot (2 \cdot \sigma'_3 + \sigma'_1) = \frac{1}{3} \cdot \sigma'_1 \cdot (2 \cdot K_0 + 1)$ and $q = (\sigma'_1 - \sigma'_3) = \sigma'_1 \cdot (1 - K_0)$;

The rate of change in mean normal effective stress with depth is therefore:

$$\frac{p'}{z} = \frac{1}{3} \cdot \gamma' \cdot (2 \cdot K_0 + 1)$$

p'/z = 4.55 kPa/m

From modified Cam-Clay the yield surface is described as:

$$\left(\frac{q}{M \cdot p'}\right)^2 + 1 - \frac{p'_0}{p'} = 0$$

Defining $\eta = q/p'$ and $p'_0 = p'$ at intersection of yield surface with hydrostatic (q = 0) axis:

$$\frac{p'_0}{p'} = 1 + \left(\frac{\eta}{M}\right)^2$$

The soil is in anisotropic stress state, so it is more useful to define the yield surface based on the intersection with the anisotropic (K_0) stress state of p'_K and q_K (with $\eta_K = q_K/p_K'$):

Therefore in K_0 condition:

$$\frac{p'_0}{p'_K} = 1 + \left(\frac{\eta_K}{M}\right)^2$$

While at the critical state ($p' = p'_C$, $q = q_C$):

$$\frac{p'_0}{p'_C} = 2$$

So:

$$\frac{p'_C}{p'_K} = \frac{1 + \left(\frac{\eta_K}{M}\right)^2}{2}$$

$$\eta_K = \frac{3 \cdot (1 - K_0)}{2 \cdot K_0 + 1} = 0.868$$

And:

$$q_c = M \cdot p'_C = \frac{1 + \left(\frac{\eta_K}{M}\right)^2}{2} \cdot M \cdot p'_K$$

i.e. in the normally consolidated zone:

$$\tau_c = \frac{1 + \left(\frac{\eta_K}{M}\right)^2}{4} \cdot M \cdot p'_K = 0.457 p'_K \text{ or } 2.08 kPa/m$$

This can also be expressed in terms of effective overburden stress, i.e.:

$$p' = \frac{1}{3} \cdot \sigma'_1 \cdot (2 \cdot K_0 + 1) \therefore \tau_c = \frac{0.457 \cdot (2 \cdot K_0 + 1)}{3} \cdot \sigma'_1 = 0.289 \sigma'_1$$

$m_1 = 1000.S_u = 457p'$ (all values in kPa) or *m_1* (in MPa) *= 0.457p'*.